28 November 2008 | $10

Science

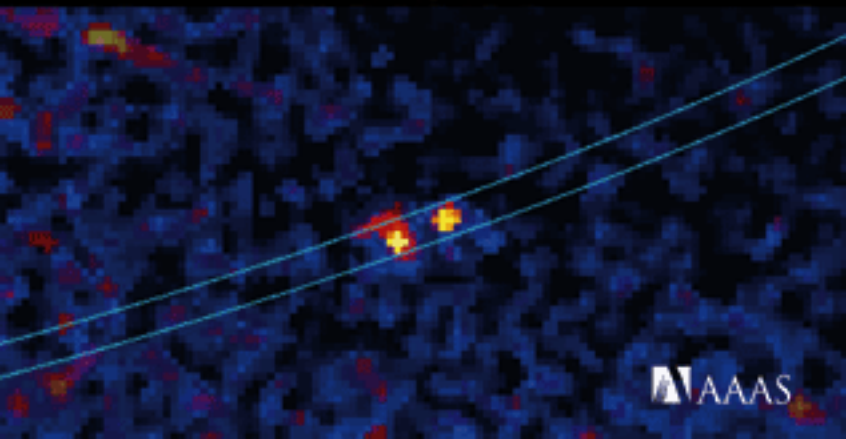

AAAS

Volume 322, Issue 5906

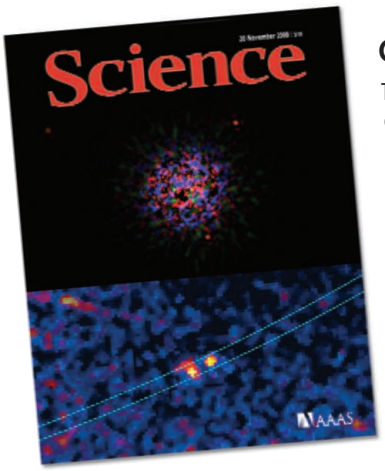

COVER

Two direct detections of extrasolar planet candidates. Top: Keck Telescope colored infrared image of star HR 8799, for which the starlight is masked, showing three surrounding planets (red dots). Bottom: Superposed Hubble Space Telescope visible images from 2 years apart, tracing the orbit of a planet surrounding the star Fomalhaut. See pages 1345 and 1348.

Images: Christian Marois/NRC Herzberg Institute of Astrophysics, Canada; Paul Kalas/University of California, Berkeley

DEPARTMENTS

1297 *Science* Online
1299 This Week in *Science*
1304 Editors' Choice
1306 Contact *Science*
1307 Random Samples
1309 Newsmakers
1342 AAAS News & Notes
1400 New Products
1401 *Science* Careers

EDITORIAL

1303 Scientists and Human Rights
by Leonard Rubenstein and Mona Younis

NEWS OF THE WEEK

Chinese Probe Unmasks High-Tech Adulteration With Melamine 1310
Will French Science Swallow Zerhouni's Strong Medicine? 1312
Giant Scope Heads Europe's Wish List 1313
SCIENCESCOPE 1313
Interest Rises in DNA Copy Number Variations—Along With Questions 1314
Science Goes Hollywood: NAS Links With Entertainment Industry 1315

NEWS FOCUS

Canada's Experimental Lakes 1316
Contaminating a Lake to Save Others
>> Science *Podcast*
Adam Reiss: A Universe Past the Braking Point 1320
University Hackers Test the Right to Expose Security Concerns 1322


1316

LETTERS

The Price of Exploration *J. B. Garvin* 1324
Research Funding: Less Should Be More *R. Sousa*
Cell Phone and DNA Story Overlooked Studies *V. G. Khurana* Response *G. Vogel*
Flaunting the Feminine Side of Research Studies *P. Greenberger*
CORRECTIONS AND CLARIFICATIONS 1326

BOOKS *ET AL.*

The Superorganism The Beauty, Elegance, and Strangeness of Insect Societies *B. Hölldobler and E. O. Wilson, reviewed by J. H. Hunt* 1327
Sun in a Bottle The Strange History of Fusion and the Science of Wishful Thinking *C. Seife, reviewed by F. N. von Hippel* 1328


1327

EDUCATION FORUM

Scientific Teaching in Practice 1329
S. Miller, C. Pfund, C. M. Pribbenow, J. Handelsman
Global Sex Differences in Test Score Variability 1331
S. Machin and T. Pekkarinen

PERSPECTIVES

A Tamed Reactive Intermediate 1333
J. B. Lambert >> Report p. 1360
Reflections on a Wall of Light 1334
P.-M. Binder
Exoplanets—Seeing Is Believing 1335
M. S. Marley >> Research Articles pp. 1345 and 1348
An Antibiotic Mimics Immunity 1337
C. Nathan >> Report p. 1392
Carbon in Charge 1338
R. L. Evans >> Report p. 1363
Controlled Chaos 1340
V. N. Uversky and A. K. Dunker >> Report p. 1365

CONTENTS continued >>

Published by AAAS

Science

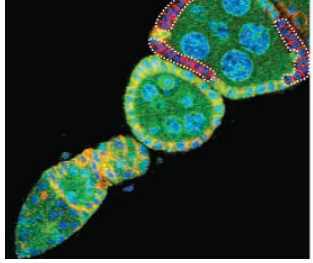

SCIENCE EXPRESS

www.sciencexpress.org

MICROBIOLOGY

AMPylation of Rho GTPases by *Vibrio* VopS Disrupts Effector Binding and Downstream Signaling

M. L. Yarbrough, Y. Li, L. N. Kinch, N. V. Grishin, H. L. Ball, K. Orth

A GI-active pathogen destroys intestinal cells, in part by improperly modifying a host signaling protein, causing loss of cell shape and contributing to cell death.

10.1126/science.1166382

PHYSICS

Universal Theory of Nonlinear Luttinger Liquids

A. Imambekov and L. I. Glazman

A theory of one-dimensional quantum liquids is generalized from linear interactions among particles to nonlinear ones, affecting, for example, predicted tunneling dynamics.

10.1126/science.1165403

DEVELOPMENTAL BIOLOGY

Drosophila Stem Cells Share a Common Requirement for the Histone H2B Ubiquitin Protease Scrawny

M. Buszczak, S. Paterno, A. C. Spradling

Stem cells in the germ line, epithelium, and intestine all require a particular modification of histone H2B to repress key differentiation genes and maintain pluripotency.

10.1126/science.1165678

MATERIALS SCIENCE

Direct Measurement of Molecular Mobility in Actively Deformed Polymer Glasses

H.-N. Lee, K. Paeng, S. F. Swallen, M. D. Ediger

Optical bleaching of a dilute molecular probe shows that when a rubbery polymer begins to flow, polymer chains become more mobile than predicted from a classical model.

10.1126/science.1165995

TECHNICAL COMMENT ABSTRACTS

ECOLOGY

Comment on "Climate-Driven Ecosystem Succession in the Sahara: The Past 6000 Years" 1326

V. Brovkin and M. Claussen

full text at www.sciencemag.org/cgi/content/full/322/5906/1326b

Response to Comment on "Climate-Driven Ecosystem Succession in the Sahara: The Past 6000 Years"

S. Kröpelin, D. Verschuren, A.-M. Lézine

full text at www.sciencemag.org/cgi/content/full/322/5906/1326c

BREVIA

CLIMATE CHANGE

A Simple Law for Ice-Shelf Calving 1344

R. B. Alley et al.

An empirical model of iceberg production as an ice shelf that buttresses a glacier spread may help to predict glacial flow and sea level rise as Earth's climate warms.

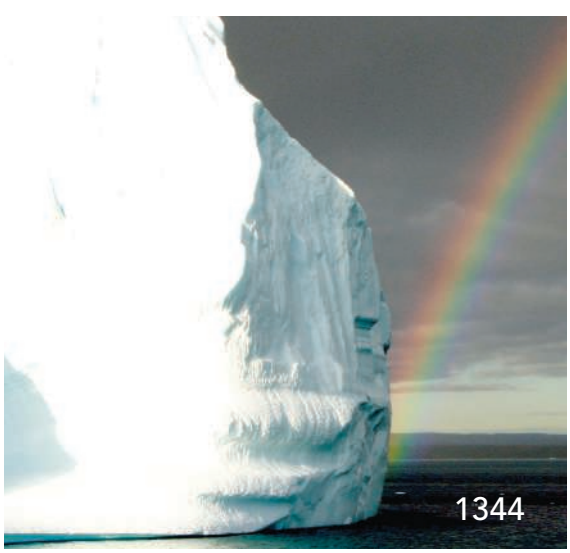

RESEARCH ARTICLES

ASTRONOMY

Optical Images of an Exosolar Planet 25 Light-Years from Earth 1345

P. Kalas et al.

Images from the Hubble Space Telescope reveal a Jupiter-sized planet, perhaps with a surrounding dust disk, orbiting about 115 astronomical units from a nearby main sequence star.

>> Perspective p. 1335

ASTRONOMY

Direct Imaging of Multiple Planets Orbiting the Star HR 8799 1348

C. Marois et al.

Infrared images from the Keck and Gemini telescopes reveal three giant planets orbiting counterclockwise around a young star, in a scaled-up version of our solar system.

>> Perspective p. 1335

CELL BIOLOGY

Detection of GTP-Tubulin Conformation in Vivo Reveals a Role for GTP Remnants in Microtubule Rescues 1353

A. Dimitrov et al.

GTP-bound tubulin is found at microtubule ends in living cells and also within microtubules, where it may promote repolymerization and avert microtubule collapse.

REPORTS

PHYSICS

Resolving Vacuum Fluctuations in an Electrical Circuit by Measuring the Lamb Shift 1357

A. Fragner et al.

A solid-state qubit in an electrical circuit connected to a vacuum field shows a shift in its transition energy level, a classic quantum effect typically seen in isolated atoms.

CONTENTS continued **>>**

Published by AAAS

REPORTS *CONTINUED...*

CHEMISTRY

A Cryptand-Encapsulated Germanium(II) Dication 1360
P. A. Rupar, V. N. Staroverov, K. M. Baines
A cage-like molecule typically used to sequester hard metal cations such as Ca^{2+} in solution proves capable of capturing the softer, elusive free germanium ion Ge^{2+}. *>> Perspective p. 1333*

GEOCHEMISTRY

Carbonatite Melts and Electrical Conductivity in the Asthenosphere 1363
F. Gaillard et al.
The electrical conductivity of molten carbonates is higher than that of silicate minerals; thus, minor amounts of carbonate melt could explain electrical signals of Earth's mantle.
>> Perspective p. 1338

BIOCHEMISTRY

Tight Regulation of Unstructured Proteins: From Transcript Synthesis to Protein Degradation 1365
J. Gsponer et al.
Yeast proteins with unstructured regions tend to be highly regulated, consistent with the idea that these regions may mediate critical regulatory protein-protein interactions.
>> Perspective p. 1340

BIOCHEMISTRY

Structural Evidence for Common Ancestry of the Nuclear Pore Complex and Vesicle Coats 1369
S. G. Brohawn et al.
The protein complex that controls entry and exit from the cell nucleus shares a structural element with vesicle coat proteins, suggesting that it is built around a lattice-like scaffold.

ECOLOGY

The Widespread Threat of Calcium Decline in Fresh Waters 1374
A. Jeziorski et al.
As calcium levels decline in Canadian lakes, populations of a keystone prey crustacean are being depleted, with likely consequences for freshwater food webs.

MEDICINE

Genomic Analysis of the Clonal Origins of Relapsed Acute Lymphoblastic Leukemia 1377
C. G. Mullighan et al.
The cells responsible for relapse of a particular type of leukemia are often not the same cells that gave rise to the original disease.
>> Science *Podcast*

PLANT SCIENCE

A Genetic Framework for the Control of Cell Division and Differentiation in the Root Meristem 1380
R. Dello Ioio et al.
The number of stem cells in plant roots is controlled by an auxin-cytokine feedback loop in which a particular gene integrates signals from both hormones.

1353

MOLECULAR BIOLOGY

Chromosome Alignment and Transvection Are Antagonized by Condensin II 1384
T. A. Hartl, H. F. Smith, G. Bosco
A *Drosophila* protein required for dissolution of homologous chromosome bundles independently prevents long-distance effects of one allele on the transcription of its homolog.

MOLECULAR BIOLOGY

An Epigenetic Role for Maternally Inherited piRNAs in Transposon Silencing 1387
J. Brennecke et al.
In *Drosophila*, small RNAs derived from transposons are inherited from the mother and directly inhibit activation of these potentially detrimental transposons in offspring. >> Science *Podcast*

MICROBIOLOGY

PA-824 Kills Nonreplicating *Mycobacterium tuberculosis* by Intracellular NO Release 1392
R. Singh et al.
An unusual drug candidate for resistant tuberculosis generates nitrous acid and thus acts as an intracellular nitric oxide donor, augmenting the innate immune system. *>> Perspective p. 1337*

CELL BIOLOGY

Absence of the SRC-2 Coactivator Results in a Glycogenopathy Resembling Von Gierke's Disease 1395
A. R. Chopra et al.
In mice, a coactivator binds to a nuclear orphan receptor and regulates glucose-6-phosphatase transcription and thus glucose homeostasis.

AAAS
ADVANCING SCIENCE, SERVING SOCIETY

SCIENCE (ISSN 0036-8075) is published weekly on Friday, except the last week in December, by the American Association for the Advancement of Science, 1200 New York Avenue, NW, Washington, DC 20005. Periodicals Mail postage (publication No. 484460) paid at Washington, DC, and additional mailing offices.

Domestic individual membership and subscription (51 issues): $144 ($74 allocated to subscription). Domestic institutional subscription (51 issues): $770; Foreign postage extra: Mexico, Caribbean (surface mail) $55; other countries (air assist delivery) $85. First class, airmail, student, and emeritus rates on request. Canadian rates with GST available upon request, GST #1254 88122. Publications Mail Agreement Number 1069624. SCIENCE is printed on 30 percent post-consumer recycled paper. **Printed in the U.S.A.**

Change of address: Allow 4 weeks, giving old and new addresses and 8-digit account number. **Postmaster:** Send change of address to AAAS, P.O. Box 96178, Washington, DC 20090–6178. **Single-copy sales:** $10.00 current issue, $15.00 back issue prepaid includes surface postage; bulk rates on request. **Authorization to photocopy** material for internal or personal use under circumstances not falling within the fair use provisions of the Copyright Act is granted by AAAS to libraries and other users registered with the Copyright Clearance Center (CCC) Transactional Reporting Service, provided that $20.00 per article is paid directly to CCC, 222 Rosewood Drive, Danvers, MA 01923. *Science* is indexed in the *Reader's Guide to Periodical Literature* and in several specialized indexes.

Printed on 30% post-consumer recycled paper.

CONTENTS continued >>

A migrating iceberg in the Atlantic.

SCIENCE**NOW**

www.sciencenow.org

HIGHLIGHTS FROM OUR DAILY NEWS COVERAGE

Did Icebergs Warm the World?
Errant ice might have driven ancient surges of carbon dioxide.

Scientists Untangle Woolly Mammoth Genome
New data give clues to creature's evolution and hardiness.

When a Flood Beats a Trickle
Old-fashioned irrigation saves water.

Can your career spare 15 minutes?

SCIENCE **CAREERS**

www.sciencecareers.org/career_development

FREE CAREER RESOURCES FOR SCIENTISTS

Tooling Up: 15 Minutes to a Better Interview
D. Jensen
The basic rules of interview courtesy and etiquette are worth reviewing.

Young Italian Scientists Take to the Streets
E. Pain
Italian scientists on short-term contracts protest cuts in research funding and jobs.

From the Archives: Cheating, Betrayal, Denial, and Lies
M. P. DeWhyse
As Thanksgiving approached, our Educated Woman realized that grad school was not everything she had anticipated.

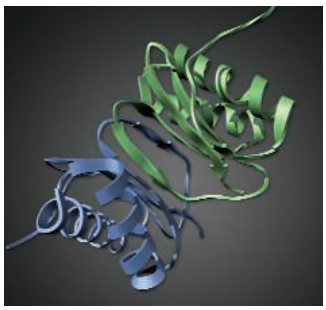

Dynein light chain dimer.

SCIENCE **SIGNALING**

www.sciencesignaling.org

THE SIGNAL TRANSDUCTION KNOWLEDGE ENVIRONMENT

EDITORIAL GUIDE: How to "Cell" a Genomic or Proteomic Screen
M. B. Yaffe
With the amount of data from screens increasing, researchers need better ways to make the information most useful.

RESEARCH ARTICLE: Identification of ROCK1 as an Upstream Activator of the JIP-3 to JNK Signaling Axis in Response to UVB Damage
P. P. Ongusaha, H. H. Qi, L. Raj, Y.-B. Kim, S. A. Aaronson, R. J. Davis, Y. Shi, J. K. Liao, S. W. Lee
The Rho-associated kinase ROCK1 mediates the cellular response to UV radiation.

RESEARCH ARTICLE: γ-Secretase Limits the Inflammatory Response Through the Processing of LRP1
K. Zurhove, C. Nakajima, J. Herz, H. H. Bock, P. May
Cleavage of the intracellular domain of the lipoprotein receptor LRP1 allows it to transcriptionally inhibit inflammatory responses.

PERSPECTIVE: An All-Purpose Tool for Axon Guidance
L. C. Schecterson and M. Bothwell
The p75 neurotrophin receptor functions as a co-receptor in three distinct systems that mediate repellant signals.

PERSPECTIVE: Dynein-Independent Functions of DYNLL1(LC8)—Redox State Sensing and Transcriptional Control
S. M. King
Stimuli that alter the dimerization state of the dynein light chain DYNLL1 influence its regulatory functions.

PODCAST
P. May and A. M. VanHook
Petra May discusses new findings about a role for LRP1 in inhibiting inflammation.

SCIENCE**PODCAST**

www.sciencemag.org/multimedia/podcast

FREE WEEKLY SHOW

Download the 28 November *Science* Podcast to hear about small RNAs and inheritance, understanding leukemic relapse, insights from Canada's experimental lakes, and more.

CREDITS: (*SCIENCE NOW*) ERIC GALBRAITH/*NATURE*; (*SCIENCE CAREERS*) COMSTOCK; (*SCIENCE SIGNALING*) CHRIS BICKEL

Separate individual or institutional subscriptions to these products may be required for full-text access.

Condensin II and Transvection >>

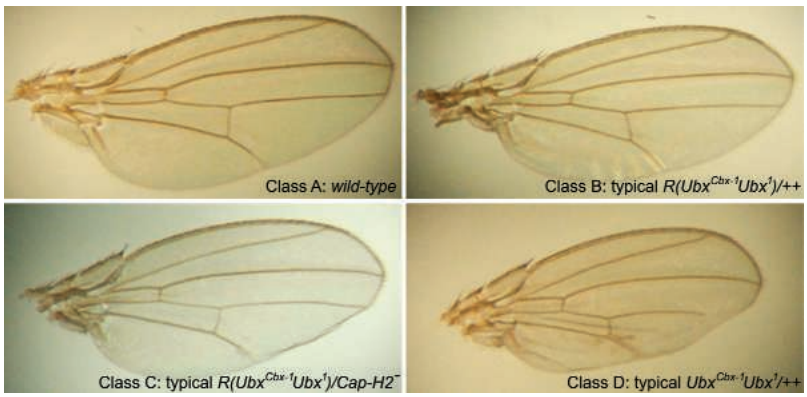

Distant regions of the genome in eukaryotic chromosomes are able to interact with each other, allowing long-range regulatory communication both in *cis*, between regions on the same chromosome, and in *trans*, between chromosomes. For example, in transvection, alleles of the same gene on chromosome homologs can cross-regulate each other. **Hartl *et al.*** (p. 1384) study the extreme case of *trans* association seen in polytene chromosomes in *Drosophila*, which each consist of many copies of an individual chromosome associated in perfect register. Condensin II subunits are involved in polytene chromosome disassembly, and these same subunits also interfere with instances of transvection in the fruit fly, suggesting that the condensin II complex may antagonize homology-dependent chromosomal interactions.

Images of Extra-Solar Planets

More than 300 planets have been found outside the solar system, most of them discovered indirectly through their influence on their parent star. Now two groups have obtained images of planets orbiting neighboring stars that resemble the Sun (see the Perspective by **Marley**, published online 13 November). **Kalas *et al.*** (p. 1345, published online 13 November; see the cover) present optical images of a planet with a mass no greater than three times that of Jupiter that orbits the star Fomalhaut 25 light-years from Earth. **Marois *et al.*** (p. 1348, published online 13 November; see the cover) present near-infrared images of three giant planets orbiting a star 128 light-years from Earth. This planetary system is reminiscent of the outer part of our solar system.

Dynamic Instability Revisited

Microtubules are intracellular polymers of the protein tubulin essential for the intracellular organization, polarization, and cell division of every eukaryotic cell. Microtubules display "dynamic instability"—alternating between tubulin polymerization and depolymerization phases separated by catastrophe and rescue events. The textbook model to explain this behavior proposes a small protective GTP-bound conformational cap at the microtubule's polymerizing extremity, the loss of which could be responsible for catastrophe transitions. However, this model does not propose any mechanistic basis for the observed rescue transitions and has not been validated in vivo. **Dimitrov *et al.*** (p. 1353, published online 16 October) generated a conformational antibody that specifically recognizes tubulin in a GTP-bound conformation and confirmed the presence of a GTP cap at the extremity of cellular microtubules. In addition, unexpected GTP-tubulin remnants inside the polymer were revealed, which may be responsible for the observed rescue events.

CREDITS (TOP TO BOTTOM): HARTL *ET AL.*; RUPAR *ET AL.*

Cation Capture

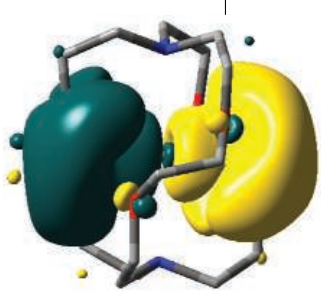

Crown ethers and cryptands—cagelike molecules in which several oxygen and/or nitrogen atoms create an inner environment hospitable to charged guests—can sequester hard metal cations, such as Mg^{2+} and Ca^{2+}, in solution. **Rupar *et al.*** (p. 1360; see the Perspective by **Lambert**) now show that a cryptand can also encapsulate a free germanium dication. This more polarizable element, sometimes termed a metalloid-like boron and silicon, has previously required tightly bound ligands to stabilize a +2 oxidation state. Examination of the cryptand-bound ion using x-ray crystallography suggests that a range of soft cations could similarly be isolated in solution environments.

"Nothing" Affects Electronic Circuits

A vacuum is not empty, but is a seething sea of virtual particles being constantly created and annihilated. When a quantum system is coupled to a vacuum, you would expect the vacuum to have an affect on your system. For atomic systems, like hydrogen, this coupling manifests itself as a small shift, the Lamb shift, in the energy levels of the hydrogen atom. Now, **Fragner *et al.*** (p. 1357) demonstrate such a Lamb shift for a more complex, many-body solid-state system—an electrical circuit. When a superconducting two-level quantum system (qubit) was placed in a cavity, a shift in energy-level transitions of the qubit were observed consistent with those predicted from theory, which may prove important in designing future quantum electronic devices.

Melt in Mantle

Some regions of Earth's mantle and deep crust have anomalously high electrical conductivities, which have usually been interpreted as indicating the presence of partial melt of mantle silicate minerals, distributed water, or high proportions of graphite. **Gaillard *et al.*** (p. 1363; see the Perspective by **Evans**) now show that the electrical conductivity of molten carbonate minerals is extremely high—orders of magnitude more than that of silicate phases. Thus, the previous anomalous observations could indicate small amounts of carbonate melt in the mantle.

Coating the Nuclear Pore

The Nuclear Pore Complex (NPC) is a 40- to 60-megadalton protein assembly that facilitates the exchange of macromolecules across the nuclear envelope. Low-resolution views of the structure and computer modeling have given general

Continued on page 1301

Published by AAAS

Continued from page 1299

insight into its organization. **Brohawn *et al.*** (p. 1369, published online 30 October) now add to the picture by providing a crystal structure of Nup85•Seh1, a module in the Nup84 complex that probably comprises the two peripheral rings of the NPC. Nup85, along with several other nucleoporins, has structural similarity to intracellular vesicle coat proteins. This similarity and mutagenesis experiments were used to define the organization of the Nup84 complex and to suggest that the NPC structural scaffold is a lattice-like coat.

Acid Baths

Ocean acidification contributes to the erosion of calcium-based biosynthetic structures like coral reefs, but we have little evidence of the effects of acidification on highly calcium-dependent organisms in fresh waters. **Jeziorski *et al.*** (p. 1374) examined the sediment records of calcium-reinforced freshwater crustaceans living in the soft-water (low pH) lakes of the Canadian Shield. During the 1970s these lakes suffered particularly from industrial acid rain. Even though the pH of many of these lakes has recovered, populations of small daphniid crustaceans have become depleted as water calcium levels continue to decline. Daphniids are keystone prey species, thus their loss predicts consequences to freshwater food webs in eastern Canada and, for similar reasons, probably also in many other parts of the Northern Hemisphere.

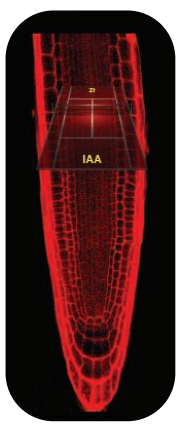

The Yin Yang of Root Regulation

The root meristem is a group of stem cells at the root tip that give rise to differentiated root tissues. The root meristem exists as a balance between new cells added by proliferation, and daughter cells removed by differentiation. The plant hormone, auxin, seems to oversee meristem cell proliferation, while the plant hormone, cytokinin, oversees differentiation. Using *Arabidopsis* plants, mutants, and expression and chromatin analysis, **Dello Ioio *et al.*** (p. 1380) find that signaling pathways from the two hormones converge on the *SHY2* gene. Cytokinin activates the *SHY2* gene, the effects of which cascade toward redistributing auxin. Auxin, on the other hand, directs degradation of the *SHY2* protein, thus stabilizing auxin distribution.

Hybrid Dysgenesis

In *Drosophila melanogaster* crosses between a strain of flies with, and a strain of flies without, a specific type of transposon in their genomes can result in infertility in the progeny—a phenomenon known as hybrid dysgenesis. However, hybrid dysgenesis is only seen in the crosses between transposon-bearing males and transposon-free females, and not the reverse cross (whose progeny are fertile), suggesting that a "protective" cytoplasmic factor is inherited through the maternal germ line. The control of mobile elements in germ cells is mediated in large part by Piwi-interacting (pi) RNAs, produced from the transposons themselves. **Brennecke *et al.*** (p. 1387) now show that piRNAs are the cytoplasmic factor in *P*- or *I*-element transposon mediated hybrid dysgenesis, transmitted through the female's egg and providing protection against transposon activation in the germ line of the newly introduced transposon. Thus, piRNAs can act directly to convey epigenetic information to progeny.

TB Prodrug Chemistry

Drug-resistant tuberculosis (TB) has emerged as a major threat to global health with few new candidates emerging to replace the rapidly dwindling array of existing agents. Among those offering promise are the bicyclic nitroimidazoles that include two candidate molecules (PA-824 and OPC-67683) currently in human clinical trials. **Singh *et al.*** (p. 1392; see the Perspective by **Nathan**) recreated the cellular machinery that metabolizes these drugs. The structure of the resulting metabolites suggested that, unlike normal biological reduction of aromatic nitro compounds, the deazaflavin-dependent nitroreductase, Fnr, reduced the imidazole ring, not the nitro group, and that the resulting reduced nitroimidazole eliminated nitrous acid as a result. Nitrous acid was detected both in vitro in the enzymatic reaction, as well as in vivo inside the bacterial cell. In addition, among a series of derivatives with very different anaerobic killing effects on *Mycobacterium tuberculosis* (the causative agent of TB), the extent of killing was directly related to the extent of release of nitrous acid. Thus, this class of compounds appears to kill anaerobic cells by acting as intracellular nitric oxide donors.

CREDIT: RICCARDO DI MAMBRO

Published by AAAS

Leonard Rubenstein is president of Physicians for Human Rights and a Randolph Jennings Senior Fellow at the United States Institute of Peace.

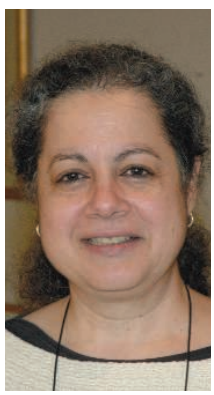

Mona Younis is director of the Science and Human Rights Program of the American Association for the Advancement of Science.

Scientists and Human Rights

ON 10 DECEMBER 1948, THE WORLD'S GOVERNMENTS MADE HISTORY WHEN THEY ADOPTED the Universal Declaration of Human Rights and agreed to ensure its "universal and effective recognition and observance." Over the course of six decades, this declaration has generated both tremendous hope and a substantial body of law obliging governments to respect, protect, and fulfill the rights inherent to all human beings. Though reaffirmed at every turn, one lesson of the past 60 years is that governments' commitment to human rights is only as strong as the demands of their citizens. As respected members of society, scientists are vital to securing governments' adherence to human rights.

Scientists have contributed valuably in making human rights a reality for all. They have defended the freedom to engage in scientific inquiry and to report their findings without interference. They have applied their knowledge and skills to reveal truths about human rights violations and have come to the aid of colleagues under attack. Notable scientific contributions to human rights include the forensic exhumation of mass graves in Argentina, the Balkans, and Rwanda that revealed evidence of war crimes and crimes against humanity; the use of DNA evidence to identify victims of mass killings in Bosnia and free wrongfully convicted prisoners in the United States; the introduction of information management techniques to illuminate large-scale human rights violations, from attacks on civilians in Kosovo to neglect of HIV/AIDS in South Africa; and, more recently, the use of satellite imagery to document the destruction of communities in remote locations around the world. Each of these cases reveals what is possible when scientists treat human rights as an area suitable for and deserving of robust scientific inquiry.

Much more could be done. In 2000, addressing the International Association for Official Statistics, Mary Robinson, then United Nations High Commissioner for Human Rights, urged that to end human suffering and achieve human rights, "What are needed are solid methodologies, careful techniques, and effective mechanisms to get the job done." Getting the job done requires engagement from science and scientists.

A good starting point is for scientists to better understand human rights, not as some vague set of aspirations, but as specific obligations of government. These obligations include the social and economic rights essential to human well-being, such as the rights to health, food, a clean environment, and as the Universal Declaration of Human Rights states, "share in scientific advancement and its benefits." Indeed, just as governments are required to respect the rights to freedom of expression and a fair trial, so too are they obligated to uphold the right to the benefits of scientific progress. Scientists have a unique and vital role in giving visibility to this neglected right, which elevates fundamental scientific values, such as equitable access to scientific knowledge, scientific freedom, and international cooperation, to universal government obligations.

Perhaps the greatest challenge is for the scientific community to become a constituency for human rights. Many scientists eschew such involvement as too "political," and thus in conflict with scientific traditions of impartiality and independent inquiry. But these and other traditions, such as rigorous analysis and peer review, are both compatible with and essential to the realization of human rights. Indeed, their contributions to human rights are limitless so long as they are applied with scientific integrity and an awareness of the boundaries of science and policy.

On the occasion of the 60th anniversary of the Universal Declaration of Human Rights, it is therefore fitting for scientists to commit to joining the global effort to realize human rights, both at home and abroad. As history and recent events have shown, we cannot take human rights for granted—to do so invites transgressions. We urge the scientific community to add its expertise and voice to global efforts to ensure that all governments respect, protect, and fulfill that which is fundamental to human life—human rights.

– Leonard Rubenstein and Mona Younis

10.1126/science.1166691

Published by AAAS

BIOCHEMISTRY

Iron Tug of War

Iron is an essential component of many enzymes, and microbes synthesize and secrete siderophores—small molecules that bind avidly to free iron in soils and in oceans—for the purpose of sequestering as much of it as they can. Many of these siderophores contain 2,3-dihydroxybenzoic acid (2,3-DHBA) as an iron-chelating moiety; not coincidentally, the mammalian innate immunity protein siderocalin defends against pathogens by enveloping 2,3-DHBA siderophores and thus blocking bacterial iron acquisition. The anthrax bacterium makes petrobactin, a siderophore that uses the less common 3,4-DHBA as its iron chelator, which enables it to evade the clutches of siderocalin.

Using biochemical and structural analyses, Pfleger *et al*. show that the *Bacillus anthracis* protein AsbF catalyzes the conversion of 3-dehydroshikimate (3-DHS) into 3,4-DHBA via a manganese-dependent formation of an enolate intermediate, followed by elimination of the C5 hydroxyl. Why does this matter? These authors show that deleting *asbF* from an otherwise deadly strain of *B. anthracis* abolishes virulence in a mouse model of inhalation anthrax. Petrobactin is produced by other pathogenic *Bacillus* species, and Fox *et al*. demonstrate that AsbF from a *B. thuringiensis* strain also dehydrates 3-DHS. — GJC

Proc. Natl. Acad. Sci. U.S.A. **105**, 17133 (2008); *Biochemistry* **47**, 10.1021/bi801876q (2008).

APPLIED PHYSICS

Structured Lasers Hit the Spot

Compact semiconductor lasers find a host of applications from optical information storage media to chemical sensors. The robust quantum cavity laser, which operates at room temperature with tunable wavelength, is the workhorse. The window from which the light is emitted can be on the order of just a few micrometers. However, this small size generally results in poor collimation; the beam fans out, which is detrimental to the areal reading capacity and requires the laser to be driven harder for sensing applications. Yu *et al.* have used a structure of concentric rings patterned into a metal layer deposited on the output facet of the laser to produce a plasmonic collimator that helps guide the output light. They find that the collimation of the output light beam can be improved by up to a factor of 30 while still retaining good output power as compared to unpatterned lasers. The improved collimation would also facilitate the coupling of light into optic waveguides and fibers for communication and possible optical computation applications. — ISO

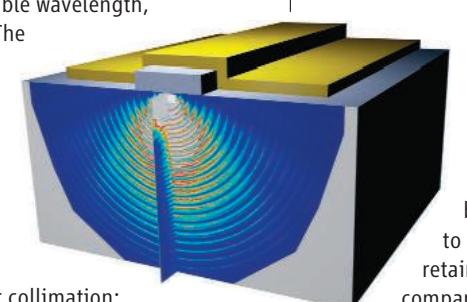

Appl. Phys. Lett. **93**, 181101 (2008).

EVOLUTION

Old-Fashioned Carbon Fixing

The grass family has evolved several innovations that have made it one of the most widespread and speciose plant families. One of these innovations has been the origin of the C_4 photosynthetic pathway, which fixes carbon to form carbohydrates at relatively high temperatures and relatively low CO_2 (in comparison to the older C_3 pathway) and which is believed to have arisen independently several times within the grass lineage.

Vicentini *et al.* have created a well-supported phylogenetic tree of the grasses and concluded that the C_4 pathway originated after a major radiation in the grasses that split the family into two large groups. They calibrated their tree with six fossils and determined that the common ancestor of the grasses appeared approximately 94 million years ago (Ma) in the upper Cretaceous and that C_4 photosynthesis originated approximately 32 Ma in the Oligocene during a period when atmospheric CO_2 levels declined. Furthermore, the authors note that parallel incidents of C_4 evolution and reversion to C_3 pathways were clustered at times that may be related to changes in global environmental conditions and that correlated with changes in global CO_2 levels. — LMZ

Global Change Biol. **14**, 10.1111/j.1365-2486.2008.01688.x (2008).

CHEMISTRY

Reacting to the HIPE

Emulsions, such as salad dressing, consist of two immiscible liquids that are blended together to form droplets of one liquid suspended in the other. Emulsifiers and stabilizers can be added to prevent the droplets from coalescing, and when the dispersed phase occupies more than 74% of the volume, the mixture is known as a high internal phase emulsion (HIPE). Gitli and Silverstein prepared HIPEs with styrene or 2-ethylhexyl acrylate monomer in the oil phase and acrylamide monomer in the aqueous phase. The monomers were polymerized and cross-

linked to form an interpenetrating porous network, with a structure similar to an open-cell foam. The presence of the acrylamide was found to alter the molecular structure of the hydrophobic polymer. Initiation of the polymerization reactions could be triggered in either the oil or water phases, or at the interphase region, and had a direct impact on the structure and properties of the polymers. For all compositions, it was possible to reversibly swell and dry the polyacrylamide component, and the authors envision that these polymers could be used in biomedical and separation applications. — MSL

Soft Matter **4**, 2475 (2008).

IMMUNOLOGY

Uric Acid Lends a Hand

Antigen-presenting cells (APCs) recognize foreign molecules—for instance, the lipopolysaccharides produced by microbial invaders—that bind to cell surface receptors, which mobilize intracellular signal transduction pathways and initiate an anti-microbial response. APCs can also be activated by environmental factors such as the uric acid crystals that are associated with gout. Whether these sorts of particulate materials engage APCs by a similar receptor-based mechanism has been unclear.

Composite image of an AFM tip (orange) holding uric acid above an APC (green).

Using atomic force microscopy (AFM), Ng *et al*. found that uric acid crystals could bind strongly (100 nN) to cellular membranes via electrostatic interactions. This caused rearrangements of cholesterol-rich lipid rafts within the plasma membrane and stimulated intracellular signaling cascades. These results indicate that, in addition to the classical receptor-ligand pairings, direct cell surface contact by particulate materials can turn on APCs. This approach furthers our understanding of how cells of the immune system can be activated and may reveal the basis of how the adjuvant alum works. — HP*

Immunity **29**, 807 (2008).

*Helen Pickersgill is a locum editor in *Science*'s editorial department.

CREDIT: NG *ET AL.*, *IMMUNITY* **29**, 807 (2008)

CHEMISTRY

Running Off Together

Surface diffusion of large organic molecules on atomically flat metal surfaces can exhibit direction anisotropy. Eichberger *et al.* show how this process can be further influenced by the interactions that result between the molecules during collisions. They used fast scanning tunneling microscopy to study the diffusion of tetrapyridylporphyrin on a Cu(111) surface between 300 and 360 K, which occurs via one-dimensional random walks. They observed an unusual increase in the jump length of dimers formed when the molecules collide with the pyridyl groups aligned parallel to one another, and an increase of more than two orders of magnitude in the diffusion rate. They suggest that the dimers form through coordination to a thermally generated copper atom from the surface; the bonding of the pyridyl group in this manner would weaken the interaction of the subunits with the surface relative to the free monomers. — PDS

Nano Lett. **8**, 10.1021/nl802995u (2008).

BIOMEDICINE

Oncogenic Fusion Disguise

Human solid tumors typically display a vast array of genetic alterations, many of which are likely to be secondary events in tumor development rather than the primary drivers of tumor growth. One goal of cancer genomics research is to identify the alterations that cause tumorigenesis and occur at high frequency in a given tumor type, as these alterations are likely to be the most informative ones with respect to the biology of the tumor as well as being the most useful ones for diagnosis and therapy. This principle is illustrated most famously by the oncogenic fusion of the *BCR* and *ABL* genes in chronic myelogenous leukemia, the discovery of which ultimately led to successful therapy. To date, however, oncogenic fusion genes have been detected only at low frequency in solid tumors that are common in the general population. Jones *et al*. suggest that this may be a problem of detection. In a study of pilocytic astrocytomas (a common low-grade brain tumor in children), they found that 29 of 44 tumors harbored a genetic alteration that fused the *BRAF* oncogene with an uncharacterized gene called *KIAA1549*. The fusion gene, which was not found in other types of brain tumors, produces a protein with constitutively active BRAF kinase activity and confers tumorigenic potential on NIH-3T3 cells. This gene rearrangement was initially detected as a tandem duplication at 7q34, raising the possibility that similar duplications seen elsewhere in the cancer genome may likewise mark the sites of bona fide oncogenic fusion genes. — PAK

Cancer Res. **68**, 8673 (2008).

Boys Take Energy

A study of 18th and 19th century Finnish farmers and fishermen provides new evidence that nature finds it more costly to produce the male mammal.

Some studies have suggested that having sons takes more out of a mother, as shown, for example, by lower birth weight in succeeding offspring. Now a multigenerational analysis by researchers at the University of Sheffield in the U.K. indicates that being next in line to a brother reduces one's reproductive success.

Evolutionary ecologist Ian Rickard and colleagues, using data from population registers of Lutheran churches, tracked the births of children and grandchildren of 653 women born between 1709 and 1815. They found 1653 surviving children born after their mothers had produced a son. These people were significantly less likely to have offspring—62%, versus 67% for those born after a sister—the researchers report this week in the *Journal of Evolution and Human Behavior*.

Ray Blanchard, a psychologist at the Clark Institute of Psychiatry in Toronto, Canada, says the study supplies new evidence that "older brothers, more than older sisters, influence certain traits in later-born siblings, and these effects are biological in nature." But what those effects are is unclear. Blanchard has found that men with older brothers are more likely to be homosexual—a trait he thinks could be related to a maternal immune response to the Y chromosome. The Sheffield researchers, however, believe the older-brother effect applies to both sexes and has something to do with "a higher physiological cost of producing sons."

Name That Rover

Snoopy? Transcendence? Grawp? U.S. students aged 5 to 18 are invited to try naming the next Mars rover, to be launched next year, in a contest sponsored by NASA together with WALL-E, a Walt Disney movie robot.

The last two rovers were named Spirit and Opportunity. The next, a six-wheeled car-sized vehicle, will have multiple chores roving over, reaching for, lasering, photographing, hammering, sniffing, cooking, and analyzing rock. Students have to accompany their suggestion with an essay explaining why it's an apt choice. The deadline is 25 January 2009, with the winner to be announced next April. For more information, go to marsrovername.jpl.nasa.gov.

This Is Your Brain Online

Elsevier is going to dump all its brain atlases onto the Internet. The science publisher has gotten together with the Allen Institute for Brain Science in Seattle, Washington, to create an online version of its extensive neuroanatomy tomes.

Called the BrainNavigator, the program will ultimately feature 3D images of more than 700 models of rat, mouse, monkey, and human brain sections. Researchers can view specific slices in 3D, micrograph, and 2D mapped images. They will also be able to upload and share their own experimental results.

Program developers solicited feedback from researchers at a rollout event at the International Spy Museum in Washington, D.C., last week during the 2008 meeting of the Society for Neuroscience. The project, to launch early next year, will take such atlases "to the next level," eclipsing other efforts in its scope and breadth, says Mike Hawrylycz of the Allen Institute. "It's a nice prototype," says Pavan Ramdya, a graduate student at Harvard University who attended the meeting. "It's not quite the Human Genome Project, but it'll get there," he says, given rapid advances in the exploding field of neuroscience.

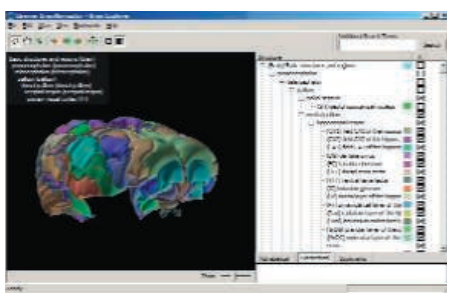

THE MANLY WORLD OF EUROPEAN SCIENCE

The United Kingdom is the big winner—and women the major losers—in the first round of grants for established ("advanced") researchers awarded by the European Research Council (ERC).

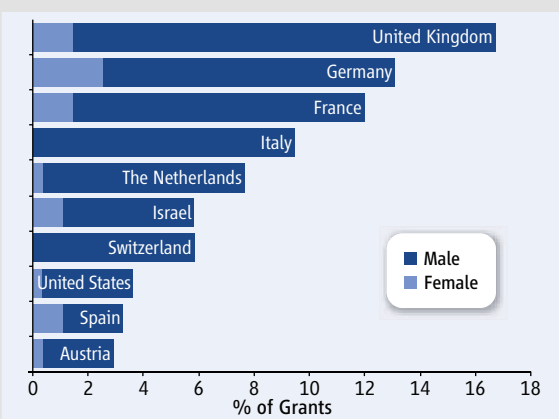

The results, released earlier this month, show that researchers from the U.K. will get more than 16% of the 275 grants, which are worth up to €3.5 million each. The top 10 nationalities are shown at left. (Some will do research in other European countries.)

Women, who made up 14% of the applicants, will get only 12% of the grants. "That was very disappointing to all of us," says ERC Vice-President Helga Nowotny, although she notes it reflects the low number of female full professors in Europe. ERC is considering remedies, Nowotny says, such as asking review panels to give candidates with unconventional career tracks special consideration and encouraging women to apply. Yet she says the agency is determined to retain excellence as the sole criterion for grants: "We cannot and will not undertake affirmative action."

CREDITS (TOP TO BOTTOM): NATIONAL GEOGRAPHIC/GETTY IMAGES; ELSEVIER; SOURCE: ERC

Two Cultures

GO WITH THE FLOW. Dance produces many good things, but good data? That's what David Kirsh, a cognitive scientist at the University of California, San Diego (UCSD), hopes to capture from British dancer and choreographer Wayne McGregor (below). Starting 26 January 2009, the Olivier Award–winner will spend 3 weeks at UCSD developing a new dance, called "Entity," under the intense scrutiny of Kirsh's research team.

The mental and social processes involved with choreography are mysterious, says Kirsh, who describes it as "using the body as a thing to think with." His plan is to use high-definition cameras and a tiny camera on McGregor's head to capture every instruction that McGregor gives to his dancers and every movement they make, from the first brainstorming session in the dance studio to the final performance. Kirsh hopes to understand the dialogue between body movement and cognition and get a better handle on the creative process. McGregor says his aim is to find a "new choreographic form with possibilities drawn from science but applied in dance."

THEY SAID IT

"I've got some in my fridge.
It tastes fine to me."

—NASA engineer Bob Bagdigian, on water derived from urine using a new wastewater recycling system that will be installed on the International Space Station (ISS) as part of a mission to renovate its living quarters. The device, developed under Bagdigian's charge, was part of the cargo transported to the ISS by seven astronauts aboard the shuttle, Endeavor, last week.

ON CAMPUS

TRAGIC RECORD. More than 6000 pages of documents related to the 16 April 2007 massacre at Virginia Polytechnic Institute and State University in Blacksburg are now available online, thanks to an effort led by computer engineering student Justin Harrison.

Now a senior, Harrison knew some of the victims killed by Seung-Hui Cho (*Science*, 27 April 2007, p. 525). The Prevail Archive (www.prevailarchive.org/archive/) was culled from the boxes of e-mails, police reports, and handwritten materials that the university released to the *Richmond Times-Dispatch*. Harrison and nine others spent 2 days scanning the documents.

Harrison says they wanted to understand how administrators reacted as the tragedy unfolded. He doesn't believe the events of that day could have been prevented, he says, "but there were so many red flags [about Cho], it's clear something more should have been done."

Got a tip for this page? E-mail people@aaas.org

IN BRIEF

Wilfrid Rall, who pioneered the application of computation modeling to neuroscience more than 5 decades ago, was awarded the inaugural $25,000 Swartz Prize for Theoretical and Computational Neuroscience at the Society for Neuroscience meeting last week. Rall, who had a background in physics before he went into neuroscience, showed in the 1950s that simulations could be used to analyze the properties and behaviors of neurons. The work laid the foundations of computational neuroscience. The prize is sponsored by the Swartz Foundation.

CELEBRITIES >>

REFORM PLATFORM. "I haven't had the chance to tell if I feel tired or not," says Toshihide Maskawa of Kyoto Sangyo University in Japan, explaining his hectic schedule since the announcement on 7 October that he had won the Nobel Prize in physics. One new responsibility is advising Japan's Ministry of Education on how to strengthen basic research and foster scientific creativity.

The panel of advisers, which includes his co-laureate Makoto Kobayashi of the High Energy Accelerator Research Organization in Tsukuba, physics laureates Leo Esaki (1973) and Masatoshi Koshiba (2002), chemistry laureates Ryoji Noyori (2001) and Koichi Tanaka (2002), and medicine laureate Susumu Tonegawa (1987), met for the first time on 7 November. One of their first pearls of wisdom, according to Shigekazu Matsuura, an official in the ministry's Research Promotion Bureau, was that "some [Japanese] professors really hope not to be upstaged by their students' accomplishments, even though this is shirking their responsibilities."

The group will meet at least once more before offering formal advice to the ministry.

(L to R): Esaki, Koshiba, Kobayashi, Tanaka, Tonegawa, Noyori, and Maskawa.

CREDITS (TOP TO BOTTOM): ROYAL OPERA HOUSE; 2008 MAINICHI NEWSPAPER CO., LTD.

Reforming French science
1312

Science in Hollywood
1315

Too late. Officials dump baby formula after finding contamination with an industrial compound.

TAINTED MILK SCANDAL

Chinese Probe Unmasks High-Tech Adulteration With Melamine

BEIJING—A weeks-long investigation into China's tainted milk scandal has left scientists astonished by the technical sophistication of those who used melamine to adulterate food products. Chinese investigators, meanwhile, are puzzling over the precise mechanisms of exposure and toxicity in infants who developed kidney damage.

At a closed workshop with U.S. experts here last week, Chinese scientists presented early results of an ongoing probe into the mass poisoning that left at least four infants dead and sickened more than 53,000 others after they drank baby formula tainted with melamine, an industrial chemical used primarily as a plastics stabilizer and fire retardant. The workshop capped a busy week in which the Chinese government trotted out measures to improve food safety, and the U.S. Food and Drug Administration (FDA) opened its first offices in China. "After melamine, there will be more transparency, more openness," says Chen Junshi, co-chair of the Sino-U.S. workshop and a risk-assessment specialist at China's Center for Disease Control and Prevention here. U.S. officials are speaking in more sweeping terms about the impact on $2 trillion worth of imports a year: "This is nothing short of a redesign of food and drug safety to meet a 21st century challenge," says U.S. Health and Human Services Secretary Michael Leavitt.

The melamine scandal came to light last September, when the central government learned that scores of infants in Gansu Province had been hospitalized with kidney stones, evidently after being fed infant formula with high levels of melamine. In the weeks that followed, powdered formula, fresh milk, and other products from some two dozen companies were found to contain melamine. Police have detained more than 30 people suspected of adulterating milk, including the general manager of one of China's largest powdered milk makers, Sanlu, based in Shijiazhuang. In an interview with *Science* last month, Premier Wen Jiabao expressed sorrow for the poisoning and vowed an aggressive response (*Science*, 17 October, p. 362).

Researchers say the adulteration was nothing short of a wholesale re-engineering of milk. Weeks ago, investigators established that workers at Sanlu and at a number of milk-collection depots were diluting milk with water; they added melamine to dupe a test for determining crude protein content. "Adulteration used to be simple. What they did was very high-tech," says Chen. Researchers have since learned that the emulsifier used to suspend melamine—a compound that resists going into solution—also boosted apparent milk-fat content.

Sanlu baby formula contained a whopping 2563 mg/kg of melamine, adding 1% of apparent crude protein content to the formula, says Jerry Brunetti, managing director of Agri-Dynamics in Easton, Pennsylvania. Milk, he notes, is only 3.0% to 3.4% protein. Chen says a dean of a school of food science told him that it would take a university team 3 months to develop this kind of concoction.

Investigators have concluded that as-yet-unidentified individuals cooked up a protocol for a premix, a solution designed to fortify foods with vitamins or other nutrients. In this case, it was deadly. Several milk-collecting companies were using the same premix, Chen says: "So someone with technical skill had to be training them."

So far, Chinese scientists have fingered only melamine as the toxic agent. Published studies on cats and rats indicate that melamine reacts with an accomplice—cyanuric acid—to form melamine cyanurate crystals found in kidney stones. Both melamine and cyanuric acid were present in wheat gluten imported from China during the North American pet-food recall last year; the mixture killed dozens of cats and sickened thousands of other pets.

In the tainted milk products, however, Chinese researchers have found only trace amounts of cyanuric acid—parts per billion, or roughly 1% of the amount of melamine in the samples, says Chen. "Our scientists concluded that melamine by itself caused the kidney stones. But one unresolved issue is how high the melamine levels have to be for

CREDIT: REUTERS/LANDOV

Published by AAAS

Polluting for science 1316

Stalking supernovae 1320

this to happen." Some experts are skeptical. George Daston, a toxicologist with Procter & Gamble Co. in Cincinnati, Ohio, who with colleagues published a study in *Toxicological Sciences* online on 9 August, doubts that "melamine alone caused the kidney stones." He says that "melamine and cyanuric acid are so tightly associated with each other, it can be difficult to extract the compounds from the contaminated products." U.S. chemists "found melamine but not cyanuric acid in their initial attempts to identify the contaminant" in pet food, says Daston; subsequent analyses, he says, uncovered significant amounts of cyanuric acid. To settle questions about the new melamine cases, Chen says, "we need more data." The World Health Organization will hold an expert consultation on these issues in Ottawa next week.

Many other strands of the tragedy have yet to be unraveled. Although it's evident that adulteration was to blame for baby formulas with high melamine levels, it's unclear whether very low levels of melamine contamination—the lowest tested level was 0.09 ppm—might have come from nonprotein nitrogen (NPN) additives in ruminant feeds or from plastic packaging. NPN additives such as biuret and urea are used in cattle feed in many countries, including the United States. The Chinese government supported research in the 1990s on NPN feed additives and has encouraged their use. Since then, a cottage industry has sprung up selling *dan bai jing* (protein essence), whose specific ingredients are unknown, for use in livestock feeds.

China has heightened its vigilance, and the odds of melamine slipping through the safety net again are vanishingly low. But the problem of adulterated livestock feeds may be harder to resolve. After FDA traced last year's poisoned pet food to gluten from China tainted with melamine scrap—melamine, cyanuric acid, and related compounds—China's agriculture ministry issued a standard for determining levels of melamine in feeds and banned the use of this and other harmful compounds in June 2007. The ban appears to have had little effect. Authorities in Hong Kong recently uncovered melamine in eggs and in fish feed.

The measures announced last week should help keep attention focused on the contamination problem. The National People's Congress is expected to pass a new food-safety law next month that would establish a food-hazard monitoring system and a risk-assessment committee under the health ministry. Meanwhile, the governing State Council ordered the ministry last month to sort out confusing food standards. For instance, soy sauce, depending on how it's made and used, is subject to four standards. One unresolved problem is segmentation of food control and inspection, with one agency overseeing farms, another one responsible for food manufacturers, and so on up to the dinner table. "Scientifically, this is a terrible system," says Chen.

Last week, FDA opened three offices in China—in Beijing, Guangzhou, and Shanghai—whose eight inspectors and technical experts will team up with Chinese experts to monitor traffic in food products. It plans to open two offices in India next month and two in Latin America in January. China's State Food and Drug Administration also plans to open U.S. offices to share technical expertise and work more closely on policing imports. The global network "will require new science for detection and investigation of contamination," says FDA Commissioner Andrew von Eschenbach.

But the challenges facing China are immense. The country has 200 million farming households and more than 500,000 food manufacturers, many of which employ fewer than 10 people, says Chen. "Most companies don't care about their reputation," he says, and can dissolve and reconstitute elsewhere. "Food adulteration is inevitable and will be with us for many years."

Chen expects food and feed adulterators to raise their game. "The sophistication of the techniques will improve the next time," he says. Li Shaomin, a management professor at Old Dominion University in Norfolk, Virginia, who studies the business environment in China, agrees. "When millions of people experiment with new ways to make money without moral self-constraint, the chance of new products that can evade existing testing methods is pretty high," he says. "Unless the people who put melamine into milk lose sleep, the product-safety problem in China will go on."

–HAO XIN AND RICHARD STONE

Brave new world. HHS Secretary Michael Leavitt and FDA chief Andrew von Eschenbach, with Chinese officials in Beijing, open the first of several FDA overseas offices to monitor imports.

CREDIT: ELIZABETH DALZIEL/AP PHOTO

Published by AAAS

FRANCE

Will French Science Swallow Zerhouni's Strong Medicine?

PARIS—Dull moments have become rare in French science and higher education. Since President Nicolas Sarkozy took office 18 months ago, heavily contested reforms have come at a frenetic pace. Still, most were child's play compared with what a high-wattage international committee prescribed in a surprisingly blunt report released on 13 November. The panel, led by former U.S. National Institutes of Health (NIH) director Elias Zerhouni, proposes a massive overhaul of French life sciences research that would create a single, strong funding agency and likely spell the death of several existing institutes.

The government has welcomed the report (tinyurl.com/inserm) as an endorsement of its own reformist program. Speaking at the 120th anniversary of the Pasteur Institute 2 weeks ago, research minister Valérie Pécresse promised Zerhouni—who grew up in Algeria and is fluent in French—that the proposals would "not remain a dead letter." But trade unions are up in arms, and Sauvons la Recherche, a left-wing researchers' movement that has fought the recent changes every step of the way, says it read the report with "astonishment" and "alarm."

The panel—which included U.S. Nobelists Harold Varmus and Peter Agre, as well as top researchers and science administrators from Switzerland, the United Kingdom, Canada, and France—had been asked to review the performance of France's National Institute for Health and Medical Research (INSERM). But it took the liberty of making a diagnosis—and prescribing a remedy—for the country's entire biological and medical research sector.

That sector is "strikingly" fragmented, the panel says: In addition to INSERM's €650 million effort, there are life science programs at the National Center for Scientific Research (CNRS), the Atomic Energy Commission, the National Cancer Institute, and at least four others. That leads to "unnecessary bureaucratic turf battles" and scientists spending "an inordinate amount of time" chasing funds, says the panel, which also criticizes INSERM's byzantine and unwieldy governance structure.

INSERM doesn't have its own institutes or campuses; most of its researchers are in so-called mixed units based at, and co-administered by, universities or other host institutes. That creates even more paperwork and "diffuses responsibility and authority," the report says. As to INSERM's scientific output, some of it excels, but the "large bulk … is published in lower-tier journals." ("Our job was to be very candid," Zerhouni says.)

Under protest. Sauvons la Recherche, which recently called on scientists to boycott the review process at two science agencies, will also fight "with all appropriate means" reforms proposed by a panel chaired by Elias Zerhouni.

What's needed, the group concludes, is bold action. That includes setting up a strong, unified agency to fund all of the life sciences—presumably a new version of INSERM. If that agency also conducts research itself, those labs should be clearly set apart, as is the case with NIH's intramural labs, Zerhouni says. The mixed units should be abolished and, in most cases, be absorbed by the university they're physically based at; INSERM could simply send them grant money. To manage science well, the universities should have more flexibility, autonomy, and strategic direction, the report says.

A lot of that jibes neatly with what the government is already trying to do, a spokesperson for Pécresse says. A law passed last year gives universities the option of cutting themselves loose from state control, and so far, 20 of them have done so. Last month, Pécresse also announced a package of measures—including financial bonuses—to make science careers more attractive, another urgent priority listed by the review panel.

The central idea of consolidating the life sciences has been gaining currency for some time in France, says neurobiologist Alain Prochiantz of the École Normale Supérieure in Paris, who co-authored a petition in favor of a single institute earlier this year. A group currently studying the problem at the ministry's request is expected to deliver a report soon that insiders believe will include a proposal for a new umbrella directorate to coordinate INSERM and the life sciences within CNRS.

But Zerhouni warns that would be "a cop-out" that could actually add a layer of unneeded complexity. "They really need to cut bureaucracy drastically," he says. Still, says biologist Jules Hoffmann, president of the French Academy of Sciences, the directorate could be an intermediate structure that would "ideally, one day, melt everything together."

Radically altering INSERM would put the French government on a collision course with the unions, warns Françoise Cavaillé, an INSERM developmental biologist who's active in SNCS, a researchers' union. National institutes such as INSERM play an indispensable role as operators of research, she says. "We don't feel like falling into the Anglo-Saxon model" in which universities compete for project-based funding.

Anger among the unions against the government was already on the rise. Sauvons la Recherche recently called on scientists to stop providing expert appraisals for the National Research Agency and the Agency for Evaluation of Research and Higher Education—two hotly contested innovations by the previous government—and demonstrations were planned in Paris and in Bordeaux for 27 November.

The panel's plans would create a tangle of practical and legal problems as well. Dissolution of the mixed units could create messy divorce fights, and Zerhouni's proposal to raise the age at which scientists get tenure—now often between 30 and 35—might run afoul of French laws that put limits on temporary labor contracts.

Still, says Zerhouni, France has little choice if it wants to stay competitive. He has been "very impressed" by the government's appetite for change; as to the unions' worries, he says: "I hope they realize this is pro-scientist. … I think people are tired of these complicated lives." **–MARTIN ENSERINK**

CREDIT: SAUVONS LA RECHERCHE

Published by AAAS

ASTRONOMY

Giant Scope Heads Europe's Wish List

European astronomers have asked policymakers to green-light a 42-meter-wide giant telescope that they promise will keep them at the forefront of world astronomy. The planned European Extremely Large Telescope (E-ELT) got top billing this week in an infrastructure road map for the field, alongside a global radio telescope called the Square Kilometer Array (SKA).

Funding the ambitious plan would give Europe "a world lead in astronomy, as it has in particle physics," says Martin Rees, the U.K.'s Astronomer Royal. That may be a tall order, however. Europe spends roughly €2 billion per year on astronomy and would have to boost that amount by 20% over the next decade to pay for all the listed projects.

Commissioned by a group of European funding bodies called Astronet, the road map lists more than a dozen projects, both ground- and space-based, that Europe's astronomers would like to achieve in the next 10 to 20 years. The proposed detectors cover the whole electromagnetic spectrum, as well as particles from space and gravitational waves.

European astronomy has always been fragmented. The European Southern Observatory (ESO) handles a number of large projects, whereas the European Space Agency (ESA) oversees most space missions. National agencies carry out many other efforts. In 2005, many of these funders formed Astronet and asked astronomers to identify their main scientific goals (*Science*, 5 October 2007, p. 35). Then they asked for a list of the tools needed to achieve them. "At the beginning, it looked almost impossible to do, because of the complexity of Europe," says astrophysicist Michael Bode of Liverpool John Moores University in the U.K., who led the exercise.

In contrast to the U.S. decadal surveys of astronomy and astrophysics, which rely heavily on "town meetings," Astronet asked a number of subject panels and user groups to work up a draft road map. It was released online earlier this year and chewed over at a symposium in June.

Some tensions emerged: Advocates for E-ELT and SKA were worried that Europe could not afford two billion-euro projects, both of which are now in the design phase. E-ELT's huge segmented mirror would give it 100 times the sensitivity of today's front-rank ground-based scopes; a decision on its construction could be made as early as 2010. Not as advanced in preparation, SKA would spread as many as 4000 radio dishes over thousands of kilometers in either Australia or South Africa (*Science*, 18 August 2006, p. 910). The Astronet road map lays out "a phased plan with a real hope of both succeeding," says Bode.

The road map also endorses a 4-meter solar telescope, a high-energy gamma-ray telescope array, and a neutrino telescope that uses a huge volume of Mediterranean seawater as its detector.

In assessing space missions, the road map closely mirrors a list of proposals that had recently been through the selection mill of ESA's Cosmic Visions program. "We were heartened by that," Bode says. Top priorities for large missions were a gravitational wave detector and an x-ray observatory. Also listed were Laplace and Tandem, proposed missions to the Jupiter and Saturn systems. Among medium-sized missions, ones to detect dark energy and study the sun stood out.

Now that Europe's astronomers have spoken, the attention is shifting to the various funding agencies. "Discussions [on E-ELT] already started some time back," says ESO Director General Tim de Zeeuw. "Our 14 member governments are actively engaged in finding ways to pay for it and build it."

–DANIEL CLERY

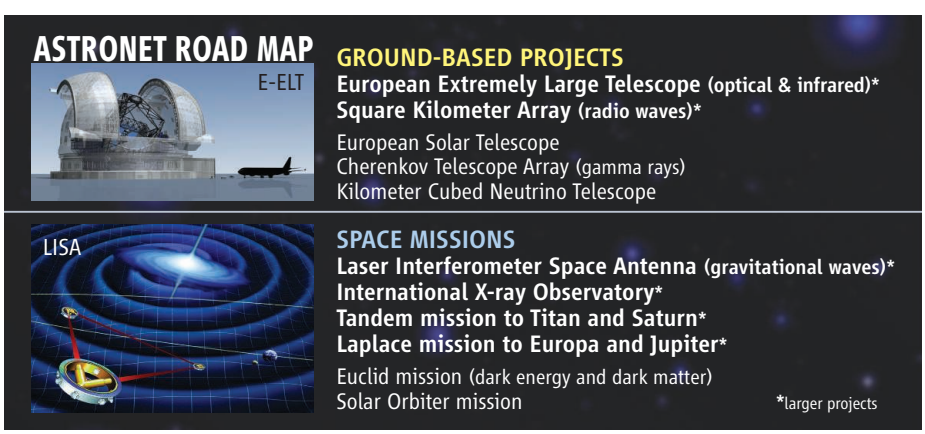

CREDITS (IMAGES, TOP TO BOTTOM): ESO; ESA

Obama Transition: Science Team Named

President-elect Barack Obama has named members of his transition team for science agencies. Nobel Prize–winning chemist Mario Molina of the University of California, San Diego, former Clinton White House officials Rosina Bierbaum and Tom Kalil, and Michael Stebbins of the Federation of American Scientists are reviewing the Office of Science and Technology Policy and the role of the science adviser. The review team for the National Science Foundation is led by Jim Kohlenberger, previously a top aide to former Vice President Al Gore, and communications lawyer Henry Rivera.

Last week, Democrats in the U.S. House of Representatives dethroned their most senior member, Representative John Dingell (D–MI), and chose Representative Henry Waxman (D–CA) to lead the powerful House Committee on Energy and Commerce. The surprising vote is expected to strengthen Obama's hand in the debate over setting limits on greenhouse gas emissions, and climate scientists say the vote augurs well for meaningful legislation in the next Congress. "It's a sea change," says Stephen Schneider of Stanford University in Palo Alto, California, adding that "they replaced seniority with 21st century thinking instead of 19th century protectionism for the auto industry."

Also last week, the Senate's failure to pass an economic stimulus package that would have helped the U.S. auto industry was also a defeat for the U.S. National Institutes of Health, which would have received a $1 billion boost under the measure. The legislation also contained $800 million for energy research.

–ELI KINTISCH

Big Push for Peanut Butter

The Bill and Melinda Gates Foundation has given $16 million to an international network led by Kathryn Dewey of the University of California, Davis, for studies in Malawi, Burkina Faso, and Ghana to develop and test a peanut butter–like food supplement that prevents malnutrition. Fat-based peanut pastes have revolutionized the treatment of malnutrition in poor countries, but their use in prevention is hotly debated (*Science*, 3 October, p. 36). "There's a huge need for more research," says Carlos Navarro-Colorado, an independent consultant on health and malnutrition in Barcelona.

–MARTIN ENSERINK

Published by AAAS

HUMAN GENETICS

Interest Rises in DNA Copy Number Variations—Along With Questions

PHILADELPHIA, PENNSYLVANIA—Like a kaleidoscope, the human genome keeps offering up new views. The latest, causing excitement here last week at the annual meeting of the American Society of Human Genetics, concerns duplicated or missing blocks of DNA, known as copy number variations (CNVs). Large CNVs, millions of DNA bases in length, have been detected for some time, for example, in children with mental retardation. But as geneticists peer closer, they are finding CNVs everywhere, in every size, all across the genome (*Science*, 7 September 2007, p. 1315). "Many of us in the field were just blown away when we realized how often all of us have regions of the genome that are missing or present in extra copies," says Jan Friedman of the University of British Columbia in Vancouver, Canada, who attended last week's meeting. "We just had no idea [the genome] was so plastic."

The study of CNVs, like any emerging field, is plagued by uncertainty. Often the technology used was not designed to detect CNVs, making results difficult to interpret. And it's not at all clear which CNVs alter the function of genes or influence disease. Last week, scientists at the meeting described links between CNVs and various cancers, schizophrenia, autism, body mass index, and Crohn's disease. But in nearly all these cases, questions remain as to whether CNVs are coincidentally present, are linked to another genetic disease driver, or are themselves causing ill health.

Many research groups are now conducting broad sweeps of genomes in various species, and in healthy and sick people, to get a sense of CNV patterns. Alexandre Reymond of the University of Lausanne in Switzerland presented unpublished research describing a survey of CNVs in mouse genomes and six different mouse tissues, including the brain, liver, and heart. Reymond wanted to learn how often CNVs popped up in different mouse strains—including wild mice caught outdoors. He was curious as to whether CNVs affected gene expression and whether expression changed across tissues and during development. He found wide effects: Genes that fell within CNVs tended to be expressed at lower levels; CNVs influenced expression of genes nearby; and the expression of affected genes varied depending on where one looked in the body.

Other CNV maps are being assembled at the Wellcome Trust Sanger Institute in Hinxton, U.K., and the Broad Institute in Cambridge, Massachusetts. Don Conrad and his colleagues at the Sanger Institute have their eyes on smaller common CNVs, as little as 500 base pairs in length. Checking about every 50 base pairs across parts of the genomes of people of African and European ancestry, they uncovered more than 10,000 CNVs—suggesting that other efforts, which have identified about 1500 common ones, are missing most CNVs. Although "there haven't been many" CNVs linked to disease yet, Conrad said in his talk, "there might be quite a few out there." Indeed, he noted that 129 of the 419 genetic-association regions pinpointed in genome-wide association studies hunting for disease DNA contain a common CNV.

The Wellcome Trust Case Control Consortium, which has scanned the genomes of thousands of people for variations in single DNA bases that might be associated with seven chronic diseases, is now performing a similar survey of copy number variation. They want to learn whether certain patterns of CNVs stand out in particular diseases. So far, they're not finding more CNVs in individuals with disease compared with those without but are finding that the CNVs in the genomes of those with, say, diabetes are not the same CNVs that show up in healthy people. The key variable with these CNVs is "kind of where they are rather than how many there are," says Matthew Hurles of the Sanger Institute, who presented the unpublished research.

In the Wellcome Trust work, as in many other CNV studies, quality control is a major challenge. Rare CNVs can trigger false positives, says Hurles, suggesting a connection to disease that isn't really there. In addition, it's easier to detect deleted DNA than it is DNA that has been duplicated, which may bias results.

Although results are often murky, some solid work points to a role for CNVs in neuropsychiatric disease. Earlier this year, research published in *The New England Journal of Medicine* tied a deletion in chromosome 16 to cases of autism, and other work linked it to cases of developmental delay. But two recent papers on schizophrenia, published earlier this year in *Science* (25 April, p. 539) and *Nature*—some data from which were also presented last week—came up with very different results. One group reported that rare CNVs were three to four times more common across the genome in those with schizophrenia than those without; the other reported 1.15 times as many. "There must be some underlying truth that explains both," says Steven McCarroll of the Broad Institute, who described his efforts to examine CNVs that might travel with DNA previously linked to disease. Technology may play a critical part, he says: "The smallest CNVs you might see on one platform but not on the other."

Despite such limitations, CNVs have become a popular target for disease gene studies. At last week's meeting, Rehab Abdel-Rahman of the University of Edinburgh in the U.K. described a CNV culled from more than 2200 cases of colorectal cancer. The CNV, which includes a gene that helps control the immune system, appeared in 14% of cancer cases but fewer than 4% of controls, she said. Other work linked CNVs to body mass index and to retinoblastoma that may be passed to children by their fathers.

One critical question is whether these CNVs are inherited or spontaneous. The latter, many believe, are much more likely to drive disease but also much less common. Another question is whether CNVs show up in many cases of a disease or just a handful. "We're still really in a learning curve," said Stephen Scherer, who studies autism genetics at Toronto's Hospital for Sick Children. Much of the work remains imprecise and very preliminary, but, he notes, "the data are getting much better."

–JENNIFER COUZIN

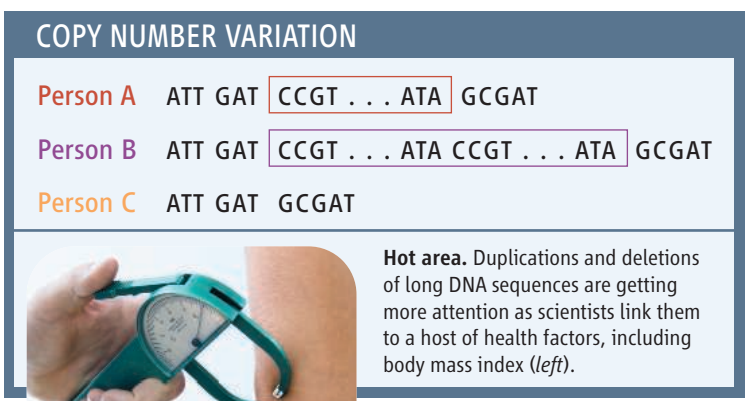

Hot area. Duplications and deletions of long DNA sequences are getting more attention as scientists link them to a host of health factors, including body mass index (*left*).

CREDIT: (IMAGE) PHOTOS.COM

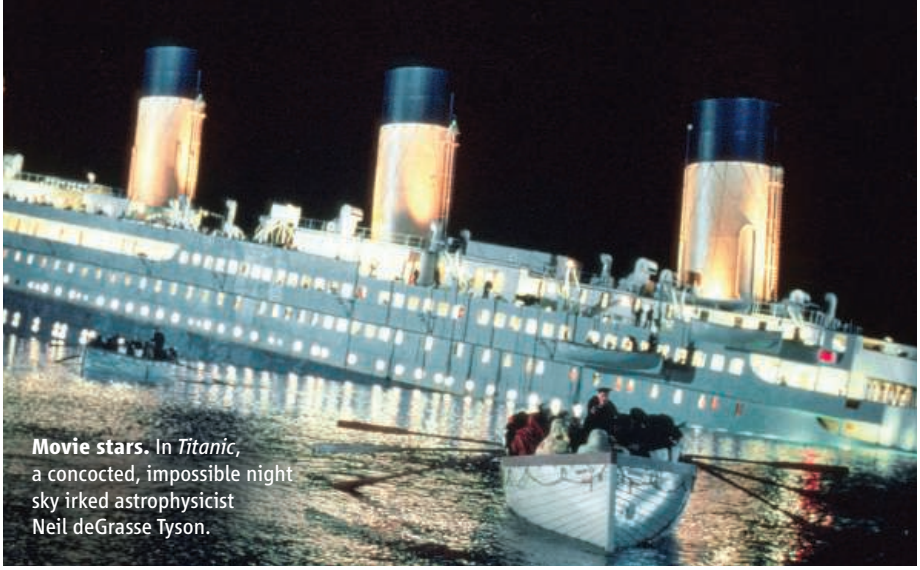

Movie stars. In *Titanic*, a concocted, impossible night sky irked astrophysicist Neil deGrasse Tyson.

SCIENCE AND SOCIETY

Science Goes Hollywood: NAS Links With Entertainment Industry

LOS ANGELES, CALIFORNIA—Near the end of the movie *Titanic*, actress Kate Winslet stands on a plank of wood and looks up at the night sky. "There was one sky Kate Winslet should be looking at," astrophysicist Neil deGrasse Tyson said at an unusual gathering of 350 Hollywood moguls and prominent scientists who met here on 20 November to launch a new collaboration called the Science & Entertainment Exchange (SEE). "It was the wrong sky. I was pissed off." Tyson, who heads the Hayden Planetarium at the American Museum of Natural History in New York City, said he met *Titanic* director James Cameron by chance and pointed out that the stars on the left side of the screen mirrored the stars on the right. "He said, 'The last time I checked, the film made $1 billion.' " Tyson says he replied, tongue in cheek, "Imagine how much more you could have made."

Aligning the stars correctly may not have helped *Titanic*'s bottom line, but Tyson's gripe does reflect a sense within the scientific community that movies and television too often botch the science—even when it would take little extra effort to get it right. With that in mind, the National Academy of Sciences (NAS) launched SEE, which it hopes will "be a service to all of Hollywood" by connecting scientific authorities to the people who produce, write, direct, and animate films and TV shows, explained NAS President Ralph Cicerone. The operation will consist of a "simple office" in Los Angeles to, as director Jerry Zucker put it, "bring our two best friends together who haven't met."

Although Hollywood is not suddenly shopping for scripts that dramatize the world of science—which many here noted rarely provides a gripping narrative—Zucker (*Airplane*, *Ghost*) and his producer wife, Janet, saw that too much distance separated the two endeavors. The Zuckers became intimately involved with the scientific community when they helped push through a 2004 proposition that created the California Institute for Regenerative Medicine to pursue stem cell research with state funds. Then one of their employees introduced them to Cicerone, and together they dreamed up SEE. A key part of their plans for SEE, which they demonstrated here, is to hold salons that enable the entertainment community to learn about cutting-edge scientific advances and discuss them with the researchers at the front. For now, NAS is bankrolling SEE's first-year budget of $490,000 from its endowment, but NAS and the Zuckers are looking for other funders.

Strange bedfellows? NAS head Ralph Cicerone (*left*) teamed with the Zuckers (*right*) to create SEE.

SEE held its glitzy inaugural—replete with fluorescent Pyrex beakers as centerpieces on the lunch tables—at 2000 Avenue of the Stars, a high-rise in Century City with spectacular views across the city. The daylong gathering featured a short film by the Zuckers that spoofed the sometimes tense relationship between Hollywood and science, but they repeatedly urged the attendees not to waste time grousing about problems. Instead, they organized six interactive salons led by leading researchers in climate change, robotics, astronomy, genomics, neuroscience, and infectious diseases. "We're not here to complain about the way you depict scientists," said Cicerone. "We want to establish a partnership. We think there really is a synergy. Certain aspects of both science and entertainment do overlap." Jerry Zucker noted that both, for example, "are very creative fields with lots of personal passion," and he joked that scientists "are just like you and me except they got perfect scores on their SATs."

The gathering brought together an eclectic who's who from two wildly different walks of life. In addition to Tyson, scientific speakers included Nobel Prize–winning physicist Steve Chu, J. Craig Venter of human genome fame, and neuroscientist V. S. Ramachandran. Hollywood attendees included cartoonist Seth MacFarlane (*Family Guy*), writer/producer Lawrence Kasdan (*Big Chill*, *Raiders of the Lost Ark*), and director/writer Kimberly Peirce (*Boys Don't Cry*). Valerie Plame Wilson, who became an accidental celebrity after the Bush Administration revealed that she worked in covert operations at the CIA, also chaired a session as a favor to the Zuckers, who are making a movie about her book, *Fair Game*.

Reviews of the get-together were largely two thumbs up. "I'm very pleased to see them doing this," said Kip Thorne, a theoretical physicist at the California Institute of Technology in Pasadena (who is working on a science-fiction movie, *Interstellar*, with Steven Spielberg). Kasdan said the day was "incredible," noting that the strong turnout at the various salons shows that the entertainment industry wants deeper ties to science.

Will SEE have what Hollywood calls legs? "I'm an experimental scientist," said Venter. "This is an interesting experiment." Venter did not mention that most experiments fail. And the entertainment community is no stranger to grand ideas that fizzle out. Then again, this is Hollywood, which is in the business of turning dreams into reality. And many scientists seem eager to help make that reality more real. **–JON COHEN**

Published by AAAS

Canada's Experimental Lakes

In remote Ontario, a network of lakes is dedicated to bold ecological manipulations. Research there has helped explain algal blooms and acid rain. As the unique outdoor lab turns 40, some wonder whether it is past its prime

In 1966, fisheries scientist Waldo Johnson had a big idea. Algal blooms were plaguing Lake Erie, and the Canadian government had created the Freshwater Institute to study the problem. Johnson, as the new director, proposed to pollute several small lakes intentionally to figure out exactly what was going on. If researchers manipulated the entire lake ecosystem, he argued, they might be able to mimic what happens in nature and find some answers.

Online
sciencemag.org
Hear more about how ELA's lakes are altered and probed on *Science*'s podcast.

The government agreed, setting aside dozens of remote lakes for research. The world-renowned facility that resulted, the Experimental Lakes Area (ELA), changed the face of freshwater ecology, ushering in an era of what researchers there call "extreme science."

Over the decades, ELA researchers and collaborators from around the world have conducted more than 50 massive experiments, including building dams and setting up fish farms. In a practice that would surely raise eyebrows elsewhere, they have dumped toxic metals, synthetic hormones, and other pollutants into pristine lakes. "Everyone has the same reaction: 'I can't believe they let you do that,'" says ELA's chief scientist Michael Paterson, a zoologist with Canada's Department of Fisheries and Oceans (DFO), which runs the facility. "We use these lakes the way medical researchers use white mice."

ELA was pivotal in fingering phosphorus from detergents as the culprit in algal blooms, and experiments in lakes there provided compelling evidence of the harm caused by acid rain. U.S. and Canadian environmental policies were forged in part on the strength of ELA's science. "It's hard to overstate the impact they've had," says James Elser of Arizona State University (ASU), Tempe.

Forty years later, ELA still hosts first-rate science, say many ecologists. With $13 million of infrastructure, finely characterized lakes, and decades of baseline data, the site can tackle problems few others can. All is not rosy, however. Researchers complain that government bureaucracy has long limited the lab's full potential, although this may change with a new arrangement for funding. Half of the staff scientists there are nearing retirement, and recruiting top talent can be a challenge. As ELA celebrates its 40th birthday, even some of the lab's old hands wonder aloud whether the place is due for some rejuvenation.

Young blood

In many ways, the stars were aligned when Johnson sketched out plans for the outdoor lab, which became useful for studying much more than eutrophication. In 1967, a pair of technicians was sent out to find an area with many lakes of various sizes, remote enough to be pristine yet within 300 kilometers of Winnipeg, where the Freshwater Institute was located. Flying by plane and helicopter, the technicians named hundreds of lakes, simply giving them sequential numbers. Eventually, 46 lakes in 17 small watersheds were selected.

The setting is ideal. The lakes and sur-

CREDITS (TOP TO BOTTOM): R. ROONEY/DFO; DFO

Published by AAAS

Probing below. Floating traps collect aquatic insects on lake 375, part of the research infrastructure at ELA.

rounding pine forests rest on granite bedrock, so there is little groundwater, which means the lake chemistry is relatively simple to study. And the diversity of the lakes' sizes and depths makes for an exceptionally versatile ecological lab.

Limnologist Jack Vallentyne, hired from Cornell University, was put in charge of assembling a crack team of scientists. He recruited respected experts from Japan, Poland, Italy, and other countries, as well as "hot, young blood," as he called the younger members of the team. In his bid to persuade scientists to move to Winnipeg and endure long, cold winters, Vallentyne touted the opportunity to do whole-lake experiments on a scale unmatched anywhere else.

In what turned out to be a strategic move, Vallentyne put a young limnologist, David Schindler of Trent University in Peterborough, Canada, in charge. In the summer of 1968, Schindler set up a field camp with a few trailers and got to work. (Schindler is a member of *Science*'s board of reviewing editors.)

ELA's original mission was to examine the problem of eutrophication. The pressing question in the late 1960s was which nutrient triggers excessive algal growth. Studies in small tanks done elsewhere had yielded conflicting data. Some scientists thought the culprit was phosphorus, principally in detergents and sewage; others thought it might be nitrogen from fertilizer and sewage, or carbon, or perhaps even trace metals.

In a now-famous experiment (*Science*, 24 May 1974, p. 897), the team divided Lake 226 with a plastic curtain and added phosphorus to one half. When it turned a distinctive murky green, they had their answer. It was an aerial photograph from this experiment that largely persuaded policymakers to phase out phosphorus from detergents. "I think that's the single most powerful image in the history of limnology," Elser says. When Schindler took the results—and the photo—to government hearings in Canada and the United States, he put ELA on the map as a hub of innovative, policy-relevant research.

Next, Schindler tackled one of the most contentious issues of the day, acid rain. In a series of experiments conducted between 1976 and 1988, researchers added sulfuric and nitric acid, pollutants that lead to acid rain, to Lake 223 and others. The results showed that the pristine ecosystem began to suffer at significantly less acidic conditions than electric utilities maintained. They also demonstrated harm cascading through the food web, with plankton species disappearing and fish not reproducing—as had been seen in lakes already damaged by acid rain. One of the key contributions of ELA, points out ecologist Gene Likens of the Cary Institute of Ecosystem Studies in Millbrook, New York, was that it provided experimental evidence that helped convince skeptics of observational studies. Schindler and his colleagues were also able to perform experiments showing that lakes would slowly recover when the pH returned to normal.

Rising star. David Schindler, shown in 1979 and today, was ELA's first director. Many credit ELA's reputation to his 2 decades of leadership.

Once again, Schindler made the rounds of government offices and congressional hearings in Canada and the United States with his data and images—this time starving trout whose prey had died and species that had vanished. Although ELA was by no means alone in studying acid rain, many say Schindler's ability to communicate science in simple, homespun terms—he appeared widely on television and in newspapers and magazines—helped spark stricter regulations on power plants. In 1990, the U.S. Congress passed major amendments to the Clean Air Act that helped reduce acid rain (*Science*, 6 November 1998, p. 1024).

They were heady times. The federal government and other funders were generous, and the researchers who flocked to the site each summer were essentially given free rein. True, there were a few rules, Schindler recalls. For example, once an experiment ended, the lake had to be restored to its original condition. Other than that, "in the early days, we could do pretty well what we pleased," he says. The camaraderie was strong. "It was nirvana when I got there," recalls John Rudd, who first arrived at ELA as a graduate student in 1972. Researchers worked full-time, brainstorming late into the night. "We lived our science together, week after week," says Rudd.

Ecology's supercollider

But change was afoot. In 1979, the Fisheries Research Board, which had been run mostly by university scientists, was dissolved; the Freshwater Institute and ELA were transferred to DFO. The move put department officials, not scientists, in charge and eventually had a large impact on the direction of the research, says Schindler.

DFO's primary focus was on marine rather than freshwater issues, and ELA gradually lost its favored status. Raising funds for experiments became increasingly hard. "We'd always fall through the cracks," Schindler recalls. Fed up, he left for the University of Alberta, Edmonton, in 1989.

Also at about that time, a few officials with the province of Ontario began to look askance

Dam impact. Flooding wetlands showed that reservoirs can release greenhouse gases and mercury.

CREDITS (TOP TO BOTTOM): D. F. BRAKKE; (INSET) UNIVERSITY OF ALBERTA CREATIVE SERVICES; DFO

WHOLE–ECOSYSTEM EXPERIMENTS

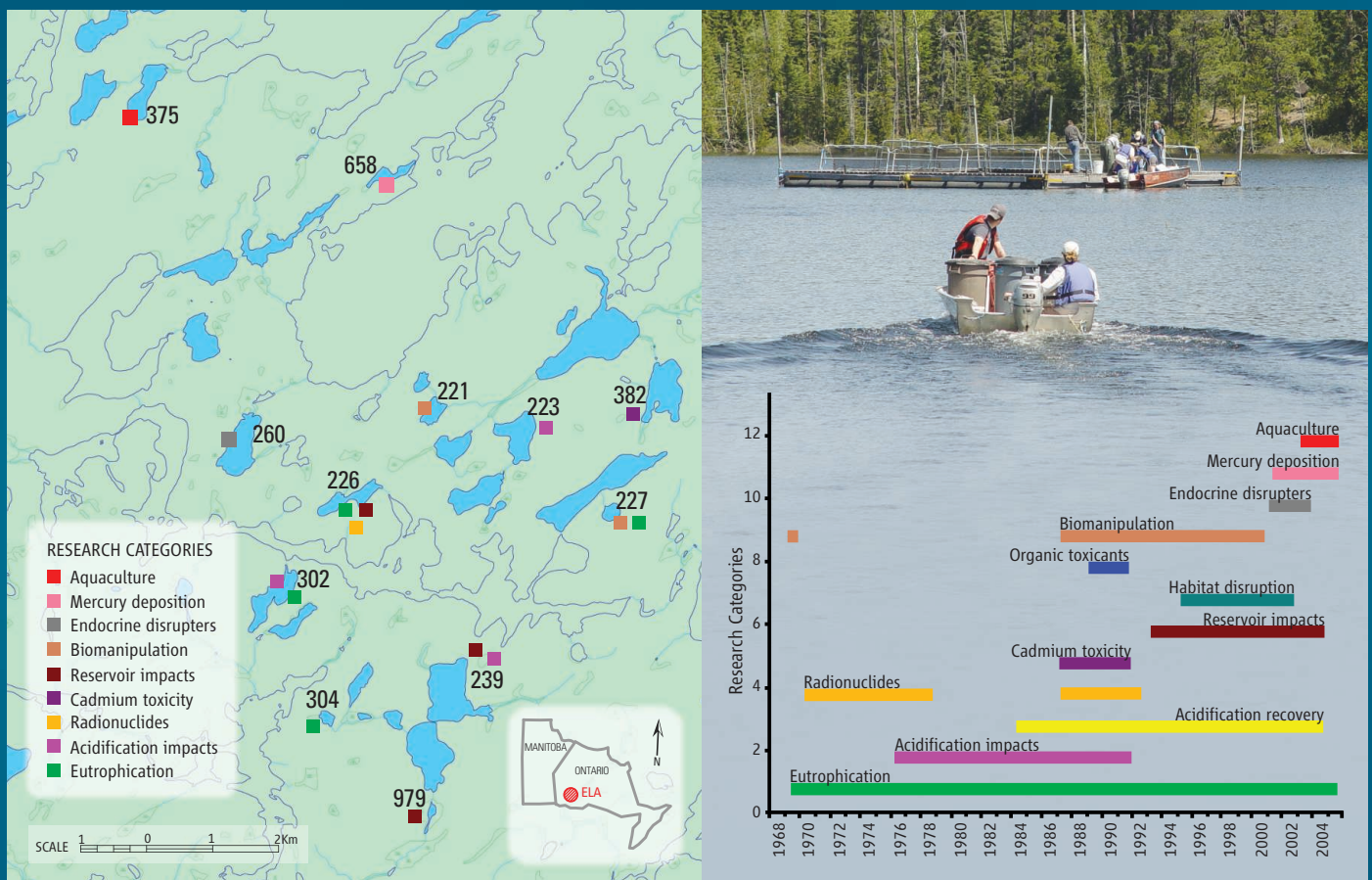

Full palate. For 40 years, researchers have conducted a broad range of experiments in 58 lakes reserved for research (some shown above). Among others, they have manipulated food webs; examined the effects of habitat disruption, such as removal of lake vegetation; and studied the impact of caged aquaculture.

at ELA's practice of dosing the lakes with one pollutant after another. One example in particular sticks in the craw of Robert Hecky, who took over as director after Schindler.

ELA scientists had been adding cadmium, a metal released from smelters and coal-fired power plants, to Lake 382 to see whether provincial regulations were tight enough to protect aquatic organisms. A few years after Schindler left, Ontario's then–minister of environment halted that work, forbidding ELA scientists from adding any more cadmium. "They threatened to shut down the whole ELA if we didn't stop," recalls a still-outraged Hecky—despite the fact that power plants were emitting greater concentrations of cadmium on a regular basis. Hecky says he soon realized that plans to add polychlorinated biphenyls to the lakes weren't going to fly, either.

The nadir came in 1996, when the federal government tried to shut ELA during a round of belt-tightening. Hecky resigned in protest. Scientific societies such as the American Society of Limnology and Oceanography rushed to ELA's defense, and the lab was saved. ELA is secure now, assures Robert Lambe, DFO's regional director in charge of the Freshwater Institute. "It's not in the crosshairs."

But the years have taken a toll, say scientists inside and outside ELA. Old-timers say that DFO grants are smaller and harder to come by now. "The federal money to conduct experiments has dried up," Rudd says. A long-term experiment on flooding of wetlands may have to be shut down if funds to repair the dam can't be found.

The biggest impact has been the decline in staffing; the number of DFO scientists working full-time at ELA has fallen by about half since the early 1990s, to six today. Researchers from other institutions still flock to the lab with the spring thaw, although now it tends to be graduate students and technicians rather than professors who stay the whole summer, Rudd says.

In terms of technological prowess, ELA remains unmatched. Over the years, DFO replaced the dented trailers with comfortable dormitories and a first-rate laboratory. ELA is still "the supercollider of ecology," says Schindler. In a recent experiment to gauge the impact of freshwater aquaculture, for instance, researchers had to build a 12-ton cage on the ice of Lake 375 in –30°C weather. Every spring, starting in 2003, the cage was stocked with 10,000 rainbow trout that had to be trucked in from nearly 1900 km away. There are not many places in the world with ELA's combination of experience setting up big infrastructure and onsite research capacity, as well as detailed background records and reference lakes, notes DFO's Cheryl Podemski, who ran the experiment.

Perhaps the most ambitious experiment of the past decade is METAALICUS (see sidebar, p. 1319), in which researchers added isotopes of mercury to Lake 658 and its watershed for 7 years in a row. The goal is to figure out how the pollutant moves

CREDITS: (MAP/TIMELINE DATA) DFO; (IMAGE) C. PODEMSKI/DFO

Published by AAAS

Contaminating a Lake to Save Others

LAKE 658, CANADA—Even at the Experimental Lakes Area (ELA), the birthplace of "big" ecological experiments, METAALICUS is ambitious. Over the past 9 years, some 15 principal investigators (PIs) from eight institutions have joined forces at this remote experimental station (see main text) to tease apart how mercury in air pollution cycles through the environment. By adding stable isotopes to Lake 658 and the surrounding watershed, researchers are studying how mercury percolates through soil and into lakes, how microbes make it bioavailable, and the rates at which it accumulates in fish. Already, the $15 million project, formally known as the Mercury Experiment to Assess Atmospheric Loading in Canada and the United States (METAALICUS), has generated policy-relevant results.

Several attributes made ELA an ideal location for METAALICUS, says one of its leaders, geochemist David Krabbenhoft of the U.S. Geological Survey in Middleton, Wisconsin. For one, the relatively low rates of background deposition to the lake made it easier to detect the tiny amounts of mercury isotopes—just 12.5 grams (a sixth of a teaspoon)—that they added each year. Even more important, the remote location and the history of successful research at ELA lowered the chance of public objections. Just in case, Canadian researchers held public briefings in Dryden and Kenora, the closest towns.

METAALICUS was years in the planning. After a 3-year pilot project at ELA, the researchers first added isotopes in June 2001, trickling ^{202}Hg throughout this 8.3-ha lake by boat. Depositing the other two isotopes— ^{198}Hg onto an adjoining wetland and ^{200}Hg onto the surrounding forest—proved far more challenging. In a nail-biting maneuver, a crop-duster had to fly low overhead repeatedly, precisely spraying an extremely dilute mist of mercury. Had a droplet of either ^{198}Hg or ^{200}Hg drifted into the lake, it would have confounded the findings.

Within 2 months, ^{202}Hg was detected in fish. In a paper published in September 2007 in the *Proceedings of the National Academy of Sciences*, the team reported that mercury levels rose by a third in young yellow perch over the first 3 years of the experiment. This suggests that lowering industrial emissions of mercury should quickly reduce fish contamination in lakes where most of the mercury falls directly from the atmosphere to the water.

The final doses of mercury were added to the ecosystem last year. Earlier this fall, a crew of technicians was busy looking for signs of isotopic mercury trickling through the forest soil. Monitoring will continue for several more years to figure out the rate at which the forest soils release mercury after it lands from the atmosphere. "It's slow, but we can't tell you whether it's 20, 100, 1000 years" for the isotopes to make their way into the lake, says biogeochemist Cindy Gilmour of the Smithsonian Environmental Research Center in Edgewater, Maryland, a co-PI on a new $570,000 U.S. National Science Foundation grant to explore the question. The work is crucial, Krabbenhoft notes, because it will provide insights into the impact that past mercury emissions will have on future fish generations.

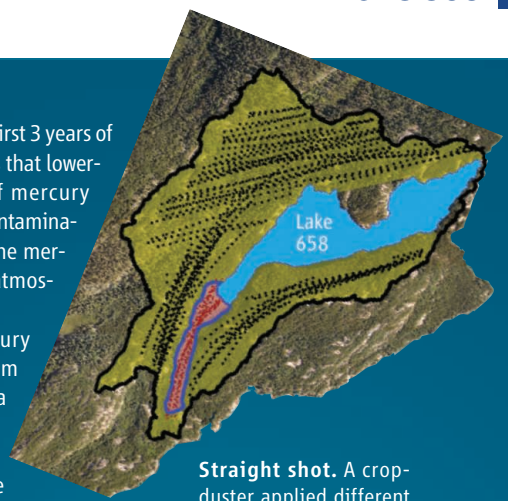

Straight shot. A crop-duster applied different isotopes of mercury (black dots) to the upland forest (green) and wetland (red).

METAALICUS is not only the largest experiment in ELA's history, but it is also the first that has moved beyond lake manipulation, ELA's original mandate, to manipulation of the surrounding terrestrial ecosystem as well. "Broadening the perspective beyond lakes adds a lot," says Stephen Carpenter of the University of Wisconsin, Madison, and would be an effective way to maximize the scientific potential of ELA. "They need to think really, really big." **–E.S.**

Trickle down. Researchers are tracking how mercury in the forest flows into Lake 658.

through the ecosystem and builds up in fish. The final dose of mercury was added in 2007, and now team members are keeping tabs on water quality and aquatic life.

Next?

Other experiments at ELA have finished their active phase as well. In 2007, all the fish were removed from the aquaculture operation for the last time. Now researchers are watching to see how the lake returns to its natural state. That's also the case with ELA's endocrine disrupter study. Over 3 years, researchers added synthetic hormones to Lake 260 to study the effects of birth-control pills in wastewater. At hormone concentrations currently found in municipal wastewater, minnow populations crashed, they found, in the first ecosystem-scale study to show the impact of these pollutants on fish populations.

But now, for the first time in ELA's storied history, no major lake manipulations are on docket. Part of the reason no big manipulations are planned is that half of the staff scientists are about to retire, says Paterson, who is "terrified" of the looming brain drain. But he is heartened by a new alliance with Environment Canada that he hopes will bring new funds to ELA and enable scientists to broaden the scope of their research again.

One key issue ELA ought to be immersed in is climate change, Paterson concedes. In fact, Rudd and Schindler tried to sell the idea of studying climate change to DFO in the 1990s, but there was no interest, they say; DFO officials felt it wasn't within the department's mandate. "For the first time, there's a major widespread problem that's going on that we're not [studying] at ELA," says Rudd, who retired in 2002 but continues to work on METAALICUS. ASU's Elser and others say ELA could have been more aggressive since then. "It helps to have senior leadership that can knock heads," Elser says.

Schindler agrees that the lab needs an infusion of fresh blood, especially someone with a bold vision for ELA's future who will battle the bureaucracy for funds. Recruiting the best and brightest isn't easy, however; government salaries aren't competitive with those at top universities, and DFO can't even offer start-up funding to set up new labs. But with three positions that will need to be filled, Paterson will soon be sifting through resumés. With any luck, he might find another Schindler in the bunch—somebody who can set the course for the next 40 years.

–ERIK STOKSTAD

CREDITS: (TOP) K. SANDILANDS/DFO, PHOTO BY ART ROBINSON; (BOTTOM) M. LUSSIER/DFO

Published by AAAS

PROFILE: ADAM RIESS

A Universe Past the Braking Point

A decade after racing to tell the world about "dark energy," an acclaimed astrophysicist pushes to streamline the search for Type Ia supernovae—celestial milestones that may help explain space's ever-accelerating expansion

On the bookcase behind Adam Riess's desk sits a framed cover of *Time* honoring Edwin Hubble, the astronomer who discovered in 1929 that the universe is expanding. On an adjacent shelf lies a stack of Riess's lab notebooks, some of which—from Riess's research as a postdoc at the University of California, Berkeley—record a discovery as dramatic as Hubble's own. During the Christmas break of 1997–98, working feverishly on a silent campus where even the heat had been switched off, the 28-year-old Riess scribbled equations and calculations based on observations of distant, exploding stars: supernovae. His analysis showed that gravity was not slowing the expansion of the universe as theory predicted. Rather, a mysterious repulsive force—or dark energy—suffused through space seemed to be accelerating that expansion.

Riess feared at first that he had made a mistake. Even after he mustered the confidence to share his shocking results, his Ph.D. adviser and collaborator Robert Kirshner asked him to triple-check his findings. "In your heart you know this is wrong," Kirshner e-mailed Riess in January 1998.

Convinced that he was right, Riess acted with hallmark urgency to publish a paper 9 months ahead of a rival team led by Saul Perlmutter of Lawrence Berkeley National Laboratory in California. Both teams have since shared credit for the discovery. In 2006, Riess, his teammate Brian Schmidt of the Australian National University in Canberra, and Perlmutter won the $1 million Shaw Prize in Astronomy. And last month, Riess won the so-called genius prize from the John D. and Catherine T. MacArthur Foundation, along with $500,000 over 5 years to spend as he pleases.

Now a professor at Johns Hopkins University in Baltimore, Maryland, Riess plans to spend part of his latest prize on a new way to search for Type Ia supernovae: exploding stars that researchers use as "standard candles" to measure astronomical distances. He hopes to equip telescopes with special filters that will eliminate the need to take spectra of supernova candidates, a process that can take up to an hour per supernova. "I like to think of them as 3D glasses for Type Ia supernovae," he says of the filters. By enabling cosmologists to use telescope time more effectively and make better use of upcoming sky surveys, he says, the technique could accelerate the study of dark energy.

Some colleagues question the merit of the idea and say it exemplifies Riess's fondness for shortcuts. "I am not enthusiastic about it," says Kirshner, who thinks false identifications will outweigh any timesaving benefit. But if Riess's plan succeeds, it could send him skating past the competition.

Disk driver. Riess is testing specially calibrated telescope filters designed to pick out stars used to calculate cosmic distances.

CREDIT: GREG SCHALER

For Riess, that is a familiar place to be. Researchers who have followed his career credit his success to luck, mathematical skill, creativity, and foresight—blended with a healthy dose of aggression. "Adam excels at beating people to the punch," says Andy Howell of Las Cumbres Observatory Global Telescope Network in California, who has co-authored papers with Riess even though he belongs to a rival team. "He isn't the most careful person in the world, but he is always first."

Bright lights, big cosmos

Riess is short and has curly reddish hair. He looks younger than his 38 years and can appear boyish if you mentally subtract the goatee from his face. When talking, he often breaks into a grin. Riess's Ph.D. student, Dan Scolnic, describes him as a down-to-earth and good-humored guy who recently dispensed some brotherly advice on dealing with a breakup. (You don't really understand relationships till you're 25, Riess told him.)

Riess played a lot of soccer growing up in Warren, New Jersey, which he says may have fostered his competitive streak. His mother was a psychologist. His father was an aeronautical engineer who quit the profession to start a frozen seafood supply store and a New York–style delicatessen. "I washed dishes there," says Riess. He likes to make the point that he was just an average kid. "I wasn't down in the basement laboratory."

Nevertheless, Riess says he was "deeply intellectually curious" about everything, pestering adults with questions. "There's a bell curve of curiosity in children. Adam was at the far end," says Riess's older sister, psychiatrist Gail Saltz. "Lots of boys bang their toys and break them. He was the kid who would bang it open to see how it worked." At the age of 8, for example, Riess stuck the antennas of his remote-controlled toy car into a socket to learn about electricity. "All the lights in the house went off," he recalls.

At school, Riess took a liking to history and science. "I remember looking at stars and my father telling me that the distances to some were so great that their light had taken

Published by AAAS

millions of years to get to us," he says. "We were seeing them the way they were millions of years ago, when dinosaurs roamed the planet. I was fascinated by this concept of cosmic time."

He was just as fascinated with technology. In seventh grade, he learned to program a TRS-80, the clunky PC of that era, and during summer vacations he worked at RadioShack. "I was ahead of the curve, but Bill Gates I was not," he says, with measured modesty.

After majoring in physics at the Massachusetts Institute of Technology in Cambridge, Riess enrolled at Harvard University and flirted with the idea of writing a thesis on the search for extraterrestrial intelligence. Instead, he joined Kirshner's lab and worked on measuring the expansion rate of the universe. Impressed by Riess's bent for math and statistics, Kirshner assigned him a problem that he felt was too mathematical for anybody else in the group: improving the measurement of distances across the universe from the brightness of Type Ia supernovae.

Type Ia supernovae are the brightest things in the universe. They begin when a burnt-out star—a white dwarf—in a binary system sucks up matter from its companion star. If the white dwarf grows to a mass known as the Chandrasekhar limit, it undergoes a thermonuclear fusion as powerful as 10 billion suns, visible billions of light-years away. Because in principle every Type Ia releases the same amount of energy, how bright they appear from Earth tells astronomers how distant they are.

Researchers learned in the early 1990s that each Type Ia actually burns a little differently, with a unique light curve representing the star's ascent to a dazzling peak and descent to darkness. Riess figured out these differences and developed a technique to characterize the light curve of an observed Type Ia, correcting for the dimming effect of dust clouds in front of it. The technique yielded more precise estimates of a supernova's distance. And that information, combined with its redshift—a change in frequency caused by the stretching of light waves across space—enabled researchers to measure the rate at which the universe was expanding when the supernova exploded.

For his postdoc, Riess joined the High-z Supernova Search Team at UC Berkeley. Led by Brian Schmidt, it had already analyzed a set of 22 nearby supernovae. Working under Alex Filippenko, Riess began analyzing observations from 12 distant supernovae and made his big discovery at the end of 1997. After overcoming his own doubts about it, Riess was frustrated by his team members' caution about publishing the finding. He knew that Perlmutter's team had more supernovae in its data set, and he pushed the others to seize the moment. "I realized that if they publish more data before we do, we wouldn't be adding very much," Riess says. Schmidt says it was Riess's laserlike focus "that enabled the High-z team to get its paper out in a timely manner."

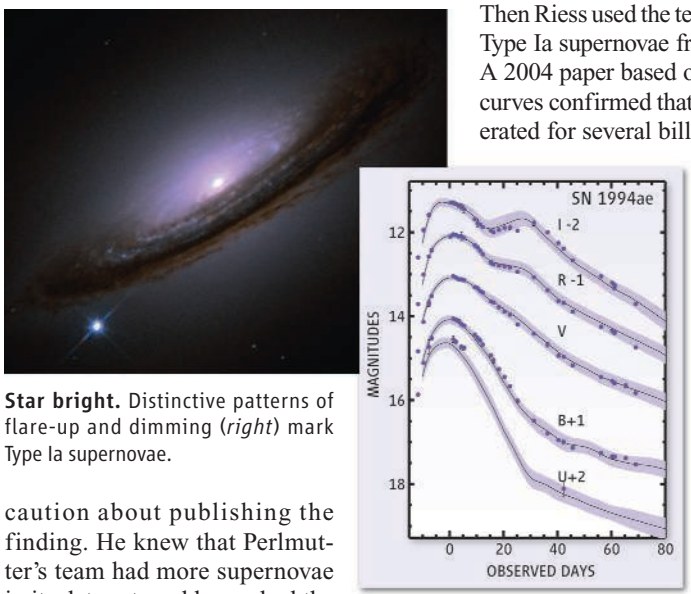

Star bright. Distinctive patterns of flare-up and dimming (*right*) mark Type Ia supernovae.

Colleagues say the work highlighted Riess's strong preference for crunching numbers over making observations. "Adam doesn't have a very good tolerance for physical discomfort. He doesn't like being too hot or too cold. His idea of astronomy is to work at home on his laptop, in his slippers," Kirshner says with a laugh. Riess agrees. "My biggest problem with observing is that I am not a night owl. When I am so sleepy, it's hard for me to make the best decisions. Did we get enough signal on this supernova? Should we move on to the next? There are people who are much better at that part than me. But I love the data!"

Harvesting stars

The 1998 paper made headlines around the world. As a follow-up, Riess decided to trace the history of dark energy. Nowadays, he reasoned, the universe is expanding because the outward push of dark energy more than balances the attractive force of gravity. At some point in the past, however, when the universe was smaller and its matter more densely packed, cosmic gravity must have outweighed dark energy, causing the universe to decelerate.

To test the idea, Riess needed a Type Ia supernova burning eons away—at a record-high redshift. By sheer serendipity, the Hubble Space Telescope had observed exactly such a star; by analyzing it, Riess and his colleagues proved in a 2002 paper that the cosmos had indeed slowed down during this early epoch. Then Riess used the telescope to find six more Type Ia supernovae from the young universe. A 2004 paper based on analysis of their light curves confirmed that the universe had decelerated for several billion years before beginning to accelerate.

Although 1000 or so Type Ia supernovae have been found, researchers need many more to better understand dark energy by quantifying the expansion history of the universe in greater detail. Riess's filter project, conceived in collaboration with Harvard astronomer Christopher Stubbs, is an attempt to leapfrog toward that goal. The filters are thick glass disks the diameter of a pancake, each designed for a different redshift. Objects seen through them with the naked eye appear dark and reddish. When he tried them on the Magellan optical telescope this summer, Riess says, the filters made Type Ia supernovae look 30% brighter or dimmer, depending on their redshift. It's a very creative idea with a potentially high payoff, says Filippenko.

Critics, however, doubt that Riess's filters will shortcut the need for observations. Astronomers have used similar filters to spot distant galaxies. But supernovae are another story, says Howell. Any filter capable of spotting their distinctive absorption and emission lines would have to let in such a broad band of wavelengths that the signal would be hard to separate from the sky's background noise. "It takes a fairly detailed spectrum to determine the type of a supernova convincingly," says Howell. "So unless he gets spectra for all of his targets," there will be errors.

Riess acknowledges that he needs many more supernovae to test the idea. If it works, he plans to implement it during the ground-based Panoramic Survey Telescope and Rapid Response System (Pan-STARRS) sky survey to be conducted from atop Mauna Kea in Hawaii.

Riess isn't worried that the discovery of dark energy would be the capstone of his career. "I can imagine that there would be some discoveries after which everything seems boring to work on," he says. "But this one really seems like the tip of an iceberg." One hopes for Riess that the peak of his career's brightness curve lies ahead.

–YUDHIJIT BHATTACHARJEE

CREDITS: NASA, ESA, THE HUBBLE KEY PROJECT TEAM, AND THE HIGH-Z SUPERNOVA SEARCH TEAM; ADAM RIESS

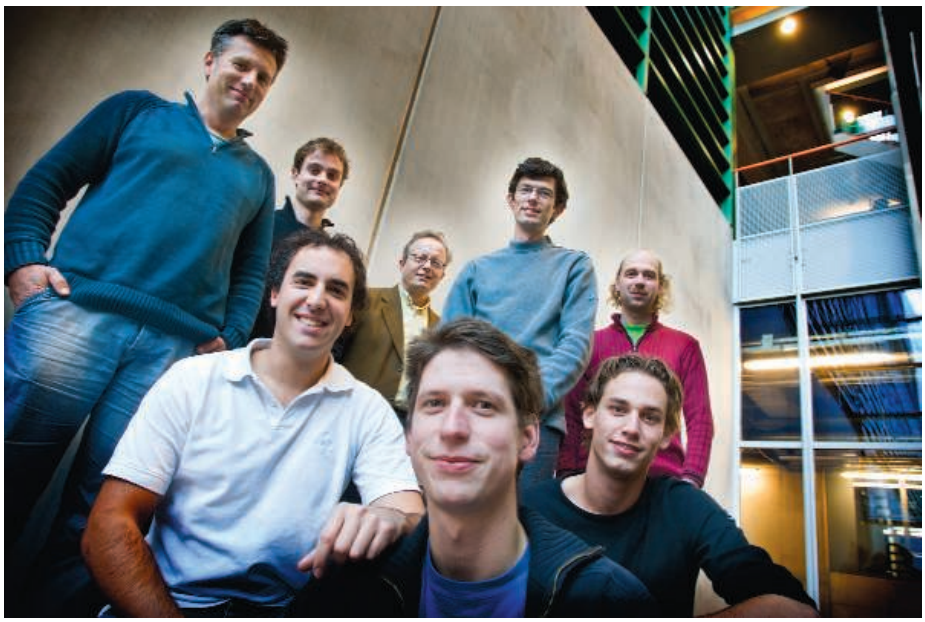

The Radboud gang. Clockwise from the left: Ronny Wichers Schreur, Gerhard de Koning Gans, Bart Jacobs, Wouter Teepe, Peter van Rossum, Ruben Muijers, Roel Verdult, and Flavio Garcia.

CREDIT: DICK VAN AALST, RADBOUD UNIVERSITY NIJMEGEN

CRYPTOGRAPHY

University Hackers Test the Right To Expose Security Concerns

When students in the Netherlands picked apart the world's most common smart card system, were they torpedoing its manufacturer or protecting the public's right to know?

NIJMEGEN, THE NETHERLANDS—In winter 2006, Roel Verdult was looking for a project for his master's thesis in computer science here at Radboud University Nijmegen. Flavio Garcia, then a doctoral student, laid down an unusual challenge. "He said, 'Well, for a goal, let's start with free parking,' " Verdult recalls. Garcia wanted Verdult to intercept and commandeer the communications between a gate controller at a parking lot and the "radio-frequency identification" (RFID) cards people wave in front of it to activate it.

Thus began an adventure that in March would lead Verdult, Garcia, and colleagues in Radboud's software security and correctness program to crack the secret messages exchanged in the world's most widely used RFID system, the MIFARE Classic. The card system opens parking gates, but it also tallies fares in the London Underground, the Netherlands' OV-Chipkaart transit system, and dozens of other transportation systems around the world. It also controls access to military bases, nuclear power plants, and myriad other buildings, the researchers say.

The team's "hack" would bring the Dutch secret service to the Radboud lab, force the country to consider replacing more than 600,000 transit fare cards, and prompt a lawsuit from the system's manufacturer, NXP Semiconductors, which sought to suppress the researchers' work. The episode has thrown a spotlight on the tension between an academic's desire to publish and the potential damage that could result. In this case, a judge ruled that the Radboud group had a right to publish their findings, as they did last month.

The company is not happy: "Broadly publishing detailed information … is, in our understanding, not responsible disclosure of sensitive information," says NXP spokesperson Alexander Tarzi. Garcia counters that, with a billion MIFARE Classic cards in circulation, the public should know they do not provide real security: "I believe the world is better off with this information out there."

A peek inside

If a hacker is supposed to be a geeky loner holed up in his cluttered bedroom, the Radboud guys don't fit the stereotype. Garcia, 30, drives a 2001 Alfa Romeo GTV sports car, used to race motocross, and says he enjoys the nightlife. Verdult, 26, practices karate and has a vicelike handshake and an easy smile. But both have been fiddling with computers since they were children. Growing up in Argentina, Garcia started programming simple video games at age 7. As an undergraduate intern at a software company, Verdult figured out how to run the company's software on computers lacking a special license chip—and alerted his boss.

To tackle the MIFARE Classic system, Verdult and Garcia built a €40 gadget to listen to the conversations between its RFID cards and readers. They joined forces with master's student Gerhard de Koning Gans, who built a similar device that talked to a reader as well. "Security evaluations are an intrinsic part of this field," says Bart Jacobs, director of Radboud's software security and correctness program. "We regularly ask our students to do them."

The Radboud team had to figure out how the MIFARE Classic reader and card scramble their messages. The messages are binary numbers—strings of 0s and 1s—that spell out commands, such as "Deduct €1.60 from the amount recorded on the card." As in many cryptographic schemes, the messages are scrambled using another sequence of 0s and 1s called a "key stream." In a conversation, each bit of each message is combined with a bit of the key stream through an "exclusive or" (XOR), a maneuver just like adding the two bits, except that the sum of 1 and 1 is set to zero. (If a command is 1100 and the key stream 0101, the XOR-scrambled message is 1001.)

Ideally, the key stream should be random, but being a machine, a MIFARE Classic reader cannot generate a truly random string of 0s and 1s. Instead, it relies on a complex but predictable recipe. (The card has the same system, which it synchronizes to the reader's.) The challenge was to figure out this secret recipe. If they could do that, the researchers could calculate the key stream to decipher any conversation or even send commands to rewrite or clone cards.

The Radboud students weren't the only ones prying into the system. Karsten Nöhl, a grad student at the University of Virginia, Charlottesville, and Henryk Plötz, a grad student at Humboldt University in Berlin, literally hacked open chips from MIFARE Classic readers and cards to see the wiring inside, as they reported at the Chaos Communication Congress in Berlin in December 2007.

At the system's heart lay a digital circuit called a linear feedback shift register (LFSR). It takes 48 0s and 1s jumbled in a row and, with each tick of the chip's clock, shifts them all one space to the left, spitting out the left-

Published by AAAS

most bit and using a feedback circuit to inject a 0 or 1 into the empty spot at the right (see diagram). A hugely long string of seemingly random bits emerges from the LFSR's left end. That output is too predictable to make a key stream, however. So, in the MIFARE Classic, certain bits of the LFSR feed into a filter function—which Nöhl and Plötz didn't reveal—for more scrambling. With each clock tick, the filter uses the current settings of those bits to calculate one bit of key stream.

Nöhl and Plötz showed parts of how the system works. But knowing how a thing works doesn't guarantee you can break into it, says Wouter Teepe, a postdoc at Radboud. "I can take apart the lock in my door to see how it works," he says. "But even if my neighbor has the same [type of] lock, knowing how it works doesn't mean I can get into his house" without the key.

Tell me your secrets

To pick that digital lock, the Radboud researchers still needed two things: the precise form of the filter function and the very first settings of the bits in the LFSR—the so-called "key" which serves as a seed for generating the key stream. The MIFARE Classic reader would soon tell them enough to deduce both. Whenever a MIFARE Classic card comes within range of a reader, the card sends its 32-bit ID number. Using that ID, the reader looks up the card's individualized key and loads it in the LFSR. To make sure the reader is legit, the card also sends a 32-bit random number called a challenge nonce that the reader must respond to correctly. The reader sends a challenge nonce of its own and then replies to the card's challenge—although now that the key has been set, these two messages and all that follow are scrambled with the key stream. Finally, the card answers the reader's nonce, ending the "initialization."

De Koning Gans and Verdult quickly found oddities in this exchange of hellos. Every time the reader was switched off and on again, it issued the same challenge nonce. For certain combinations of a card's ID and nonce, even the scrambling of the reader's nonce remained the same. That suggested that the ID number and nonce, XORed together, fed into the LFSR, marching in from the right like jurors into a box, presumably to scramble things even more.

Oddly, instead of 32-bit IDs and nonces, the reader would also accept ones 48 bits long. That flaw meant that researchers could set all the bits in the LFSR. It also meant that they could feel out the filter function by changing the bits one by one while keeping everything else the same. "Basically, we could choose the input of the filter function and also tell what comes out," says Peter van Rossum, an assistant professor at Radboud. "If you stare at it long enough, you can figure out what [the function] is."

Knowing the filter, the researchers needed only the initial 48-bit setting of the LFSR—the key—to calculating the appropriate key stream. Verdult found that if a card didn't reply to a reader's challenge, then the reader sent a 32-bit "halt" command, but it would scramble it. That was a blunder because hackers could strip out the easily guessed message to get the 32-bit stretch of key stream that scrambles it. The team found a way to snare 32 more bits as well.

In principle, the Radboud hackers were done. If they fed a reader a valid ID and any old nonce, it would reveal 64 bits of key stream. From those bits they could work backward to find the 48-bit key and then generate the entire key stream. In practice, that calculation would take months. Then Ronny Wichers Schreur, a 42-year-old doctoral student at Radboud, noticed that only every other bit of the LFSR feeds into the filter function. That meant the odd and even bits of the key stream could be treated separately, slicing one huge problem into two far smaller ones that could be solved within a second.

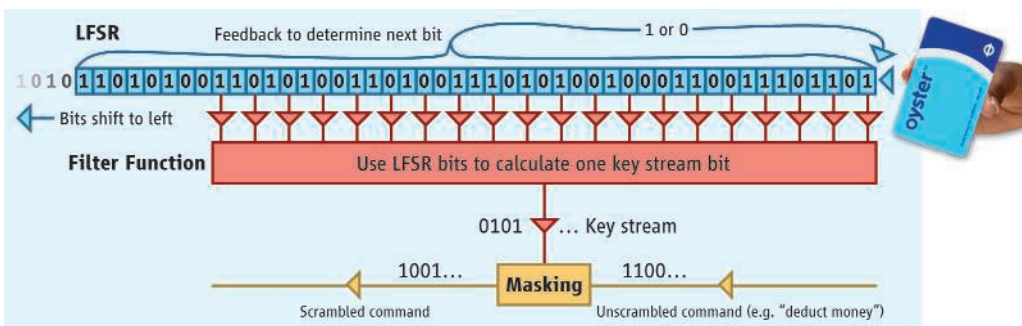

Scramble. As bits step through the LFSR, some feed the filter function, which makes the key stream used to scramble messages. A card's ID feeds into the LFSR, but that lets hackers control its bits.

To prove the system had been broken, three members of the team went to London to take a free subway ride. Using de Koning Gans's device, they sensed the ID number of an Oyster Card and fed it into a turnstile to get the card's key. Back in their hotel room, they loaded the key into a reader they'd bought for a few hundred euros and then recharged the card at will. At Radboud, they filmed themselves using a similar approach to clone a passerby's building-access card.

An unscrambled "Halt!" message

Group-leader Jacobs knew that cracking the system was "immediately a matter of national security." On Friday, 7 March, he told university officials, who immediately informed the Dutch government. The next day, two agents from AIVD, the Dutch secret service, showed up. On Sunday, the researchers alerted NXP. They planned to keep quiet until they could publish, giving NXP time to address the problem. But on 12 March, the Netherlands' Minister of the Interior, Guusje ter Horst, announced that the system had been compromised. In a press conference that day, the researchers promised not to divulge the hack's details until autumn.

NXP wanted them hushed for far longer. In June, it sued to stop publication, arguing that it would violate the company's copyrights and damage the company and its clients. The university had to fight back, says Roelof de Wijkerslooth de Weerdesteyn, president of the executive board of Radboud: "It is the responsibility of scientists to go for the truth and to publish the truth."

The Dutch court agreed. On 18 July in the district court of Arnhem, Judge R.J.B. Boonekamp found that NXP couldn't claim copyright to a design it had kept secret and that the company hadn't shown that publication would cause enough damage to warrant limiting the scientists' freedom of expression.

On 6 October, at the European Symposium on Research in Computer Security in Málaga, Spain, Garcia presented the team's work, delivering a paper rich in conceptual detail but short on how-to pointers for hackers. Nevertheless, by month's end, anonymous hackers had posted on the Web a computer program for attacking MIFARE Classic readers.

Bruce Schneier, a security technologist in Minneapolis, Minnesota, says that NXP created its own problems by ignoring a key principle of cryptography: Good systems use designs that are so hard to crack that the details can be made public. "Only very bad systems rely on secrecy," Schneier says. NXP has apparently taken that lesson begrudgingly to heart: While continuing to market the MIFARE Classic, it has introduced a new RFID card system that uses a public design. **–ADRIAN CHO**

CREDIT: TRANSPORT FOR LONDON 2005

Hoping for fusion 1328

Learning to teach 1330

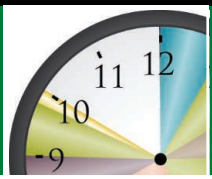

LETTERS

edited by Jennifer Sills

The Price of Exploration

NASA IS IN THE FINAL THROES OF IMPLEMENTING THE MOST POWERFUL SURFACE RECONnaissance mission ever undertaken to Mars. Dubbed the Mars Science Laboratory (MSL), it represents NASA's first life inference mission equipped with instruments capable of detecting the chemical building blocks of life more than an order of magnitude more sensitive than those used by the Viking mission of the 1970s. MSL will also demonstrate multiple technical capabilities needed to enable a future robotic Mars sample return mission.

In his 31 October Letter ("Viewing NASA's Mars budget with resignation," p. 672), former NASA Associate Administrator S. A. Stern suggested that excessive cost growth of MSL is deeply damaging NASA's overall planetary exploration agenda and destroying the opportunity for a future Mars sample return mission. He blames senior NASA leaders for disbanding his MSL independent technical review team, which he claims forced his resignation.

Let's roll. Wheels have been fitted to NASA's Mars Science Laboratory (MSL) rover, which is being assembled at NASA's Jet Propulsion Laboratory, Pasadena, California. The rover has a ground clearance of about 60 cm, or 2 feet, and is about the size of a small automobile.

Now is the time to set the record straight. NASA consolidated its independent standing review boards to streamline the process for all major flight programs in 2007. The MSL Standing Review Board remains in effect and was never disbanded.

Stern also claims that MSL was "assigned" a cost level of $650 million. He fails to mention when and by whom. The $650 million cost was a placeholder assigned to a medium-class Mars rover mission by the National Research Council Solar System Decadal Survey committee in 2002, before NASA had developed a basis of cost estimate for MSL. This served as input to NASA studies from 2000 to 2004 to fully define the MSL mission and culminated in the competitive selection of its science payload in late 2004.

At that time, the overall mission was baselined at a cost of $1.4 billion, not including several costs associated with the radioisotope power system. Given the experience with the cost of the Mars Exploration Rovers and the increased scientific and technical scope of the MSL mission, the so-called assigned value of $650 million is not credible. Stern's own New Horizons flyby mission to Pluto cost NASA more than $650 million; it is unrealistic to expect that a 700-kg analytical laboratory that must soft-land on Mars and drive around with 100 kg of scientific instruments could possibly cost less than a planetary flyby mission.

Indeed, MSL's 2 years of intensive surface science operations are difficult to compare to any missions in the $650 million price class given typical science-per-dollar metrics. The established NASA cost to implement MSL as of the time of its confirmation review was $1.55 billion (August 2006), which grew due to NASA-wide issues with thermal protection system materials in 2007 to approximately $1.7 billion. The total cost growth of the MSL mission development since NASA confirmed the mission is typical of other Mars exploration missions successfully flown over the past decade. The cost to fly MSL in 2009 will be less than the cost (in today's dollars) of flying a nonmobile Viking Lander laboratory to Mars, and MSL includes a whole new generation of instruments and mobility.

NASA has an exemplary record of honoring its commitments to implement flagship-class missions that frequently "rewrite the textbooks" as they discover how the universe operates. To abandon MSL at this time would represent an unprecedented break with this guiding philosophy. As President John F. Kennedy once stated, we choose to do these things not because they are easy, but because they are hard. NASA succeeded with Apollo to the Moon, Hubble to the universe, and Cassini to Saturn. The agency is ready now to assault the martian frontier with MSL.

JAMES. B. GARVIN

Sciences and Exploration Directorate, NASA Goddard Space Flight Center, Greenbelt, MD 20771, USA. E-mail: james.b.garvin@nasa.gov

Note

1. The author is the former NASA Chief Scientist for Mars Exploration, NASA Headquarters, 2000 to 2005.

Research Funding: Less Should Be More

THE POLICY FORUM "STRUCTURAL DISEQUIlibria in biomedical research" by M. S. Teitelbaum (1 August, p. 644) discussed structural problems in U.S. biomedical research funding, particularly NIH funding, but neglected to mention one of the most perverse structural problems in the system: Scientists are incentivized to secure as much

CREDIT: NASA/JPL

Published by AAAS

Glimpsing demons

1334

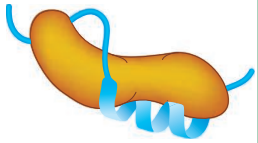

Controlling intrinsic disorder

1340

funding as possible for their work, irrespective of whether an increase in funding leads to a proportionate increase in productivity.

The problem can be illustrated by a simple comparison. Suppose a pharmaceutical company has hired two researchers to run two new research labs. After 6 years, both researchers are evaluated and both have been similarly productive in terms of papers, patents, and new drugs in the pipeline. However, one researcher has sustained this productivity with a modest budget of $800,000 per year, whereas the other has constantly requested funds from the company for more equipment, more technicians, and more resources and now spends $3 million per year of the company's money. Which researcher is the company more likely to reward and promote to a position of greater responsibility?

Now, let's switch to a research university or medical school and talk about two assistant professors who, at the end of 6 years, have been similarly productive in terms of papers and other achievements. One has done so with a single RO1, whereas the other has managed to secure three major grants. Which assistant professor will the deans and administrators be more enthusiastic about promoting and rewarding with raises, endowed chairs, and other perks?

The discrepancy between the financial priorities in these two settings is no mystery. At the company, the funding for research comes out of the company's pocket, and it has an interest in encouraging economic efficiency in scientific output. At the university or medical school, the funding comes from outside the institution, and there is an interest in maximizing the money secured for research, irrespective of its effect on actual productivity.

Even if the academic research model is self-correcting in the long run, would it not be more economically efficient in the first place to eliminate the incentives to secure funding over and above what a scientist feels he can most effectively use?

How can we remove these incentives? There must be a change in culture. No prestige should be attached to the level of funding that an investigator has managed to secure. The most basic of truths must be emphasized: Money is a means, not an end. We do not do science to get money. We get money to do science. Funding cannot be a measure of productivity, because scientists do not produce research dollars. Research dollars are produced by taxpayers (and to a lesser extent by philanthropists and charitable individuals). The amount of money spent by a researcher is not a measure of his productivity, but of his consumption, and might even be counted on the negative side of the ledger when he is evaluated.

RUI SOUSA

Department of Biochemistry, University of Texas Health Science Center, San Antonio, TX 78229–3900, USA. E-mail: sousa@biochem.uthscsa.edu

Cell Phone and DNA Story Overlooked Studies

IN HER WIDELY CITED NEWS OF THE WEEK story "Fraud charges cast doubt on claims of DNA damage from cell phone fields" (29 August, p. 1144), G. Vogel writes, "The only two peer-reviewed scientific papers showing that electromagnetic fields (EMFs) from cell phones can cause DNA breakage are at the center of a misconduct controversy at the Medical University of Vienna." Notwithstanding the allegations on both sides of the fence in this unresolved controversy, Vogel's opening comment and the title of her article are misleading. In fact, there are many other peer-reviewed papers from laboratories in at least seven countries, including the United States, showing that cell phone or similar low-intensity EMFs can break DNA or modulate it structurally [e.g., (*1*–*9*)].

VINI G. KHURANA

Department of Neurosurgery, The Canberra Hospital, Australian National University, Canberra, ACT, Australia. E-mail: vgkhurana@gmail.com

References

1. R. J. Aitken, L. E. Bennetts, D. Sawyer, A. M. Wiklendt, B. V. King, *Int. J. Androl*. **28**, 171 (2005).
2. W. Baohong *et al*., *Toxicology* **232**, 311 (2007).
3. J. Y. Kim *et al*., *Environ. Toxicol*. **23**, 319 (2008).
4. H. Lai, N. P. Singh, *Int. J. Radiat. Biol*. **69**, 513 (1996).
5. S. Lixia *et al*., *Mutat. Res*. **602**, 135 (2006).
6. R. Paulraj, J. Behari, *Mutat. Res*. **596**, 76 (2006).
7. J. L. Phillips *et al*., *Bioelectrochem. Bioenerget*. **45**, 103 (1998).
8. T. Nikolova *et al*., *FASEB J*. **19**, 1686 (2005).
9. M. Mashevich *et al*., *Bioelectromagnetics* **24**, 82 (2003).

Letters to the Editor

Letters (~300 words) discuss material published in *Science* in the previous 3 months or issues of general interest. They can be submitted through the Web (www.submit2science.org) or by regular mail (1200 New York Ave., NW, Washington, DC 20005, USA). Letters are not acknowledged upon receipt, nor are authors generally consulted before publication. Whether published in full or in part, letters are subject to editing for clarity and space.

Response

MY INTENTION WAS NOT TO IMPLY THAT THERE were only two papers showing any effects of EMFs. There are many publications that show effects of EMFs on DNA, but the citations listed here do not directly contradict the quoted sentence. Some see an effect in combination with other known agents that damage DNA. One finds an effect of microwaves, but in the range of microwave ovens and wireless LANs, not cell phones. Others look at DNA damage (for example, chromosome duplications), but not breakage. Several show mixed results: One finds a decrease in DNA breaks in three sets of exposed cells and an increase in one. Since the story was published, however, I have been made aware of a paper by Yao *et al*. (*1*), which also reported single-strand DNA breaks caused by EMFs equivalent to those from cell phones. I regret any misunderstanding the sentence caused.

GRETCHEN VOGEL

Reference

1. K. Yao *et al*., *Mol. Vision* **14**, 964 (2008).

Flaunting the Feminine Side of Research Studies

BIOLOGICAL DIFFERENCES BETWEEN WOMEN and men exist in the prevalence, presentation, and response to treatment for many diseases. In 2001, the Institute of Medicine confirmed that sex is a vital variable that should be considered when designing and analyzing studies at all levels of biomedical research (*1*). To appropriately evaluate the success of women's representation in clinical trials, we must focus on the inclusion of women (and men) in studies of conditions that affect both sexes. Discussions of raw counts of overall research participation and inclusion of single-sex studies hide the fact that women's inclusion still lags in some key areas, despite the recent gains reported by C. Holden in the News story "Women abound in NIH trials" (Special Section on Clinical

Trials and Tribulations, 10 October, p. 219).

Recently, a 2008 review of National Heart, Lung, and Blood Institute (NHLBI)–funded cardiovascular disease (CVD) randomized controlled clinical trials from 1997 to 2006 found that women were underrepresented based on general population incidence as reported by the American Heart Association's Heart Disease and Stroke Statistics report. "The mean percent of women enrolled in all trials was 27% versus 53% of all patients with CVD who are women" (*2*).

Moreover, studies that include similar numbers of men and women rarely analyze or report the results by sex (*3*). This hampers our ability to understand the differences between men and women and to use this knowledge to improve health care outcomes.

PHYLLIS GREENBERGER

Society for Women's Health Research, 1025 Connecticut Avenue, N.W., Washington, DC 20002, USA. E-mail: phyllis@womenshealthresearch.org

References

1. Institute of Medicine of the National Academies, *Exploring the Biological Contributions to Human Health: Does Sex Matter?* (www.iom.edu/CMS/3740/5437.aspx).
2. E. S. H. Kim *et al.*, *J. Am. Coll. Cardiol.* **52**, 672 (2008).
3. L. A. Blauwet *et al.*, *Mayo Clin. Proc.* **82**, 166 (2007).

CORRECTIONS AND CLARIFICATIONS

This Week in *Science*: "Oxygen torn apart" (14 November, p. 1021). In the fourth sentence, O^{2+} should have been O_2^+. The HTML version has been corrected.

Special Section on Genetics of Behavior: News: "Wanted: Math gene" by C. Holden (7 November, p. 894). The link between the *CHRM2* gene and IQ was incorrectly represented. That link was first established by Danielle Posthuma and colleagues at Vrije University, Amsterdam, in 2006 and reconfirmed in follow-up studies. The work by Danielle Dick replicated those findings.

TECHNICAL COMMENT ABSTRACTS

COMMENT ON "Climate-Driven Ecosystem Succession in the Sahara: The Past 6000 Years"

Victor Brovkin and Martin Claussen

Kröpelin *et al.* (Research Articles, 9 May 2008, p. 765) interpreted a sediment record from Lake Yoa in the east-central part of North Africa as support for a weak biogeophysical climate-vegetation feedback in the Sahara during the mid-Holocene. We argue that the new data do not invalidate earlier modeling results on strong land-atmosphere coupling in the Western Sahara for which the Lake Yoa record is far less representative.

Full text at www.sciencemag.org/cgi/content/full/322/5906/1326b

RESPONSE TO COMMENT ON "Climate-Driven Ecosystem Succession in the Sahara: The Past 6000 Years"

S. Kröpelin, D. Verschuren, A.-M. Lézine

The Lake Yoa record and archaeological data provide adequate evidence that mid-Holocene aridification did not occur abruptly across all of North Africa. Modeling results on the issue of abrupt versus gradual desiccation of the Sahara are sufficiently diverse that paleoecological data from a continuous natural archive can usefully guide the evaluation of model parameters responsible for this diversity.

Full text at www.sciencemag.org/cgi/content/full/322/5906/1326c

Comment on "Climate-Driven Ecosystem Succession in the Sahara: The Past 6000 Years"

Victor Brovkin[1]* and Martin Claussen[1,2]

Kröpelin *et al.* (Research Articles, 9 May 2008, p. 765) interpreted a sediment record from Lake Yoa in the east-central part of North Africa as support for a weak biogeophysical climate-vegetation feedback in the Sahara during the mid-Holocene. We argue that the new data do not invalidate earlier modeling results on strong land-atmosphere coupling in the Western Sahara for which the Lake Yoa record is far less representative.

Abrupt climate changes in the past provide invaluable insights on rapid climate dynamics in the future. The climate system is full of numerous feedbacks between different system components, such as vegetation and atmosphere, and North Africa might be one of the important tipping points in the system (*1*). That is why a question about the abruptness of past changes in this region requires detailed investigation.

Kröpelin *et al.* (*2*) presented fascinating details of desiccation of the east-central part of North Africa over the past 6000 years. Although we acknowledge the progress in paleoclimatic reconstruction, we disagree with some of the authors' conclusions. Kröpelin *et al.* state that their data imply a "disagreement with modeling results indicating abrupt mid-Holocene vegetation collapse," suggesting "that the implicated biogeophysical climate-vegetation feedback may have been relatively weak." We argue that the new data do not invalidate earlier hypotheses and modeling results (*3*–*6*).

The proposed biogeophysical feedback between vegetation cover and precipitation in the Sahara (e.g., *5*–*7*) operates through modification of surface albedo (a fraction of solar irradiation reflected back to space) and moisture recycling in the presence of plants. In North Africa, the difference in albedo values between vegetated surfaces and desert can be particularly large, with bare ground albedo values exceeding 0.5 in some areas (*8*, *9*). Vegetated surface traps more solar irradiation and warms the air column over land. Elevated temperature contrast between the land and adjusted ocean leads to an intensification of the regional atmospheric circulation, which results in more rainfall. As shown in modeling studies by Claussen and Gayler (*4*) and Renssen *et al.* (*3*), the biogeophysical feedback is most relevant for the Western Sahara (Fig. 1). The eastward increase in aridity in mid-Holocene Sahara is supported by geological data. Although sparsely distributed pollen records reveal that a large part of the Sahara in the mid-Holocene was covered with steppe or xerophytic shrubs (*10*), some reconstructions suggest that the western part of the Sahara was more humid than its eastern part (*11*).

The first computer simulation of transient Holocene dynamics of the Sahara was undertaken by using the CLIMBER-2 model (*12*) which does not resolve any difference between the western and the eastern part of the Sahara. In this simulation, the transition from a "green" to a barren Sahara took place within several hundred years about 5000 years before the present (yr B.P.) at a much faster pace than the driving force of changes in summer insolation. The geological records of dust transport into the North Atlantic (*13*) exhibit an even faster transition from weak to strong dust flux around 5500 yr B.P. Certainly, the dust records should be interpreted with care because the abrupt change in the dust depositions may reflect not only a decrease in vegetation cover but also an increase in the source area of the dust caused by lake desiccations.

Later model results about abruptness of North African vegetation changes in mid-Holocene give a more mixed picture. In the transient simulation with the ECBILT-CLIO-VECODE model (*3*), high climate variability masked out the abrupt climate changes in the Western Sahara. However, increased climate instability about 6000 yr B.P. was interpreted as a system shift from moist to dry regime. Liu *et al.* (*14*) used another fast climate-vegetation model, FOAM-LPJ, and found the abrupt changes not in the western but in the eastern part of the Sahara (Fig. 1), although the later results do not seem to be supported by the Lake Yoa record (*2*). Abrupt vegetation changes in the Eastern Sahara simulated by FOAM-LPJ (*14*) are associated not with the strong biogeophysical feedback but with a nonlinear response of

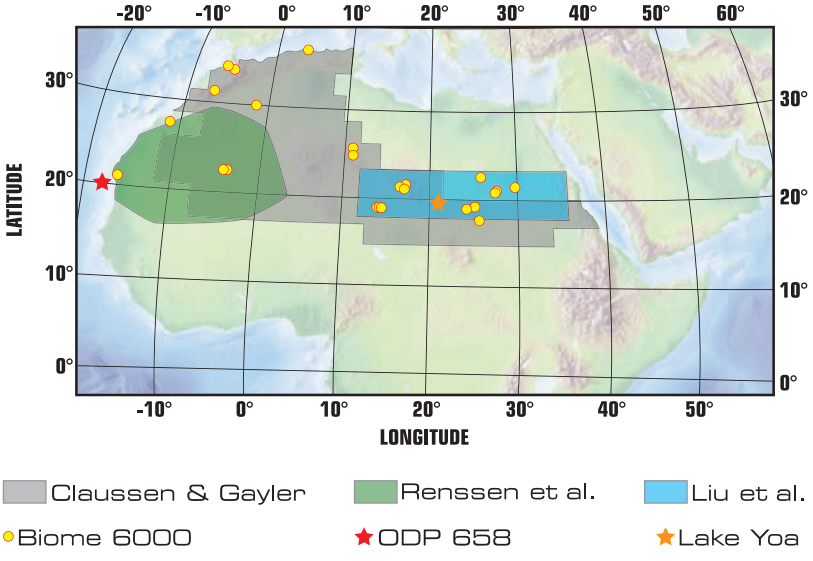

Fig. 1. Simulated difference between mid-Holocene and present-day vegetation cover, revealing changes mainly in the Western part of the Sahara, the focus of earlier hypotheses of abrupt ecosystem change in the Sahara. Gray shading indicates changes from mid-Holocene vegetated state to present-day desert (*4*); the green shaded area has more than 30% reduction in vegetation cover during the Holocene (*3*). A strong positive biogeophysical feedback between vegetation cover and precipitation in the Western Sahara found in (*3*, *4*) may result in an abrupt shift from wet to dry regime. The blue shaded area indicates the area of abrupt vegetation changes attributed to a nonlinear response of vegetation to precipitation from simulation by Liu *et al.* (*14*). The stars indicate the position of Lake Yoa (19.03°N, 20.31°E) and Ocean Drilling Program site 658C (20.45°N, 18.35°W). The record from Lake Yoa does not seem to show evidence of abrupt ecosystem transitions (*2*), whereas the marine sediment core reveals an abrupt change in dust transport from the continent (*13*). Yellow circles indicate sites with mid-Holocene steppes or xerophytic shrubs from the BIOME-6000 database (*10*).

[1]Max Planck Institute for Meteorology, Bundesstraße 55, 20146 Hamburg, Germany. [2]Meteorological Institute, University of Hamburg, Bundesstraße 55, 20146 Hamburg, Germany.

*To whom correspondence should be addressed. E-mail: victor.brovkin@zmaw.de

vegetation cover to precipitation. In contrast, model studies (*3*, *4*) that simulate mid-Holocene expansion of vegetation cover into the Western Sahara (Fig. 1) attribute a substantial part of this expansion to the strong coupling between land and atmosphere. Detailed understanding of model differences regarding the strength of biogeophysical feedback requires further investigation.

In conclusion, the jury is still out on the invalidation of the earlier assertion of abrupt ecosystem changes in the Sahara. To prove or falsify the hypothesis on abrupt changes in the Western Sahara, a convincing summary of terrestrial paleoclimatic records from this region has to be presented. Until then, the conclusion of Kröpelin *et al*. (*2*) on weak biogeophysical feedback is not justified in general.

References

1. M. Scheffer, S. Carpenter, J. A. Foley, C. Folke, B. Walker, *Nature* **413**, 591 (2001).
2. S. Kröpelin *et al*., *Science* **320**, 765 (2008).
3. H. Renssen, V. Brovkin, T. Fichefet, H. Goosse, *Geophys. Res. Lett.* **30**, 1061 (2003).
4. M. Claussen, V. Gayler, *Glob. Ecol. Biogeogr.* **6**, 369 (1997).
5. J. G. Charney, *Q. J. R. Meteorol. Soc.* **101**, 193 (1975).
6. V. Brovkin, M. Claussen, V. Petoukhov, A. Ganopolski, *J. Geophys. Res. Atmos.* **103**, 31613 (1998).
7. M. Claussen, *Clim. Dyn.* **13**, 247 (1997).
8. W. Knorr, K. G. Schnitzler, Y. Govaerts, *Geophys. Res. Lett.* **28**, 3489 (2001).
9. E. A. Tsvetsinskaya *et al*., *Geophys. Res. Lett.* **29**, 1353 (2002).
10. D. Jolly *et al*., *J. Biogeogr.* **25**, 1007 (1998).
11. H.-J. Pachur, P. Hoelzmann, *J. Afr. Earth Sci.* **30**, 929 (2000).
12. M. Claussen *et al*., *Geophys. Res. Lett.* **26**, 2037 (1999).
13. P. deMenocal *et al*., *Quat. Sci. Rev.* **19**, 347 (2000).
14. Z. Liu *et al*., *Quat. Sci. Rev.* **26**, 1818 (2007).

17 July 2008; accepted 30 October 2008
10.1126/science.1163381

Response to Comment on "Climate-Driven Ecosystem Succession in the Sahara: The Past 6000 Years"

S. Kröpelin,[1]* D. Verschuren,[2] A.-M. Lézine[3]

The Lake Yoa record and archaeological data provide adequate evidence that mid-Holocene aridification did not occur abruptly across all of North Africa. Modeling results on the issue of abrupt versus gradual desiccation of the Sahara are sufficiently diverse that paleoecological data from a continuous natural archive can usefully guide the evaluation of model parameters responsible for this diversity.

We thank Brovkin and Claussen (*1*) for their insightful comment and the opportunity to clarify our findings (*2*). We agree with the authors to the point that our reconstruction of gradual desiccation of the terrestrial ecosystem in the east-central Sahara does not necessarily imply weak biogeophysical feedback in the western Sahara and that land-atmosphere and/or atmosphere-vegetation interactions there may have been sufficiently different to have resulted in a distinct regional trajectory of mid-Holocene desiccation. The principal objective of our study (*2*) was to correct the popular notion (e.g., *3*–*6*) that the iconic record of Saharan dust deposition in marine sediments off the Mauritanian coast (*7*) represents Holocene landscape evolution across North Africa, including the central and eastern Sahara, and that climate-modeling results (*8*) supposedly support this exaggerated viewpoint.

We consider our paleoecological record from northern Chad to be representative for a sizable portion of the central and eastern Sahara (*2*). The conclusions of our study are consistent with the regional chronologies of multi-indicator archaeological evidence from shifting prehistoric occupation sites in the Egyptian and Sudanese Sahara, which similarly suggest a continuous southward retreat of monsoonal rainfall causing gradual environmental deterioration during the middle Holocene (*9*), notwithstanding transitory climatic perturbations that are a common feature of all desert margins.

We are aware of the moisture gradient between the western and eastern parts of the Sahara that is treated as such in recent climate-vegetation simulations (e.g., *10*–*12*). However, some state-of-the-art general circulation climate models (*13*) have suggested that landscape desiccation was gradual in both the eastern and western Sahara, consistent with our reconstruction, whereas other experiments with similar models (*11*, *14*) simulated mid-Holocene vegetation collapse exactly for the region where Lake Yoa is located [blue shaded area in figure 1 in (*1*)]. Also, the mechanisms considered responsible for abrupt vegetation changes observed in various model output are diverse: a positive vegetation-climate feedback due to modification of surface albedo (*15*, *16*), a threshold response of vegetation to particular modes of climate variability (*14*), microscale vegetation-soil feedback (*12*, *17*), or a transition from negative to positive vegetation-climate feedback at increasing time scales (*18*). Clearly, modeling results on the issue of abrupt versus gradual desiccation of the Sahara are sufficiently diverse that paleoecological data from a continuous natural archive (*2*) can usefully guide the evaluation of model parameters responsible for this diversity.

We subscribe to the caution formulated by Brovkin and Claussen (*1*) about the inferred rapidity of the mid-Holocene transition from a "green" to a barren Sahara recorded in the Ocean Drilling Program site 658 sediment sequence (*7*). Here we agree with Holmes (*19*) that the abrupt increase in dust flux at that location may be partly due to the relatively sudden desiccation of one or more large and shallow lake basins in the source area of dust delivered to the Atlantic Ocean offshore Mauritania; today this is mostly northern Mauritania and central Algeria. However, we are less optimistic than Brovkin and Claussen that a new summary of terrestrial climate-proxy records from the western Sahara will conclusively resolve the issue of whether ecosystem changes there were gradual or abrupt. All known depositional sequences from the region are incomplete over the critical time interval, and a continuous and high-quality paleoenvironmental archive comparable to the Lake Yoa sequence is unlikely to be found.

[1]Africa Research Unit, Institute of Prehistoric Archaeology, University of Cologne, Jennerstraße 8, D-50823 Köln, Germany. [2]Limnology Unit, Department of Biology, Ghent University, K. L. Ledeganckstraat 35, B-9000 Ghent, Belgium. [3]Laboratoire des Sciences du Climat et de l'Environnement, Unité mixte de recherche 1572, CNRS-CEA-UVSQ, L'Orme des Merisiers, F-91191 Gif-Sur-Yvette, France.

*To whom correspondence should be addressed. E-mail: s.kroe@uni-koeln.de

References

1. V. Brovkin, M. Claussen, *Science* **322**, 1326 (2008); www.sciencemag.org/cgi/content/full/322/5906/1326b.
2. S. Kröpelin *et al.*, *Science* **320**, 765 (2008).
3. M. Scheffer, S. Carpenter, J. A. Foley, C. Folke, B. Walker, *Nature* **413**, 591 (2001).
4. J. A. Foley, M. T. Coe, M. Scheffer, G. L. Wang, *Ecosystems (N.Y., Print)* **6**, 524 (2003).
5. J. A. Rial *et al.*, *Clim. Change* **65**, 11 (2004).
6. T. M. Lenton *et al.*, *Proc. Natl. Acad. Sci. U.S.A.* **105**, 1786 (2008).
7. P. deMenocal *et al.*, *Quat. Sci. Rev.* **19**, 347 (2000).
8. M. Claussen *et al.*, *Geophys. Res. Lett.* **26**, 2037 (1999).
9. R. Kuper, S. Kröpelin, *Science* **313**, 803 (2006).
10. H. Renssen, V. Brovkin, T. Fichefet, H. Goosse, *Geophys. Res. Lett.* **30**, 1184 (2003).
11. Z. Liu *et al.*, *Quat. Sci. Rev.* **26**, 1818 (2007).
12. R. H. H. Janssen *et al.*, *Glob. Change Biol.* **14**, 1104 (2008).
13. P. Braconnot *et al.*, *Clim. Past* **3**, 279 (2007).
14. Z. Liu *et al.*, *Geophys. Res. Lett.* **33**, L22709 (2006).
15. V. Brovkin, M. Claussen, V. Petoukhov, A. Ganopolski, *J. Geophys. Res. Atmos.* **103**, 31613 (1998).
16. M. Claussen, *Clim. Dyn.* **13**, 247 (1997).
17. M. Scheffer, M. Holmgren, V. Brovkin, M. Claussen, *Glob. Change Biol.* **11**, 1003 (2005).
18. Y. Wang *et al.*, *Clim. Past* **4**, 59 (2008).
19. J. A. Holmes, *Science* **320**, 752 (2008).

8 August 2008; accepted 31 October 2008
10.1126/science.1163483

EVOLUTION

All for One and One for All

James H. Hunt

Few scientists win a Pulitzer Prize. In 1991, Bert Hölldobler and Edward O. Wilson did for their magisterial *The Ants* (*1*). Now these distinguished collaborators offer *The Superorganism: The Beauty, Elegance, and Strangeness of Insect Societies*. In this ambitious book, they seemingly have three goals. Hölldobler and Wilson reprise and update themes from *The Ants* while broadening their survey to include other social insects (most notably honeybees). In a thread woven throughout the narrative, they argue that colonies of social insects should be seen and studied as superorganisms, a naturally selected level of organization a step above individual organisms. And they present the work in a format apparently intended to attract the broadest possible readership of both specialists and nonspecialists. This suggests the authors' probable primary motivation—they are advocating a conceptual framework for understanding insect sociality that has been out of favor for four decades.

Hölldobler and Wilson begin by updating the superorganism concept. They hold that "[t]he principal target of natural selection in the social evolution of insects is the colony, while the unit of selection is the gene." They then treat this claim in detail through a historical and theoretical dissection of gene-centered, altruistic worker–centered, and colony-centered perspectives along with the controversies, sometimes heated, that have accompanied them. They seek synthesis under the umbrella of multilevel selection, which Wilson and David Sloan Wilson have recently advocated in general and specialist articles (*2, 3*). Ensuing chapters address the "sociogenesis" of colonies and two main organizing principles for social insect colonies, division of labor and communication. Several chapters on ants, the forte of both authors, round out the book. Each chapter after the introduction is a stand-alone review of its topic, rich in content and sometimes daunting in detail. The chapter on ponerine ants, in particular, exemplifies the quantity, quality, and diversity of research on ants during the past two decades.

Numerous color photographs and original drawings illustrate interesting behaviors and traits, making the book enjoyable to page through and inviting to general readers. Literature citations appear as footnotes, which may be reader-friendly but results in the repetition of individual references (sometimes even more than once on a page). A glossary covers much, but not all, of the technical jargon. Even so, one wonders whether many general readers will make it through the long chapter on communication, much less through the book as a whole.

Ultimately, the book will be judged by its success in advancing the perspective that natural selection acts on social insects more strongly at the colony level than at the levels of individual organisms or genes. Most readers will be convinced of the clarity that the superorganism concept brings to an understanding of honeybees and behaviorally advanced ants. Some readers will remain skeptical, however, that the superorganism concept sheds much light on the origin, rather than elaboration, of sociality.

An intriguing aspect of the book is hinted at in the introduction, made apparent in the discussion of genetic social evolution, and finally explicitly acknowledged in the penultimate chapter: the co-authors disagree on which social insect colonies should be called superorganisms. Wilson favors broad application of the concept, beginning with the origin of sociality, whereas Hölldobler holds an individual-centered view of the origin of sociality and reserves the superorganism concept for species that have passed the "point of no return" marked by obligately sterile workers (*4*). Perhaps this disagreement would have been resolved if the authors had given greater attention to social insects such as termites, sweat bees, and wasps—all of which offer more promising pathways to enlighten the origins of social behavior than do ants or honeybees. Indeed, in several of the few places where research on wasps is sketchily described, that research is mischaracterized or incorrectly cited. Thus, the book is not a comprehensive review of social insects, and it falls short of being a gateway to understanding the origins of insect sociality.

But, let praise be given where it is due. For the focal topics, and especially when ants are featured, the technical reviews are comprehensive and up to date and will be of lasting value. Moreover, it is timely and appropriate that the authors have undertaken to restore the superorganism to the conceptual framework and working lexicon for envisioning and discussing insect sociality. The book doesn't hard-sell the superorganism concept; there is no ringing conclusion at its end, for example. Instead, each case study or discussion topic concludes with a soft-sell assertion that the preceding passage clearly shows natural selection to be acting more strongly at the colony level than on individuals. The detailed contents will entice researchers to repeatedly return to the book. On every visit, they will re-encounter the superorganism message and, in doing so, grow accustomed to and comfortable with it. Our future discourses on insect sociality will thus be improved. *Superorganism* offers a clear and compelling picture showing that, in already-social insects, natural selection acts more strongly on colonies than on individuals to shape the genotypes and phenotypes of a colony's members—thereby giving rise to the sophisticated nest architectures, amazing (and amazingly complex) behaviors, and substantial ecological impacts that are the hallmarks of social insects.

CREDIT: JAMES H. HUNT

Without blueprint or supervision. Social insects, such as these Brazilian wasps (*Polybia emaciata*), construct complex nests by following behavior algorithms that reflect natural selection at the colony level.

The Superorganism
The Beauty, Elegance, and Strangeness of Insect Societies

by Bert Hölldobler and Edward O. Wilson

Norton, New York, 2008. 544 pp. $55, C$60.50, £30. ISBN 9780393067040.

The reviewer is at the Department of Entomology, North Carolina State University, Raleigh, NC 27695, USA. E-mail: jim_hunt@ncsu.edu

References

1. B. Hölldobler, E. O. Wilson, *The Ants* (Harvard Univ. Press, Cambridge, MA, 1990).
2. D. S. Wilson, E. O. Wilson, *Am. Sci.* **96**, 380 (2008).
3. D. S. Wilson, E. O. Wilson, *Q. Rev. Biol.* **82**, 327 (2007).
4. H. K. Reeve, B. Hölldobler, *Proc. Natl. Acad. Sci. U.S.A.* **104**, 9736 (2007).

10.1126/science.1167005

ENERGY

Promising the Sun

Frank N. von Hippel

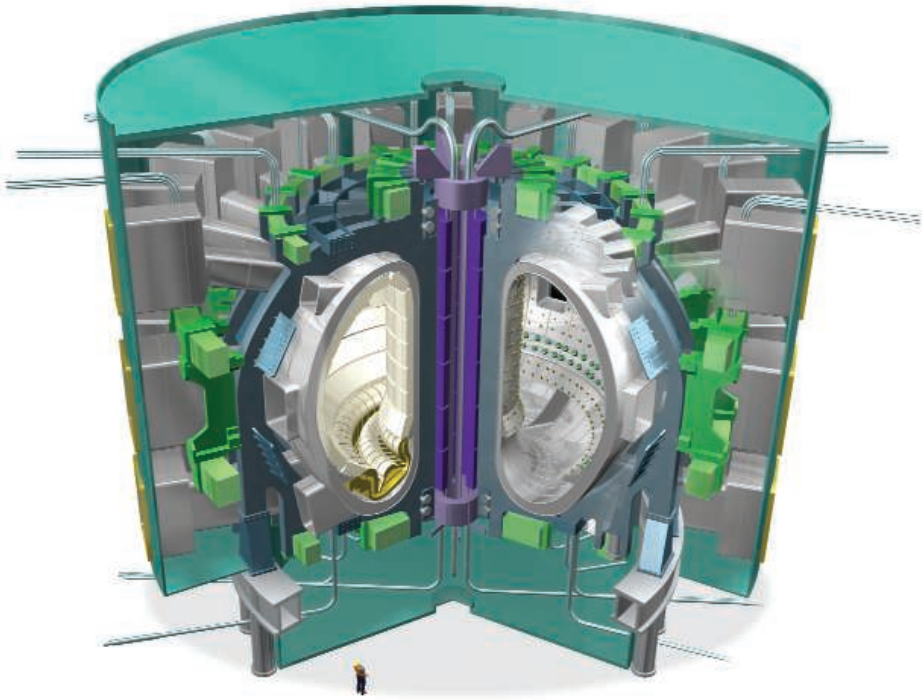

A vessel for hope. An artist's conception ITER, showing magnets and internal components inside the cryostat.

As its subtitle indicates, *Sun in a Bottle* focuses on the historic overoptimism of fusion-energy scientists. Charles Seife offers an interesting and technically mostly correct account, but he covers such a diverse range of case studies that the book does not really hang together.

Seife (a journalism professor at New York University) devotes a third of the book to fusion bombs, a third to the controversies over cold fusion and bubble fusion, and a third to the two approaches to which almost all the fusion-energy effort has gone: magnetic confinement and inertial confinement.

The chapters on fusion bombs describe overoptimistic and obsessive promotions by Edward Teller: first of his original flawed design for a hydrogen bomb and then, during the 1950s, of a bizarre program to use nuclear explosions for such purposes as making canals and harbors and fracturing underground gas-bearing rock. Both stories are well known and Seife adds little new material, but they are worth retelling.

The chapters on cold fusion and bubble fusion contain the most original material. However, they describe primarily the follies of individual scientists and are hardly a basis for indicting the whole field of fusion energy. Seife was a news writer for *Science* when it published the first article claiming to have established experimentally that the high temperatures generated in collapsing bubbles can cause fusion (*1*). Remarkably, Seife's article reporting widespread skepticism about the claims and criticism of *Science*'s editor for publishing them appeared in the same issue (*2*).

Sun in a Bottle
The Strange History of Fusion and the Science of Wishful Thinking

by Charles Seife

Viking (Penguin), New York, 2008. 310 pp. $25.95, C$28.50. ISBN 9780670020331.

Seife discusses the last 30 years of research on magnetic and inertial-confinement fusion (the first a civilian program and the second a spin-off of nuclear-weapons work) in two short chapters. Once again, as he details, the pioneers were overly optimistic. It was much more difficult than they expected to get much more energy out of the fuel than they put in, and researchers have moved to ever bigger and more costly machines.

In the case of magnetic fusion, the focus is now on the proposed 6-billion-euro International Thermonuclear Experimental Reactor (ITER), designed to produce 500 megawatts of fusion thermal power in pulses of several minutes' duration. In the inertial-confinement approach, the $4 billion National Ignition Facility is now nearing completion at the Lawrence Livermore National Laboratory. It will use huge lasers to implode and heat a millimeter-sized pellet of deuterium and tritium (or of plutonium). In addition to research on fusion ignition and energy gain, its primary purposes include studying the properties of nuclear-weapon materials at temperatures and pressures approaching those realized in nuclear explosions.

Seife doesn't see much difference between fusion and fission energy sources. He argues that fusion is saddled with its own radioactive waste problem because neutron transmutation of a fusion reactor's inner lining makes it highly radioactive. He does not find it important that, with proper choice of materials, the half-life of the fusion-induced radioactivity can be limited to decades, while the half-lives of the plutonium and other transuranic elements produced in uranium-fueled power reactors run a thousand times longer. Strangely, in comparing fusion and fission, Seife doesn't even mention reactor safety or nuclear-weapon proliferation. Here, fusion could have qualitative advantages. It does not need or produce any fissile materials, and it could not generate a Chernobyl-scale release of long-lived radioactivity.

It seems unlikely, however, that any of the current approaches to fusion energy will be able to compete economically with fission power as currently practiced in the United States: irradiating low-enriched uranium fuel in water-cooled reactors and then storing the spent fuel indefinitely. The U.S. Department of Energy has advocated a much more expensive approach to fission in which spent fuel would be chemically processed in plants costing tens of billions of dollars and the plutonium and other transuranic elements would be recycled in costly molten-sodium-cooled reactors. Magnetic-confinement fusion might be able to compete in that league—and it would be a lot less worrisome than a system fueled by nuclear-weapons materials. There is no good reason to move away from relatively cheap and proliferation-resistant "once-through" fission, however. There is therefore time to continue to wait and see whether Seife's "wishful thinkers" will finally come up with a viable fusion-energy option.

The reviewer is at the Program on Science and Global Security, Woodrow Wilson School of Public and International Affairs, Princeton University, Princeton, NJ 08542–4601, USA. E-mail: fvhippel@princeton.edu

References

1. R. P. Taleyarkhan *et al.*, *Science* **295**, 1868 (2002).
2. C. Seife, *Science* **295**, 1808 (2002).

10.1126/science.1167754

THE PIPELINE

Scientific Teaching in Practice

A new generation of university scientists is learning to teach using a scientific teaching approach.

Sarah Miller,[1] Christine Pfund,[2] Christine Maidl Pribbenow,[1,3] Jo Handelsman[1]*

The United States educates and trains outstanding scientists. Doctoral students emerge as rigorous experimentalists and strong analytical thinkers, intellectually prepared for the diverse employment opportunities that await them. Problems persist, however, in two areas: preparing undergraduate students as scientists and preparing graduate students to teach (*1*, *2*). Both deficiencies can be addressed by implementing programs that train graduate students to teach. Although there have been repeated calls for such programs (*1*–*3*), and descriptions of some (*4*), little work has assessed their impact on the practices and philosophies of the participants.

In contrast to graduate education, undergraduate science education is based largely on facts rather than analytical thinking. Effective teaching methods based on how people learn are known (*5*, *6*), but are not often applied in undergraduate classrooms. Similarly, graduate students and postdoctoral researchers (postdocs) who will become teachers of undergraduates are not taught how to use these teaching methods. Graduate students and postdocs who learn how to foster scientific curiosity, reasoning, and problem-solving will be prepared to produce a generation of science undergraduates who think scientifically.

Here, we describe a program that trains graduate students and postdocs to practice scientific teaching. Hallmarks of scientific teaching are methods that encourage students to construct new knowledge and to develop scientific ways of thinking, provide both students and instructors with feedback about learning, and foster success for all students. Scientific teaching aims to create classrooms that reflect the true nature of science and promotes teaching as a scholarly endeavor.

The Teaching Fellows Program

At the University of Wisconsin–Madison, we developed the Teaching Fellows Program, which is an 8-week course entitled, "Teaching Biology," followed by development of teaching materials and their implementation in the classroom. Fellows partner with UW-Madison biology instructors to develop teachable units, built on a scientific teaching framework (*5*), that address challenges in the instructors' courses. As they develop their materials in teams of two to three, fellows learn an iterative process of instructional design: develop concrete learning goals, design activities to meet the goals, and revise instruction based on evaluation of progress toward the goals. Peer review and dissemination are embedded in the process. Details about coursework, the teachable-unit design (see table, below) and evaluation rubric, evaluation instruments, and data collected are provided (*7*).

Since 2003, all 63 fellows who have completed the Teaching Fellows Program have been named "Howard Hughes Medical Institute (HHMI) Teaching Fellows." The fellows worked with 21 faculty and staff to create 35 distinct instructional materials for undergraduate biology courses, designed or redesigned two complete courses, created two instructional videos, developed two online learning modules, and produced a series of video podcasts. Collectively, the fellows have used these materials to teach over 1900 undergraduate students in 14 courses (ranging from 15 to 250+ students per course) at UW-Madison.

Here, we report the impact of the Teaching Fellows Program, based on assessment of the 44 fellows who participated between 2004 and 2007 and the 17 teachable units they developed and posted online. These fellows were graduate students (89%) and postdocs (11%) from diverse fields of biology, mostly white (91%), and of both sexes (66% female, 34% male). Most aspired to careers as faculty at small undergraduate colleges (63%) and/or large research universities (31%).

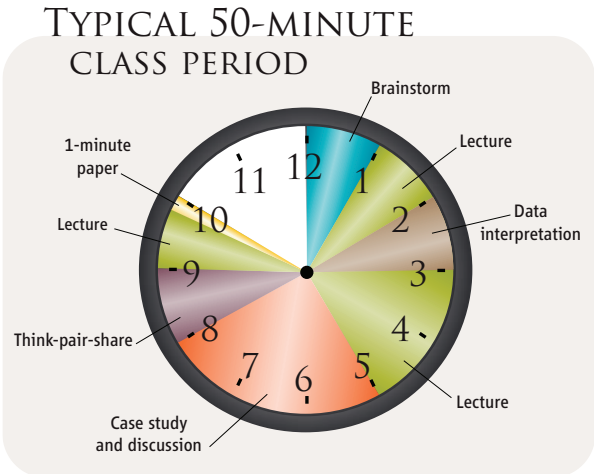

Classroom implementation. Analysis of teachable units developed by fellows for lecture-style classes revealed that 66% of class time was devoted to active learning events.

Examples of Teachable Units

Influenza—active learning exercises in which students learn about virus structure and life cycle; students model the epidemiology of outbreaks of viral diseases based on hypothetical viruses with various quantitative features

The Bacterial Side of the Story—case study in which students learn how horizontal gene transfer, mutations, selection, and human behavior lead to widespread antibiotic resistance

Statistical Tools for Biology—active learning exercises in which students learn how to use statistics to guide experimental design; links to inquiry-based lab experiments on behavior and population biology of *Daphnia magna*

http://scientificteaching.wisc.edu/materials

Assessment Methods

To determine whether and to what extent the fellows put scientific teaching into practice, we used a mixed-methods design (*8*) with both qualitative and quantitative data collection and analysis. We analyzed the materials created by the fellows (teachable units, evaluation reports, publications, and teaching philosophies) and deployed electronic surveys. First, we coded each teachable unit for evidence of active learning and assessment events, statements of diversity considerations, indications of quantitative or reflective approaches to teaching, and inclusion of methods that foster discovery. Examples of active learning included students engaging in small-group discussion; analyzing a case study; and responding to clicker questions, multiple-choice, and conceptual questions that can be answered individually by students with a wireless hand-held device during a lecture. We included as evidence of active learning only instances in which the exercise necessitated engagement of most or all students

[1]Wisconsin Program for Scientific Teaching, Department of Bacteriology, University of Wisconsin–Madison, Madison, WI 53706, USA. [2]Delta Program for Research, Teaching, and Learning, University of Wisconsin–Madison, Madison, WI 53706, USA. [3]Wisconsin Center for Education Research, University of Wisconsin–Madison, Madison, WI 53706, USA.

*Author for correspondence. E-mail: joh@bact.wisc.edu

Published by AAAS

(i.e., not a question posed by the instructor and answered by only one student). Second, we determined how many fellows published papers about their teachable units. Third, fellows completed exit surveys about their level of knowledge and skill before and after (*9*) participating in the Teaching Fellows Program, rating their ability to develop active learning strategies, myriad assessments, and inclusive classrooms.

To assess philosophical aspects of the fellows' approaches to teaching, we analyzed their written teaching philosophy statements and responses to survey questions. We used a teaching philosophy rubric (*10*), adapted to include components of scientific teaching and learner-centered approaches. Statements of teaching philosophy from the beginning of the program (submitted as part of the applications) were compared with those written 9 months later, at the end of the program. In addition, surveys measured the fellows' attitudes after participating in the program. Respondents indicated their level of agreement with statements such as: "I am a good teacher" and "I feel that I am part of a community of scientific teachers." Averages were calculated from responses of three cohorts of fellows.

Evidence of Practice

Fellows created teachable units that devoted, on average, >66% of class time to active learning events (see figure, page 1329). Each class period contained an average of four to five discrete active learning events, and 82% of fellows explained in their written description of the teachable units how the activities served the dual purposes of actively engaging students and assessing their knowledge or skill.

Teaching fellows included teaching methods to reach diverse students. Active learning and assessment events ranged from single clicker questions to multipart case studies; 71% of teachable units accounted for diverse learning styles; and 53% referred to race, ethnicity, culture, gender, socioeconomic issues, or international and/or global contexts. For example, Cloud-Hansen, *et al*. (*11*) stated as a learning goal, "Students will be able to critically analyze information to support a position on a complex and current scientific issue, while also justifying the political and socio-economic impact." No units, however, mentioned accommodating disability (e.g., physical, learning, or psychological) as a way to create inclusive classrooms, although this element of diversity was addressed in "Teaching Biology."

All teachable units described learning goals for one or more content areas; most teachable units (76%) also stated the expectation that students would learn one or more aspects of scientific discovery, such as the scientific method, science as an iterative process based on empirical evidence, historical context of science, group problem-solving, critical thinking, or communication of scientific ideas.

Nearly every teachable unit (94%) included some form of baseline data collection to assess students' prior knowledge or misconceptions; 47% followed up with a post-unit survey to gauge learning gains. Homework assignments and exams typically involved questions that represented multiple levels of understanding from knowledge to evaluation and reflected the established learning goals.

All fellows evaluated learning, and many (41%) generated a report about the results, four of which were published in peer-reviewed journals (*11*–*14*). These publications provide evidence that the undergraduate students who were taught by the teaching fellows gained knowledge in specific subject areas, learned skills in solving complex problems, and retained what they learned months later.

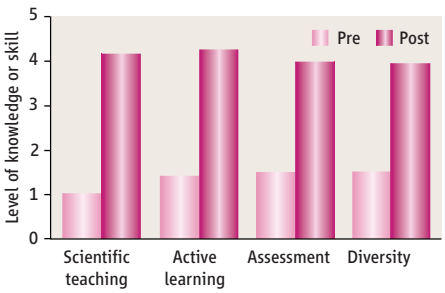

Learning gains for fellows. ($n = 25$; $P < 0.05$.)

Fellows reported significant gains in skill or knowledge for the core elements of scientific teaching. Across all categories, fellows reported an average skill or knowledge level of 1.7 ("low") before and 3.8 ("high") after completing the program (see chart above).

A Philosophy of Scientific Teaching

A comparison of teaching philosophies written before and after participation in the program ($n = 31$), demonstrated a shift in fellows' focus on the teacher to focus on the learner, as evidenced through comments in the philosophies about the responsibility of students for their own learning, the role of the teacher as guide, and the importance and implementation of a variety of teaching methods to facilitate student engagement in learning. For example, using a scale of 1 to 3, the average fellows' score shifted significantly ($P < 0.05$) from a baseline number of 2.0 ("average") to an exit score of 2.5 ("average" to "superior") in the category "View of the Learner," which demonstrated a deeper understanding of the learners and their role in their own classroom success.

An excerpt from a fellow's statement illustrates a typical learner-centered philosophy:

> Although the teacher is present and engaged in the activities, active learning exercises place the learning responsibility into the hands of the student and require that the student come to class prepared to learn. This attitudinal shift alone will enhance learning because the student is ready and willing to participate.

After participating in the program, most survey respondents indicated that scientific teaching is a difficult but worthwhile effort (86%), that they were confident they are good teachers (96%), and that they felt part of a scientific teaching community (96%).

Conclusions

This study indicates that the Teaching Fellows Program effectively trains scientific teachers, as reflected through practice, philosophy, and the products created. Fellows learned the key elements of scientific teaching (active learning, assessment, and diversity) and integrated them into their teaching practices. Fellows acquired a scholarly approach to teaching, developed classrooms that reflect the nature of science, moved from teacher-centered toward student-centered teaching philosophies, and contributed to the development of a community of scientific teachers through partnerships with other instructors, online teaching materials, and peer-reviewed publications.

References and Notes

1. National Research Council, *Bio2010: Transforming Undergraduate Education for Future Research Biologists* (National Academies Press, Washington, DC, 2003).
2. F. J. Rutherford, *Science for All Americans* (Oxford Univ. Press, New York, 1990).
3. J. Handelsman *et al*., *Science* **304**, 521 (2004).
4. D. G. Markowitz, M. J. DuPré, *CBE Life Sci. Educ.* **6**, 233 (2007).
5. J. Handelsman, S. Miller, C. Pfund, *Scientific Teaching* (W. H. Freeman, New York, 2007).
6. National Research Council, *How People Learn* (National Academies Press, Washington, DC, 1999).
7. Materials, methods, and other items are available as supporting material on *Science* Online.
8. J. Creswell, V. L. Plano Clark, *Designing and Conducting Mixed Methods Research* (Sage Publications, Thousand Oaks, CA, 2006).
9. T. C. M. Lam, P. Bengo, *Am. J. Eval.* **24**, 65 (2003).
10. D. J. Schonwetter *et al*., *Int. J. Acad. Dev.* **7**, 1 (2002).
11. K. A. Cloud-Hansen *et al*., *CBE Life Sci. Educ.* **7**, 302 (2008).
12. D. J. Kelley *et al*., *CBE Life Sci. Educ.* **7**, 202 (2008).
13. A. R. Phillips *et al*., *CBE Life Sci. Educ.* **7**, 96 (2008).
14. A. L. Robertson, A. R. Phillips, *CBE Life Sci. Educ.* **7**, 89 (2008).
15. We thank all the teaching fellows and instructors who participated in this study. Supported by HHMI Professors grant and NSF-CCLI grant no. 0618821.

Supporting Online Material

www.sciencemag.org/cgi/content/full/322/5906/1329/DC1

10.1126/science.1166032

ASSESSMENT

Global Sex Differences in Test Score Variability

International testing results show greater variance in boys' scores than in girls' scores.

Stephen Machin[1] and Tuomas Pekkarinen[2]

Do boys and girls differ in their intellectual and cognitive abilities and, if so, in what way? These questions have raised considerable debate, both in terms of average performance and in terms of variability around the average.

Empirical research on gender differences in achievements produces mixed conclusions, with some evidence that favors boys and some that favors girls (*1*–*4*). In many countries, girls show superior performance in school examinations, which is also reflected in higher rates of attendance in tertiary education. In addition, girls have been improving their position relative to boys (*5*, *6*). In countries with a more gender-equal culture, the gender gap that is usually in favor of boys in average mathematics test scores is erased or even reversed in favor of girls (*7*).

At the same time, some research focuses on the notion that there are more males at the upper end of the distributions of educational and professional success (*8*). Oft-cited examples include there being more male than female Nobel Prize winners and the inequity of wages in the labor market in favor of males (*9*, *10*). Studies of talented individuals who succeed at the very highest levels, especially in science, highlight substantial male overrepresentation (*11*).

These outcomes can be generated by various kinds of distributions describing the educational and intellectual make-up of boys and girls. Differences in the gender composition of the high-scoring group can be a consequence of gender differences in the mean or variance of the test scores or both. Given that recent research has shown that gender differences in the mean test scores are not a robust phenomenon internationally (*7*), it is of interest to explore whether the gender differences in the variance of test scores are a more universal outcome.

The idea that males are intellectually and educationally more variable than females dates back a long time and is embedded in cultural history. Early academic entries are represented by late 19th century texts from Ellis (*12*) and Galton (*13*). Modern comment [e.g., (*14*)] can be quite critical of the motives of those who postulate that gender differences in variances exist.

Most of the evidence regarding gender-dependent differences in the mean and variance of intellectual and cognitive abilities is based on U.S. data (*15*, *16*), because most of the data containing test scores are from the United States. But data sources from other countries exist as well. We have therefore investigated whether the phenomenon of "higher variance" is an accurate characterization of boys' educational performance relative to girls from a wider sample of countries (*17*).

GENDER GAPS VARY BUT DIFFERENCES IN VARIABILITY ARE A ROBUST PHENOMENON

Reading	Global	OECD	Non-OECD	United States
Mean M-F gap	-0.30**	-0.32**	-0.27**	-0.32**
M-F gap at 5th quantile	-0.45**	-0.53**	-0.41**	-0.46**
M-F gap at 95th quantile	-0.20**	-0.23**	-0.14**	-0.20**
M-F Variance Ratio	1.15**	1.17**	1.19**	1.17**
M-F Ratio in bottom 5%	2.20**	2.38**	2.05**	2.45**
M-F Ratio in top 5%	0.58**	0.56**	0.68**	0.60**
Mathematics	**Global**	**OECD**	**Non-OECD**	**United States**
Mean M-F gap	0.10**	0.10**	0.11**	0.07*
M-F gap at 5th quantile	0.03**	0.02	0.06**	-0.11**
M-F gap at 95th quantile	0.20**	0.22**	0.22**	0.22**
M-F Variance Ratio	1.13**	1.13**	1.16**	1.19**
M-F Ratio in bottom 5%	0.94**	0.98	0.86**	1.21**
M-F Ratio in top 5%	1.70**	1.69**	1.70**	1.72**

Gaps and ratios. In the table, M refers to male and F to female. Gaps are M-F differences at the mean, 5th, and 95th quantiles in standard deviation units. Variance ratio refers to male variance divided by female variance, and ratios in top and bottom 5% refer to the ratio of number of males and females who scored in the top and bottom 5% of the distribution. Results for the full data are presented here; USA is excluded from OECD results. For full results, see SOM, *$P < 0.05$; **$P < 0.01$.

Research Method and Findings

We examined boy-girl differences in test score performance from the 2003 OECD (Organization for Economic Co-operation and Develop-ment) Programme for Inter-national Student Assessment (PISA), a survey of 15-year-olds who are enrolled in full- or part-time education in industrialized countries (*18*). The PISA survey contains data on individual student performance for 41 countries. Here, we analyze mathematics and reading test scores by country, focusing on differences in the mean and variance of these test scores. The test scores are standardized to have a mean of 500 and a standard deviation of 100 across the OECD countries.

Reading. We calculated the international standardized mean differences in reading test scores as the sex difference in means divided by the standard deviation, and differences in variance as the male-to-female variance ratio. In all 41 countries, the boy-girl mean difference is negative, indicating that girls generally outscore boys (see table, top, and table S1). In 35 out of 41 countries, the boy-girl variance ratio indicates, with statistical significance ($P < 0.05$), that the population of boys displays greater variance than does the population of girls (see the table above and table S1).

[1]Department of Economics, University College London, London, WC1 6BT, UK, and Centre for Economic Performance, London School of Economics, London, WC2A 2AE, UK. [2]Department of Economics, Helsinki School of Economics, 00101 Helsinki, Finland; Government Institute for Economic Research (VATT), 00101 Helsinki, Finland; and Department of Econonmics and Statistics, Åbo Akademi University, 20500 Turku, Finland.

*Author for correspondence. E-mail: tuomas.pekkarinen@hse.fi

Published by AAAS

Mathematics. With the same comparisons for mathematics, the mean difference is positive, which indicates that boys generally outscore girls (see table, bottom, and table S2). In 37 of 41 countries, the boy-girl variance ratio indicates with statistical significance ($P < 0.05$) that the population of boys displays greater variance than does the population of girls (see the figure below and table S2).

Tip and tail. There are differences for the two tests. On both math and reading tests, boys predominate in two of the four extreme scoring categories (low reading, high math), with girls predominating in the high reading and low math category (see table, top and bottom, and columns 4 and 5 of tables S1 and S2). For mathematics, in 35 of the 41 countries, there are more boys than girls in the top 5%. For reading, 36 of 41 countries have more girls than boys in the top 5% of scores, and 39 of 41 countries have more boys than girls in the bottom 5% of scores.

Gender gaps. Gender gaps at the 5th and 95th quantiles of the reading distribution favor girls, but tend to be smaller at the 95th quantile than at the 5th quantile. In mathematics, on the other hand, the gender difference at the 5th quantile is statistically significant at the 5% level only in 18 countries, and the sign of this difference varies across countries. In mathematics, the gender difference at the 95th quantile favors boys in 36 countries ($P < 0.05$) (see table S2).

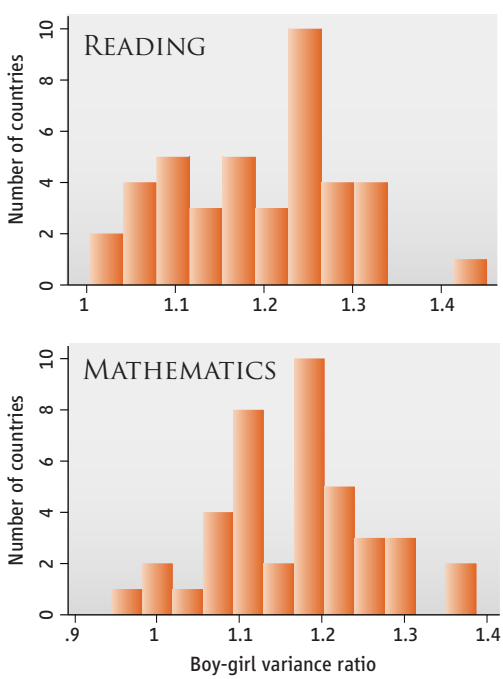

Variance ratios in countries that participated in PISA 2003. In the majority of countries, male variability is higher than female variability in both reading and math.

Variance and test performance. For both reading and mathematics tests in all 41 countries, the boy-girl variance ratio shows a positive correlation ($r = 0.21$ for reading and $r = 0.26$ for mathematics) with the mean test score performance (fig. S1, A and B). In countries with better test score performance, the boy-girl variance ratio is significantly higher ($P < 0.05$) than in countries where the children score more poorly (table S3). We find no relation between the Gender Gap Index of the World Economic Forum (*19*) and the variance ratios for either math or reading (table S3 and fig. S2, A and B), unlike the relation previously identified between the Gender Gap Index and the gender gap in average test scores (*7*).

Other data sources. To further probe the robustness and wider applicability of these findings, we have also studied gender differences in variance from other international data sources. We analyzed results from (i) the Trends in International Mathematics and Science Study (TIMMS) given in 2003, which tested 9- and 13-year-olds in mathematics and science; and (ii) the Progress in International Reading Literacy Study (PIRLS), given in 2001, which tests reading skills of 10-year-olds (*20*, *21*). Data from both studies indicate higher variance for boys in most countries (table S4).

Implications and Conclusions

Our analysis of international test score data shows a higher variance in boys' than girls' results on mathematics and reading tests in most OECD countries. How this translates into educational achievement is a matter open for discussion. Higher variability among boys is a salient feature of reading and mathematics test performance across the world. In almost all comparisons, the age 15 boy-girl variance difference in test scores is present. This difference in variance is higher in countries that have higher levels of test score performance.

Sex differences in means are easier to characterize: It is evident from the PISA data that boys do better in mathematics, and girls do better in reading. This has a compositional effect on the variance differences as well. The higher boy-girl variance ratio in mathematics comes about because of an increased prevalence of boys in the upper part of the distribution, but the higher variance in reading is due to a greater preponderance of boys in the bottom part of the test score distribution. Because literacy and numeracy skills have been shown to be important determinants of later success in life (for instance, in terms of earning higher wages or getting better jobs), these differing variances have important economic and social implications (*22*).

We therefore confirm that 15-year-old boys do show more variability than girls in educational performance, with specifics that differ according to whether mathematics or reading are being studied and tested. These results imply that gender differences in the variance of test scores are an international phenomenon and that they emerge in different institutional settings.

References and Notes

1. A. Jensen, in *Intelligence: Genetic and Environmental Influences*, R. Cancro, Ed. (Grune and Stratton, New York, 1971).
2. E. Maccoby, C. Jacklin, *The Psychology of Sex Differences* (Stanford Univ. Press, Stanford, 1974)
3. J. S. Hyde, *Am. Psychol.* **60**, 581 (2005).
4. D. Kimura, *Neuroendocrinol. Lett.* **23**, 67 (2002).
5. S. Machin, S. McNally, *Oxf. Rev. Econ. Policy* **21**, 357 (2005).
6. J. S. Hyde, S. M. Lindberg, M. C. Linn, A. B. Ellis, C. C. Williams, *Science* **321**, 494 (2008).
7. L. Guiso, F. Monte, P. Sapienza, L. Zingales, *Science* **320**, 1164 (2008).
8. K. Bayard, J. Hellerstein, D. Neumark, K. Troske, *J. Labor Econ.* **21**, 887 (2003).
9. S. Bertsch McGrayne, *Nobel Prize Women in Science: Their Lives, Struggles, and Momentous Discoveries* (Joseph Henry Press, National Academy of Sciences, Washington, DC, 2001).
10. W. Arulampalam, A. L. Booth, M. L. Bryan, *Ind. Labor Relat. Rev.* **60**, 163 (2007).
11. C. Muller *et al.*, *Science* **307**, 1043 (2005).
12. H. Ellis, *Man and Woman: A Study of Secondary and Tertiary Sexual Characters* (Heinemann, London, 1894).
13. F. Galton, *Hereditary Genius: An Inquiry into Its Laws and Consequences* (Macmillan, London, 1869).
14. N. Noddings, *Rev. Educ. Res.* **62**, 85 (1992).
15. A. Feingold, *Rev. Educ. Res.* **59**, 185 (1992).
16. L. V. Hedges, A. Nowell, *Science* **269**, 41 (1995).
17. Materials and methods are available as supporting material on *Science* Online.
18. *PISA, The 2003 Assessment Framework – Mathematics, Reading, Science, and Problem Solving Knowledge and Skills* (OECD, Paris, 2003); www.pisa.oecd.org/.
19. R. Hausmann, L. D. Tyson, S. Zahidi, *The Global Gender Gap Report* (World Economic Forum, Geneva, Switzerland, 2006).
20. M. O. Martin, Ed., *TIMMS 2003 User Guide for the International Database* (TIMSS & PIRLS International Study Center, Boston College, Chestnut Hill, MA, 2005); http://timss.bc.edu/.
21. E. J. Gonzales, A. M. Kennedy, Eds., *PIRLS 2001 User Guide for the International Database* (Boston College, Chestnut Hill, MA, 2003); http://timss.bc.edu/.
22. E. Leuven, H. Oosterbeek, H. Van Ophen, *Econ. J.* **114**, 466 (2004).

Supporting Online Material

www.sciencemag.org/cgi/content/full/322/5906/1331/DC1

10.1126/science.1162573

CHEMISTRY

A Tamed Reactive Intermediate

The highly reactive germanium dication is isolated by trapping it in a molecular cage.

Joseph B. Lambert

For more than 100 years (*1*), chemists have hypothesized unobserved intermediates in reaction schemes—seemingly invisible chemical spirits that explain the experimental facts. Often, such species are the key to understanding entire areas of chemistry. Indirect evidence may point to their existence, but their high reactivity shortens their lifetime and prevents isolation. Under particular circumstances, reactive intermediates have been isolated and characterized, but establishing the existence of an entirely new class of intermediates is rare indeed. The isolation of a novel reactive intermediate by Rupar *et al*. on page 1360 of this issue (*2*) is thus a remarkable and exciting achievement.

The organic chemistry of reactive intermediates has focused largely on carbenium ions (R_3C^+), carbanions ($R_3C{:}^-$), and carbenes ($R_2C{:}$). Open-shell intermediates (with unpaired electrons) include neutral ($R_3C^\bullet$) and charged radicals. Much of the reactivity of these organic intermediates comes from their charges and their deviations from a closed shell of eight electrons. Thus, higher charge and further loss of electrons from the closed shell might imply even greater reactivity and more difficulty in isolation. A series of six-electron carbon intermediates can be imagined by successively removing a ligand without its electron pair (R^+) from the carbenium ion, resulting in R_3C^+, $R_2C{:}$, $R\ddot{C}{:}^-$, and $:\ddot{C}{:}^{2-}$. A series of increasingly electron-deficient carbon species is generated by successive removal of ligands with their electron pair ($R{:}^-$) from the carbanion, resulting in $R_3C{:}^-$, $R_2C{:}$, $RC{:}^+$, and $C{:}^{2+}$, with eight, six, four, and two valence electrons, respectively. At the end of each series is an unknown, doubly charged atomic ion that lacks all coordination with other ligands or molecules. Of the seven distinct species, only three to date have been isolated and characterized in stable forms. Possibly the most reactive of the unknown species is carbon with two positive charges and only two valence electrons, $C{:}^{2+}$.

Rupar *et al.* now report the isolation of the germanium(II) dication, $Ge{:}^{2+}$, which is the germanium analog of $C{:}^{2+}$ (both germanium and carbon are in group 14 of the periodic table). No previous doubly charged ion of a nonmetal has been reported, except in highly coordinated forms such as $R_3Ge{:}^{2+}$ (*3*). Singly charged, monocoordinated silicon, germanium, and tin cations exist, which are analogs of $RC{:}^+$ (*4*, *5*).

Nonmetallic cations such as $Ge{:}^{2+}$ differ from the many metallic cations of general chemistry, such as Na^+ and Ca^{2+}, in many important ways. Whereas the metallic cations have four valence electron lone pairs, $Ge{:}^{2+}$ possesses just one lone pair (explicitly drawn) and three empty orbitals in the valence shell. The metallic cations are loosely solvated in aqueous solution, whereas the empty orbitals of $Ge{:}^{2+}$ would react instantly with any nucleophile such as water. The legendary reactivity of the carbenium and silylium cations (R_3C^+ and R_3Si^+) derives from their single empty orbital.

For decades, chemists have aimed to tame high reactivity by finding friendly environments with low reactivity and by arranging steric protection around the reactive species. The preparation of the free silylium cation relied on these techniques (*6*). In 1991, Cram *et al*., in a paper famously entitled "The Taming of Cyclobutadiene," reported isolation of the highly reactive four-membered ring containing two double bonds by protecting it within a molecular cage or prison (*7*). The cage lacked molecular components that could react with cyclobutadiene and barred external molecules from reacting with it. Many molecular cages have been used to encapsulate ions or molecules (*8*), but only a few have served to accommodate reactive intermediates. Rupar *et al.* now use a cryptand cage, composed of carbon chains interspersed with nitrogen and oxygen atoms, to isolate $Ge{:}^{2+}$ from reactive neighbors.

But is their germanium cation free, or "naked" as many authors like to call such species? A truly free cation must resemble its analog in vacuum, free of all surrounding species. No atoms can be within bonding distance. This extreme criterion was, for example, fulfilled in the case of the silyl cation (*6*). In the present case, there is no doubt from the mass spectrum that the imprisoned atom is germanium and from the x-ray data that the triflate counterions are well removed from bonding distances. The remaining suspects are the atoms of the cryptand (see the figure).

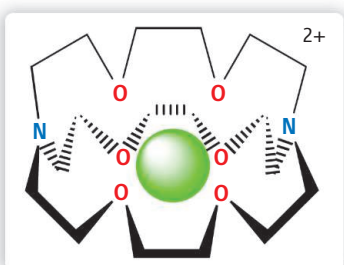

The sequestered germanium dication. Germanium with two positive charges ($Ge{:}^{2+}$) resides inside a chemical shell without any closely bonded atoms (*2*). Carbon and hydrogen atoms are not shown.

The carbon and hydrogen atoms are nonreactive and well removed from the germanium, but what about the nitrogen and oxygen atoms? It seems likely that there is some interaction between germanium and these other atoms, as germanium falls midway on the line connecting the two nitrogens and is equidistant from the six oxygens. The experimentally determined distances (Ge–N, 2.524 Å; Ge–O, 2.4856 Å) are well outside typical Ge–N (1.85 Å) and Ge–O (1.80 Å) single-bond lengths. The Ge–O distance, however, is similar to that (2.4 Å) between the solvent O and Ge in the $GeCl_2$-dioxane complex, in which germanium is not considered entirely free (*9*). The fractional bond orders calculated from the crystallographic parameters are 0.11 for Ge–N and 0.10 for Ge–O, indicating that there is little bonding between Ge and any single atom. Six oxygens and two nitrogens, however, each provide this small amount of bonding, so that the total bonding accumulates.

It is noteworthy that germanium is midway between the two nitrogens, indicating a single-minimum rather than a double-minimum potential well. This situation is reminiscent of hydrogen bonds, in which hydrogen can reside in either type of well. Shorter distances favor the single minimum. At longer distances, the hydrogen bond moves to a double minimum (*10*). It is possible, then, that a larger cryptand would allow germanium to move off center and have stronger bonding interactions with one nitrogen or with one or more oxygen atoms.

Department of Chemistry, Northwestern University, Evanston, IL 60208, USA. E-mail: jlambert@northwestern.edu

Published by AAAS

These reservations qualify as quibbles. Without a doubt, Rupar *et al.* have created a nearly naked germanium(II) dication, a species for which there is no precedent in nonmetallic inorganic chemistry. It may have interesting synthetic applications, as a template for adding two to four groups to germanium. Germanium-73 nuclear magnetic resonance measurements could clarify to what extent germanium is free. Finally, the successful isolation of this species suggests that it may be possible to prepare other unprecedented cations from groups 13 to 17—such as Ga^{+}, Si^{2+}, P^{3+}, As^{3+}, and Sb^{3+}—by imprisonment.

References

1. A. Lapworth, *J. Chem. Soc.* **85**, 32 (1904).
2. P. A. Rupar, V. N. Staroverov, K. M. Baines, *Science* **322**, 1360 (2008).
3. P. A. Rupar, V. N. Staroverov, P. J. Ragogna, K. M. Baines, *J. Am. Chem. Soc.* **129**, 15138 (2007).
4. T. Probst, O. Steigelmann, J. Riede, H. Schmidbaur, *Angew. Chem. Int. Ed.* **29**, 1397 (1990).
5. P. Jutzi *et al.*, *Science* **305**, 849 (2004); published online 1 July 2004 (10.1126/science.1099879).
6. J. B. Lambert, Y. Zhao, S. M. Zhang, *J. Phys. Org. Chem.* **14**, 370 (2001).
7. D. J. Cram, M. E. Tanner, R. Thomas, *Angew. Chem. Int. Ed.* **30**, 1024 (1991).
8. J.-M. Lehn, *Supramolecular Chemistry: Concepts and Perspectives* (Wiley-VCH, Weinheim, Germany, 1995).
9. M. K. Denk, M. Khan, A. J. Lough, K. Shuchi, *Acta Crystallogr. C* **54**, 1830 (1998).
10. R. G. Snyder, J. A. Ibers, *J. Chem. Phys.* **36**, 1356 (1962).

10.1126/science.1167321

PHYSICS

Reflections on a Wall of Light

Single-photon cooling of atoms offers a rare view of a real-life Maxwell's demon.

P.-M. Binder

Optical traps allow atoms to be cooled to ultralow temperatures, where the atoms can form exotic quantum states of matter. Studies to date have, however, been mostly confined to half a dozen or so atomic systems. The recently reported cooling of atoms (*1*) with a one-way wall of light (*2*, *3*) now provides the opportunity to experiment with over 80% of the elements in the periodic table at temperatures of just a few microkelvin. In addition, these selective barriers that allow the trapping of cold atoms are also practical realizations of a familiar mythical being that has accompanied physicists for well over a century: Maxwell's demon. My aim here is to discuss the role played by entropy and information in this particular cooling technique. I will look in turn at the wall, the Maxwell demon (in general), and then both.

In the new method, the atoms are first slowed and trapped magnetically (*4*), creating a tilted potential for the atoms (see the figure, green area). The one-way wall is then implemented by moving two laser beam sheets, tuned to different frequencies (red and blue in the figure), across the magnetic trap. The frequencies are carefully chosen so that one beam acts as a repulsive barrier for atoms in one state ("1") and as an attractive well for atoms in another state ("2"). Low-energy atoms in state 2 go right through the approaching wall and then encounter the second beam that induces an irreversible transition from state 2 to 1, emitting a single photon in the process (see the figure, left panel). With this approach, the captured atoms in state 1 can be gently shepherded to the center of the trap by the wall, where they can be contained for some time.

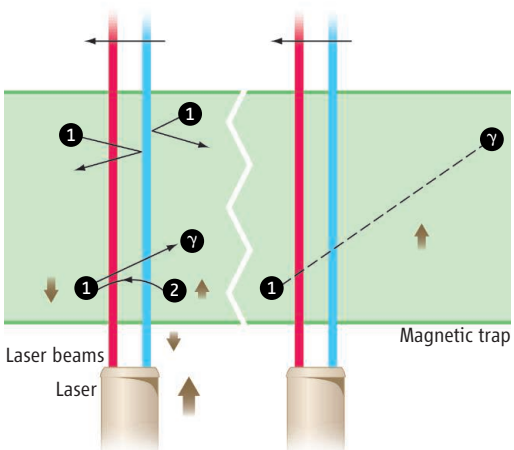

Reflectively trapped. Green: magnetic trap. Red and blue: laser beam sheets that form the wall. Left of the wall: optical trap. (**Left**) Two atoms in state 1 reflect off the left-moving wall (upper part); a slow atom gets trapped, transitions from state 2 to 1, and emits a photon γ (middle part). The laser increases the net entropy of the universe as illustrated by the relative size of the arrows (bottom part). (**Right**) As the trapped atom and the emitted photon move apart, decoherence increases the total entropy, and the Second Law is safe (once again).

Demons were introduced by James Clerk Maxwell in 1871 to help illustrate the statistical nature of the Second Law of Thermodynamics, which forbids the spontaneous appearance of temperature gradients in a body at equilibrium or the full conversion of microscopic internal energy into organized work. Alternatively, the law can be stated in terms of the entropy of a closed system, which must never spontaneously decrease. Maxwell's nimble-fingered creatures that try to defeat the Second Law by sorting fast and slow gas atoms into two compartments have been analyzed in depth by physicists and philosophers. Arguments over what exactly happens to demons and the environment as the entropy of the gas decreases in apparent violation of the Second Law have helped sharpen our understanding of the crucial concepts of measurement and information. One can attribute to Leo Szilard the discovery of the bit, the unit of information, as part of his 1929 Maxwell's demon paper (*5*).

The generally accepted solution to the missing entropy problem, which arises in the above scenario of ordering the gas atoms, came in two steps. Following Szilard's ideas, it was believed that in the process of measuring the gas atoms as they were being manipulated by the demons, the demons acquired information that somehow offset the entropy decrease of the atoms, thus rescuing the Second Law. But in subsequent work in the 1980s, Charles Bennett (*6*) invoked earlier work of Rolf Landauer (*7*) to argue that any decrease in the entropy of the universe caused by the sorting of atoms will not be regained by the demon while measuring the atom, a possibly reversible process. This is so because atoms and demons become highly correlated and their joint entropy is about the same as their individual entropy. Instead, entropy increases later when the demon's memory of the measurement is erased as the demon returns to its "initial state" and becomes ready for another measurement. A volume by Leff and Rex (*8*) contains most of the work described in these two paragraphs.

Expanding on an existing entropy analysis of the cooling process (*9*), the following picture emerges: Each slow atom being trapped emits a photon at the light wall ("measure-

Department of Physics and Astronomy, University of Hawaii, Hilo, HI 96720–4091, USA. E-mail: pbinder@hawaii.edu

ment"); atom-photon pairs are highly correlated, so the photons do not add to the overall entropy. As atoms are collected at the center of the trap, their entropy decreases. The corresponding entropy increase that saves the Second Law does not happen right away but rather as atoms and photons become uncorrelated (*10*) when they drift apart and interact with their surroundings (see the figure, right panel), especially through absorption and scattering of the photons ("erasure"). Note how closely this recapitulates the century-long discovery of the original solution.

There is an additional source of irreversibility not present in the familiar rigid container habitat of the demon. The walls of the optical trap come from a (macroscopic) laser unit, which generates entropy: As photons are collected into a highly organized beam, their entropy is lowered (*11*), but this is more than offset by the laser warming up and transferring energy to its surroundings (see bottom of left panel).

Single-photon cooling of atoms is still being perfected and will extend our ability to probe into the details of the physical world (*1*). A wonderful bonus from this quantum optics experiment is the opportunity to observe a real-life Maxwell's demon in action and to be able to follow the intricate flows of information and entropy in a tangible laboratory setting.

References and Notes

1. G. N. Price *et al.*, *Phys. Rev. Lett.* **100**, 093304 (2008).
2. J. J. Thorn, E. A. Schoene, T. Li, D. A. Steck, *Phys. Rev. Lett.* **100**, 240407 (2008).
3. A. Marian, B. Friedrich, *Nat. Photonics* **2**, 463 (2008).
4. E. Narevicius *et al.*, *Phys. Rev. Lett*. **100**, 093003 (2008).
5. L. Szilard, *Z. Physik* **53**, 840 (1929).
6. C. H. Bennett, *Sci. Am.* **257**, 108 (1987).
7. R. Landauer, *IBM J. Res. Dev.* **5**, 182 (1961).
8. H. S. Leff, A. F. Rex, Eds., *Maxwell's Demon 2* (IOP, Bristol, UK, 2003).
9. A. Ruschhaupt, J. G. Muga, M. G. Raizen, *J. Phys. B: At. Mol. Opt. Phys.* **39**, 3833 (2006).
10. S. Lloyd, *Phys. Rev. A* **56**, 3374 (1997).
11. X. L. Ruan, S. C. Rand, M. Kaviany, *Phys. Rev. B* **75**, 214304 (2007).
12. I thank the Research Corporation (award CC5885) for financial support.

10.1126/science.1166681

ASTRONOMY

Exoplanets—Seeing Is Believing

Direct observations have been made of the infrared and optical signatures of planets orbiting distant stars.

Mark S. Marley

The bonanza of extrasolar planet discoveries, more than 300 at last count, has been enabled mainly by two indirect methods—radial-velocity surveys, which detect the motion of the star induced by its orbiting partner, and searches for planets that transit their primary stars. Both methods can reveal the architecture of planetary systems (masses and orbits), and the transiting planets also yield a second harvest (radii, densities, and atmospheric properties inferred partly from absorption of the star's light). Transit characterization methods depend upon proximity of the target planet to the primary star and so far tell us nothing about planets at large orbital separations. The holy grail in planet detection has thus been direct imaging because any planet spatially separated from its primary star is amenable to follow-up characterization. Although there have been previous claims of such detections (*1*, *2*), we ultimately know a planetary system when we see it. Thanks to two papers in this issue—by Kalas *et al*. on page 1345 (*3*) and Marois *et al*. on page 1348 (*4*)—we now have compelling images of the glow of faint planetary companions—not only adjacent to but clearly orbiting stars. Kalas *et al.* present optical Hubble Space Telescope images of what is likely to be a planet with a mass a few times that of Jupiter orbiting the famous bright A star Fomalhaut. Marois *et al.* present a series of infrared images of three giant planets orbiting the A-type star HR 8799 in the constellation Pegasus. The planets (see the figure) are seen in nearly face-on, circular orbits spaced not unlike those of the solar system's giants at larger scale.

Direct imaging of planets is eminently challenging, particularly for ground-based telescopes observing through the blurring effects of the atmosphere, as faint planets are lost in the scattered and diffracted glare of their primary stars. The tools required for planet-imaging searches include adaptive optics techniques, which correct for the blurring of the atmosphere, and coronagraphs, which block out most of the star's light (a technique developed to study the Sun's corona).

Earlier mileposts on the road to images of planets orbiting stars have included the brown dwarf Gliese 229 B (*5*), which orbits an M star, and the several–Jupiter-mass object 2MASS 1207 B (*1*), which orbits a brown dwarf (see the figure). Neither of these low-mass objects nor other contenders fits the planet profile. Gliese 299 B is massive enough to fuse deuterium, which requires a mass greater than about 13 times Jupiter's mass (M_{Jup}) (*6*), and the object that 2MASS 1207 B orbits is not a star—its mass is less than ~75 M_{Jup}, the minimum required to permit fusion of hydrogen to helium (*7*).

The systems studied by Marois *et al.* and by Kalas *et al.* are notable for their similarities. Dusty debris disks, presumably arising from collisions of planetesimals, and perhaps shepherded by the new planets, surround both stars. A similar disk is likely present in our own solar system (*8*). The primary stars in both systems are younger, brighter, warmer, and more massive than the Sun. Although main-sequence A stars are generally not amenable to radial-velocity planet searches, more than a dozen giant planets have been detected by such surveys around evolved A-type stars, and trends suggest that the likelihood of a giant planetary companion increases with stellar mass (*9*).

Although images of faint companions orbiting their primary stars are captivating, their masses must be inferred from their brightness. Unlike stars, giant planets fade as they radiate away the heat of their formation. Thus, estimates of the masses of these planets depend upon how bright and how old they are. Marois *et al.* constrain the total luminosity of each companion to HR 8799 by combining images taken in several different spectral bandpasses, each of which covers a limited range of wavelengths in the infrared. They then compare the luminosities with theoretical models for giant-planet evolution, assuming an estimated stellar age of 30 to 160 million years, and conclude that all three objects have masses well below the ~13 M_{Jup} planet threshold. However, the evolution models at these ages can be sensitive to assumed initial conditions (*10*). Higher-resolution near-infrared spectra of the planets and long-term astrometric measurements of their orbits will ultimately refine their masses. Nevertheless, the multiple objects, faint luminosities, young ages, small companion-to-primary mass ratios, circular, well-spaced

NASA Ames Research Center, Moffett Field, CA 94035, USA. E-mail: mark.s.marley@nasa.gov

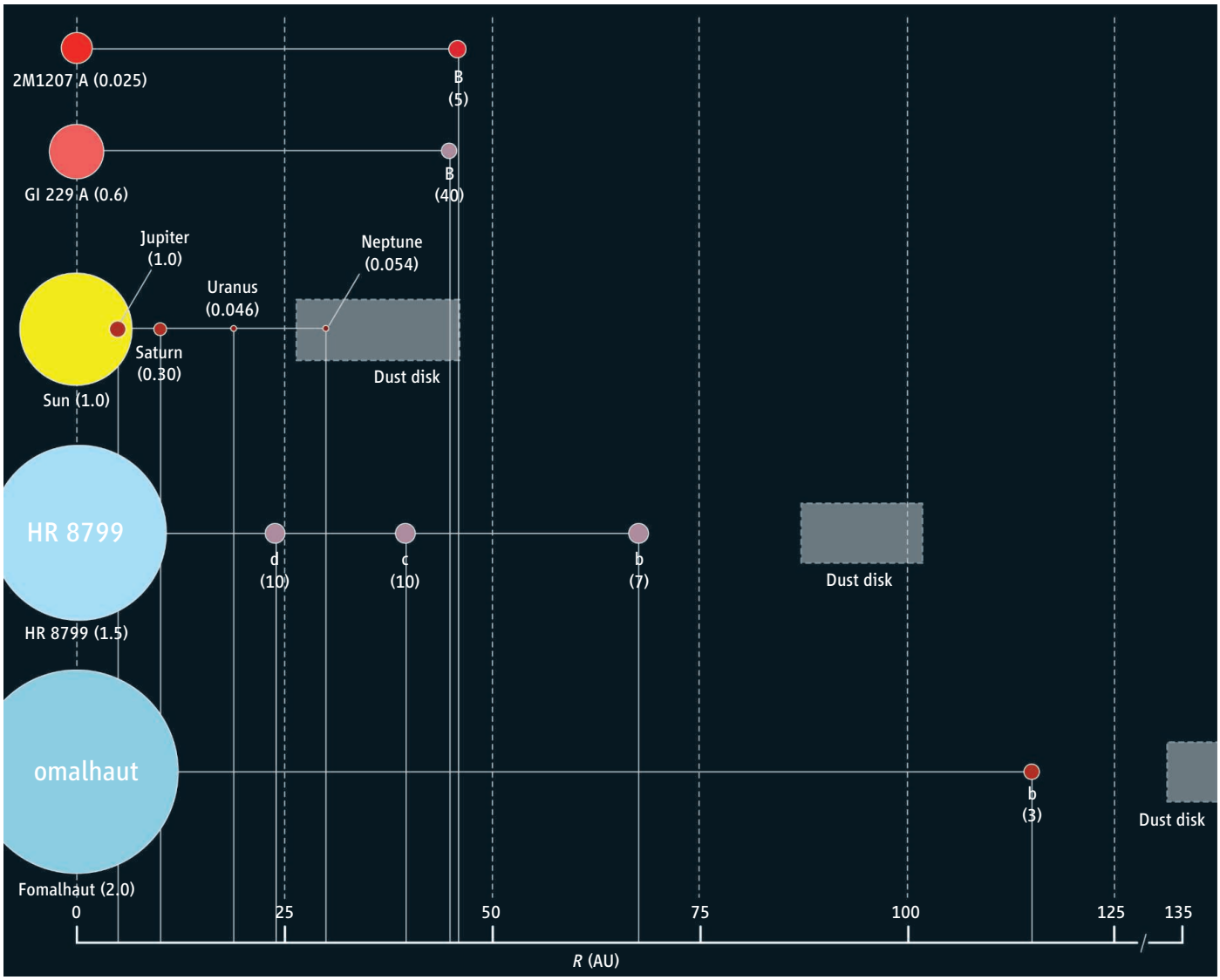

Distant stellar systems. This schematic diagram compares the directly imaged Fomalhaut and HR 8799 systems to the solar system and two other well-known binary systems. All companions are plotted at the correct projected orbital distance *R* from their primaries. Sizes and distances are shown on consistent—but separate—linear scales. The approximate locations of the known dust disk around Fomalhaut, as well as the disks inferred to be present around HR 8799 and the Sun, are also shown. Numbers in parentheses below each object are masses, for the primaries in units of the Sun's mass and for the companions in units of Jupiter's mass. Masses for all of the companions beyond the solar system are uncertain, in some cases (including Gl 229 B and 2M1207 B) by at least 50%. Stellar colors are suggestive; companions with similar (arbitrary) colors have comparable atmospheric temperature. AU, astronomical units.

orbits, and associated dust disk recount a compelling story.

For Fomalhaut's companion, the plot is more complex: Apparently, planetary thermal emission is detected in only a single spectral bandpass. Kalas *et al.* must rely upon spectra from model atmosphere calculations that have never been validated in this temperature regime and upper limits from nondetections at other wavelengths for their mass estimate. The lack of gravitational disruption to this system's dust belt places an independent (but still model dependent) constraint on the planet's mass (<3 M_{Jup}). Together, the available data imply a very cool atmospheric temperature (400 K or less) and possibly a bright circumplanetary ring. If confirmed, this object will be the coolest and lowest-mass body imaged outside of the solar system.

The difficult path to ascertaining masses of these planets foreshadows the challenges that will be faced if space-based coronagraphic telescopes, such as NASA's proposed Terrestrial Planet Finder, directly image extrasolar terrestrial planets in reflected starlight. For such mature objects, there will be no connection between stellar age and planet mass; thus, the mass of planets detected only by imaging will be uncertain. Images of dots—even pale blue ones that recall Earth—orbiting other stars will be ultimately unsatisfying without knowledge of their mass. Partly for this reason, the NASA-NSF Exoplanet Task Force (*11*) advocated an astrometric planet-finding space mission that could measure masses of even terrestrial planets around nearby stars. Lacking such direct measures, the masses of future planetary discoveries will continue to hinge on the veracity of theory.

However, for the two systems now in hand, the prospects are bright. Spectroscopic and photometric observations should determine how the atmospheric composition of the planets compares to that of their primary stars, a key test of planet-formation models. In our own solar system, the atmospheric abundance of heavy elements in giant planets

CREDIT: C. BICKEL/*SCIENCE*

Published by AAAS

exceeds that of the Sun, increases with orbital distance, and is smallest in the most massive planet. It will be fascinating to see if similar trends are found elsewhere. We can further expect a race to the bottom as portraits of smaller, colder, and older giant planets, found ever closer to their parent stars, are teased out from the glare of those stars by increasingly sophisticated techniques.

References

1. G. Chauvin *et al.*, *Astron. Astrophys.* **425**, L29 (2004).
2. D. Lafrenière, R. Jayawardhana, M. H. van Kerkwijk, *Astrophys. J. Lett.*, in press; available at http://arXiv.org/abs/0809.1424.
3. P. Kalas *et al.*, *Science* **322**, 1345 (2008); published online 13 November 2008 (10.1126/science.1166609).
4. C. Marois *et al.*, *Science* **322**, 1348 (2008); published online 13 November 2008 (10.1126/science.1166585).
5. T. Nakajima *et al.*, *Nature* **378**, 463 (1995).
6. D. Saumon *et al.*, *Astrophys. J.* **460**, 993 (1996).
7. A. Burrows, *et al.*, *Astrophys. J.* **406**, 158 (1993).
8. J.-C. Liou, H.A. Zook, *Astrophys. J.* **118**, 580 (1999).
9. J. A. Johnson, *et al.*, *Astrophys. J.* **675**, 784 (2008).
10. M. Marley *et al. Astrophys. J.* **655**, 541 (2007).
11. J. I. Lunine *et al.*, *Report of the Exoplanet Task Force to the Astronomy and Astrophysics Advisory Committee* (2008); available at http://arXiv.org/abs/0808.2754.

Published online 13 November 2008;
10.1126/science.1167569
Include this information when citing this paper.

MICROBIOLOGY

An Antibiotic Mimics Immunity

Certain compounds generate reactive nitrogen intermediates in bacteria, contributing to their antimicrobial effect.

Carl Nathan

When German scientist Paul Ehrlich developed the drug arsphenamine to treat syphilis in 1908, he launched an approach to produce antibacterial compounds that was benchmarked over the next half-century by Nobel Prizes to Domagk for sulfonamides; Fleming, Florey, and Chain for penicillin; and Waksman for streptomycin. Ehrlich's own Nobel Prize honored his idea that immunity depends on soluble, specific, endogenous, antimicrobial macromolecules. However, it was his realization that exogenous small molecules could also protect the host that founded modern medicine. Beyond taking inspiration from immunity, however, the Ehrlichian approach to chemotherapy ignored the immune system in that it treated the host as no more than a complex bacteriologic culture vessel. In 1931, Avery and Dubos (*1*) introduced the alternative concept that an antimicrobial—in their case, a bacterial enzyme that degraded another bacterium's capsule—could cure the host by preventing the pathogen from defending itself against attack by the host's immune system. Their idea was advanced by the discovery of small molecules that synergize with host immunity by inactivating bacterial counter defenses (*2*, *3*). On page 1392 of this issue, Singh *et al*. (*4*) discover a third form of the relation between antimicrobial chemotherapy and host immunity: An antibacterial agent can mimic immunity by generating an important chemistry of the immune response.

Reactive nitrogen intermediates generated by the host enzyme inducible nitric oxide synthase are critical for controlling infection by *Mycobacterium tuberculosis* (Mtb) in mice (*5*). PA-824 is a nitroimidazole that is bactericidal to Mtb both in aerobic conditions and at very low oxygen levels (hypoxic conditions) (*6*). Singh *et al*. find that nitroimidazoles kill Mtb under hypoxic conditions at least in part by undergoing enzyme-catalyzed denitration, which generates reactive nitrogen intermediates. It now becomes reasonable to test nitroimidazole analogs for their capacity to produce reactive nitrogen intermediates as a functionally relevant assay to determine their potential to kill Mtb under hypoxic conditions. The new findings illumine the functions of three bacterial factors: the deazaflavin cofactor F_{420}, the F_{420}-dependent nitroreductase family (which activates PA-824), and the $F4_{420}$-dependent glucose 6-phosphate dehydrogenase (which redox-cycles F_{420}). Thus, Mtb can become resistant to nitroimidazoles by mutating the activating enzyme, enzymes that make its cofactor, or the enzyme that redox-cycles the cofactor (*7*).

The discoveries of Singh *et al*. have potential medical importance. Tuberculosis is the third leading cause of death and disability in the world. What makes Mtb so hard to eradicate is its penchant to stop replicating for prolonged periods. Nonreplicating Mtb latently infects about one-third of humanity. Its resumption of growth in a proportion of individuals sustains the pandemic of active tuberculosis; even then, some bacteria remain nonreplicating. It seems that the immune system rarely eradicates Mtb, but rather drives much of it into nonreplication through diverse mechanisms including deprivation of carbohydrate, iron, oxygen, and certain amino acids, and the generation of reactive nitrogen intermediates and reactive oxygen intermediates (*8*). Today's chemotherapeutics target processes by which Mtb increases biomass, and thus, are chiefly active against replicating Mtb. By contrast, nonreplicating Mtb is relatively tolerant to conventional chemotherapeutics (*8*). This creates another relation between chemotherapy and immunity: When immunity imposes bacteriostasis, it works at cross-purposes with chemotherapy that selectively kills

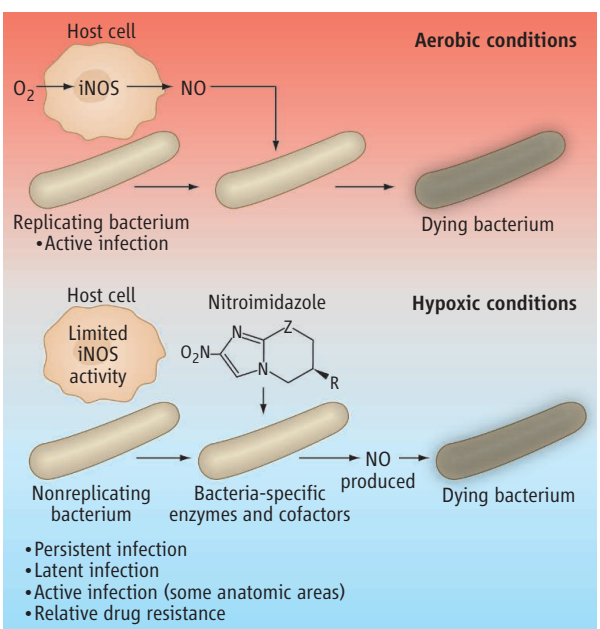

Same chemical strategy. Under aerobic conditions, host cells produce nitric oxide (NO) via the enzyme inducible nitric oxide synthase (iNOS). NO can kill replicating bacteria. Under hypoxic conditions, bacteria enter a state of nonreplicative persistence and host cell NO production is limited. Certain nitroimidazoles can generate NO (and other reactive nitrogen intermediates) within the bacteria under both aerobic and hypoxic conditions. Under hypoxic conditions, these reactive nitrogen intermediates contribute to killing the bacteria.

The Department of Microbiology and Immunology, Weill Cornell Medical College, New York, NY 10065, USA. E-mail: cnathan@med.cornell.edu

replicating Mtb. This is believed to necessitate treatment that is more prolonged (6 to 24 months or more) than for any other curable bacterial infection (besides leprosy, another mycobacterial disease). Interruption of treatment is commonplace and selects for airborne spread of multi–drug-resistant (~450,000 cases per year) and extensively drug-resistant tuberculosis (~45,000 cases per year). Over 80% of the latter cases have been fatal in a leading U.S. treatment center (*9*). Hence, it is urgent to find new drugs effective against nonreplicating Mtb (*2*).

What makes reactive nitrogen intermediates such good host-derived antimicrobials is their multiplicity of targets. Known targets of reactive nitrogen intermediates within an Mtb bacterium include the adaptive transcriptional response of Mtb when the bacterium dwells within activated macrophages (*10*), the pathogen's DNA (*11*), at least 29 of its enzymes (*12*), and a metallothionein from which nitric oxide displaces copper in a toxic form (*13*). Likewise, their multiplicity of targets makes reactive nitrogen intermediates potentially toxic for the host. Nitroimidazoles appear to have improved on immunity in two respects (see the figure). First, they generate reactive nitrogen intermediates when activated by F_{420}-dependent nitroreductases. Neither the nitroreductases nor F_{420} are produced by the host. Thus, the reactive nitrogen intermediates donated by nitroimidazoles may arise only in the pathogen, which may restrict their actions to Mtb and perhaps the host cells in which Mtb resides. Second, nitroimidazoles generate reactive nitrogen intermediates not just aerobically, but also anaerobically, when the host enzyme (inducible nitric oxide synthase) cannot.

The findings of Singh *et al.* raise many questions. Does the drug tolerance of nonreplicating Mtb really explain why chemotherapy takes so long to treat tuberculosis? It is not yet known whether nitroimidazoles kill nonreplicating Mtb when nonreplication is imposed by stringencies other than hypoxia. Another nitroimidazole, OPC-67683, is in clinical trials for tuberculosis, but whether it also kills nonreplicating Mtb by donating reactive nitrogen intermediates is not known. And does the host generate reactive nitrogen intermediates from nitroimidazoles? If so, is this mutagenic or otherwise toxic?

The physiologic role of deazaflavin-dependent nitroreductases may be to repair endogenous molecules that become nitrated in Mtb as it dwells in its natural host, humans. Consistent with this, mutant Mtb that are defective in F_{420} synthesis are hypersensitive to reactive nitrogen intermediates (*11*), which suggests that F_{420}-dependent enzymes repair bacterial molecules that reactive nitrogen intermediates have modified. How might Mtb encounter reactive nitrogen intermediates in humans? During anaerobic respiration, Mtb may generate its own reactive nitrogen intermediates by donating an electron to nitrate (*14*). Nitrate enters human body fluids from the diet and from auto-oxidation of nitric oxide produced by nitric oxide synthases. In less hypoxic sites, host-derived reactive nitrogen intermediates may modify components of Mtb, because Mtb-infected human tissue macrophages often express functional inducible nitric oxide synthase (*15*).

Some antimicrobials are proficient at killing replicating bacteria, but risk being rendered less effective by bacteriostatic immunity (*8*). Others synergize with host immunity by inactivating bacterial counterdefenses (*2*, *3*). Singh *et al*. show that some antimicrobials can mimic immunity by generating one of its chemistries. Chemotherapy can also mimic immunity by inhibiting the same bacterial targets as immunity, with synthetic chemicals that bacteria have not evolved the means to detoxify. For example, reactive nitrogen intermediates nitrosylate Mtb's ATP synthase (*12*); the same enzyme is targeted by a diarylquinoline that is in clinical trials (*16*). The challenge now is to develop more compounds of each class with good pharmaceutical properties and to exploit the power of their combinations.

References and Notes

1. O. Avery, R. Dubos, *J. Exp. Med.* **54**, 73 (1931).
2. R. Bryk *et al*., *Cell Host Microbe* **3**, 137 (2008).
3. C. I. Liu *et al*., *Science* **319**, 1391 (2008).
4. R. Singh *et al., Science* **322**, 1392 (2008).
5. J. D. MacMicking *et al*., *Proc. Natl. Acad. Sci. U.S.A.* **94**, 5243 (1997).
6. C. K. Stover *et al*., *Nature* **405**, 962 (2000).
7. U. H. Manjunatha *et al*., *Proc. Natl. Acad. Sci. U.S.A.* **103**, 431 (2006).
8. C. Nathan *et al*., *Tuberculosis (Edinburgh)* **88** (suppl. 1), S25 (2008).
9. E. D. Chan, M. J. Strand, M. D. Iseman, *N. Engl. J. Med.* **359**, 657 (2008).
10. D. Schnappinger *et al*., *J. Exp. Med.* **198**, 693 (2003).
11. K. H. Darwin *et al*., *Science* **302**, 1963 (2003).
12. K. Y. Rhee, H. Erdjument-Bromage, P. Tempst, C. F. Nathan, *Proc. Natl. Acad. Sci. U.S.A.* **102**, 467 (2005).
13. B. Gold *et al*., *Nat. Chem. Biol.* **4**, 609 (2008).
14. C. D. Sohaskey, *J. Bacteriol.* **190**, 2981 (2008).
15. C. Nathan, *Science* **312**, 1874 (2006).
16. K. Andries *et al*., *Science* **307**, 223 (2005).

17. C.N. is supported by the Abby and Howard P. Milstein Program in Chemical Biology of Infectious Diseases. The Department of Microbiology and Immunology is supported by the William Randolph Hearst Foundation. Thanks to B. Bryk, S. Ehrt, B. Gold, G. Lin, K. Rhee, L. P. Sorio de Carvalho, and G. Vogt for helpful comments.

10.1126/science.1167452

GEOCHEMISTRY

Carbon in Charge

Rob L. Evans

Laboratory data suggest that enhanced conductivity in the deep mantle can be caused by extremely small amounts of carbon-rich melt.

The mantle is Earth's largest reservoir of carbon (*1*). Carbon is released to the ocean or atmosphere through volcanic processes and is recycled back into the mantle in subduction zones, where oceanic plates are pushed under continents. Over the lifetime of our planet, this exchange of carbon between the mantle and the oceans and atmosphere may have influenced climate. Furthermore, the volcanism that takes melt from deep in the mantle to form new sea floor is the most important and dynamic process that shapes Earth's surface. An entirely new sea floor is formed every ~200 million years, a blink of the eye in the geologic time scale. On page 1363 of this issue, Gaillard *et al.* shed light on the likely sources of carbon-rich melt within the mantle (*2*) and call into question models of mantle electrical conductivity structure involving water.

Most of the silica-rich melt that is extracted from the mantle through upwelling at mid-ocean ridges comes from the uppermost ~110 km of the mantle. Melting to these depths requires the influence of water and carbon dioxide, both of which lower the melting point of the mantle (*3*). However, this leaves another 300 km of upper mantle untapped. Geophysical data from an experiment on the southern East Pacific Rise (*4*), a super-fast spreading center, and measurements on the melting point of carbonated mantle (*5*) suggest that small amounts of melting—producing in this case a carbon-rich (or carbonatite)

Department of Geology and Geophysics, Woods Hole Oceanographic Institution, Woods Hole, MA 02543, USA. E-mail: revans@whoi.edu

melt—could begin as deep as 300 km. Such a deep source would change the size of the melt reservoir and the scale of carbon extraction from the mantle. Carbon-rich melts are also a potential link in another exchange of carbon between the mantle and the Earth surface: diamonds.

However, the melt fractions predicted by some geophysical measurements have not matched those that fit geochemical predictions. Geochemical analyses predict very low melt fractions (typically much less than 1% by volume) at these great depths. Gaillard *et al*. now present laboratory data showing that carbonatite melts, the kind that would be produced at depths of ~200 to 300 km, are considerably more electrically conductive than the silicate melts produced by mantle melting beneath mid-ocean ridges. A more conductive melt means that less melt is needed to increase bulk conductivity to a given level and thus to explain geophysical observations. For example, the same increase in conductivity produced by 1% silicate melt can be achieved by just 0.02% carbonatite melt. This extremely small volume fraction can be detected by measuring the bulk electrical conductivity of the deep mantle, whereas other geophysical methods are insensitive to such low melt fractions.

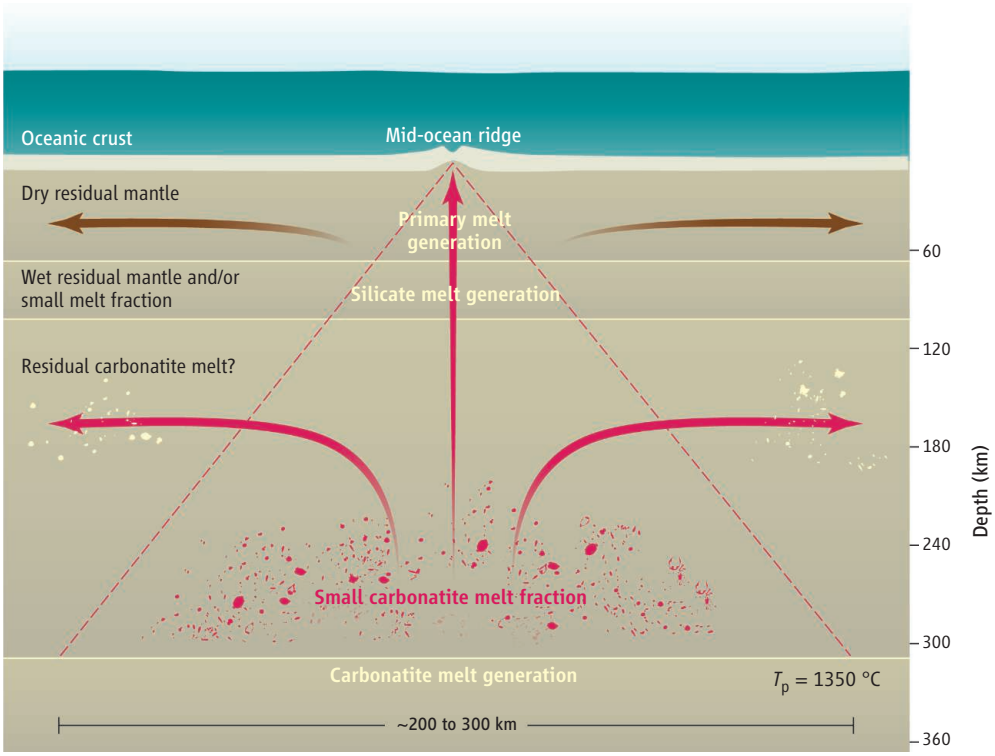

Melt riddles. Melt generation beneath mid-ocean ridges is thought to extend perhaps as deep as 300 km. At these depths, the melts produced are the carbonatites discussed by Gaillard *et al*. (*2*). The combination of upwelling mantle flow and the buoyancy of the melt causes the melt to rise. Melt that migrates toward the mid-ocean ridge seems to come from a relatively broad area of mantle (roughly delineated by the dashed lines). At depths of ~110 km, under the influence of CO_2 and water, silicate melting begins (*5*). These silicate melts mix with the carbonatites, potentially reducing their bulk conductivity. Evidence for conductive regions at depths between ~60 and 120 km at distances more than 50 km away from the ridge crest ("off-axis") suggest either water (*9*) or melt (*2*) that does not escape at the ridge and is transported away from the spreading center. The deeper Pacific basin-wide conductive layer (*7*) could also be due to very small amounts of carbonatite melt, although it is unclear why such melt would remain in place and not rise upward under buoyancy.

So far so good. But other controversies remain regarding processes at shallower depths. One controversy has been whether conductivity measurements can detect the presence of water (in the form of hydroxyl and hydrogen) dissolved in olivine and, if so, whether they can untangle this signature from that of melt. Water content is a mantle property as important as carbon. The ability of the mantle to convect is related to its viscosity, and water contents at levels likely for the mantle reduce its viscosity (making it easier for the mantle to flow) by about 2 orders of magnitude (*6*).

A survey of the mantle conductivity across the Pacific basin from Hawaii to Oregon showed enhanced conductivity at depths of ~200 km (*7*). The authors discounted deep melt as an explanation, largely because the melt would have to be a stable and continuous feature across such a large expanse of mantle. Instead they argued that water, in the form of hydrogen dissolved in olivine, could account for the high conductivity (*8*). This interpretation suggested higher conductivity in the direction of plate spreading, a feature that their data could not resolve.

More recent data from the East Pacific Rise showed enhanced conductivity that was interpreted in terms of water (*3*, *9*), in the shallower depth range where silicate melting kicks in. The data require an anisotropic conductivity, consistent with the water conductivity model. However, recent laboratory measurements have yielded differing results as to the degree to which hydrogen can impact bulk conductivity and whether it can cause anisotropic conductivity (*10*, *11*).

Gaillard *et al*. prefer to explain the shallow conductivity anomaly at the East Pacific Rise by carbonatite melt. The authors take the view that hydrogen in olivine does not produce an anisotropic conductivity and that it only has a modest impact on bulk conductivity (*10*), but this result requires an extrapolation of the extant laboratory results. Other laboratory results (*11*) are consistent with a conductivity anomaly caused by hydrogen. Gaillard *et al*. do not argue in favor of a dry mantle, but rather that carbonatites can mask the ability of conductivity to measure mantle water content. Because carbonatites will mix with silicate melts at shallower depths (*12*), this conclusion is depth-dependent, and the conductivity of a silicate-carbonatite melt mix remains unknown. A deeper conductor beneath the East Pacific Rise is entirely consistent with the Gaillard *et al.* model of carbonatite melt. Deep conductors in the Andean subduction zone (*13*) may also be consistent with small amounts of melt from carbonated oceanic crust (*14*).

A key part of the water/melt controversy is whether melt can form an anisotropic network compatible with the observed conductivity. Is the melt distribution controlled by regional stresses or by surface energies and buoyancy acting at the grain scale? If it is the former, as Gaillard *et al.* claim, then melt would be the preferred explanation; some seismologists have also argued in favor of melt (*15*). If it is the latter, then there could still be a small amount of silicate melt present that would impact seismic velocities and even conductivity, but most of the anisotropic conductivity

CREDIT: FIGURE ADAPTED FROM (4)

Published by AAAS

would come from the effects of water. Furthermore, the independent observations that Gaillard *et al*. use to argue in favor of melt predict a sheet-like melt network would not cause anisotropic conductivity, especially if the conduction arises from highly conductive carbonatite melts.

If Gaillard *et al*.'s explanation is correct, then small volumes of carbonatite melt are rafted away from the ridge crest. For the melt to conduct, it needs to be interconnected throughout the mantle—and there is good reason to expect it to be interconnected (*16*). Carbonatites are highly buoyant (*17*) and, in general, interconnected melt is thought to be mobile. Yet, if the conductor away from the ridge crest on the East Pacific Rise is caused by carbonatite melt, then this trace amount of melt appears to be trapped: The overlying 60 to 70 km of mantle are highly resistive, show no sign of melt, and thus appear to prevent upward flow. Similarly, the deeper conductor across the Pacific Basin appears to be stable. Substantial volumes of melt could be floating about in the asthenosphere (the actively convecting part of the mantle), and its fate merits further investigation. Perhaps it plays a role in seamount formation. Perhaps it is released through faults in the overriding lithosphere. Or perhaps it stays put.

Resolving the water/melt controversy may be tricky: It is difficult to conceive of a field experiment that could rule one mechanism in or out. Areas with temperatures below the mantle melting point would also be too cold for the water mechanism to affect conductivity, and the interdependence between melting and water content similarly make it difficult to untangle the two. But regardless of this debate, at least the deep melt fractions inferred from geophysics can now be revised, and petrologists and geophysicists can move several steps closer to agreement.

References and Notes

1. N. H. Sleep, K. Zahnle, *J. Geophys. Res.* **106**, 1373 (2001).
2. F. Gaillard, *Science* **322**, 1363 (2008).
3. R. Dasgupta *et al*., *Geology* **35**, 135 (2007).
4. K. Baba *et al.*, *J. Geophys. Res.* **111**, B02101 (2006).
5. R. Dasgupta, M. M. Hirschmann, *Nature* **440**, 659 (2006).
6. G. Hirth, D. L. Kohlstedt, *Earth and Planet. Sci. Lett*. **144**, 93 (1996).
7. D. Lizarralde *et al.*, *J. Geophys. Res.* **100**, 17837 (1995).
8. S. Karato, *Nature*, **347**, 272 (1990).
9. R. L. Evans *et al.*, *Nature* **437**, 249 (2005).
10. T. Yoshino *et al*., *Nature* **443**, 973 (2006).
11. D. J. Wang *et al*., *Nature* **443**, 977 (2006).
12. W. Lee, P. J. Wyllie, *Contrib. Mineral. Petrol.* **127**, 1 (1997).
13. J. Booker *et al*., *Nature* **429**, 399 (2004).
14. M. Walter *et al*., *Nature* **454**, 622 (2008).
15. Y. Yang *et al*., *Earth Planet. Sci. Lett*. **258**, 260 (2007).
16. W. G. Minarik, E. B. Watson, *Earth Planet. Sci. Lett*. **133**, 423 (1995).
17. D. P. Dobson *et al.*, *Earth Planet. Sci. Lett*. **143**, 207 (1996).
18. Thanks to A. Saal, G. Hirth, G. Gaetani, and R. Dasgupta for answering questions on carbonatite melts.

10.1126/science.1166260

BIOCHEMISTRY

Controlled Chaos

The availability and abundance of intrinsically disordered proteins inside a cell is under tight control.

Vladimir N. Uversky[1,2] and A. Keith Dunker[1]

The cornerstone of modern protein structural biology is the sequence-structure-function paradigm, according to which a protein's function depends on its folding into a unique three-dimensional structure. Thus, proteins are traditionally viewed as rigid or semi-rigid "blocks," whose specificity and catalytic power are determined by the unique fit of a correct substrate onto the preformed and sturdy surface of the enzyme's active site (*1*). But the discovery of proteins that are wholly disordered or contain lengthy disordered segments, yet are functional (*2*–*6*), has wreaked havoc on the lock-and-key world view that demands highly organized proteins. Such disordered proteins are abundant, diverse, vital, dynamic, and chaotic, and on page 1365 of this issue, Gsponer *et al*. (*7*) reveal how these disorganized proteins are tightly controlled inside the cell.

The concept of ill-structured but functional proteins has raised many questions. For example, although some disordered proteins (and disordered regions within proteins) have been characterized in vitro, whether they are "real" and exist in vivo has not been clear. The abundance of these proteins and protein regions in various proteomes, their structural and dynamical properties, and their functional repertoire have not been understood. It also remains unknown whether intrinsic disorder in a protein is encoded by the amino acid sequence, or what the turnover rates are of such proteins in a cell. More generally, it is not clear how intrinsically disordered proteins are regulated inside the cell.

Bioinformatics has begun to play a crucial role in shaping the study of intrinsically disordered proteins, bringing coherence to proteins that were previously viewed as individual outliers (*8*). Disorderedness is now linked to amino acid sequence. Intrinsically disordered proteins (and regions) are generally enriched in most polar and charged residues and are depleted of hydrophobic residues (other than proline), and this distinction forms the basis of computational tools for disorder prediction (*4*, *5*, *8*, *9*).

The main functions of intrinsically disordered proteins include transducing intracellular signals, regulating processes including the cell division cycle, and recognizing various binding partners (e.g., ligands, other proteins, and nucleic acids). These are complementary to the common catalysis and transport activities of proteins with well-defined, stable three-dimensional structures (*3*, *5*, *6*, *10*–*12*). Structurally, intrinsically disordered proteins range from completely unstructured polypeptides to extended partially structured forms to compact disordered ensembles containing substantial secondary structure (*10*, *11*). Intrinsically disordered regions are highly abundant in nature [>50% of eukaryotic proteins likely contain at least one disordered region ≥30 amino acids in length (*5*)]. Furthermore, many proteins encoded by various genomes are likely to be wholly disordered [e.g., >20% of eukaryotic proteins are expected to be mostly disordered (*13*)].

The rates (*14*) and patterns (*15*) of amino acid substitutions within intrinsically disordered proteins over evolutionary time are distinct from those within structured proteins and are consistent with lack of structure. Therefore, these evolutionary characteristics support the existence of disorder inside the cell. Also, polypeptide segments that are present in some proteins but absent in others as a result of alternative splicing of the encoding messenger RNA (mRNA) are much more often intrinsically disordered than ordered (*16*). Furthermore, new segments that become

[1]Institute for Intrinsically Disordered Protein Research, Center for Computational Biology and Bioinformatics, Department of Biochemistry and Molecular Biology, Indiana University School of Medicine, Indianapolis, IN 46202, USA. [2]Institute for Biological Instrumentation, Russian Academy of Sciences, 142290 Pushchino, Moscow Region, Russia. E-mail: vuversky@iupui.edu

added to proteins (probably through the conversion of a noncoding DNA sequence to a coding sequence) typically lack structure and fall into the class of intrinsically disordered regions (*17*). Thus, it is not surprising that proteins and protein regions that are disordered are often associated with human diseases (*18*).

Gsponer *et al*. assigned all proteins of the budding yeast *Saccharomyces cerevisiae* to one of three groups according to their predicted levels of intrinsic disorder: highly ordered proteins (0 to 10% predicted disorder), moderately disordered proteins (10 to 30% predicted disorder), and highly disordered proteins (30 to 100% predicted disorder). The authors then evaluated correlations between these groups and the various steps of protein synthesis and degradation.

To collate the transcription of genes encoding intrinsically disordered and ordered proteins, Gsponer *et al*. compared the synthesis and degradation rates of the corresponding mRNAs. Although the rates of transcription of genes encoding both classes of proteins were comparable, mRNAs encoding intrinsically disordered proteins were generally less abundant because of their increased degradation (see the figure).

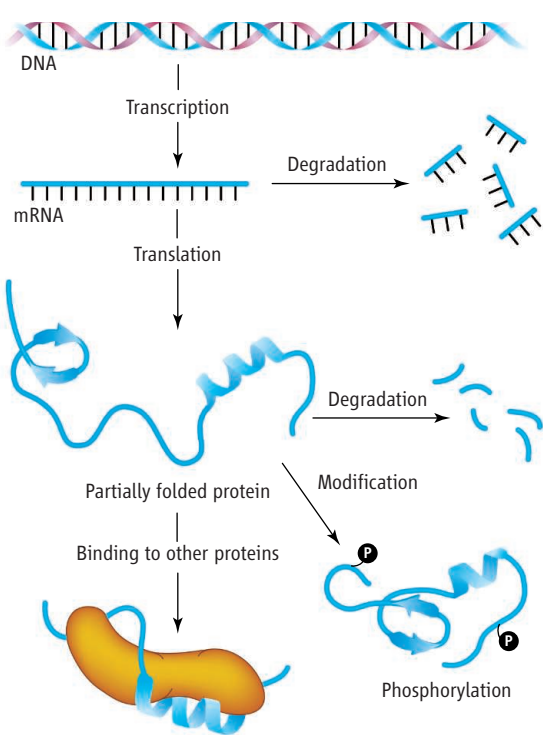

Disorder management. As a result of fast mRNA degradation, slow translation of mRNA into protein, and fast protein degradation, the overall amount of intrinsically disordered proteins inside a cell is less, and their half-lives are generally shorter, than those of ordered proteins. However, some disordered proteins can be present at high quantities and for long periods of time if they are modified (such as by phosphorylation) or interact with some specific binding partners.

At the protein level, intrinsically disordered proteins were less abundant than ordered proteins because of their lower rates of synthesis and shorter half-lives. Because the stability of certain proteins can be modulated by chemical modifications such as phosphorylation (*19*), Gsponer *et al*. examined a specific enzyme-substrate network in yeast. Intrinsically disordered proteins were substrates of twice as many kinases (enzymes that phosphorylate proteins) as were ordered proteins. The majority of kinases whose substrates were mostly intrinsically disordered proteins either were regulated in a manner that depended on the stage of the cell division cycle or were activated upon exposure to particular stimuli or stress. Therefore, protein modifications not only may serve as important regulatory mechanisms for the fine-tuning the functions of intrinsically disordered proteins, but may also be necessary to tightly control the availability of these proteins under different conditions.

Comparable trends were found in proteins of the fission yeast *Schizosaccharomyces pombe* and in proteins of *Homo sapiens*, suggesting that unicellular and multicellular eukaryotes regulate the availability of intrinsically disordered proteins similarly. Overall, Gsponer *et al*. demonstrate evolutionarily conserved tight control of synthesis and clearance of most intrinsically disordered proteins. This stringent regulation is directly related to the involvement of such proteins in cell signaling, in which it is crucial that proteins be available in appropriate amounts yet not be present longer than needed. In addition, some intrinsically disordered proteins could be present in cells in large amounts and/or for long periods of time because of either specific chemical modifications or interactions with other factors that promote changes in their cellular localization or protect them from degradation (*5*, *19*, *20*).

The observations made by Gsponer *et al*. clearly show that the chaos seemingly introduced into the protein world by the discovery of these proteins is under tight control. These findings are in a good agreement with a recently published study showing that both the measured amount of RNA in a bacterium (*Escherichia coli*) and the predicted amount of protein expression correlate positively with the predicted fraction of disordered regions in *E. coli* proteins (*21*). The disorder predictions match with the experimentally elucidated disordered regions for several highly expressed proteins that were predicted to have a high degree of disorder. It was proposed that higher synthesis and degradation rates could make the amount of intrinsically disordered proteins very sensitive to the environment, with slight changes in either production or degradation leading to significant shifts in the amount of protein present.

The discovery of new functions of intrinsically disordered proteins is a goal for the future, as well as a better understanding of how these proteins have evolved. Another important aim will be the elaboration of new experimental methods and computational tools for the discovery and structural and functional characterization of intrinsically disordered proteins and regions, both inside cells and in a crowded milieu in vitro. Uncovering the interplay between intrinsic protein disorder and the pathogenesis of human diseases has just begun.

References and Notes

1. E. Fischer, *Ber. Deutsch. Chem. Ges.* **27**, 2985 (1894).
2. P. Romero *et al.*, *Pac. Symp. Biocomput.* **3**, 437 (1998).
3. P. E. Wright, H. J. Dyson, *J. Mol. Biol.* **293**, 321 (1999).
4. V. N. Uversky, J. R. Gillespie, A. L. Fink, *Proteins* **41**, 415 (2000).
5. A. K. Dunker *et al.*, *J. Mol. Graph. Model.* **19**, 26 (2001).
6. P. Tompa, *Trends Biochem. Sci.* **27**, 527 (2002).
7. J. Gsponer, M. E. Futschik, S. A. Teichmann, M. M. Babu, *Science* **322**, 1365 (2008).
8. P. Radivojac *et al.*, *Biophys. J.* **92**, 1439 (2007).
9. F. Ferron, S. Longhi, B. Canard, D. Karlin, *Proteins* **65**, 1 (2006).
10. A. K. Dunker, Z. Obradovic, *Nat. Biotechnol.* **19**, 805 (2001).
11. V. N. Uversky, *Protein Sci.* **11**, 739 (2002).
12. H. J. Dyson, P. E. Wright, *Nat. Rev. Mol. Cell. Biol.* **6**, 197 (2005).
13. C. J. Oldfield *et al.*, *Biochemistry* **44**, 1989 (2005).
14. C. J. Brown *et al.*, *J. Mol. Evol.* **55**, 104 (2002).
15. P. Radivojac, Z. Obradovic, C. J. Brown, A. K. Dunker, *Pac. Symp. Biocomput.* **7**, 589 (2002).
16. P. R. Romero *et al.*, *Proc. Natl. Acad. Sci. U.S.A.* **103**, 8390 (2006).
17. S. Fukuchi, K. Homma, Y. Minezaki, K. Nishikawa, *J. Mol. Biol.* **355**, 845 (2006).
18. V. N. Uversky, C. J. Oldfield, A. K. Dunker, *Annu. Rev. Biophys. Mol. Biol.* **37**, 215 (2008).
19. M. Grimmler *et al.*, *Cell* **128**, 269 (2007).
20. P. Tompa, *FEBS Lett.* **579**, 3346 (2005).
21. O. Paliy, S. M. Gargac, Y. Cheng, V. N. Uversky, A. K. Dunker, *J. Proteome Res.* **7**, 2234 (2008).
22. Supported by NIH grants R01 LM007688-01A1 (V.N.U. and A.K.D.) and GM071714-01A2 (V.N.U. and A.K.D.) and by the Molecular and Cellular Biology Program of the Russian Academy of Sciences (V.N.U.). We gratefully acknowledge the support of the IUPUI Signature Centers Initiative.

10.1126/science.1167453

AAAS ABELSON SEMINAR

In Pursuit of Cures, Researchers Track Impact of Stress on the Brain

Researchers are looking deep into the circuitry of the brain to understand how stress affects synapses and even molecules, and that may yield therapies for ills ranging from Alzheimer's disease and alcoholism to post-traumatic stress disorder, speakers said at the annual Philip Hauge Abelson Advancing Science Seminar.

At the day-long conference, 10 prominent neurobiologists, psychologists, and genetics researchers demonstrated that the cutting-edge science of stress has moved far past the general notion that stress is a pervasive but superficial complaint. Researchers at the forefront today are pinpointing the molecular mechanisms by which stress leads to poor health.

These data will help researchers develop new drugs to treat stress-related disorders, but they also underscore stress's importance as a risk factor for disease and a major cause of illness and death around the world, said Harvard Provost Steven E. Hyman at the close of the conference.

"We need to be really rigorous with ourselves about what the mechanisms are, because it is not easily and broadly accepted in society and by policy-makers that negative experience or stress gets internalized in a way that leaves indelible or very difficult-to-erase traces in the body that affect health," said Hyman.

The new biology of stress suggests that not all stress is unhealthy, and the evolutionary benefits of short-term stress are clear, said keynote speaker Robert Sapolsky, the John A. and Cynthia Fry Gunn Professor of Neurology and Neurological Sciences at Stanford University. Stressful situations can prompt a surge of energy, a flood of hormones, and quick thinking—all of which probably evolved as a way to allow us to evade and outsmart our ancient predators, he said.

This stress response might be harnessed to enhance immunity during vaccination and surgery, said Firdaus Dhabhar of the Institute for Immunity, Transplantation and Infection at Stanford University. Dhabhar and colleagues have shown that the hormones produced during the stress of knee surgery can strengthen the immune response and promote recovery up to a year later.

Sapolsky's decades-long field studies of baboon troops in Kenya illustrate the host of disorders that can occur when stress continues for a long time. The baboons "spend 3 hours a day getting the calories they need," said Sapolsky. "That means they have 9 hours a day to be god-awful terrible to some other baboon." Lower-ranking baboons that bear the brunt of this behavior tend to have higher blood pressure, less "good" cholesterol, lower levels of white blood cells, insulin resistance, and suppressed sperm production, his studies show.

Stress in the wild. Olive baboon field studies underscore the health effects of long-term stress.

"I think it's important to realize that in some cases [stress] is protective, but if you push the signal too long, then it becomes deleterious," said Richard I. Morimoto, director of the Rice Institute for Biomedical Research at Northwestern University. Morimoto discussed stress's effects at the molecular level and its implications for neurodegenerative disorders such as Huntington's and Alzheimer's disease.

Many of the speakers focused on the neurochemical changes induced by stress, particularly among children. Martha J. Farah, director of the Center for Cognitive Neuroscience at the University of Pennsylvania, shared data from several studies suggesting a link between the stress of childhood poverty and diminished functioning in areas of the brain necessary for language, memory, and self-control.

The brain's "stress axis" of hormonal response by the hypothalamic, pituitary, and adrenal glands can be altered by nurturing, at least according to rat-rearing studies. The amount of stimulation newborn rats receive can affect the sensitivity of the stress axis, said Darlene Francis, an assistant professor of neuroscience, psychology, and public health at the University of California, Berkeley. "Differences in the stress-axis may then render populations more vulnerable—or resilient—to the slings and arrows of life," she explained.

Other researchers are looking for ways to harness the brain's response to stress to treat diseases such as alcoholism, where some preliminary studies suggest that manipulating anti-stress hormones can relieve the symptoms of alcohol dependence, said Markus Heilig of the National Institute on Alcohol Abuse and Alcoholism.

The molecular mechanisms of how the brain creates, stores, and recalls memories might be an apt treatment target for post-traumatic stress disorder, according to several speakers. In the future, "we might have a patient retrieve a memory, give a drug or some other manipulation that blocks the re-storage of the memory, and as a result, maybe weaken or dampen the emotional impact of that memory," explained Joseph LeDoux, Henry and Lucy Moses Professor of Science at the Center for Neural Science at New York University.

The "Science, Stress, and Human Health" seminar was planned in honor of Philip Abelson, who served as editor of the journal *Science* for 22 years, and then as senior advisor to AAAS until shortly before his death, at the age of 91, in 2004. Recordings from the seminar are available at www.aaas.org/go/abelson.

—Ginger Pinholster and Becky Ham

SCIENCE DIPLOMACY

Pickering: Science Can Defuse Global Conflicts

The United States is locked in a challenging conflict with Iran over nuclear proliferation fears. Economic competition and environmental issues inject tension into the U.S. relationship with China. Some analysts fear a sequel to the U.S.-Russia Cold War. But former U.S. Ambassador Thomas Pickering, in a talk at AAAS, suggested a common tool for addressing each conflict: science diplomacy.

Recalling the lessons of his nearly 40-year diplomatic career as ambassador to Russia, Israel, and four other countries, Pickering said that shared interests in science and technology can help the United States build a productive relationship with its strongest competitors and foes while dampening the possibility of more volatile confrontations.

"If you look around the world, despite what is certainly a serious decline in U.S. … popular-

Published by AAAS

ity, the science issue has not faded from the center of foreign interest in us," said Pickering, now chairman of the international consulting firm Hills and Co.

In his wide-ranging, 90-min interview with foreign affairs journalist and analyst Arnaud de Borchgrave, Pickering discussed how the United States might approach its diplomatic relationships with key nations such as Iran, where the United States has sought a halt to the country's advancing nuclear program.

Pickering said the United States has not "run out the string for diplomacy" with Iran, and suggested that direct talks—without preconditions—would be a good strategy for the next U.S. administration to pursue. But he advised against a meeting with Iranian President Mahmoud Ahmadinejad before lower-level talks take place. The United States has said it would not negotiate directly unless Iran agrees to stop all uranium enrichment for its nuclear program.

Arnaud de Borchgrave and Thomas Pickering.

To defuse mounting tensions with Russia, Pickering recommended a strategy that has been successful in the U.S. relationship with China—building a positive agenda of cooperative efforts instead of focusing solely on negative policies. "We can sit down—as we must—and figure out those long series of questions in which we have a common interest," he said.

When Pickering served as U.S. ambassador to India in the early 1990s, "the one set of questions that we worked on—that was the one bright star in U.S.-India relations—was our science cooperation," he said. "Indians still value it very highly."

Pickering listed disarmament, nonproliferation, energy, climate change, development, health, food, water, and immigration as worldwide diplomatic issues that cannot be resolved "without good science and without the work of science."

"In the contemporary world, science and diplomacy have to be intimately connected," said Norman Neureiter, director of the AAAS Center for Science, Technology and Security Policy. "As Colin Powell said, 'Diplomacy is the front line of national security.' When the talking stops, that's when the shooting starts. In a nuclear world, that can be really serious."

The 7 October event was cosponsored by the AAAS Center for Science, Technology and Security Policy and the new AAAS Center for Science Diplomacy.

—Molly McElroy and Becky Ham

ETHICS

AAAS and Academies Launch Ambitious Research Integrity Site

In the wake of several prominent research scandals and a recent study suggesting that scientific misconduct often goes unreported, a new Web site from the National Academies and AAAS offers a comprehensive resource on research integrity.

Drawn from a variety of multimedia sources, the site is one of the few online portals to offer regularly updated information on misconduct and integrity across scientific disciplines.

"It's a documentation of what the community and others are trying to do to preempt misconduct and to react to it effectively when it does occur," said Mark S. Frankel, director of the AAAS Scientific Freedom, Responsibility and Law Program.

Topics from the use of animals in research to data sharing are explored through the site's links to recent literature, news stories, teaching guides, conference information, and research guidelines from public and private research institutions. The site also acknowledges the "global nature of science and the worldwide search for research collaborators" by including extensive links to international materials, said Frankel.

As a resource that can be regularly updated, the site has "tremendous potential," said Richard Bissell, executive director for policy and global affairs at the Academies' National Research Council. "Rather than being a fixed book on the shelf, it can draw on new specific challenges in research ethics, which are often technological."

Bissell said research scandals such as the stem cell fraud committed by South Korean scientists and data suppression by some industry-funded researchers has brought scientific misconduct into sharp relief for policy-makers and the public. In June, a survey of researchers funded by the U.S. National Institutes of Health estimated that 1000 cases of scientific misconduct go unreported each year.

One of the site's strengths, said Frankel, is that it can serve as a hub to Web sites from government agencies and other institutions that have "case studies, role-playing exercises, syllabi, and teaching materials" specific to the issues faced by their researchers.

The site, at www.aaas.org/go/integrity, was funded in part through an endowment established by an anonymous AAAS member to promote honesty in scientific research, especially through collaboration between AAAS and the National Academies.

—Becky Ham

COMMUNICATION

AAAS Names Science Journalism Winners

An ambitious series on memory and the brain, a look at whether research supports widespread use of anti-cholesterol medications, and a broadcast account of the contentious battle over intelligent design in Dover, Pennsylvania, are among the winners of the 2008 AAAS Science Journalism Awards.

Large newspaper—(Circulation >100,000): Terry McDermott, *Los Angeles Times,* for "Chasing Memory" (series), 19 to 22 August 2007.

Small newspaper—(Circulation <100,000): Kara Platoni, *East Bay Express,* for "In Search of Life" (series), 4 July and 11 July 2007.

Magazine: John Carey, *Business Week,* for "Do Cholesterol Drugs Do Any Good?" 28 January 2008.

Television: Joseph McMaster and Gary Johnstone, WGBH/NOVA and Vulcan Productions, for "Judgment Day: Intelligent Design on Trial," 13 November 2007.

Radio: Daniel Grossman, WBUR, Boston, for "Meltdown: Inside Out," December 2007.

Online: Stefan Lovgren, National Geographic News, for "Megafishes," 24 July and 7 November 2007; 29 April 2008.

Children's science news: Yoon Shin-Young, *Children's Science Donga,* for "Roadkill, Horror on Roads," 15 June 2008.

Yoon Shin-Young of South Korea is the first international winner of the children's award since it was introduced in 2005.

The awards, established in 1945, are sponsored by Johnson & Johnson Pharmaceutical Research & Development, L.L.C. Winners in each category will be awarded $3000 and a plaque. The winners will pick up their plaques at a reception at the AAAS Annual Meeting in Chicago in February.

—Earl Lane

2009 ELECTION

A Call for Nominations

AAAS members may suggest nominees (including themselves) for president-elect and the Board of Directors for election in the fall of 2009. For a list of this year's candidates, see AAAS News & Notes in the 26 September 2008 issue of *Science;* for a list of current Board members, go to www.aaas.org/aboutaaas/organization/board.shtml

Please send the suggested nominee's curriculum vitae no later than 29 December to Gretchen Seiler, AAAS Executive Office, 1200 New York Avenue, N.W., Washington, DC, 20005. Suggested nominees will be considered by the AAAS Committee on Nominations at their winter meeting.

Published by AAAS

A Simple Law for Ice-Shelf Calving

Richard B. Alley,[1]* Huw J. Horgan,[1] Ian Joughin,[2] Kurt M. Cuffey,[3] Todd K. Dupont,[4] Byron R. Parizek,[5] Sridhar Anandakrishnan,[1] Jeremy Bassis[6]

Subfreezing ice flowing from Greenland and Antarctica typically forms floating extensions, called ice shelves, before calving icebergs into surrounding seas. A major problem for ice-sheet models is that no physically based law for the calving process has been established (*1*). Ice-shelf buttressing from friction with embayment walls or local sea-floor highs restrains ice-sheet flow; reduction of this buttressing contributes to sea-level rise through faster flow of nonfloating ice feeding ice shelves (*2*). Side friction and the probability of encountering a sea-floor high increase with ice-shelf length, which cannot be calculated without a calving law.

A complete calving law for ice shelves will include forcing (e.g., waves, tides, and collisions with passing icebergs), geometry and material properties (e.g., thickness, temperature, and density), and preexisting flaws (e.g., surface and basal crevasses). However, because calving is dominated by opening of cracks transverse to flow, we hypothesize that along-flow ice shelf spreading is the dominant control on calving.

To test this hypothesis, we assembled (Fig. 1) new [supporting online material (SOM) text] and published data from a range of ice shelves (table S1), chosen to be representative rather than comprehensive. Except for a few spectacular examples, which we avoided, calving flux greatly exceeds length changes. Thus, velocity near the front closely approximates calving flux (c), whereas the along-flow gradient in that velocity gives the appropriate spreading rate ($\dot{\varepsilon}$). All data avoid shear margins and are primarily near center lines.

Results are consistent with our hypothesis. The optimal power-law fit, $c = 15{,}000\,\dot{\varepsilon}^{0.43}$ m/year, explains 91% of the variance (62% for a linear regression in log-log space); using $c = 12{,}000\,\dot{\varepsilon}^{0.33}$ for linear dependence on spreading stress explains 88% of variance (43% log-log).

Residuals indicate slower calving for narrower shelves. Side shear rotates crack-opening stresses away from the calving front, while favoring smaller bergs and shear fractures that can heal easily. The model $c = 0.039(\dot{\varepsilon}w)^{1.9}$ m/year (with half-width w in meters) explains over 95% of the variance (92% in log-log space). Calving rate does correlate with thickness H, but a power-law fit for $c(H)$ explains only 69% of the variance (84% log-log); residuals from the fits involving $c(\dot{\varepsilon})$ and $c(\dot{\varepsilon}w)$ do not strongly correlate with H. Nonetheless, the spreading stress increases with H, and one might expect fracturing, and hence calving, to depend on the rate of deformational work done and thus to be proportional to $\dot{\varepsilon}H$. The best-fit power law including ($\dot{\varepsilon}wH$) is $c = 0.022(\dot{\varepsilon}wH)^{0.98}$ m/year; Fig. 1 shows the linear fit through the origin $c = 0.016\ \dot{\varepsilon}wH$ m/year, with each explaining 89% of the variance (93% log-log) (SOM text). The data do not allow choice among these or some other possible relations, but the latter is physically motivated and simple.

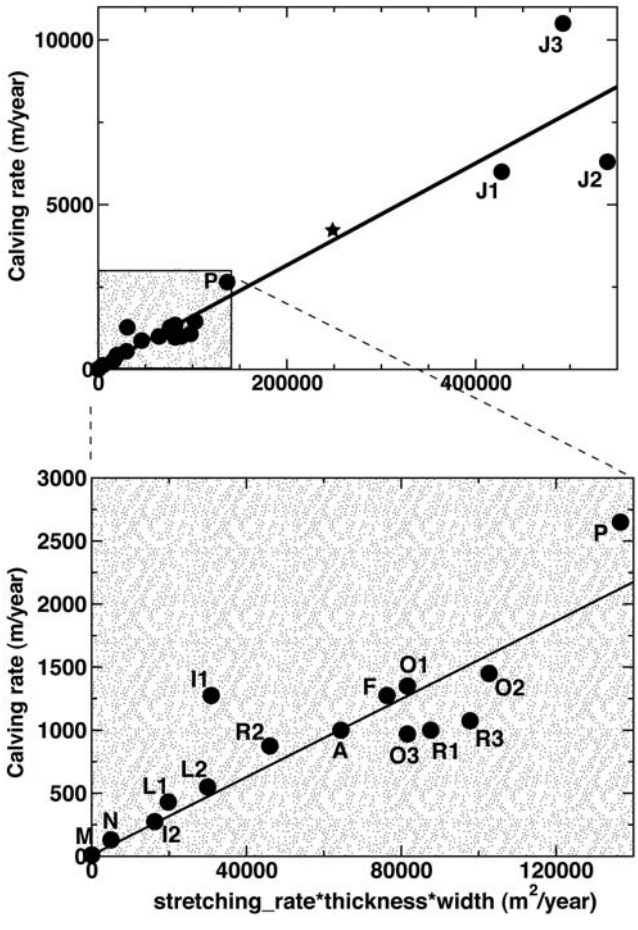

Fig. 1. Calving rate (estimated as observed ice-front velocity) against the product of ice-shelf near-front thickness, half-width, and strain rate (estimated as along-flow gradient in along-flow velocity taken about one iceberg width from the calving front). Letters identify shelves (table S1): A, Amery; F, Filchner; I, Riiser; J, Jakobshavn; L, Larsen B; M, McMurdo; N, Nivlisen; O, Ronne; P, Pine Island; and R, Ross. All of the points are near ice-shelf center lines except R1, R3, O1, and O3, which are well away from shear margins and which do not greatly influence the regression line shown. Columbia Glacier (star) (SOM text) is also indicated for reference; it lacks an ice shelf and is not included in any regressions.

One implication of c increasing with $\dot{\varepsilon}$ is that almost any unbuttressed ice shelf will be unconditionally unstable because thickness (hence spreading rate) decreases in the flow direction but velocity increases; a calving event will move the ice front into thicker, faster-spreading, and hence faster-calving, ice that is supplied more slowly. Numerical experiments (*3*) indicate that appropriate buttressing stabilizes ice shelves. This appears consistent with observations: extremely elongated "ice tongues" are possible from sufficiently fast input of sufficiently thin (hence slowly spreading) ice, shelves are commonly observed to terminate near buttressing points, and rapid shelf shrinkage has occurred after loss of buttressing.

Although we have not learned the complete calving law, we suggest that the relations derived here from intercomparison of ice shelves may be more encouraging than any obtained previously for this vexing problem and so merit additional testing and cautious implementation in ice-flow models.

References and Notes

1. M. F. Meier, in *Sea-Level Change* (National Academy Press, Washington, DC, 1990), pp. 171–189.
2. T. K. Dupont, R. B. Alley, *Geophys. Res. Lett.* **32**, L04503 10.1029/2004GL022024 (2005).
3. T. K. Dupont, R. B. Alley, H. Horgan, I. Joughin, paper presented at the 14th Annual West Antarctic Ice Sheet Meeting/joint meeting with Filchner-Ronne Ice Shelf Program, Sterling, VA, 7 September 2008.
4. Partial funding was provided by NSF (including grants 0424589, 0440899, 0531211, 0758274, and 0809106), NASA NRA04OES02, and the Gary Comer Science and Education Foundation. We thank two anonymous reviewers.

Supporting Online Material

www.sciencemag.org/cgi/content/full/322/5906/1344/DC1
SOM Text
Table S1
References

30 June 2008; accepted 12 September 2008
10.1126/science.1162543

[1]Department of Geosciences, Pennsylvania State University (Penn State), University Park, PA 16802, USA. [2]Applied Physics Laboratory, University of Washington, Seattle, WA 98105, USA. [3]Department of Geography, University of California, Berkeley, CA 94720, USA. [4]Department of Earth System Science, University of California, Irvine, CA 92697, USA. [5]Mathematics and Geoscience, Penn State Dubois, Dubois, PA 15801, USA. [6]Scripps Institution of Oceanography, La Jolla, CA 92037, USA.

*To whom correspondence should be addressed. E-mail: rba6@psu.edu

CORRECTED 2 JANUARY 2009; SEE LAST PAGE

Optical Images of an Exosolar Planet 25 Light-Years from Earth

Paul Kalas,[1]* James R. Graham,[1] Eugene Chiang,[1,2] Michael P. Fitzgerald,[3] Mark Clampin,[4] Edwin S. Kite,[2] Karl Stapelfeldt,[5] Christian Marois,[6] John Krist[5]

Fomalhaut, a bright star 7.7 parsecs (25 light-years) from Earth, harbors a belt of cold dust with a structure consistent with gravitational sculpting by an orbiting planet. Here, we present optical observations of an exoplanet candidate, Fomalhaut b. Fomalhaut b lies about 119 astronomical units (AU) from the star and 18 AU of the dust belt, matching predictions of its location. Hubble Space Telescope observations separated by 1.73 years reveal counterclockwise orbital motion. Dynamical models of the interaction between the planet and the belt indicate that the planet's mass is at most three times that of Jupiter; a higher mass would lead to gravitational disruption of the belt, matching predictions of its location. The flux detected at 0.8 μm is also consistent with that of a planet with mass no greater than a few times that of Jupiter. The brightness at 0.6 μm and the lack of detection at longer wavelengths suggest that the detected flux may include starlight reflected off a circumplanetary disk, with dimension comparable to the orbits of the Galilean satellites. We also observe variability of unknown origin at 0.6 μm.

About 15% of nearby stars are surrounded by smaller bodies that produce copious amounts of fine dust via collisional erosion (*1*). These "dusty debris disks" are analogs to our Kuiper Belt and can be imaged directly through the starlight they reflect or thermal emission from their dust grains. Debris disks may be gravitationally sculpted by more massive objects; their structure gives indirect evidence for the existence of accompanying planets [e.g., (*2*, *3*)]. Fomalhaut, an A3V star 7.69 pc from the Sun (*4*), is an excellent example: A planet can explain the observed 15 AU offset between the star and the geometric center of the belt, as well as the sharp truncation of the belt's inner edge (*3*, *5*–*7*). With an estimated age of 100 to 300 million years (My) (*8*), any planet around Fomalhaut would still be radiating its formation heat and would be amenable to direct detection. The main observational challenge is that Fomalhaut is one of the brightest stars in the sky (apparent visual magnitude $m_V = 1.2$ mag); to detect a planet around it requires the use of specialized techniques such as coronagraphy to artificially eclipse the star and suppress scattered and diffracted light.

Detection of Fomalhaut b. Coronagraphic observations with the Hubble Space Telescope (HST) in 2004 produced the first optical image of Fomalhaut's dust belt and detected several faint sources near Fomalhaut (*6*). Fomalhaut's proper motion across the sky is 0.425 arc sec per year in the southeast direction, which means that objects that are in the background will appear to move northwest relative to the star. To find common proper motion candidate sources, we observed Fomalhaut with the Keck II 10-m telescope in 2005 and with HST in 2006 (*9*). In May 2008, a comprehensive data analysis revealed that Fomalhaut b is physically associated with the star and displays orbital motion. Follow-up observations were then conducted at Gemini Observatory at 3.8 μm (*9*).

Fomalhaut b was confirmed as a real astrophysical object in six independent HST observations at two optical wavelengths (0.6 μm and 0.8 μm; Fig. 1 and table S1). It is comoving with Fomalhaut, except for a 0.184 ± 0.022 arc sec (1.41 ± 0.17 AU) offset between 2004 and 2006 ($\Delta T = 1.73$ years) corresponding to 0.82 ± 0.10 AU year^{-1} projected motion relative to Fomalhaut (*9*). If Fomalhaut b has an orbit that is coplanar and nested within the dust belt, then its semimajor axis is $a \approx 115$ AU, close to that predicted by Quillen (*7*). An object with $a = 115$ AU in near-circular Keplerian motion around a star with mass 2.0 times that of the Sun has an orbital period of 872 years and a circular speed of 3.9 km s^{-1}. The six Keplerian orbital elements are unconstrained by measurements at only two epochs; however, by comparing the deprojected space velocity ($5.5^{+1.1}_{-0.7}$ km s^{-1}) with the circular speed, we

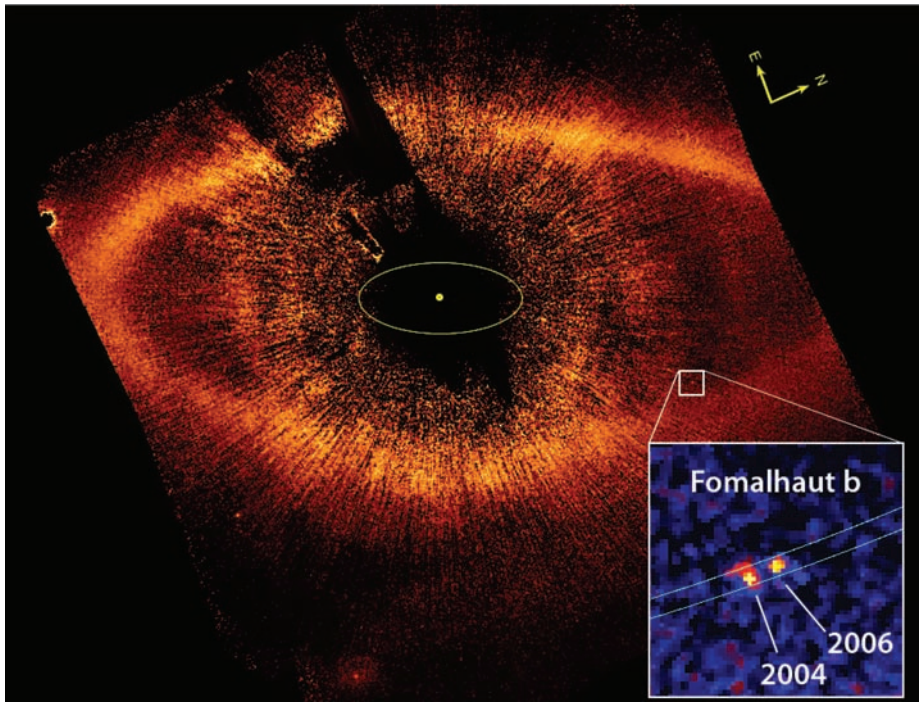

Fig. 1. HST coronagraphic image of Fomalhaut at 0.6 μm, showing the location of Fomalhaut b (white square) 12.7 arc sec radius from the star and just within the inner boundary of the dust belt. All the other apparent objects in the field are either background stars and galaxies or false positives. The fainter lower half of the dust belt lies behind the sky plane. To obtain an orientation with north up and east left, this figure should be rotated 66.0° counterclockwise. The yellow circle marks the location of the star behind the occulting spot. The yellow ellipse has a semimajor axis of 30 AU at Fomalhaut (3.9 arc sec) that corresponds to the orbit of Neptune in our solar system. The inset is a composite image showing the location of Fomalhaut b in 2004 and 2006 relative to Fomalhaut. Bounding Fomalhaut b are two elliptical annuli that are identical to those shown for Fomalhaut's dust belt (*6*), except that here the inner and outer annuli have semimajor axes of 114.2 and 115.9 AU, respectively. The motion of Fomalhaut b therefore appears to be nested within the dust belt.

[1]Astronomy Department, University of California, Berkeley, CA 94720, USA. [2]Department of Earth and Planetary Science, University of California, Berkeley, CA 94720, USA. [3]Institute of Geophysics and Planetary Science, Lawrence Livermore National Laboratory, Livermore, CA 94551, USA. [4]Exoplanets and Stellar Astrophysics Laboratory, Goddard Space Flight Center, Greenbelt, MD 20771, USA. [5]MS 183-900, Jet Propulsion Laboratory, California Institute of Technology, Pasadena, CA 91109, USA. [6]Herzberg Institute for Astrophysics, Victoria, British Columbia V9E 2E7, Canada.

*To whom correspondence should be addressed. E-mail: kalas@astron.berkeley.edu

find a lower limit on the eccentricity of 0.13 (95% confidence) by assuming that Fomalhaut b is at periastron. Thus, our observations are consistent with bound Keplerian motion, although the exact range of allowable eccentricity depends sensitively on poorly known uncertainties in orbital inclination, apsidal orientation, and host stellar mass.

Fomalhaut b is located near the faint half of the belt seen in stellar light backscattered by dust grains. Therefore, it lies behind the sky plane (the Earth–Fomalhaut–Fomalhaut b angle is 126°), at ~51° past conjunction as it orbits counterclockwise. Although faint, Fomalhaut b is still 100 times as bright as reflected light from a Jupiter-like planet at that radius from Fomalhaut (*9*).

Dynamical models of planet-belt interaction. We constrained the mass of Fomalhaut b by modeling its gravitational influence on the dust belt, reproducing properties of the belt inferred from the HST scattered-light images. Our model assumes that Fomalhaut b is solely responsible for the observed belt morphology. This assumption implies that the orbits of the belt and of Fomalhaut b are apsidally aligned. The deprojected space velocity and current location of Fomalhaut b are nominally inconsistent with this expectation. Apsidal misalignment may imply the existence of additional perturbers; then the mass estimates derived from our single-planet models are upper limits.

Our modeling procedure comprises four steps. First, for a given mass and orbit of Fomalhaut b, we create a population of several thousand parent bodies stable to gravitational perturbations from the planet. These parent bodies, modeled as test particles, do not undergo close encounters with Fomalhaut b over a 100-My period. Initial parent body orbits have semimajor axes between 120 and 140 AU, and their eccentricities and longitudes of periastron are purely secularly forced by the planet (*10*). Initial inclinations of parent bodies are randomly and uniformly distributed within 0.025 rad of Fomalhaut b's orbital plane, and remaining orbital angles are drawn at random. After 100 My, parent body orbits differ somewhat from these initial conditions; most survivors have semimajor axes of >130 AU. The forced orbits thus constructed are nested ellipses with eccentricity of ~0.11 that approximate the observed belt morphology. Forced orbits are expected to result from interparticle collisions, which dissipate random motions and compel planetesimals to conform toward closed, nonintersecting paths (*11*).

This elliptical annulus of parent bodies is termed a "birth ring" (*12*); erosive collisions among parent bodies give birth to smaller but more numerous dust grains. The observed scattered stellar light predominantly arises not from parent bodies but rather from their dust progeny. Thus, the second step of our procedure is to track dust trajectories. We take each parent to release a dust grain with the same instantaneous position and velocity as its parent's. The trajectory of a grain of given β (force of radiation pressure relative to that of stellar gravity; β scales inversely as grain radius) is then integrated forward under the effects of radiation pressure and Poynting-Robertson drag. We carry out integrations for $\beta \in (0, 0.00625, 0.0125, \ldots, 0.4)$. For β approaching the radiation blowout value of ~½, grains execute highly elongated orbits whose periastra are rooted within the birth ring. Integrations last 0.1 My, corresponding to the collisional lifetime of grains in Fomalhaut's belt, as estimated from the inferred optical depth of the belt.

Third, we superpose the various β integrations to construct maps of optical depth normal to the belt plane. To reduce the shot noise associated with a finite number of grains, we smear each grain along its orbit: Each grain is replaced by an elliptical wire whose linear density along any segment is proportional to the time that a particle in Keplerian motion spends traversing that segment. We compute the optical depth presented by the collection of wires, weighting each β integration according to a Dohnanyi (*13*) grain size distribution. This distribution, which reflects a quasi-steady collisional cascade in which parent bodies grind down to grains so small they are expelled by radiation pressure, is assumed to hold in the birth ring, where dust densities are greatest and collision rates are highest.

The final step is to compare the optical depth profile of our dynamical model with that of a scattered-light model adjusted to fit the 2004 HST image of Fomalhaut's belt (*6*). We focus on the one belt property that seems most diagnostic of planet mass and orbit: the belt's inner edge, having a semimajor axis of $a_{inner} = 133$ AU according to the scattered-light model. This edge marks the outer boundary of the planet's chaotic zone (*7*). The chaotic zone is a swath of space, enclosing the planet's orbit, that is purged of material because of dynamical instabilities caused by overlapping first-order mean-motion resonances (*14*). For a given planet mass M, we adjust the planet's semimajor axis a until the dynamical model's optical depth attains half its maximum value at a_{inner} (Fig. 2, bottom). Applying this procedure, we find that

$$a_{inner} - a = 2.0(M/M_*)^{2/7}a \qquad (1)$$

where M_* is the central stellar mass.

Two trends that emerge from our modeling imply that the mass of the planet should be low. First, as M increases, the planet more readily perturbs dust grains onto eccentric orbits, and the resultant optical depth profile becomes too

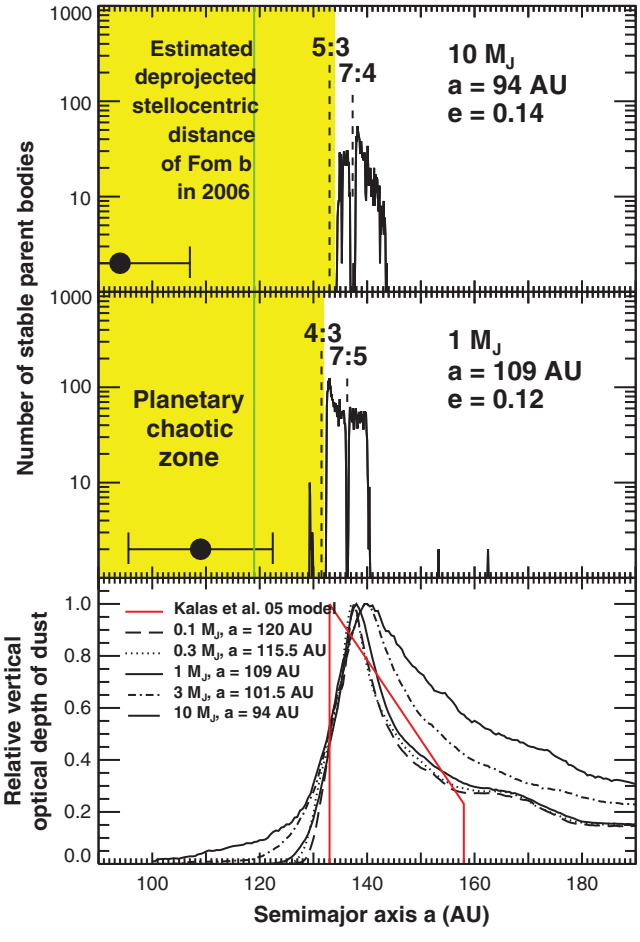

Fig. 2. Dynamical models of how Fomalhaut b gravitationally sculpts the belt [see also (*15*)]. (**Top** and **middle**) Histograms of time-averaged semimajor axes of parent bodies that survive 100-My integrations with Fomalhaut b, whose parameters are chosen to reproduce the belt's inner edge at 133 AU and ellipticity of 0.11. Parent bodies are evacuated from Fomalhaut b's chaotic zone (yellow region). Gaps open at the planet's resonances, akin to the solar system's Kirkwood gaps. Black circles and bars mark the range of stellocentric distances spanned by the model orbits for Fomalhaut b. The apocentric distance for 10 M_J is inconsistent with the observed stellocentric distance of Fomalhaut b (green line). The 1-M_J model is consistent. (**Bottom**) Vertical optical depth profiles of dust generated from parent bodies. The planet orbit is tuned so that the optical depth is at half maximum at 133 AU, the location of the inner edge of the scattered-light model from (*6*) (red curve), which itself is an idealized and non-unique fit to the HST data. Although the dynamical and scattered-light models do not agree perfectly, lower planet masses are still inferred because they do not produce broad tails of emission at $a >$ ~140 AU. At $a >$ ~160 AU, the HST data are too uncertain to constrain any model.

broad at distances greater than ~140 AU (Fig. 2, bottom). Second, for the belt to remain undisrupted, larger-mass planets must have smaller orbits, violating our estimate for the current stellocentric distance of Fomalhaut b (Fig. 2, top and middle). Together, these considerations imply that $M < 3$ Jupiter masses (M_J). This upper limit supersedes those derived previously (*7*), as the quantitative details of our model are more realistic [see also (*15*)]: The belt as a whole is modeled, not just its inner edge; parent bodies are handled separately from dust grains, and only the latter are used to compare with observations; stellar radiation pressure is accounted for; parent bodies are screened for dynamical stability over the system age; and grain-grain collisions are recognized as destructive, so that dust particle integrations are halted after a collision time.

Model planet atmospheres. Comparison between our photometric data and planet atmosphere model–derived spectra indicate that Fomalhaut b may be a cooling jovian-mass exoplanet with an age of 100 to 300 My (Fig. 3). A planet atmosphere model with effective temperature T_{eff} = 400 K and radius 1.2 R_J, for which the bolometric luminosity is 3.4×10^{-7} times that of the Sun ($L_\odot$) (*16*, *17*), reproduces the observed 0.8-μm flux. This model implies that the luminosity of Fomalhaut b is lower than that of any other object observed outside the solar system, and thus that it is not a young brown dwarf or a more massive object. Theoretical cooling tracks of objects with T_{eff} = 400 K and ages of >100 My are insensitive to uncertain initial conditions [see figure 1 of (*16*)]. The luminosity on these tracks is given by $L \sim 2 \times 10^{-7}\,[M/(2\,M_J)]^{1.87}\,(t/200\text{ My})^{-1.21}\,L_\odot$, implying that the mass of Fomalhaut b is 1.7 to 3.5 M_J. The error in the mass is dominated by the age uncertainty.

Relative to the planet atmosphere models, the flux of Fomalhaut b is too faint by at least a factor of 3 at 1.6 μm, and the upper limit set by observations at 3.8 μm is only marginally consistent with the models. However, the various models disagree with each other by similar factors at 1.6 μm, partly because of theoretical uncertainties associated with the strengths of the CH_4 vibrational bands. Moreover, our hypothesized effective temperature is near the condensation temperature of water clouds, and such clouds are a large source of uncertainty in planet atmosphere models. Nonetheless, our observations at 1.6 μm and 3.8 μm exclude a warmer (more massive) planet.

Choosing a 400 K, 46 m s^{-2}, 5× solar abundance model from (*16*) as a baseline, we can investigate the effects of gravity and composition with the use of theoretical exoplanet model spectra (*16*, *17*). The elevated abundance set is chosen to be representative of solar system gas giants. The temperature and gravity of this model are a good match to a 2.5 M_J exoplanet with an age of 200 My. As previously noted, this model accounts for the 0.8-μm flux but overpredicts the 1.6-μm band flux by a factor of 3. Cooler models (350 K) cannot simultaneously reproduce the 0.8-μm flux without violating the long-wavelength flux limits, whereas for hotter models (500 K) the 1.6-μm upper limit becomes particularly problematic. If there is a significant thermal photospheric contribution to the 0.8-μm flux, then 400 K is a rough upper limit to the temperature of the object.

The 400 K solar abundance model has reduced methane opacity, which causes it to be unacceptably bright in the H band. The colors and fluxes also depend on the surface gravity. Models from (*16*) for 10 m s^{-2} and 215 m s^{-2} are also available; the colors of the low-gravity model are too red in both the 0.8- to 1.6-μm and 0.8- to 3.8-μm ranges to be acceptable. Thus, if the gravity is lower than our nominal assumption, corresponding to a ~0.5 M_J object, then we estimate that the upper limit on temperature is raised by about 50 K. The colors of the high-gravity 400 K model are similar to those of the 46 m s^{-2} one.

Other sources of optical emission. From 0.6 to 0.8 μm, Fomalhaut b is bluer than the models predict (Fig. 3). Furthermore, between 2004 and 2006 Fomalhaut b became fainter by ~0.5 mag at 0.6 μm. Photometric variability and excess optical emission cannot be explained by exoplanet thermal radiation alone. The 0.6-μm flux might be contaminated by Hα emission (*9*) that is detected from brown dwarfs (*18*, *19*). Variable Hα emission might arise from a hot planetary chromosphere heated by vigorous internal convection, or trace hot gas at the inner boundary of a circumplanetary accretion disk, by analogy with magnetospheric emission from accreting T Tauri stars [e.g., (*20*)]. If a circumplanetary disk is extended, the starlight it reflects might contribute to the flux detected at 0.6 and 0.8 μm. To explain our observed fluxes requires a disk radius of ~20 to 40 R_J, comparable to the orbital radii of Jupiter's Galilean satellites (*9*). The need for additional sources of luminosity implies that the mass inferred from the 0.8-μm flux alone is an upper limit.

As remarkably distant as Fomalhaut b is from its star, the planet might have formed in situ. The dust belt of Fomalhaut contains three Earth masses of solids in its largest collisional parent bodies. Adding enough gas to bring this material to cosmic composition would imply a minimum primordial disk mass of 1 M_J, comparable to the upper mass limit of Fomalhaut b. Alternatively, the planet might have migrated outward by interacting with its parent disk (*21*) or by gravitationally scattering off another planet in the system and having its eccentricity mildly damped by dynamical friction with surrounding disk material (*22*).

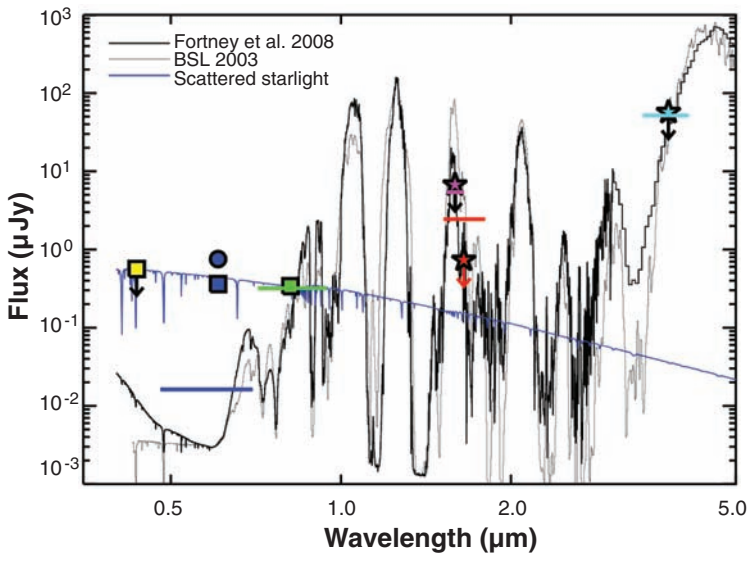

Fig. 3. Photometry on Fomalhaut b shows the F435W 3σ upper limit (yellow square), two F606W measurements (blue square, 2006; blue circle, 2004), the F814W photometry (green square), 3σ upper limits for Keck observations in the CH_4 passband (purple solid star) and in the H band (red solid star), and a 3σ upper limit for Gemini observations at L′ (light blue star). This is a log-log plot. If we first assume that the F606W variability is due to Hα emission and the F814W detection is due to planet thermal emission, we then proceed to fit a planet atmosphere model from Fortney *et al.* (*16*) to the F814W flux. The heavy solid line represents the same planet atmosphere model smoothed to R = 1200 with planet radius 1.2 R_J, gravity 46 m s^{-2}, and T = 400 K (roughly 1 to 3 M_J at 200 My). The horizontal colored lines mark the equivalent broad-band flux found by integrating the model spectrum over the instrumental passband. Other models from Burrows *et al.* [BSL; (*17*)] give a similar spectrum (light solid line), although a factor of 3 to 4 brighter in the CH_4 and H bands. The model predicts that the planet candidate should have been detected with Keck in the H band, although this prediction is only a factor of 3 above our limit. The discrepancy could arise from uncertainties in the model atmosphere (which has never been tested against observation), or from the possibility that the F606W and F814W detections include stellar light reflected from a circumplanetary dust disk or ring system. The solid blue line intersecting the optical data represents light reflected from a circumplanetary disk (with radius 20 R_J and a constant albedo of 0.4) and with stellar properties adopted from (*23*). See table S2 for more information about the HST filters used.

References and Notes

1. D. E. Backman, F. C. Gillett, in *Cool Stars, Stellar Systems and the Sun*, J. L. Linsky, R. E. Stencel, Eds. (Springer-Verlag, Berlin, 1987), pp. 340–350.
2. D. Mouillet, J. D. Larwood, J. C. B. Papaloizou, A. M. Lagrange, *Mon. Not. R. Astron. Soc.* **292**, 896 (1997).
3. M. C. Wyatt *et al.*, *Astrophys. J.* **527**, 918 (1999).
4. One parsec (pc) = 3.09×10^{18} cm.
5. K. Stapelfeldt *et al.*, *Astrophys. J. Suppl. Ser.* **154**, 458 (2004).
6. P. Kalas, J. R. Graham, M. Clampin, *Nature* **435**, 1067 (2005).
7. A. Quillen, *Mon. Not. R. Astron. Soc.* **372**, L14 (2006).
8. D. Barrado y Navascues, *Astron. Astrophys.* **339**, 831 (1998).
9. See supporting material on *Science* Online.
10. C. D. Murray, S. F. Dermott, *Solar System Dynamics* (Cambridge Univ. Press, Cambridge, 1999).
11. B. Paczynski, *Astrophys. J.* **216**, 822 (1977).
12. L. E. Strubbe, E. I. Chiang, *Astrophys. J.* **648**, 652 (2006).
13. J. W. Dohnanyi, *J. Geophys. Res.* **74**, 2531 (1969).
14. J. Wisdom, *Astron. J.* **85**, 1122 (1980).
15. E. Chiang, E. Kite, P. Kalas, J R. Graham, M. Clampin, *Astrophys. J.*, in press; http://arxiv.org/abs/0811.1985.
16. J. J. Fortney *et al.*, *Astrophys. J.* **683**, 1104 (2008).
17. A. Burrows, D. Sudarsky, J. I. Lunine, *Astrophys. J.* **596**, 587 (2003).
18. A. J. Burgasser *et al.*, *Astron. J.* **120**, 473 (2000).
19. C. Marois, B. Macintosh, T. Barman, *Astrophys. J.* **654**, L151 (2007).
20. L. Hartmann, R. Hewett, N. Calvet, *Astron. J.* **426**, 669 (1994).
21. D. Veras, P. J. Armitage, *Mon. Not. R. Astron. Soc.* **347**, 613 (2004).
22. E. B. Ford, E. I. Chiang, *Astrophys. J.* **661**, 602 (2007).
23. J. Davis *et al.*, *Astron. Nachr.* **326**, 25 (2005).

24. Supported by HST programs GO-10598 (P.K.) and GO-10539 (K.S. and J.K.), provided by NASA through a grant from the Space Telescope Science Institute (STScI) under NASA contract NAS5-26555; NSF grant AST-0507805 (E.C.); the Michelson Fellowship Program, under contract with JPL, funded by NASA (M.P.F.); and a Berkeley Fellowship (E.S.K.). Work at LLNL was performed under the auspices of the U.S. Department of Energy under contract DE-AC52-07NA27344. We thank the staff at STScI, Keck, and Gemini for supporting our observations.

Supporting Online Material

www.sciencemag.org/cgi/content/full/1166609/DC1
SOM Text
Fig. S1
Tables S1 to S4
References

30 September 2008; accepted 5 November 2008
Published online 13 November 2008;
10.1126/science.1166609
Include this information when citing this paper.

Direct Imaging of Multiple Planets Orbiting the Star HR 8799

Christian Marois,[1,2,3]* Bruce Macintosh,[2] Travis Barman,[4] B. Zuckerman,[5] Inseok Song,[6] Jennifer Patience,[7] David Lafrenière,[8] René Doyon[9]

Direct imaging of exoplanetary systems is a powerful technique that can reveal Jupiter-like planets in wide orbits, can enable detailed characterization of planetary atmospheres, and is a key step toward imaging Earth-like planets. Imaging detections are challenging because of the combined effect of small angular separation and large luminosity contrast between a planet and its host star. High-contrast observations with the Keck and Gemini telescopes have revealed three planets orbiting the star HR 8799, with projected separations of 24, 38, and 68 astronomical units. Multi-epoch data show counter clockwise orbital motion for all three imaged planets. The low luminosity of the companions and the estimated age of the system imply planetary masses between 5 and 13 times that of Jupiter. This system resembles a scaled-up version of the outer portion of our solar system.

During the past decade, various planet detection techniques—precision radial velocities, transits, and microlensing—have been used to detect a diverse population of exoplanets. However, these methods have two limitations. First, the existence of a planet is inferred through its influence on the star about which it orbits; the planet is not directly discerned [photometric signals from some of the closest-in giant planets have been detected by careful analysis of the variations in the integrated brightness of the system as the planet orbits its star (*1*)]. Second, these techniques are limited to small (transits) to moderate (precision radial velocity and microlensing) planet-star separation. The effective sensitivities of the latter two techniques diminish rapidly at semimajor axes beyond about 5 astronomical units (AU). Direct observations allow discovery of planets in wider orbits and allow the spectroscopic and photometric characterization of their complex atmospheres to derive their physical characteristics.

There is indirect evidence for planets in orbits beyond 5 AU from their stars. Some images of dusty debris disks orbiting main-sequence stars (the Vega phenomenon) show spatial structure on a scale of tens to hundreds of astronomical units (*2*). The most likely explanation of such structure is gravitational perturbations by planets with semimajor axes comparable to the radius of the dusty disks and rings [see references in (*3*)].

The only technique currently available to detect planets with semimajor axes greater than about 5 AU in a reasonable amount of time is infrared (IR) imaging of young, nearby stars. The detected near-IR radiation is escaped internal heat energy from the recently formed planets. During

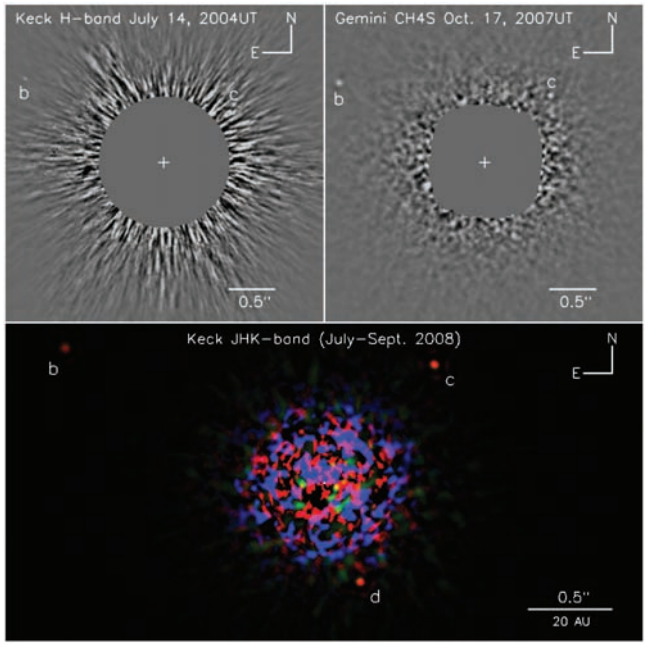

Fig. 1. HR 8799bcd discovery images after the light from the bright host star has been removed by ADI processing. (**Upper left**) A Keck image acquired in July 2004. (**Upper right**) Gemini discovery ADI image acquired in October 2007. Both b and c are detected at the two epochs. (**Bottom**) A color image of the planetary system produced by combining the J-, H-, and Ks-band images obtained at the Keck telescope in July (H) and September (J and Ks) 2008. The inner part of the H-band image has been rotated by 1° to compensate for the orbital motion of d between July and September. The central region is masked out in the upper images but left unmasked in the lower to clearly show the speckle noise level near d.

[1]National Research Council Canada, Herzberg Institute of Astrophysics, 5071 West Saanich Road, Victoria, BC V9E 2E7, Canada. [2]Lawrence Livermore National Laboratory, 7000 East Avenue, Livermore, CA 94550, USA. [3]Astronomy Department, University of California, Berkeley, CA 94720, USA. [4]Lowell Observatory, 1400 West Mars Hill Road, Flagstaff, AZ 86001, USA. [5]Physics and Astronomy Department and Center for Astrobiology, University of California, Los Angeles, CA 90095, USA. [6]University of Georgia, Department of Physics and Astronomy, 240 Physics, Athens, GA 30602, USA. [7]University of Exeter, School of Physics, Stocker Road, Exeter EX4 4QL, UK. [8]Department of Astronomy and Astrophysics, University of Toronto, 50 St. George Street, Toronto, ON M5S 3H4, Canada. [9]Département de Physique and Observatoire du Mont Mégantic, Université de Montréal, C.P. 6128, Succursale Centre-Ville, Montréal, QC H3C 3J7, Canada.

*To whom correspondence should be addressed; E-mail: christian.marois@nrc-cnrc.gc.ca

ERRATUM

Post date 2 January 2009

Research Articles: "Optical images of an exosolar planet 25 light-years from Earth" by P. Kalas *et al.* (28 November 2008, p. 1345). In the abstract, the phrase "matching predictions of its location" was inadvertently added to the end of two different sentences during final corrections. The phrase correctly appears at the end of the third sentence, whereas the fifth sentence should read "Dynamical models of the interaction between the planet and the belt indicate that the planet's mass is at most three times that of Jupiter; a higher mass would lead to gravitational disruption of the belt."

the past decade, hundreds of young stars with ages ≤100 million years (My) have been identified within ~100 pc of Earth (*4*, *5*), and many of these have been imaged in the near-IR with ground-based adaptive optics (AO) systems and with the Hubble Space Telescope. Direct imaging searches for companions of these stars have detected some objects that are generally considered to be near or above the mass threshold 13.6 M_{Jup} dividing planets from brown dwarfs [see (*6*) for an example and (*7*) for a list of known substellar objects orbiting stars] and one planetary mass companion that is orbiting a brown dwarf, not a star (*8*). Recently, Lafrenière *et al*. (*9*) have detected a candidate planet near a young (5 My old) star of the Upper Scorpius association, but a proper motion analysis is required to confirm that it is bound to the host star and not an unrelated low-mass member of the young association. In this issue, Kalas *et al*. report the detection, in visible light, of a candidate planetary mass companion near the inner edge of the Fomalhaut debris disk (*10*). Nondetections of the candidate companion at near-IR wavelengths suggest that the detected visible flux may be partially host-star light-scattering off circumplanetary dust rather than photons from the underlying object. A statistical Bayesian analysis of a dedicated AO survey of nearby young F-, G-, and K-type stars shows that exoplanets are relatively rare at separations >20 AU around stars with masses similar to the Sun (*11*).

Bright A-type stars have been mostly neglected in imaging surveys because the higher stellar luminosity offers a less favorable planet-to-star contrast. However, main sequence A-type stars do have some advantages. The higher-mass A stars can retain heavier and more extended disks and thus might form massive planets at wide separations, making their planets easier to detect. Millimeter interferometric continuum observations of the nearest Herbig Ae stars, the precursors to A-type stars, indicate that these are encircled by disks with masses up to several times the Minimum Mass Solar Nebula (*12*), the minimum amount of solar abundance material (0.01 M_{Sun}) required to form all planets in the solar system (*13*). Associated millimeter line observations resolve these gas disks and indicate that their outer radii are 85 to 450 AU (*12*). The most exceptional example of a young A-star disk is the one orbiting IRAS 18059-3211, which is estimated to have a mass of 90 times the Minimum Mass Solar Nebula and an outer radius extending to ~3000 AU (*14*). Radial velocity surveys of evolved A stars do seem to confirm these hypotheses by showing a trend of a higher frequency of planets at wider separations (*15*). In this article, we describe the detection of three faint objects at 0.63″, 0.95″, and 1.73″ (24, 38, and 68 AU projected separation, respectively) (Fig. 1) from the dusty and young A-type main sequence star HR 8799, show that all objects are co-moving with HR 8799, and describe their orbital motion and physical characteristics.

HR 8799 stellar properties. HR 8799 [also V342 Peg and HIP114189, located 39.4 pc (*16*) from Earth] is the only star known that has simultaneously been classified as γ Doradus (variable), λ Bootis (metal-poor Population I A-type star), and Vega-like (far-IR excess emission from circumstellar dust) (*17*, *18*). A fit to the Infrared Astronomical Satellite (IRAS) and Infrared Space Observatory (ISO) photometry indicates that it has a dominant dust disk with temperature of 50 K (*3*, *19*). Such black-body grains, in an optically thin disk, would reside ~75 AU (~2″) from HR 8799. This would place the dust just outside the orbit of the most distant companion seen in our images (Fig. 1), similar to the way the Kuiper Belt is confined by Neptune in our solar system.

The fractional IR luminosity ($L_{IR}/L_{bol} = 2.3 \times 10^{-4}$) (*19*, *20*) is too bright to come from a geo-

Table 1. HR 8799 Planetary System Data.

	HR 8799		
Spectral type	A5V		
Mass	1.5 ± 0.3 M_{Sun} (*17*)		
Luminosity	4.92 ± 0.41 L_{Sun} (*17*)		
Distance	39.4 ± 1.0 pc (128 ± 3 ly) (*16*)		
Proper motion [east, north]	[107.88 ± 0.76, −50.08 ± 0.63] mas/year (*16*)		
Age	60 (30–160) My		
Metallicity	Log[(M/H)/(M/H)$_{Sun}$] = −0.47 (*17*)		
J, H, Ks, L′	5.383 ± 0.027, 5.280 ± 0.018, 5.240 ± 0.018, 5.220 ± 0.018		
	Separation with respect to the host star in [east, north]″		
	HR 8799b	c	d
2004 July 14 (±0.005″)	[1.471, 0.884]	[−0.739, 0.612]	–
2007 Oct. 25 (±0.005″)	[1.512, 0.805]	[−0.674, 0.681]	–
2008 July 11 (±0.004″)	[1.527, 0.799]	[−0.658, 0.701]	[−0.208, −0.582]
2008 Aug. 12 (±0.002″)	[1.527, 0.801]	[−0.657, 0.706]	[−0.216, −0.582]
2008 Sept. 18 (±0.003″)	[1.528, 0.798]	[−0.657, 0.706]	[−0.216, −0.582]
Projected sep. (AU)	68	38	24
Orbital motion (″/year)	0.025 ± 0.002	0.030 ± 0.002	0.042 ± 0.027
Period for face-on cir. orbits (years)	~460	~190	~100
M_J (1.248 μm)	16.30 ± 0.16	14.65 ± 0.17	15.26 ± 0.43
M_H (1.633 μm)	14.87 ± 0.17	13.93 ± 0.17	13.86 ± 0.22
M_{CH4S} (1.592 μm)	15.18 ± 0.17	14.25 ± 0.19	14.03 ± 0.30
M_{CH4L} (1.681 μm)	14.89 ± 0.18	13.90 ± 0.19	14.57 ± 0.23
M_{Ks} (2.146 μm)	14.05 ± 0.08	13.13 ± 0.08	13.11 ± 0.12
$M_{L'}$ (3.776 μm)	12.66 ± 0.11	11.74 ± 0.09	11.56 ± 0.16
Luminosity (L_{Sun})	−5.1 ± 0.1	−4.7 ± 0.1	−4.7 ± 0.1
T_{eff} (K)	870 (800–900)	1090 (1000–1100)	1090 (1000–1100)
Radius (R_{Jup})	1.2 (1.1–1.3)	1.2 (1.2–1.3)	1.2 (1.2–1.3)
Mass (M_{Jup})	7 (5–11)	10 (7–13)	10 (7–13)

metrically thin, flat disk orbiting at such large distances from HR 8799. Such an optically thin disk would need to be warped or "puffed up" in the vertical direction, plausibly by the gravitational influence of nearby planets. Submillimeter photometry indicates a dust mass of 0.1 Earth masses (*21*), making it one of the most massive debris disks detected by IRAS (*19*).

When planets form, gravitational potential energy is released and turned into heat in their interiors. Because planets do not possess any internal nuclear energy source to maintain their temperature, they cool down and become less luminous with time. For massive planets, this self-luminosity can dominate over their stellar insolation for hundreds of millions or billions of years. With some assumptions on the initial conditions at the time of formation, a planet's mass can be derived simply by estimating the planet's luminosity and the system age. Our age estimate for HR8799 is based on four lines of evidence: the star's galactic space motion, the star's position in a color-magnitude diagram, the typical age of λ Boo and γ Dor class stars, and the large mass of the HR 8799 debris disk.

Most young stars in the solar neighborhood have Galactic space motions (UVW) that fall in limited ranges. HR 8799's space motion with respect to the Sun, as calculated from published distance, radial velocity, and proper motion, is UVW = (–11.9, –21.0, –6.8 km s^{-1}) (*16*, *22*). This UVW is similar to that of other stars with an age between that of the TW Hydra association [8 My (*4*, *5*)] and the Pleiades [125 ± 8 My (*23*)]. The UVW of HR 8799 is similar to that of members of the 30-My-old, southern hemisphere, Columba and Carina Associations (*5*). Calculations of the UVW of the young stars HD 984 and HD 221318, which lie near HR 8799, show that their space motions are similar to that of HR 8799. We estimate the ages of HD 984 and HD 221318 to be 30 and 100 My, respectively, whereas the Foundation and Evolution of Planetary Systems team estimates the age of HD 984 to be 40 My (*24*). Overall, the UVW of HR 8799 is clearly consistent with those of young clusters and associations in the solar neighborhood. Of course, in this UVW range of young stars, there are also older stars with random motions; so other, independent, methods must also be employed to place limits/constraints on the age of HR 8799.

HR 8799 is also found below the main sequence of the Pleiades, α Per (age 70 My) and IC2391 (age 50 My) on a Hertzsprung-Russell diagram. This is consistent with a younger age compared to that of the Pleiades (*25*). Even with the more recent Tycho measurement and correcting for the star's low metallicity, so that the star's visible-light B-V color is increased and lies between 0.26 and 0.3, HR 8799 still lies low on the Hertzsprung-Russell diagram when plotted against known young stars (*25*), consistent with our young age estimate.

The λ Boo stars are generally thought to be young, up to a few 100 My old (*26*). The γ Dor class stars are probably also young; they are seen in the Pleiades and in NGC 2516 (age ~100 My), but not in the Hyades (age ~650 My) (*27*).

Finally, the probability that a star has a massive debris disk like HR 8799 declines with age (*19*). Considering all of the above, we arrive at an estimate of age 60 My and a range between 30 and 160 My, consistent with an earlier independent estimate of 20 to 150 My (*20*). The conservative age upper limit for HR 8799 is chosen to be the ~5- σ upper limit to the Pleiades age.

Observations. The sensitivity of high-contrast ground-based AO imaging is limited primarily by quasistatic speckle artifacts; at large separations (>0.5″), the main source of speckles is surface errors on the telescope primary mirror and internal optics. To remove this noise, we used angular differential imaging (ADI) in our observations (*28*, *29*). This technique uses the intrinsic field-of-view rotation of altitude/azimuth telescopes to decouple exoplanets from optical artifacts. An ADI sequence is obtained by keeping the telescope pupil fixed on the science camera and allowing the field-of-view to slowly rotate with time around the star. Our observations were obtained in the near-IR (1.1 to 4.2 microns), a regime where the planets are expected to be bright and where the AO system provides excellent image correction. ADI sequences at various wavelengths were acquired using the adaptive optics system at the Keck and Gemini telescopes and the corresponding facility near-IR cameras, NIRC2 and NIRI, between 2007 and 2008 (Fig. 1). During each observing sequence, we typically obtained a mix of unsaturated short-exposure images of the star, to determine its precise location and brightness, together with a set of 30-s exposures that overexposed the central star but had maximum sensitivity to faint companions. Some coronagraphic images were also acquired with NIRC2 to benefit from the simultaneous photometric calibration achievable with a partially transmissive focal plane mask. The b and c companions were first seen in October 2007 Gemini data; the d component was first detected in Keck data in 2008. The b and c components were also visible

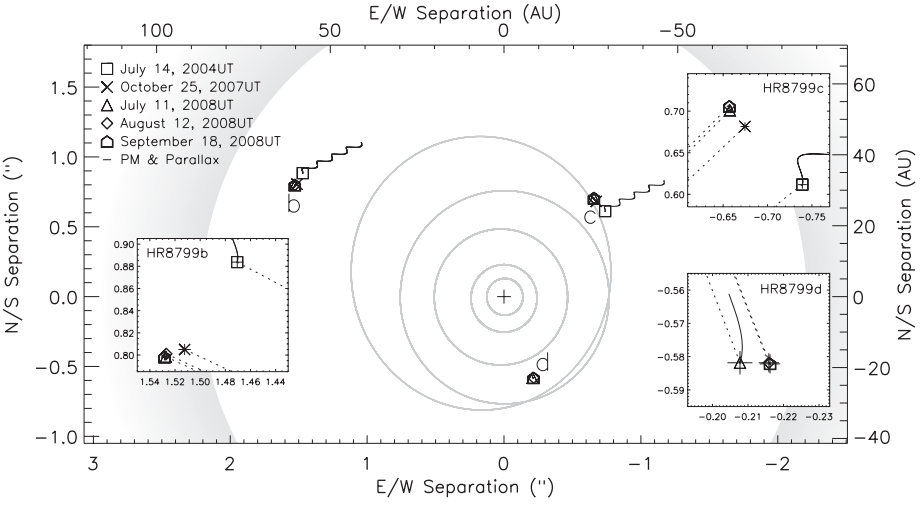

Fig. 2. HR 8799bcd astrometric analysis. The positions of HR 8799bcd at each epoch are shown in both the overall field of view and in the zoomed-in insets. The solid oscillating line originating from the first detected epoch of each planet is the expected motion of unbound background objects relative to the star over a duration equal to the maximum interval over which the companions were detected (4 years for b and c, two months for d). All three companions are confirmed as co-moving with HR 8799 to 98 σ for b, 90 σ for c and ~6 σ for d. Counter-clockwise orbital motion is observed for all three companions. The dashed lines in the small insets connect the position of the planet at each epoch with the star. A schematic dust disk—at 87 AU separation to be in 3:2 resonance with b while also entirely consistent with the far-infrared dust spectrum—is also shown. The inner gray ellipses are the outer Jovian-mass planets of our solar system (Jupiter, Saturn, Uranus and Neptune) and Pluto shown to scale.

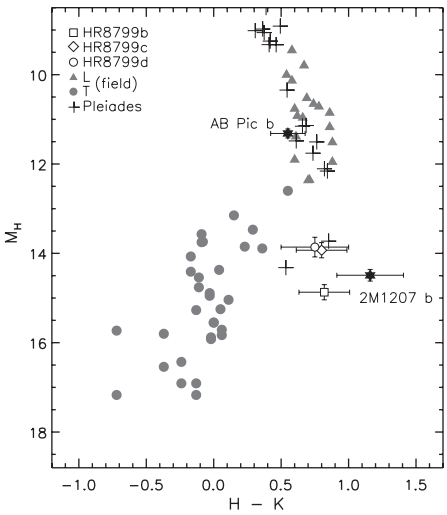

Fig. 3. Absolute magnitude in H-band versus H-K color. Old field (gray dots) and young Pleiades brown dwarfs (pluses) are shown along with two very low-mass brown dwarfs/planetary mass companions (filled black symbols). Open symbols are HR 8799b (square), c (diamond), and d (circle).

in a reanalysis of non-ADI Keck data obtained for a related program in 2004 [the data sets and the reduction technique are described further in the supporting online material (SOM)].

Astrometric analysis. After the initial detection of the companions, we evaluated their positions relative to the star to confirm that they are co-moving with it (possibly including orbital motion) and not unrelated background or foreground objects (Table 1, table S2, and Fig. 2). Because HR 8799b was visible in the 2004 Keck images, we have more than 4 years of time baseline for proper motion measurements. With the large proper motion of HR 8799 (0.13″/year), the HR 8799b object is shown to be bound at a significance of 98 times the estimated 1-σ uncertainty. Additionally, the data show that it is orbiting counter-clockwise. It moved 25 ± 2 milliarcseconds (mas)/year (0.98 AU/year) southeast during the 4-year period. Its detected orbital motion is near perpendicular to the line connecting the planet and primary, suggesting that the system is viewed nearly pole-on and that the orbit is not very eccentric. The near face-on perspective is further supported by the slow projected rotational velocity of HR 8799 [~40 km sec^{-1} (*17*)]; this is well below average for late-A and early-F type stars (*30*). If we assume that it has a semimajor axis of 68 AU, a circular orbit, a pole-on view, and a host stellar mass equal to 1.5 solar masses, then the orbital period and motion of HR 8799b are ~450 years and 0.93 AU/year (24 mas/year) respectively, consistent with our measurements.

HR 8799c is also detected, at lower significance, in the 2004 data set. The measurement of its 4-year proper motion confirms that it is bound to the star at the 90-σ level. Its orbit is also counter-clockwise at 30 ± 2 mas/year (1.18 AU/year). For its semimajor axis of 38 AU, the orbital period is ~190 years and the expected orbital motion is 1.25 AU/year (32 mas/year). Again, the orbital motion is close to being perpendicular to the line connecting the planet to the primary.

HR 8799d was first detected in the July 2008 data set. The 2 months of available proper motion measurements are sufficient to confirm that it is bound to the star at the ~6-σ level. The available data are also consistent with a counter-clockwise orbital motion of 42 ± 27 mas/year (1.65 AU/year). For a semimajor axis of 24 AU, the orbital period is 100 years and the expected orbital motion is 1.57 AU/year (40 mas/year).

HR 8799bcd photometric analysis. All three companions are intrinsically faint and have red near-IR colors that are comparable to those of substellar-mass objects with low effective temperatures (Table 1). Compared to old field brown dwarfs (objects with masses between planets and stars), all three companions lie at the base of the L dwarf spectral sequence—objects known to be cool and have dusty clouds in their atmospheres (Fig. 3). Two candidate free-floating Pleiades brown dwarfs, with comparable colors and absolute K-band magnitudes to HR 8799c and d, are consistent with a mass of ~11 M_{Jup} from evolutionary models (*31*). If HR 8799 is (as is likely) younger than the Pleiades, the c and d companions would be even less massive. HR 8799b is fainter than all of the known Pleiades substellar members and thus is below 11 M_{Jup} (Fig. 3). All three companions stand apart from the older, more massive brown dwarfs in a color-magnitude diagram. The known distance to HR 8799, and photometry for each companion that covers a substantial fraction of the spectral energy distribution (SED), allow for a robust measurement of the bolometric luminosity (L_{bol}). We fit a variety of synthetic SEDs (generated with the PHOENIX model atmosphere code) to the observed photometry for each companion, assuming that their atmospheres were either cloud-free, very cloudy, partly cloudy (50% coverage), or radiated like black bodies. This fitting process is equivalent to simultaneously determining bolometric corrections for each band-pass for various model assumptions. Luminosities were also obtained using the K-band bolometric corrections for brown dwarfs (*32*). Although the different models produce different estimates of effective temperature, the range of L_{bol} for each object is small (Table 1), indicating that our estimate is robust against the uncertainty in the details of the atmosphere and clouds (see the SOM for more details).

The cooling of hydrogen-helium brown dwarfs and giant planets is generally well understood; however, the initial conditions associated with the formation of objects from collapsing molecular clouds or core accretion inside a disk are uncertain. Consequently, theoretical cooling tracks of objects at young ages may not be reliable. Recent efforts to establish initial conditions for cooling tracks based on core-accretion models have produced young Jupiter-mass planets substantially fainter (<10^{-5} L_{Sun}) than predicted by traditional models (*33*). However, these hybrid models do not yet include a realistic treatment of the complex radiative transfer within the accretion shock and thus provide only lower limits on the luminosity at young ages. Warmer, more luminous planets originating from core accretion cannot be ruled out.

Although HR 8799 is young, its upper age limit (~160 My) is near the time when the dif-

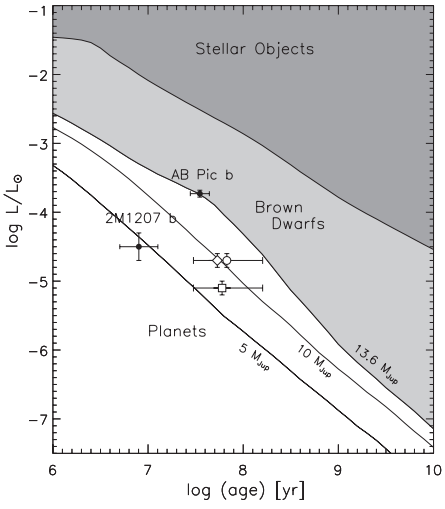

Fig. 4. Luminosity versus time for a variety of masses (*34*). The three coeval points are HR 8799b (square), c (diamond), and d (circle); c and d data points are displaced horizontally for clarity. The locations of the low mass object AB Pic b on the planet/brown dwarf dividing line and a planetary mass companion (2M1207b) to the brown dwarf 2M1207 are also shown [note that alternative models proposed for 2M1207 lead to somewhat larger luminosity and mass (~8 M_{Jup}) for the companion (*42*)]. The deuterium burning mass limit, currently believed to be ~13.6 M_{Jup}, has been incorporated into a "working definition" of a planet by the International Astronomical Union and is used here to separate planets (which also must orbit a star) from brown dwarfs. The boundary between stars and brown dwarfs is set by stable hydrogen burning.

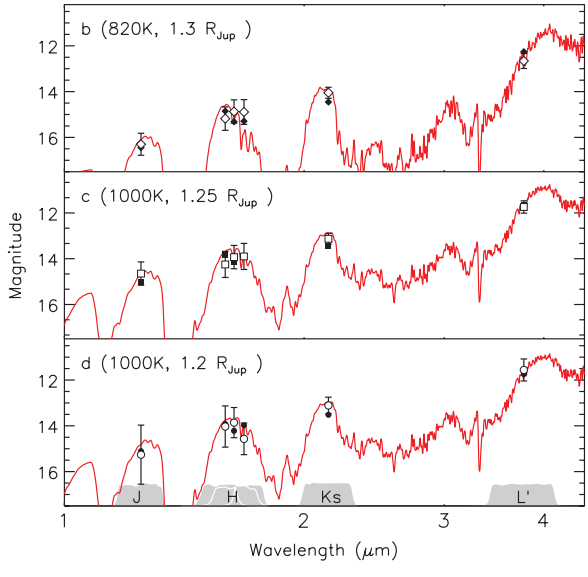

Fig. 5. Synthetic spectra from model atmospheres containing clouds located between 10 and 0.1 bar of pressure are compared to the measured fluxes (with 3-σ error bars) for HR 8799 b, c, and d. Response curves for each filter band pass are indicated along the *x* axis. The predicted magnitudes from the synthetic spectra, averaged over the filter passbands, are shown by the filled symbols.

ferences among cooling tracks with various initial conditions are not so dramatic and, given the uncertainties associated with all planet evolution models, standard cooling tracks are as reliable at these ages as other hybrid models. Figure 4 compares the measured luminosities and age range for HR 8799 bcd to theoretical "hot start" cooling tracks for a variety of masses (*34*).

The region occupied by all three companions falls below the lowest mass brown dwarf, well inside the planet regime. The masses derived from the luminosities, cooling tracks, and best age for bcd are, respectively, 7, 10, and 10 M_{Jup}. See Table 1 for values of additional important properties derived from the cooling track comparison, with uncertainties based on our current best age range. In the very unlikely event that the star is older than our estimated upper limit, it would need to be >300 My old for all three objects to be brown dwarfs.

The large planet masses and orbital radii in the HR 8799 system are challenging to explain in the context of a core-accretion scenario. A number of factors such as stellar mass (*35*), metallicity (*36*), disk surface density (*37*), and planet migration in the disk (*38*) influence the core-accretion process. The stellar mass of HR 8799 is larger than that of the Sun. The star's metallicity is low, especially in refractory elements, but for a λ Boo star this is usually attributed to the details of the star's accretion and atmospheric physics rather than an initial low metallicity for the system (*26*).

The exceptionally dusty debris disk around HR 8799 may indicate that the proto-planetary disk was massive and had a high surface density, factors conducive to planet formation. Alternatively, the giant planets in the HR 8799 system may have formed rapidly from a gravitational instability in the early disk (*39*, *40*). Some models (*40*) of such instabilities do favor the creation of massive planets (>6 M_{Jup}).

As suggested by the color-magnitude diagram (Fig. 3), each companion appears to be at the edge of (or inside) the transition region from cloudy to cloud-free atmospheres. Current planet atmosphere models have difficulties fitting the color and spectrum features of these objects. The physical mechanism responsible for the clearing of clouds in ultracool atmospheres is not fully understood, but recent cloud models with vertical stratification have had some success at simulating/producing photometric properties in this transition region (*41*). A modified PHOENIX atmospheric model was developed that incorporates cloud stratification. These updated models were found to match well-known brown dwarfs located in the cloudy/cloud-free transition region. With the cloud stratification model, PHOENIX is capable of producing spectra that are consistent with the observed photometry and the bulk properties (effective temperature, radius, and gravity) predicted by the cooling tracks (Fig. 5). Clearly these synthetic models do not reproduce all of the photometric data, but given the difficulty of cloud modeling, the agreement is sufficient to support the effective temperatures and radii determined from the cooling tracks.

Conclusions. The three co-moving companions of HR 8799 are different from known field objects of similar effective temperature; the only similar object known is the planetary mass companion to the brown dwarf 2M1207. Low luminosities of these companions and the young age for HR 8799 indicate that they have planetary masses and are not brown dwarfs. The nature of the system provides an additional indirect line of evidence for planetary-mass companions (and hence a low age). There are no known systems where multiple brown dwarfs independently orbit a star; the only systems we know of with multiple companions in independent orbits are the exoplanetary systems discovered from the precision radial velocity method. Interestingly, our observations show that the HR 8799 planets orbit in the same direction, similar to the planets in our own solar system and consistent with models of planet formation in a disk. In many ways this resembles a scaled-up version of our solar system. HR 8799 has a luminosity of 4.9 L_{Sun}, so the radius corresponding to a given equilibrium temperature is 2.2 times as large as the corresponding radius in our solar system. Because formation processes will be affected by luminosity—for example, the location of the snow line where water can condense on rocky material to potentially form giant planet cores—one can view the three planetary companions as having temperature-equivalent projected orbital separations of 11, 17, and 31 AU, to be compared with 9.5, 19, and 30 AU for Saturn, Uranus, and Neptune, respectively. The HR 8799 planets are also consistent with formation through instabilities in a massive protoplanetary disk, which may form objects with masses above 5 M_{Jup} (*40*), but the core-accretion scenario cannot yet be ruled out.

The presence of these massive planets still leaves dynamic room for other Jovian-mass planets or even lower mass terrestrial planets in the inner part of the system. In our survey, we only observed a few early-type stars before making this detection, compared to similar imaging surveys of young G-, K-, and M-type stars that have covered more than a few hundred targets. This may indicate that Jovian-mass planetary companions to early-type stars are much more common at separations beyond ~20 AU, consistent with what was suggested by radial velocity surveys of evolved A-type stars (*15*).

References and Notes

1. D. Deming, *Proc. IAU Symposium* **253**, in press; arXiv:0808.1289 astro-ph.
2. P. Kalas, J. R. Graham, M. Clampin, *Nature* **435**, 1067 (2005).
3. B. Zuckerman, I. Song, *Astrophys. J.* **603**, 738 (2004).
4. B. Zuckerman, I. Song, *Annu. Rev. Astron. Astrophys.* **42**, 685 (2004).
5. C. A. O. Torres, G. R. Quast, C. H. F. Melo, M. E. Sterzik, *Handbook of Star Forming Regions Vol. II. Astronomical Society of the Pacific*, in press; arXiv:0808.3362 astro-ph.
6. T. Nakajima *et al*., *Nature* **378**, 463 (1995).
7. B. Zuckerman, I. Song, *Astron. Astrophys*, in press; arXiv:0811.0429 astro-ph.
8. G. Chauvin *et al*., *Astron. Astrophys.* **425**, 29 (2004).
9. D. Lafrenière *et al*., *Astrophys J.*, in press; arXiv:0809.1424v2 astro-ph.
10. P. Kalas *et al*., *Science* **322**, 1345 (2008); published online 13 November 2008 (10.1126/science.1166609).
11. D. Lafrenière *et al*., *Astrophys. J.* **660**, 770 (2007).
12. V. Mannings, A. I. Sargent, *Astrophys. J.* **490**, 792 (1997).
13. S. J. Weidenschilling, *Astrophys. Space Sci.* **51**, 153 (1977).
14. V. Bujarrabal, K. Young, D. Fong, *Astron. Astrophys.* **483**, 839 (2008).
15. J. Johnson *et al*., *Astrophys. J.* **670**, 833 (2007).
16. E. van Leeuwen, *Astron. Astrophys.* **474**, 653 (2007).
17. R. O. Gray, A. B. Kaye, *Astron. J.* **118**, 2993 (1999).
18. K. Sadakane, M. Nishida, *Publ. Astron. Soc. Pac.* **98**, 685 (1986).
19. J. H. Rhee, I. Song, B. Zuckerman, M. McElwain, *Astrophys. J.* **660**, 1556 (2007).
20. A. Moór *et al*., *Astrophys. J.* **644**, 525 (2006).
21. J. P. Williams, S. M. Andrews, *Astrophys. J.* **653**, 1480 (2006).
22. R. E. Wilson, *General Catalogue of Stellar Radial Velocities* (Carnegie Institute, Washington, DC, Publ. 601, 1953).
23. J. R. Stauffer, G. Schultz, J. D. Kirkpatrick, *Astrophys. J.* **499**, 199 (1998).
24. J. Najita, J. P. Williams, *Astrophys. J.* **635**, 625 (2005).
25. B. Zuckerman, *Annu. Rev. Astron. Astrophys.* **39**, 549 (2001).
26. R. O. Gray, C. J. Corbally, *Astron. J.* **124**, 989 (2002).
27. K. Krisciunas, R. A. Crowe, K. D. Luedeke, M. Roberts, *Mon. Not. R. Astron. Soc.* **277**, 1404 (1995).
28. C. Marois *et al*., *Astrophys. J.* **641**, 556 (2006).
29. D. Lafrenière *et al*., *Astrophys. J.* **660**, 770 (2007).
30. F. Royer, J. Zorec, A. E. Gómez, *Astron. Astrophys.* **463**, 671 (2007).
31. S. L. Casewell *et al*., *Mon. Not. R. Astron. Soc.* **378**, 1131 (2007).
32. D. A. Golimowski *et al*., *Astrophys. J.* **127**, 3516 (2004).
33. M. S. Marley *et al*., *Astrophys. J.* **655**, 541 (2007).
34. I. Baraffe *et al*., *Astron. Astrophys.* **402**, 701 (2003).
35. S. Ida, D. N. C. Lin, *Astrophys. J.* **626**, 1045 (2005).
36. S. Ida, D. N. C. Lin, *Astrophys. J.* **616**, 567 (2004).
37. J. J. Lissauer, *Icarus* **69**, 249 (1987).
38. W. K. M. Rice, P. J. Armitage, *Astrophys. J.* **598**, 55 (2003).
39. A. P. Boss, *Science* **276**, 1836 (1997).
40. R. R. Rafikov, *Astrophys. J.* **621**, 69 (2005).
41. D. Saumon, M. S. Marley, *Astrophys J.*, arXiv:0808.2611 (2008).
42. C. Ducourant *et al*., *Astron. Astrophys.* **477**, 1 (2008).

43. We thank the Keck and Gemini staff, particularly T. Armandroff, B. Goodrich, and J.-R. Roy, for support with the follow-up observations. We thank the University of California–Los Angeles (UCLA) galactic center team, especially J. Lu, for the NIRC2 plate scale and North orientation errors. We are indebted to E. Becklin and R. Racine for their contributions in the earliest stages of this research. C.M. and D.L. are supported in part through postdoctoral fellowships from the Fonds Québécois de la Recherche sur la Nature et les Technologies. Portions of this research were performed under the auspices of the U.S. Department of Energy by Lawrence Livermore National Laboratory under contract DE-AC52-07NA27344 and also supported in part by the NSF Science and Technology CfAO, managed by the University of California–Santa Cruz under cooperative agreement AST 98-76783. We acknowledge support by NASA grants to UCLA and Lowell Observatory. R.D. is supported through a grant from the Natural Sciences and Engineering Research Council of Canada. The data were obtained at the W.M. Keck and Gemini Observatories. This publication makes use of data products from the Two Micron All Sky Survey and the SIMBAD database (http://simbad.u-strasbg.fr/simbad).

Supporting Online Material

www.sciencemag.org/cgi/content/full/1166585/DC1
Materials and Methods
Tables S1 and S2
References

30 September 2008; accepted 5 November 2008
Published online 13 November 2008;
10.1126/science.1166585
Include this information when citing this paper

Detection of GTP-Tubulin Conformation in Vivo Reveals a Role for GTP Remnants in Microtubule Rescues

Ariane Dimitrov,[1,2]* Mélanie Quesnoit,[1,2,3]* Sandrine Moutel,[2,4] Isabelle Cantaloube,[3] Christian Poüs,[3,5]† Franck Perez[1,2]†‡

Microtubules display dynamic instability, with alternating phases of growth and shrinkage separated by catastrophe and rescue events. The guanosine triphosphate (GTP) cap at the growing end of microtubules, whose presence is essential to prevent microtubule catastrophes in vitro, has been difficult to observe in vivo. We selected a recombinant antibody that specifically recognizes GTP-bound tubulin in microtubules and found that GTP-tubulin was indeed present at the plus end of growing microtubules. Unexpectedly, GTP-tubulin remnants were also present in older parts of microtubules, which suggests that GTP hydrolysis is sometimes incomplete during polymerization. Observations in living cells suggested that these GTP remnants may be responsible for the rescue events in which microtubules recover from catastrophe.

Microtubules are highly dynamic tubulin polymers that are essential for intracellular organization and cell division. They display a dynamic instability, with alternating phases of growth and shrinkage separated by catastrophe and rescue events (*1*, *2*). Tubulin polymerizes in a guanosine triphosphate (GTP)–bound form and hydrolyzes GTP in the polymer with a slight delay. This creates a GTP cap at the growing end of microtubules (*2*–*4*). Loss of the GTP cap promotes catastrophic events, whereas microtubule rescues result from uncharacterized stochastic events.

Even though the characteristics of the GTP cap have been well studied in vitro, the evidence that such a cap exists in vivo is lacking, essentially because no antibodies specific for the GTP-bound conformation of tubulin are available. The GTP-bound tubulin dimer is in a straighter conformation than the guanosine diphosphate (GDP)–bound dimer (*5*), and even when constrained in the lattice, GDP-tubulin does not have the same conformation as GTP-tubulin (*6*, *7*). This suggests that it should be possible to make conformational antibodies that specifically recognize GTP-bound tubulin in the polymer. Conformational antibodies specific for GTP-bound Rab6 were selected in vitro by antibody phage display (*8*). Here, we selected a recombinant antibody specific for the GTP-bound conformation of tubulin in the polymer. We used this antibody to localize GTP-tubulin in cellular microtubules.

[1]CNRS UMR144, Institut Curie, 26 rue d'Ulm, 75248 Paris Cedex 05, France. [2]Institut Curie, Centre de Recherche, 26 rue d'Ulm, 75248 Paris Cedex 05, France. [3]Biochimie et Biologie Cellulaire–JE2493, Université Paris-Sud 11, IFR141–Faculté de Pharmacie, 92296 Châtenay-Malabry, France. [4]Institut Curie, Translational Research Department, 26 rue d'Ulm, 75248 Paris Cedex 05, France. [5]Biochimie-Hormonologie, AP-HP, Hôpital Antoine Béclère, 92141 Clamart, France.

*These authors contributed equally to this work.
†These authors contributed equally to this work.
‡To whom correspondence should be addressed. E-mail: franck.perez@curie.fr

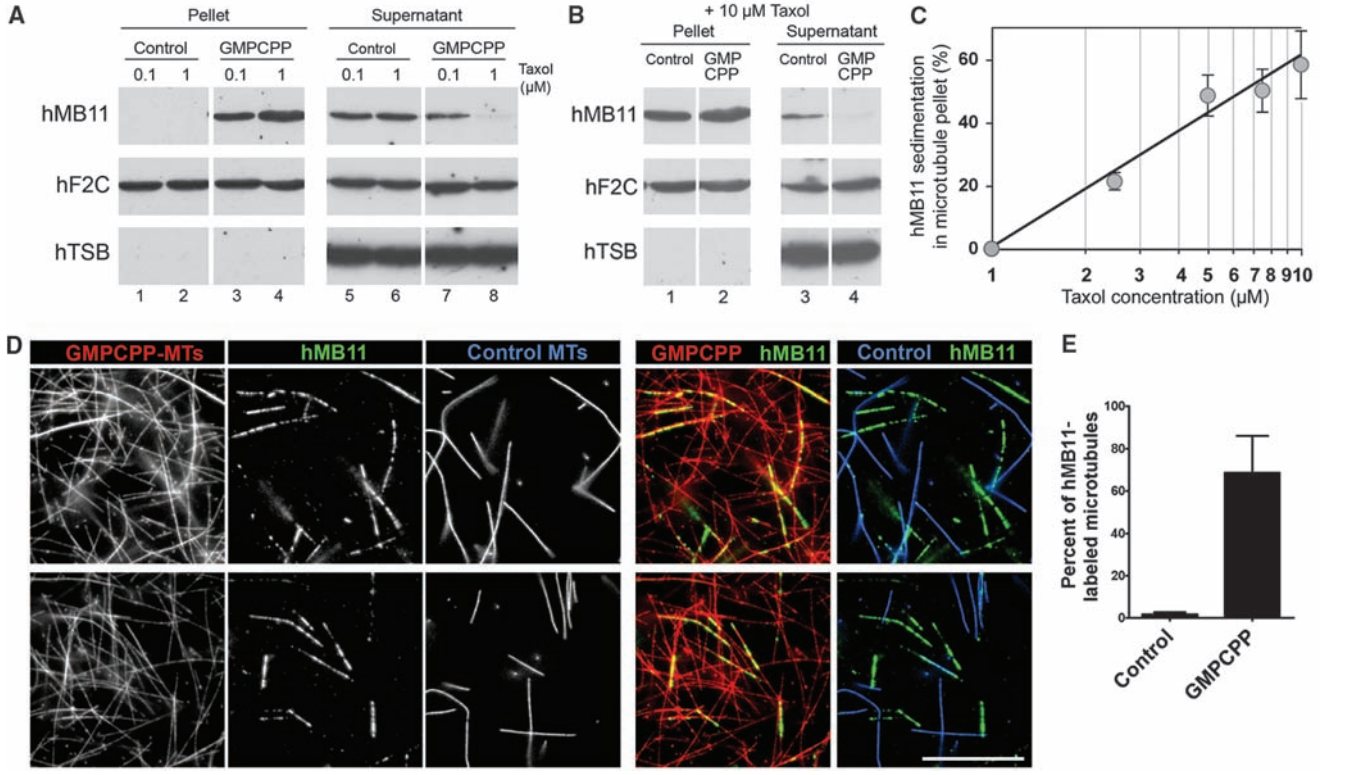

Fig. 1. Conformational detection of microtubules by the antibody hMB11. (**A**) Microtubules were polymerized in the presence of GTP (control) or GMPCPP. After stabilization with taxol, they were incubated with hMB11, anti-tsg101 (hTSB), or anti-tubulin (hF2C). After centrifugation, antibodies in pellets (lanes 1 to 4) and supernatants (lanes 5 to 8) were analyzed by immunoblot. Only hMB11 cosedimented specifically with GMPCPP microtubules. (**B** and **C**) Cosedimentation experiments were carried out as in (A) but in the presence of 10 μM taxol. Binding of hMB11 to control microtubules depended on taxol concentration (C). Data are means ± SEM of four experiments. (**D**) Fluorescent microtubules assembled separately with GMPCPP (red) or GTP (blue) were stabilized with 1 μM taxol, mixed together, and stained with hMB11 (green). (**E**) Quantification of hMB11 staining (mean ± SD, $N = 585$, two experiments).

Selection of a recombinant antibody specific for the GTP-bound conformation of tubulin. We screened a phage display library of recombinant scFv (single-chain fragment variable) against guanosine 5′-*O*-(3′-thiotriphosphate) (GTP-γ-S)–loaded tubulin and selected a series of recombinant antibodies to tubulin (*9*) (fig. S1). One scFv, named hMB11 (scFv MB11 fused to the Fc domain of human immuno-

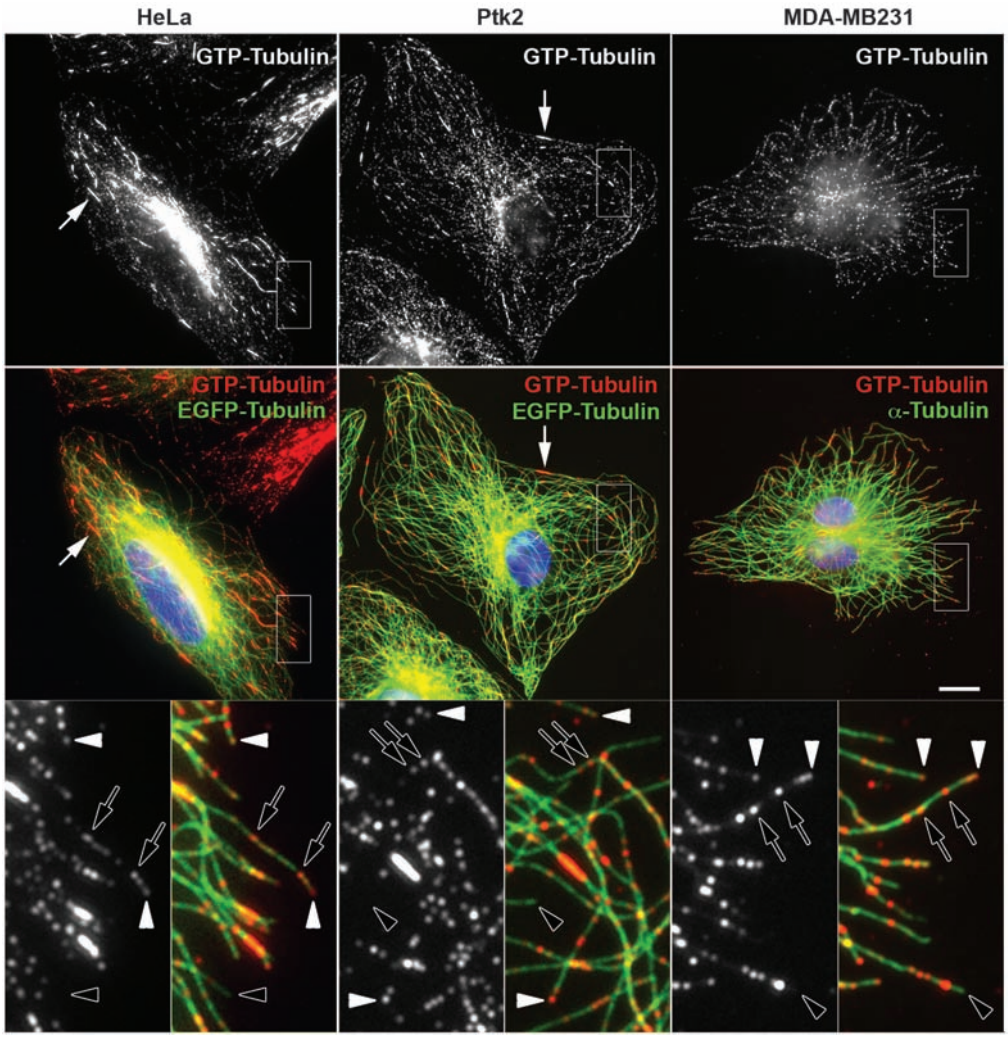

Fig. 2. Detection of GTP-tubulin by immunofluorescence in mammalian cells. Cultured cells were processed for hMB11 immunostaining (*9*) and microtubules were stained with the hF2C antibody (MDA-MB231 cells) or by GFP-tubulin expression (HeLa and Ptk2 cells). Boxed regions are shown enlarged (×5) below. Some microtubule ends were stained by hMB11 (white arrowheads); others were not (open arrowheads). hMB11 also detected GTP-tubulin dots inside the polymers (open arrows). In HeLa or Ptk2, extended stretches corresponding to microtubule bundling were also strongly stained (white arrows). Scale bar, 10 μm.

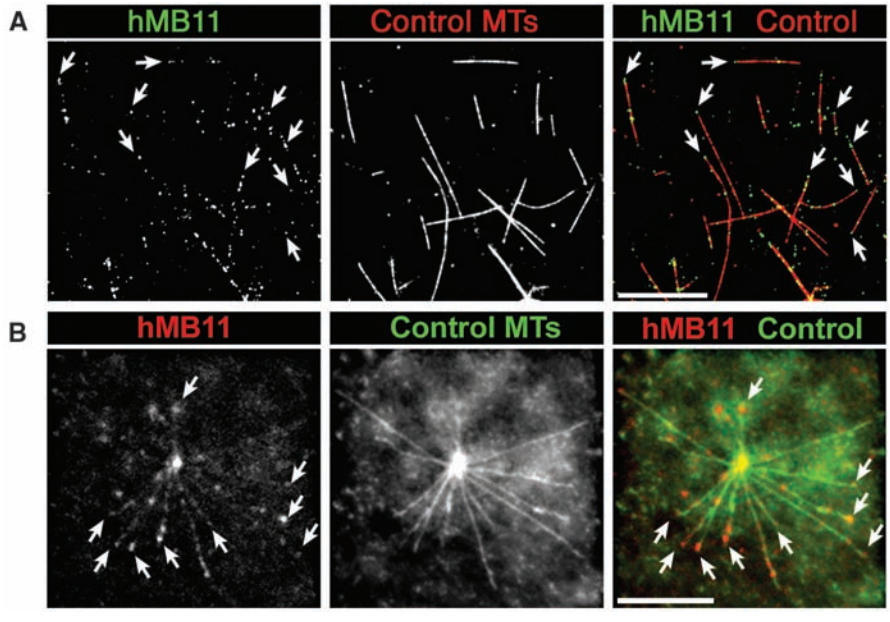

Fig. 3. Staining of in vitro polymerized microtubules by hMB11. (**A**) Microtubules were assembled in vitro as in Fig. 1D in the presence of GTP and directly stained with hMB11 before being diluted in taxol and observed by fluorescence microscopy. In these conditions, hMB11 labeled discrete dots along polymerized microtubules. The arrows show microtubule ends stained by hMB11. Scale bar, 10 μm. (**B**) Microtubules were polymerized for a short period of time (15 min, 37°C) from centrosomes incubated with purified tubulin and labeled with hMB11 (red) and hF2C (green). Note that in addition to internal dots, hMB11 stained the majority of microtubule plus ends (arrows). Scale bar, 10 μm.

globulin G), was found to be conformation-specific. It did not recognize denatured tubulin by immunoblotting and seemed not to bind to native nonpolymerized tubulin. However, hMB11 cosedimented specifically with microtubules polymerized in the presence of guanylyl 5′-(β,γ-methylenediphosphonate) (GMPCPP), a nonhydrolyzable GTP analog, and not with control microtubules assembled in the presence of GTP (Fig. 1A). In this experiment, low concentrations of taxol (0.1 to 1 μM) were used to prevent depolymerization of control microtubules. When a higher concentration of taxol was used, hMB11 bound to both control and GMPCPP microtubules (Fig. 1, B and C),which suggests that it recognized a conformation and not the nucleotide itself.

We then used hMB11 to stain by immunofluorescence a mixture of microtubules polymerized from pure tubulin in the presence of GTP or GMPCPP (Fig. 1D). Under these conditions, hMB11 stained only GMPCPP microtubules [representing 68.6 ± 17.3% (SD) of MB11-positive microtubules] and not control microtubules (1.8 ± 0.9%). The remaining 29.7 ± 16.6% were bundles of both GMPCPP and control microtubules. Despite varying experimental conditions, not all GMPCPP-containing microtubules were stained by MB11, which suggests that some microtubules possessed conformational defects under these conditions.

Detection of tubulin in GTP conformation in cellular microtubules. We next used hMB11 to localize GTP-tubulin in cellular microtubules by immunofluorescence. Because of its conformational binding, hMB11 staining was very sensitive to structural alterations occurring after fixation (*10*). It was best to use unfixed cells permeabilized in the presence of glycerol and/or low taxol concentration to prevent microtubule depolymerization. In three representative cell lines (HeLa, Ptk2, and MDA-

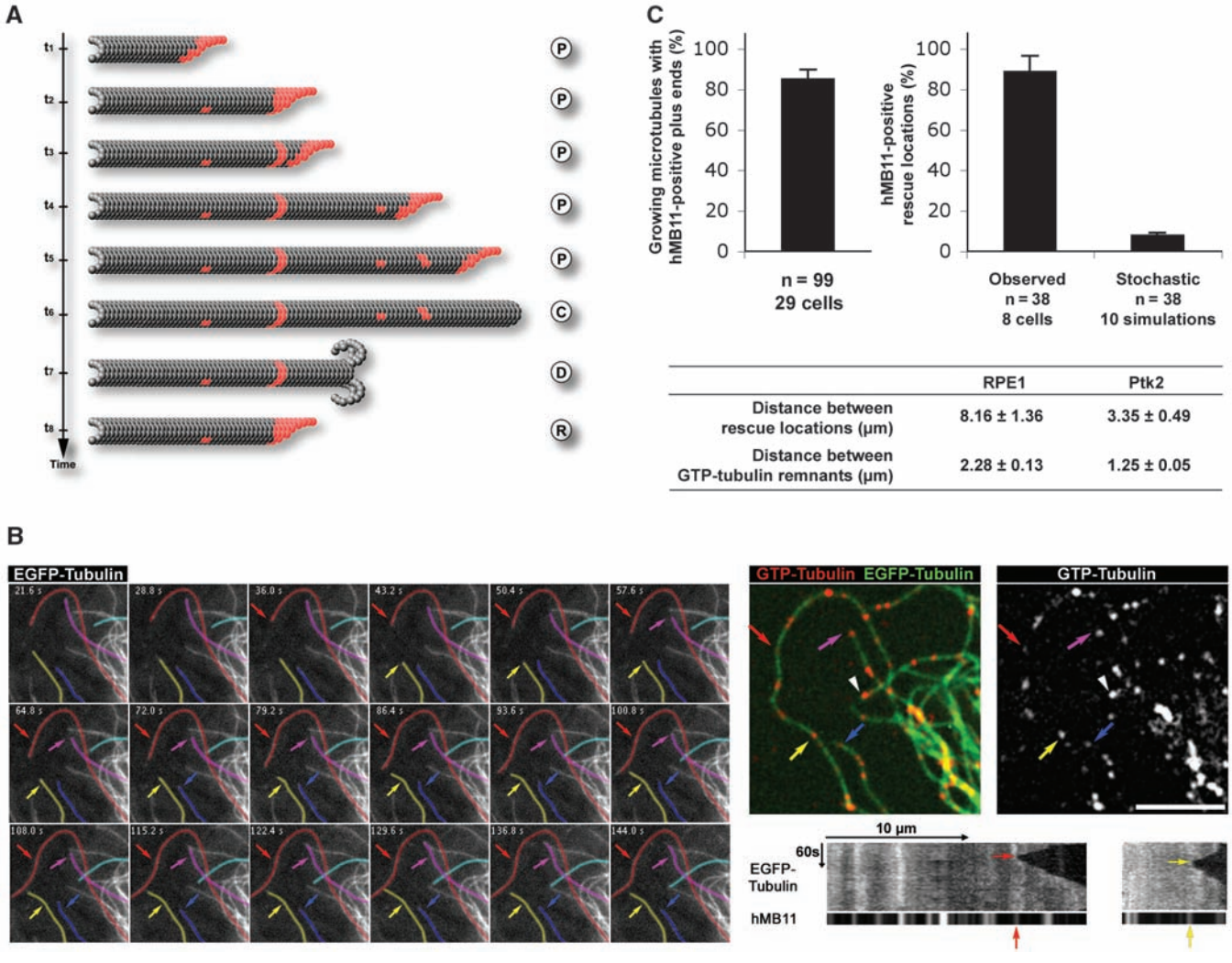

	RPE1	Ptk2
Distance between rescue locations (μm)	8.16 ± 1.36	3.35 ± 0.49
Distance between GTP-tubulin remnants (μm)	2.28 ± 0.13	1.25 ± 0.05

Fig. 4. A GTP-remnant model for microtubule dynamic instability. (**A**) Model for microtubule dynamics showing GTP-tubulin (red) in a GTP cap during polymerization (P) and in inner microtubule regions. Upon cap loss, the probability of catastrophe (C) increases and the microtubule depolymerizes (D) until its end reaches a GTP-tubulin remnant. A GTP end is restored and the probability of microtubule polymerization increases, allowing its rescue (R). (**B**) Ptk2 cells stably expressing GFP-tubulin were imaged at the indicated times. Rescue events (colored arrows) and the tip of a growing microtubule (arrowhead) are indicated. After cytosol extraction, cells were stained with hMB11 (red) and imaged again, often showing GTP-tubulin remnants at rescue locations. Scale bar, 10 μm. The two kymographs show the dynamics of the microtubules highlighted in red and yellow (top) aligned with hMB11 staining (bottom). Note the good coincidence of rescue position and GTP remnants. (**C**) Quantification of experiments done as in (A), showing the proportion of polymerizing microtubules stained by hMB11 at their plus ends and the proportions of GTP-tubulin remnants that colocalized with rescue locations in Ptk2 cells (means ± SEM). The proportion that would be expected in stochastic conditions is shown for reference at the right (Monte Carlo simulation, table S1) (*9*). The table shows that the rescue frequency varies with the distribution of GTP-tubulin remnants (means ± SEM, comparison of Ptk2 and RPE1 cells) (*9*) (table S1).

MB231), hMB11 stained the tips of only a fraction of microtubules (Fig. 2, white arrowheads representing 63 ± 4.5% of visible ends), whereas other microtubule ends were unstained (Fig. 2, open arrowheads). This was expected because the GTP-cap model proposes that only microtubules growing at the time of staining should be capped with GTP-tubulin. The observed proportion was very close to the 60% of growing microtubules identified in interphase cells (*11*).

In addition to the microtubule tip staining predicted by the GTP-cap model, we also observed an unexpected GTP-tubulin staining. First, hMB11 labeled long internal stretches in areas where microtubules formed bundles (Fig. 2, white arrows), although not all bundles were positive. The occurrences of these stretches depended on the cell line used. It is not known whether the GTP domains of microtubules are prone to bundling (as observed upon long incubation with taxol; see fig. S2) or whether microtubules retain a GTP conformation due to bundling and/or to specific binding proteins. Second, hMB11 detected dots along individual microtubules, which we have termed "GTP remnants," that looked randomly distributed (Fig. 2, open arrows). GTP caps and GTP remnants were also detected in mitotic cells and were more abundant in spindle than in astral microtubules (fig. S3).

Microtubules polymerized in vitro from GTP-tubulin were similarly stained by hMB11 at some of their ends and on discrete internal regions (Fig. 3A). To determine whether labeled ends could correspond to GTP caps, we stained microtubule asters that had polymerized from centrosomes for a short period of time. As predicted by the GTP-cap model, the majority of microtubule plus ends (73% of 226 microtubules in 22 asters) were labeled (Fig. 3B, arrows). Intriguingly, and as shown above, a few discrete internal microtubule regions were also decorated. One possibility is that hMB11 may be directed against a domain in tubulin that would face the lumen of the tube and thus only be accessible at plus ends and on random structural defects along microtubules. This seems unlikely, however, because hMB11 decorated microtubules all along their length when expressed intracellularly while fused to mCherry (fig. S4).

We propose that hMB11 stains GTP-bound or GDP–inorganic phosphate (GDP-Pi)–bound tubulin dimers that have been trapped in small regions of the microtubules. A molecular mechanical model indeed predicted that the presence of GTP dimers in the lattice would only locally perturb the microtubule structure (*12*). Experimentally, GTP or GDP-Pi tubulin have been detected in microtubules (*13*–*16*). However, more recent studies have failed to detect GTP-bound or GDP-Pi–bound subunits in microtubules, and the presence of very small caps has been proposed (*3*, *4*, *17*, *18*), although this has recently been challenged (*19*). In any case, only a small fraction of GTP-tubulin is present inside the polymer.

Coincidence of GTP remnants with microtubule rescue domains. The presence of GTP-tubulin conformation in microtubules suggests a model for dynamic instability (Fig. 4A) that would provide some mechanistic basis to the seemingly stochastic rescue events. In this model, GTP hydrolysis is not always complete and some tubulin dimers persist in a GTP conformation in the polymer. Upon depolymerization, these GTP remnants will become exposed. If GTP hydrolysis does not resume, any remnant as small as a single tubulin layer (*4*) may behave as a polymerization-prone GTP cap, thereby promoting microtubule rescue. The GTP remnants may explain the frequent rescue events observed when polymerizing microtubules experience shortening (*19*). Note that growing GTP caps are structurally shaped as open sheets, whereas uncovered internal GTP remnants may exhibit blunt ends.

To test our model, we analyzed the dynamic behavior of microtubules in Ptk2 cells stably expressing a GFP (green fluorescent protein)–tubulin fusion protein and performed retrospective staining of GTP remnants. Figure 4B and movie S1 show such a sequence in which various events can be identified in particular microtubule rescues (arrows). The polymerizing microtubule exhibited a GTP cap (Fig. 4B, white arrowhead), as did more than 80% of the microtubules that were growing at the time of cell extraction (Fig. 4C). A large fraction of the rescue events recorded [88.8 ± 7.8% (SEM); 38 rescues, 35 microtubules, eight cells] occurred at locations where GTP remnants were retrospectively identified, thus supporting the GTP remnant model (see kymographs, Fig. 4B). A Monte Carlo simulation predicted that only 7.77 ± 1.53% coincidence would be expected to occur by chance (*9*) (Fig. 4C and table S1). GTP remnant distribution was roughly proportional to rescue frequency (see the comparison between RPE1 and Ptk2 cell lines, Fig. 4C), even though only one-third of GTP remnants seemed to rescue microtubules efficiently. In addition, GTP remnants could be found in newly polymerized portions of microtubules that had never encountered a rescue event (fig. S5), which suggests that the GTP remnants are most probably the cause rather than the consequence of rescue.

On the basis of these findings, we wrote simulation software to visualize the different models of microtubule dynamic instability (*9*) (MTsimul v1.4; fig. S6 and movie S2). According to the GTP-cap model, rescue depends on the probability of GDP tubulin present at the tip of the depolymerizing microtubule to start polymerizing again. Under the GTP-remnant model, rescues are linked to the probability of GTP hydrolysis. This implies that rescue locations are memorized in the polymer during the seconds or minutes before actual rescues, allowing cells to predetermine their microtubule life span. Factors may exist that would regulate GTP-remnant frequency and thus microtubule stability.

References and Notes

1. T. Mitchison, M. Kirschner, *Nature* **312**, 237 (1984).
2. A. Desai, T. J. Mitchison, *Annu. Rev. Cell Dev. Biol.* **13**, 83 (1997).
3. D. N. Drechsel, M. W. Kirschner, *Curr. Biol.* **4**, 1053 (1994).
4. M. Caplow, J. Shanks, *Mol. Biol. Cell* **7**, 663 (1996).
5. H. W. Wang, E. Nogales, *Nature* **435**, 911 (2005).
6. I. Arnal, R. H. Wade, *Curr. Biol.* **5**, 900 (1995).
7. C. Elie-Caille *et al.*, *Curr. Biol.* **17**, 1765 (2007).
8. C. Nizak *et al.*, *Science* **300**, 984 (2003).
9. See supporting material on *Science* Online.
10. E. Draberova, V. Viklicky, P. Draber, *Eur. J. Cell Biol.* **79**, 982 (2000).
11. G. S. Diamantopoulos *et al.*, *J. Cell Biol.* **144**, 99 (1999).
12. M. I. Molodtsov *et al.*, *Biophys. J.* **88**, 3167 (2005).
13. M. F. Carlier, D. Didry, C. Simon, D. Pantaloni, *Biochemistry* **28**, 1783 (1989).
14. R. Melki, M. F. Carlier, D. Pantaloni, *Biochemistry* **29**, 8921 (1990).
15. M. F. Carlier, D. Didry, C. Valentin-Ranc, *J. Biol. Chem.* **266**, 12361 (1991).
16. C. A. Dougherty, R. H. Himes, L. Wilson, K. W. Farrell, *Biochemistry* **37**, 10861 (1998).
17. M. Caplow, J. Shanks, *Biochemistry* **37**, 12994 (1998).
18. A. Vandecandelaere, M. Brune, M. R. Webb, S. R. Martin, P. M. Bayley, *Biochemistry* **38**, 8179 (1999).
19. H. T. Schek 3rd, M. K. Gardner, J. Cheng, D. J. Odde, A. J. Hunt, *Curr. Biol.* **17**, 1445 (2007).

20. We thank P. Benaroch for the selection of the TSB antibody, A. Khodjakov for the Ptk2 GFP-tubulin cell line, F. Severin and T. Hyman for help and advice, J. Sillibourne and D. Job for reading and commenting on the manuscript, and B. Goud for his constant support. Supported by the Institut de Recherches International Servier and the Association pour la Recherche sur le Cancer (ARC) (M.Q.), by the French Ministry of Research and the Association Française contre les Myopathies (A.D.), and by CNRS, the Agence Nationale de la Recherche (ANR non thématique), the Human Frontier Science Program Organization, ARC, and French Ministry of Research grant ACI-BCMS 338.

Supporting Online Material

www.sciencemag.org/cgi/content/full/1165401/DC1
Materials and Methods
Figs. S1 to S6
Table S1
Movies S1 to S3
Simulation software MTsimul 1.4 (for Mac OS X and Windows)

3 September 2008; accepted 8 October 2008
Published online 16 October 2008;
10.1126/science.1165401
Include this information when citing this paper.

Resolving Vacuum Fluctuations in an Electrical Circuit by Measuring the Lamb Shift

A. Fragner,[1] M. Göppl,[1] J. M. Fink,[1] M. Baur,[1] R. Bianchetti,[1] P. J. Leek,[1] A. Blais,[2] A. Wallraff[1]*

Quantum theory predicts that empty space is not truly empty. Even in the absence of any particles or radiation, in pure vacuum, virtual particles are constantly created and annihilated. In an electromagnetic field, the presence of virtual photons manifests itself as a small renormalization of the energy of a quantum system, known as the Lamb shift. We present an experimental observation of the Lamb shift in a solid-state system. The strong dispersive coupling of a superconducting electronic circuit acting as a quantum bit (qubit) to the vacuum field in a transmission-line resonator leads to measurable Lamb shifts of up to 1.4% of the qubit transition frequency. The qubit is also observed to couple more strongly to the vacuum field than to a single photon inside the cavity, an effect that is explained by taking into account the limited anharmonicity of the higher excited qubit states.

The concept of the vacuum field was originally invoked as an explanation for the natural linewidths of atoms in free space and given its physical interpretation in terms of virtual particles within the framework of quantum field theory (*1*). The electromagnetic vacuum leads to a number of observable effects (*2*), most notably the Casimir forces (*3*), which cause mechanical displacements of parallel conducting plates in vacuum; the Purcell effect (*4*), which governs the spontaneous emission of a quantum system coupled to a cavity field; and the Lamb shift (*5*, *6*), a radiative level shift that was first observed in hydrogen atoms. The Lamb shift has since been investigated in a number of experiments in the atomic domain (*7*–*9*), in which it is also being established as an ultra-high precision test of the theory of quantum electrodynamics (QED) (*10*). The interaction with the vacuum fluctuations is the underlying reason for the spontaneous emission of radiation from any excited quantum system (*11*). The same effect also triggers the well-known process of vacuum Rabi oscillations in cavity QED (*12*–*15*). Quantum fluctuations have been demonstrated to determine the spontaneous emission lifetime of superconducting quantum bits (qubits) (*16*); they also serve as a benchmark for amplifiers and the squeezing of quantum noise at the quantum limit (*17*, *18*) or for detecting the zero-point motion of nanomechanical oscillators (*19*).

We observed the cavity-enhanced Lamb shift of an individual superconducting two-level system coupled to a high-quality factor resonator with a large vacuum-field strength (*14*) in an architecture known as circuit QED (*20*, *21*). Our measurements were carried out with a superconducting transmon-type qubit (*22*), a Cooper pair box (*23*) with a large ratio of Josephson-to-charging-energy (E_J/E_C). Its energy-level spectrum (*22*) is controlled by a flux Φ threading the loop formed by the two parallel Josephson junctions (Fig. 1B) that determine the Josephson energy $E_J = E_J^{max}|\cos(\pi\Phi/\Phi_0)|$, where E_J^{max} is the maximum Josephson energy of the two tunnel junctions and Φ_0 is the magnetic flux quantum. The electrostatic energy of the qubit $E_C = e^2/2C_\Sigma$ is determined by its total capacitance C_Σ, with e being the electron charge. The qubit is strongly coupled to a coplanar transmission-line resonator (*20*, *21*) with a fundamental resonance frequency $\omega_r/2\pi = 6.44$ GHz and a photon decay rate $\kappa/2\pi \approx 1.6$ MHz. The transmon qubit provides for both a large dipole-coupling strength to the resonator

[1]Department of Physics, Eidgenössische Technische Hochschule–Zurich (ETHZ), CH-8093 Zurich, Switzerland. [2]Département de Physique, Université de Sherbrooke, Sherbrooke, Québec J1K 2R1, Canada.

*To whom correspondence should be addressed. E-mail: andreas.wallraff@phys.ethz.ch.

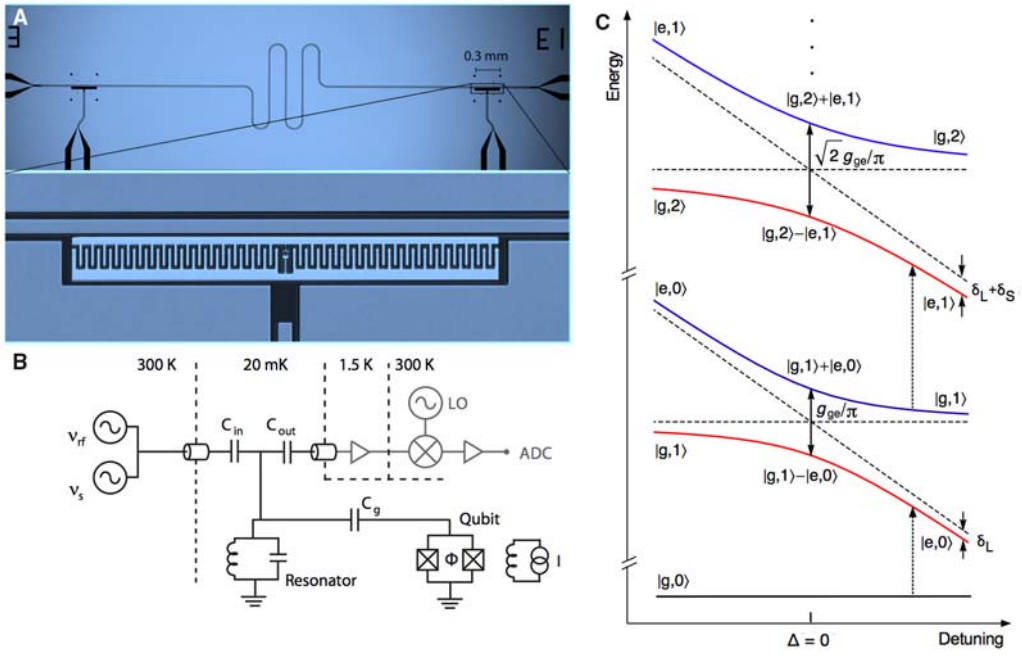

Fig. 1. Sample, experimental setup and energy-level diagram. (**A**) (Top) Optical image of the superconducting coplanar waveguide resonator with the transmon-type superconducting qubit embedded at the position shown boxed. (Bottom) Magnified view of boxed area, showing the qubit with dimensions 300 by 30 μm^2 close to the center conductor. (**B**) Simplified circuit diagram of the setup, similar to the one used in (*21*). We capacitively coupled the qubit at temperature 20 mK to the radiation field contained in the resonator through C_g. We coupled the resonator, represented by a parallel LC circuit, to input and output transmission lines via the capacitors C_{in} and C_{out}. We controlled the qubit transition frequency via a current-biased (I) coil generating a magnetic flux Φ threading the qubit loop. Microwave signal generators for populating the resonator with photons (ν_{rf}) and for exciting the qubit spectroscopically (ν_s) are shown. By using ultralow-noise amplifiers at 1.5 K and a mixer at 300 K, we down-converted the transmitted microwave signal with a local oscillator (LO) and digitized with an analog-to-digital converter (ADC) for measuring the qubit and photon states. (**C**) Energy levels of the coupled (solid lines) and uncoupled (dashed lines) qubit/cavity system versus detuning Δ. The corresponding states and their characteristic energy shifts are indicated (see text for details).

(*14*, *24*) and long relative coherence times at the expense of limited anharmonicity in the energy-level spectrum (*16*, *22*, *25*). Optical images of our device and a simplified circuit diagram of the setup are shown in Fig. 1, A and B.

The coupled qubit/cavity system is well described by a Jaynes-Cummings Hamiltonian

$$\hat{H} = \hbar\omega_{ge}\hat{\sigma}_{ee} + \hbar\omega_r\hat{a}^\dagger\hat{a} + \hbar g_{ge}(\hat{\sigma}_{ge}^\dagger\hat{a} + \hat{a}^\dagger\hat{\sigma}_{ge}) \quad (1)$$

where ω_{ge} denotes the transition frequency from the ground state ($|g\rangle$) to excited state ($|e\rangle$) of the qubit and $\hat{\sigma}_{ij} = |i\rangle\langle j|$ are the corresponding operators acting on the qubit states. The dynamics of the cavity field of frequency ω_r is described by the creation and annihilation operators $\hat{a}^\dagger$, $\hat{a}$ acting on the photon number states $|n\rangle$ and the dipole coupling strength between qubit and cavity is given by g_{ge}. Equation 1 can be generalized to take into account additional qubit levels (*22*, *24*).

In the resonant limit $\Delta = \omega_{ge} - \omega_r \to 0$, a single quantum of energy is coherently exchanged between the qubit and the cavity (*21*, *24*), which are described by the joint-dressed qubit-field state vectors $|n\pm\rangle \equiv (|g,n\rangle \pm |e,n-1\rangle)/\sqrt{2}$ (Fig. 1C). A qualitatively different regime is obtained when qubit and cavity are far detuned from each other ($|\Delta| >> g_{ge}$). In this dispersive limit, the two systems do not exchange energy resonantly, instead their interaction manifests itself in the form of frequency shifts (*20*, *21*, *26*). The qubit transition frequency ω_{ge} is renormalized by the dispersive interaction and experiences a detuning-dependent ac Stark shift $\delta_S \sim 2\, n\, g_{ge}^2/\Delta$ for a cavity field populated with $n = \langle\hat{a}^\dagger\hat{a}\rangle$ photons (*26*), as well as a Lamb shift $\delta_L \sim g_{ge}^2/\Delta$ due to its interaction with the vacuum fluctuations, $\langle\hat{a}^\dagger\hat{a}\rangle = 0$ (Fig. 1C). In our circuit QED setup, we are able to adjust the size of the Lamb and Stark shifts by controlling the detuning Δ between the resonator frequency and the qubit frequency. A similar approach has been used in an experiment with Rydberg atoms interacting with the vacuum field in a three-dimensional microwave cavity (*8*).

To resolve the relatively small Lamb shift of our solid-state quantum system, an accurate measurement of the characteristic qubit parameters and their dependence on the control variables was essential. We determined the qubit transition frequency and its periodic modulation with applied magnetic flux by measuring the cavity-transmission spectrum (*24*) and simultaneously performing qubit spectroscopy with a dispersive measurement of the cavity frequency shift (*26*). With this procedure, we can determine both the flux periodicity and the flux offset because of magnetic offset fields to an accuracy of better than $10^{-3}\,\Phi_0$. From here on, we express the applied magnetic field in terms of a normalized flux Φ/Φ_0. Adjusting the applied flux bias to $\Phi/\Phi_0 = 0$, the qubit is tuned to its maximum transition frequency $\omega_{ge}/2\pi = 7.84$ GHz, which we determined spectroscopically. At this bias point, we also determined the transition frequency $\omega_{gf}/2\pi$ between ground $|g\rangle$ and second excited qubit state $|f\rangle$ via two-photon absorption spectroscopy (*22*, *25*), which yields an anharmonicity of $\alpha = (\omega_{ge} - \omega_{ef})/2\pi \sim 250$ MHz. With these two quantities, we were able to in turn determine the maximum Josephson coupling energy $E_J^{max} = 35.11$ GHz and the charging energy of our device $E_C = 231.7$ MHz at maximum positive detuning from the cavity, in which the dispersive shifts are small. To check for consistency, similar measurements have been performed down to negative detunings of $|\Delta|/2\pi \sim 3$ GHz. The excitation spectrum of our qubit, including its higher excited states, is fully determined by E_J^{max}, E_C, and the flux periodicity (*22*).

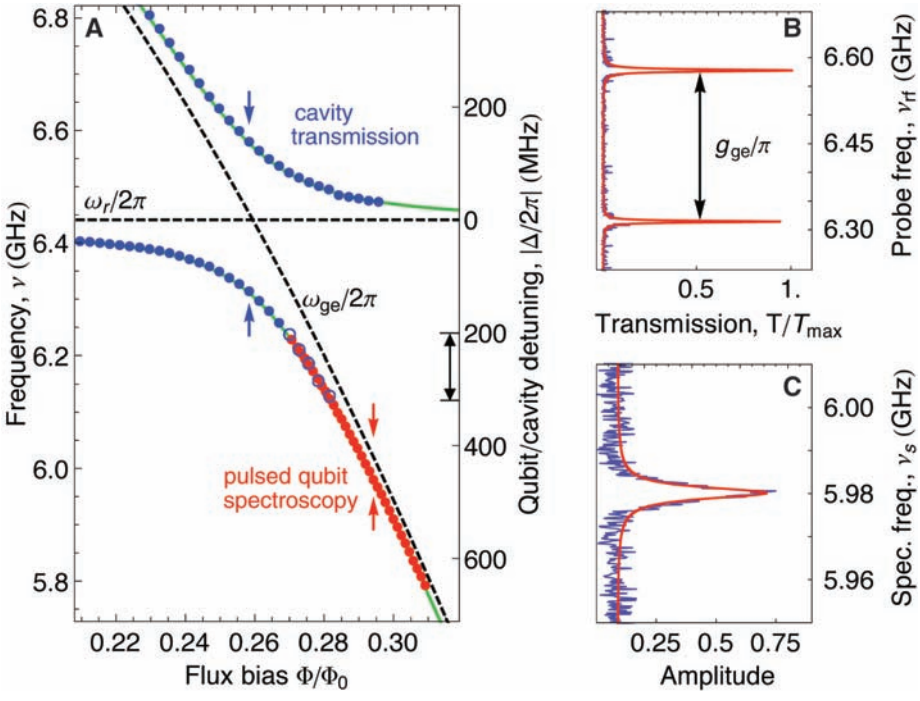

Fig. 2. Spectrum of the coupled qubit/cavity system. (**A**) Measured transition frequencies of cavity (blue circles) and qubit (red circles) versus normalized flux bias Φ/Φ_0. The dashed horizontal line is the cavity transition frequency ω_r, and the dashed slanted line is the calculated bare qubit-transtion frequency ω_{ge}. The green solid lines are the numerically calculated eigenfrequencies of the coupled system. Overlap of resonator transmission (open blue circles) and qubit spectroscopy data (solid red circles) is indicated by black arrows on the detuning axis (see text for details). (**B**) Measured resonant vacuum Rabi mode–split cavity transmission spectrum T (blue line) versus probe frequency ν_{rf} at flux bias, indicated by blue arrows in (A). The solid red line is a fit to a double-peak Lorentzian. (**C**) Measured spectroscopic qubit line shape (blue line) versus spectroscopy frequency ν_s at flux bias, indicated by red arrows in (A). The solid red line is a fit to a Lorentzian.

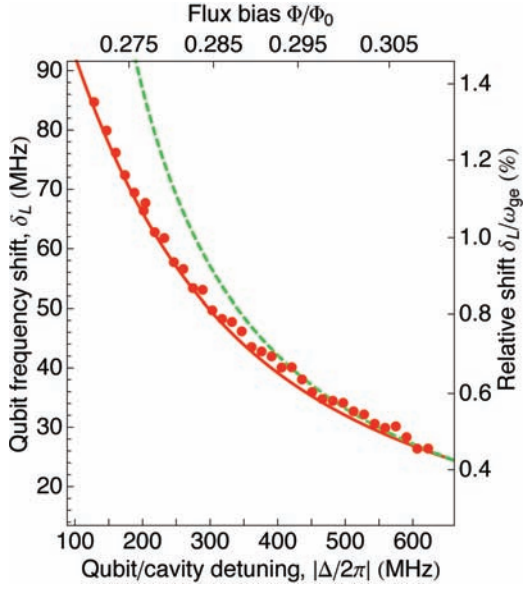

Fig. 3. Lamb shift. Difference between measured qubit-transition frequency $\tilde{\omega}_{ge}/2\pi$ dressed by the vacuum-field fluctuations (red circles) and calculated bare qubit-transition frequency $\omega_{ge}/2\pi$ versus qubit-cavity detuning $\Delta/2\pi$ (bottom axis) and normalized flux bias Φ/Φ_0 (top axis). The right axis shows the Lamb shift as a percentage relative to the bare qubit transition frequency. The red line is the predicted Lamb shift calculated with exact numerical diagonalization of the generalized Jaynes-Cummings Hamiltonian, and the dashed green line is g_{ge}^2/Δ from a dispersive approximation of Eq. 1.

We then determined the resonant qubit/field coupling strength g_{ge} by measuring the anticrossing of the flux-tunable qubit and the fixed-frequency resonator. The extracted frequencies $\nu_{1\pm}$ of the qubit/cavity superposition states $|n\pm\rangle$ for $n = 1$ photon are shown as blue circles in Fig. 2A as measured with a probe tone power populating the resonator field with much less than one photon on average. Here, the energies of the $|1\pm\rangle$ states were determined by measuring the photonic component of the joint qubit/field-state vector. On resonance ($\Delta = 0$), in which the joint states have equal qubit and photon character, we extracted the coupling strength $g_{ge}/2\pi = 133$ MHz from the observed vacuum Rabi-mode splitting (Fig. 2B), which in turn also allowed us to calculate the coupling between higher transmon levels and the cavity (*22*). The measured eigenfrequencies $\nu_{1\pm}$ were in excellent agreement with the exact numerical solution of the generalized Jaynes-Cummings Hamiltonian, taking into account higher qubit levels (Fig. 2A, solid green lines), at which we considered the qubit spectrum up to the fifth excited state and resonator states up to $|4\rangle$. At this point, we fully determined the parameters that govern the coupled qubit/resonator system and set out to spectroscopically measure the Lamb shift of the qubit because of the coupling to the fundamental mode of the resonator.

Using magnetic flux bias, we detuned the qubit to well below the cavity-resonance frequency ($|\Delta| >> g_{ge}$), at which the joint qubit/field state has a predominantly qubit character ($|e,0\rangle$) (Fig. 1C). We then spectroscopically determined the transition frequency $\tilde{\omega}_{ge}/2\pi$ between $|g,0\rangle$ and $|e,0\rangle$ by probing the resonator response in a dispersive quantum nondemolition measurement (*26*), which measures the qubit component of the joint state. At the largest investigated detuning ($|\Delta| \sim 620$ MHz), this state has a predominantly qubit character with ~99.5% probability for $|e,0\rangle$ and ~0.5% for $|g,1\rangle$ (*20*). In a typical qubit spectral line (Fig. 2C), the qubit line width is on the order of $\delta_{ge} \sim 3$ MHz, slightly power-broadened by the spectroscopy tone. Here it is important to point out that first we applied a long microwave pulse to the qubit to prepare a fully mixed state. Only after this, we applied a measurement tone to the resonator, the amplitude of which was used to readout the qubit state (*26*). In this pulsed spectroscopy scheme, excitation and measurement tones were separated in time, and the cavity was left approximately in the vacuum state $|0\rangle$, when the spectroscopy pulse was applied to the qubit. In contrast, performing a measurement with a continuous tone at the cavity frequency simultaneously with the spectroscopy pulse would result in an observation of a photon number-split qubit spectrum. In that case, the strong dispersive coupling leads to distinct, well-separated qubit lines that correspond to the individual photon number states, as is discussed theoretically in (*27*) and observed experimentally in (*28*).

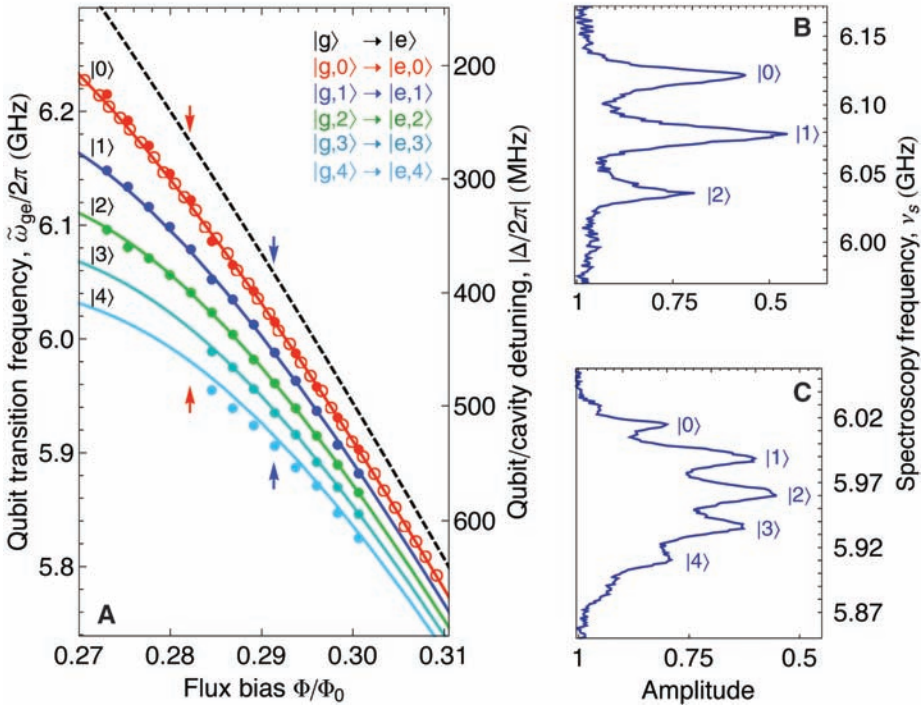

Fig. 4. Number splitting and ac Stark shift. (**A**) Spectroscopically measured qubit-transition frequency $\tilde{\omega}_{ge}/2\pi$ (data points) dressed by a weak coherent field. The solid circles with colors (red, dark blue, green, aquamarine, and light blue) correspond to number-split qubit transitions with $n = 0$, 1, 2, 3, and 4 photons, as indicated in the upper right-hand corner. Open circles are pulsed spectroscopy data from Fig. 2A. The solid lines are corresponding dressed-state energy levels calculated by exact diagonalization of the generalized Jaynes-Cummings Hamiltonian, and the dashed line is the bare qubit-transition frequency. (**B** and **C**) Measured number-split qubit spectrum at flux bias are indicated by blue and red arrows in (A). The photon number states $|n\rangle$ corresponding to each peak are indicated.

We then sequentially reduced the detuning Δ and extracted the qubit transition frequency from the maximum in the pulsed spectroscopic line (Fig. 2C). The extracted dressed frequencies $\tilde{\omega}_{ge}/2\pi$ are shown as red circles in Fig. 2A. We observed that the measured frequencies coincide for all detunings with the frequencies of the $|1-\rangle$ state calculated from an exact numerical diagonalization of the generalized Jaynes-Cummings Hamiltonian accounting for the first five transmon levels. The difference between the measured and the bare qubit transition frequency (dashed slanted line), resulting from the interaction with the vacuum fluctuations, was clearly observed and well-resolved by many line widths. This represents a direct spectroscopic observation of the Lamb shift in a solid-state system and demonstrates the dispersive interaction of a superconducting qubit with the vaccuum field in a cavity.

We explicitly extracted the Lamb shift from the data versus flux-controlled detuning by subtracting the measured qubit transition frequency $\tilde{\omega}_{ge}/2\pi$ from the calculated bare frequency $\omega_{ge}/2\pi$, as shown by red circles in Fig. 3. For the measured range of detunings, we found that the Lamb shift varies from about 30 MHz at a detuning of $|\Delta|/2\pi \sim 620$ MHz to 85 MHz at $|\Delta|/2\pi \sim 130$ MHz, corresponding to a maximum value of roughly 1.4% of the bare qubit-transition frequency. The data are in good agreement with the Lamb shift that was calculated from the generalized Jaynes-Cummings Hamiltonian, including counter-rotating terms, shown as the solid red line in Fig. 3. For comparison, the Lamb shift g_{ge}^2/Δ expected from a simple dispersive approximation of Eq. 1 is shown as a dashed green line in the same plot. The dispersive approximation is in good agreement with the data for large Δ and is seen to break down for small Δ. The Bloch-Siegert shift (*29*) is small for the given coupling strengths in our sample and could not be resolved.

Over a range of detunings (Fig. 2A, black arrows), the energy of the coupled qubit/resonator system was extracted both from the photonic component, measured by probing the cavity resonance frequency, and the qubit component, measured spectroscopically. We observed virtually identical, and thus consistent, frequencies in the overlap region of the data from the two independent measurements (Fig. 2A, open blue and solid red circles).

Finally, we checked that the observed energy shifts were indeed solely due to the vacuum fluctuations of the radiation field and not confused with ac Stark shifts induced by residual photons in the cavity. To do so, we applied a continuous-wave coherent microwave field at the resonator frequency with the qubit in the ground state, populating the cavity with a small mean number of photons. We simultaneously used the same tone to perform a dispersive measurement of the qubit state. The resulting number-split qubit spectra (*27*, *28*) under weak qubit driving are shown in Fig. 4, B and C, for two different detunings (Fig. 4A, arrows). Each individual peak can be clearly associated with a photon number state

$|n\rangle$ of the cavity. The extracted peak frequencies for $n = 0$, 1, 2, 3, and 4 photons are plotted as solid circles in Fig. 4A. The corresponding transitions are also indicated by dotted arrows in Fig. 1C. Again, we clearly observed that the qubit frequency is Lamb-shifted with respect to its bare frequency by the vacuum state of the cavity. The pulsed spectroscopy data of Fig. 2A (open circles) are also in good agreement. Moreover, we resolved the quantum ac Stark-shifted qubit-transition frequencies of the corresponding photon number states $|n\rangle$ and their dependence on the flux-controlled detuning. As before, we were able to explain the observed frequencies of the individual transitions accurately, solving the generalized Jaynes-Cummings Hamiltonian numerically by taking into account up to five qubit (g, e, f, h, and i) and five cavity levels ($n = 0$, 1, 2, 3, and 4 photons) (Fig. 4A, solid lines). Only for $n = 4$ photons, small deviations between data and theory were observed. These are probably related to the limited accuracy with which the resonant frequency can be extracted from the number-split line, the width of which scales with $n\kappa$. This data consistently demonstrates that the measured frequency shift for an empty cavity ($n = 0$ photons) can be associated with the vacuum fluctuations of the cavity radiation field.

As a final check, we determined the background thermal photon number in our circuit QED system by probing the resonant vacuum Rabi-mode splitting. A small thermal population of the $|1\pm\rangle$ states can be detected through the transitions from the first doublet of the Jaynes-Cummings ladder into the second doublet $|1\pm\rangle \rightarrow |2\pm\rangle$, appearing as weak lines in the transmission spectrum of the resonator. The effective temperature of the radiation field was estimated to be $T_r \approx 90$ mK, corresponding to a mean thermal photon number of $\bar{n}_{th} \approx 0.03$, where we have analyzed in detail the amplitudes of these lines in the vacuum Rabi-mode splitting (*30*, *31*).

Another observation concerns the relative size of the Lamb and ac Stark shifts. In general for a two-level system, the ac Stark shift per photon is expected to be twice as large as the shift induced by the vacuum field. However, we made the surprising observation that the measured Stark shift per photon is in fact smaller than the Lamb shift (Fig. 4A). This phenomenon can be explained by considering the higher excited states of our qubit beyond $\{|e\rangle,|g\rangle\}$. As discussed theoretically in (*22*), the ac Stark shift per photon is renormalized by the presence of the third transmon level $|f\rangle$ and consequently reduced by a factor proportional to the level of anharmonicity. For the given measured anharmonicity of our artificial atom, we indeed reached the limit of $\delta_S/n < \delta_L$. In this way, the qubit appeared to couple more strongly to the vacuum field than to a single photon inside the cavity. Similarly, for two coupled strictly harmonic quantum oscillators, only a Lamb shift but no photon number–dependent Stark shift is expected, a situation that was approached in our experiments because of the limited anharmonicity of the qubit.

The Lamb shift induced in a solid-state quantum system by the vacuum fluctuations of the electromagnetic field in a resonator was observed spectroscopically. In resolving this effect, we explicitly demonstrate the presence of dispersive vacuum-field interactions in circuit QED and show that these can exceed the interaction with a photon-populated field. The clear observation of vacuum fluctuations in this strongly coupled system should serve as a motivation for further experiments aimed at investigating other effects triggered by quantum fluctuations of electromagnetic or even nanomechanical degrees of freedom in solid-state systems (*19*, *32*).

References and Notes

1. J. Schwinger, *Selected Papers on Quantum Electrodynamics* (Dover, New York, 1958).
2. P. W. Milonni, *The Quantum Vacuum: An Introduction to Quantum Electrodynamics* (Academic Press, New York, 1994).
3. H. Casimir, D. Polder, *Phys. Rev.* **73**, 360 (1948).
4. E. M. Purcell, *Phys. Rev.* **69**, 681 (1946).
5. W. E. Lamb, R. Retherford, *Phys. Rev.* **72**, 241 (1947).
6. H. Bethe, *Phys. Rev.* **72**, 339 (1947).
7. D. J. Heinzen, M. S. Feld, *Phys. Rev. Lett.* **59**, 2623 (1987).
8. M. Brune *et al*., *Phys. Rev. Lett.* **72**, 3339 (1994).
9. M. Marrocco, M. Weidinger, R. T. Sang, H. Walther, *Phys. Rev. Lett.* **81**, 5784 (1998).
10. M. Niering *et al*., *Phys. Rev. Lett.* **84**, 5496 (2000).
11. D. Walls, G. Milburn, *Quantum Optics* (Springer-Verlag, Berlin, 1994).
12. S. Haroche, J. Raimond, *Exploring the Quantum: Atoms, Cavities, and Photons* (Oxford Univ. Press, New York, 2006).
13. G. Khitrova, H. M. Gibbs, M. Kira, S. W. Koch, A. Scherer, *Nat. Phys.* **2**, 81 (2006).
14. R. J. Schoelkopf, S. M. Girvin, *Nature* **451**, 664 (2008).
15. J. Ye, H. J. Kimble, H. Katori, *Science* **320**, 1734 (2008).
16. A. A. Houck *et al*., *Phys. Rev. Lett.* **101**, 080502 (2008).
17. J. Clarke, A. Braginsky, *The SQUID Handbook* (Wiley-VCH, Berlin, 2006).
18. M. A. Castellanos-Beltran, K. Irwin, G. Hilton, L. Vale, K. Lehnert, *Nat. Phys*. 10.1038/nphys1090 (2008).
19. C. Regal, J. Teufel, K. Lehnert, *Nat. Phys.* **4**, 555 (2008).
20. A. Blais, R. S. Huang, A. Wallraff, S. M. Girvin, R. J. Schoelkopf, *Phys. Rev. A* **69**, 062320 (2004).
21. A. Wallraff *et al*., *Nature* **431**, 162 (2004).
22. J. Koch *et al*., *Phys. Rev. A* **76**, 042319 (2007).
23. V. Bouchiat, D. Vion, P. Joyez, D. Esteve, M. H. Devoret, *Phys. Scr.* **T76**, 165 (1998).
24. J. M. Fink *et al*., *Nature* **454**, 315 (2008).
25. J. Schreier *et al*., *Phys. Rev. B* **77**, 180502 (2008).
26. D. I. Schuster *et al*., *Phys. Rev. Lett.* **98**, 049902 (2007).
27. J. Gambetta *et al*., *Phys. Rev. A* **74**, 042318 (2006).
28. D. I. Schuster *et al*., *Nature* **445**, 515 (2007).
29. F. Bloch, A. Siegert, *Phys. Rev.* **57**, 522 (1940).
30. I. Rau, G. Johansson, A. Shnirman, *Phys. Rev. B* **70**, 054521 (2004).
31. L. Bishop *et al*., *arXiv:0807.2882v1* (2008).
32. E. K. Irish, K. Schwab, *Phys. Rev. B* **68**, 155311 (2003).

33. We thank G. Blatter for stimulating discussions and L. Bishop, P. Studer, J. Koch, and R. Schoelkopf for their support in analyzing vacuum Rabi-mode spectra in the presence of thermal photons. This work was supported by the Swiss National Science Foundation and ETHZ. P.J.L. was supported by the European Commission with a Marie Curie Intra-European Fellowship. A.B. was supported by the Natural Sciences and Engineering Research Council of Canada, Canadian Institute for Advanced Research, and Fonds Québécois de la Recherche sur la Nature et les Technologies.

11 August 2008; accepted 20 October 2008
10.1126/science.1164482

A Cryptand-Encapsulated Germanium(II) Dication

Paul A. Rupar, Viktor N. Staroverov, Kim M. Baines*

Unlike cations of metals such as sodium or calcium, oxidized silicon and germanium centers generally require strongly bound covalent ligands. We report the synthesis and characterization of a germanium(II) dication in the form of the salt (Ge·cryptand[2.2.2])$(O_3SCF_3)_2$. The salt is isolated in 88% yield from the reaction of cryptand [2.2.2] and an N-heterocyclic carbene complex of $GeCl(O_3SCF_3)$ as an air-sensitive, white solid. The crystal structure of the salt shows minimal interaction between the cryptand-encapsulated germanium(II) ion and the two $^-O_3SCF_3$ counterions. These results suggest a widely expanded role of cryptands and related molecules in stabilizing nonmetallic cations.

For over a century, the periodic table has been an icon of science, providing a unifying vision for a seemingly diverse range of chemical facts. On the basis of their positions in the table, the main-group metals of groups 1 and 2 are expected to, and indeed form, stable free cations in solution with only weak coordination of the solvent. In contrast, elements in groups 13 to 15—particularly those of the first few periods: boron, silicon, phosphorus, and germanium—tend not to form cations, preferring to bond covalently to ligands. Despite the expectations, chemists have succeeded in synthesizing silylium (*1*, *2*) and germylium monocations with a vacant coordination site (*3*–*5*) in the condensed phase by employing two key strategies: (i) the use of bulky ligands and/or (ii) the use of noncoordinating counterions (*6*). Both tactics effectively stop the coordination of a fourth ligand to complete the octet at silicon or germanium (*7*, *8*). This methodology has been extended to silicon(II) and germanium(II) cations, which have only a single covalently bound ligand, as

Department of Chemistry, University of Western Ontario, London, Ontario, Canada N6A 5B7.

*To whom correspondence should be addressed. E-mail: kbaines2@uwo.ca

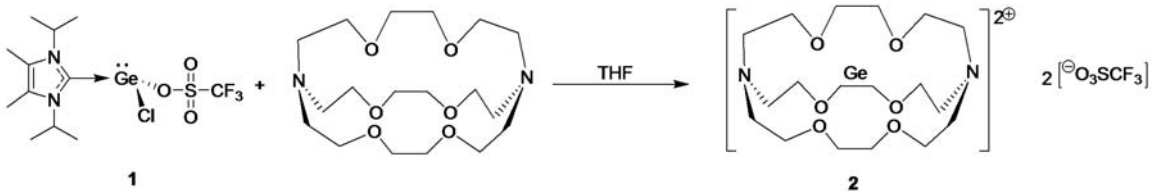

1

Scheme 1.

exemplified by the synthesis of $Cp^*Si^+ B(C_6F_5)_4^-$ (where Cp* is pentamethylcyclopentadienyl) (*9*, *10*) and the earlier syntheses of germanium derivatives (*11*). Dicationic silicon(II) and germanium(II) are no less intriguing targets, both as formidable synthetic challenges and as potentially useful reagents (*12*, *13*). However, the possibility of synthesizing a condensed-phase dicationic group 14 species with a lone pair of electrons, three unoccupied valence orbitals, and no tightly bound (covalent) ligands has always appeared remote. If the previous strategies are to be followed, the crucial question is how to remove the remaining tightly bound ligand and replace it with another noncoordinating counterion.

We have previously employed N-heterocyclic carbenes (NHCs) to synthesize stable germanium(II) complexes for use as precursors for the synthesis of germanium-containing compounds (*14*, *15*). In addition to serving as synthons of neutral GeX_2 fragments by displacement of the labile carbene, NHC-GeX_2 complexes, with the judicious selection of X (where X is a good leaving group), may act as precursors to cationic germanium(II). We recently reported a dicationic complex of germanium, featuring a central Ge atom with three NHC ligands synthesized from an NHC complex of GeI_2 (*16*). Although this complex carries a +2 charge, the central germanium atom is strongly bound to the three carbenes, and therefore, the positive charge is shared by the substituents. In search of a chemical environment capable of supporting dicationic germanium(II) in the condensed phase, we considered the use of cryptands, which are bicyclic macromolecular polyether cages commonly used to sequester metallic cations (*17*). We reasoned that in the absence of covalently bound ligands to provide steric shielding or electronic stabilization, the Ge^{2+} cation would need protection in three dimensions; cryptands satisfy this requirement. When we examined the literature, we were surprised that there are no reports, with the exception of protonated species (for example, NH_4^+) (*17*), of a cryptand containing a mononuclear metalloid or nonmetal element carrying a cationic charge (*18*–*20*). Given the success of cryptands in binding metallic cations, we postulated that a cationic germanium could be isolated and stabilized with the use of the appropriately sized cryptand. Because cryptands can completely encapsulate their host cation and protect it from nucleophilic counterions and solvents, the use of cryptands may allow the isolation of a more highly charged germanium species. Thus, we have investigated the reaction between cryptand [2.2.2], which is known to accommodate a diverse range of positively charged species, and an NHC complex of $GeCl(O_3SCF_3)$ (*15*), a germanium(II) precursor with labile ligands.

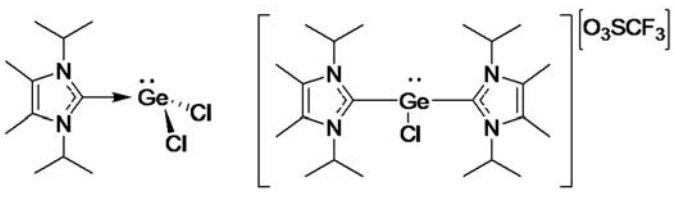

3 4

Scheme 2.

The addition of cryptand [2.2.2] to a solution of **1** (*15*) in tetrahydrofuran (THF) results in the rapid precipitation of a white powder (Scheme 1) (*21*). After stirring the reaction mixture for 24 hours, we collected the precipitate and then redissolved it in deuterated acetonitrile for study by nuclear magnetic resonance (NMR) spectroscopy. The ^1H NMR spectrum of the product showed only three distinct signals that were assigned to a cryptand moiety. The simplicity of the spectrum suggests that the macrocycle remains in a highly symmetrical environment. Signals attributable to a carbene moiety were not observed. The ^{19}F NMR spectrum showed a single resonance typical of a triflate anion. Crystals of the precipitate were grown and identified by single crystal x-ray diffraction as the salt **2** (*21*). The primary species in the unit cell is a dicationic germanium located inside the cavity of the cryptand (Fig. 1). The $(Ge{\cdot}cryptand[2.2.2])^{2+}$ complex has D_3 symmetry with the germanium directly in the center of the cage. No solvent molecules are occluded within the crystal. The triflate counterions show no interaction with the germanium (fig. S3); the closest triflate–oxygen–germanium approach is 5.32 Å. Previous examples of unsaturated cations of group 14 utilized very weakly or noncoordinating anions to maintain discrete cation/anion separation in the condensed phase; triflate is not considered a weakly or noncoordinating anion (*6*). The observation that the cryptand [2.2.2] is able to exclude the triflates from the coordination sphere of the dicationic germanium attests to the stabilizing effect of the cryptand on the cation and its ability to provide steric shielding.

Notably absent in the spectral data of the collected precipitate was evidence of either the carbene moiety or the chlorine atoms originally present in **1**. However, two other germanium-containing compounds were identified in the mother liquor: (i) the NHC $GeCl_2$ complex **3** (*16*) and (ii) the cationic dicarbene complex **4** (Scheme 2) (*21*). Presumably, with the precipitation of **2**, the displaced chloride and carbene react rapidly with two equivalents of **1**, displacing the labile triflate and forming **3** and **4**, respectively. On the basis of compounds **2** to **4** being the primary products of the reaction, the stoichiometry of the reaction shown in Scheme 1 is three equivalents of **1** per equivalent of cryptand. When the reaction is carried out with the correct stoichiometry, the isolated yields of **2** to **4** are 88%, 81%, and 96%, respectively. We believe that the driving force for the reaction is probably the precipitation of the $(Ge{\cdot}cryptand[2.2.2])^{2+}$ complex, which is insoluble in the reaction solvent (THF).

Considering that cryptand [2.2.2] has a strong affinity for metallic ions, the possibility exists that the central atom within the cryptand is not germanium but instead is an adventitious metallic cation. We used three different analytical techniques to obtain evidence that germanium is present. Combustion elemental analysis of the bulk powder was consistent with the molecular formula of **2**: $GeC_{20}N_2O_{12}F_3S_2$. Second, electrospray ionization mass spectrometry shows the expected mass/charge signals for **2**, with an isotopic distribution that is characteristic of germanium (fig. S1). Finally, energy-dispersive x-ray spectroscopy (EDX) showed signals confirming the presence of germanium (fig. S2).

The electron-rich cryptand cavity substantially contributes to the ability of cryptands to attract and stabilize guest cations. Cryptand [2.2.2] has six oxygen and two nitrogen atoms, all of which have identifiable electron lone pairs oriented into the cavity of the macrocycle. The experimental Ge–N and Ge–O distances in the crystals of **2** are 2.524(3) and 2.4856(16) Å, respectively. These

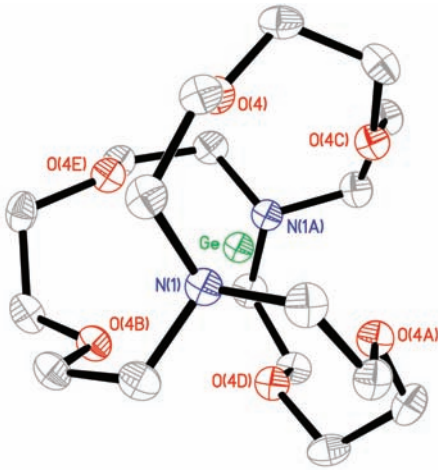

Fig. 1. Thermal ellipsoid plot (30% probability surface) of **2**. Triflate anions and hydrogen atoms have been omitted for clarity. Selected distances between atoms (in Å): Ge–N1 = 2.524(3) and Ge–O4 = 2.4856(16).

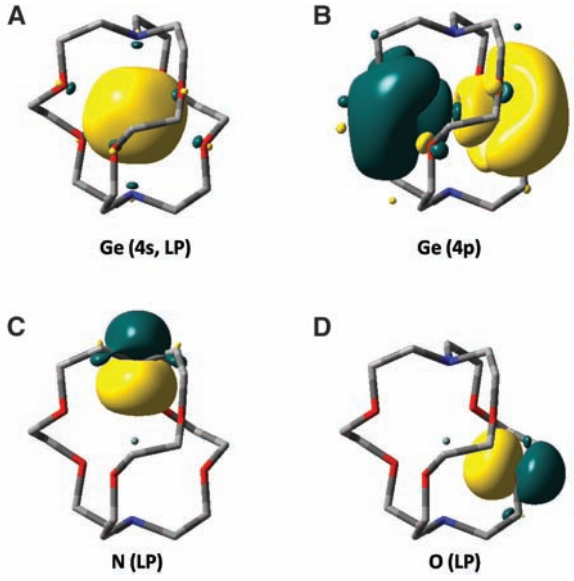

Fig. 2. Selected NBOs of (Ge·cryptand[2.2.2])$^{2+}$ complex computed at the experimental solid-state D_3 geometry using the PBE1PBE functional and the 6-311+G(2d,p) basis set. (**A**) Occupied lone pair on Ge. (**B**) Unoccupied orbital on Ge. (**C**) Lone pair on N. (**D**) Lone pair on O. The isosurface value for all plots is 0.03 bohr$^{-3/2}$. Hydrogen atoms are omitted for clarity. The valence electrons of Ge are not involved in any substantial bonding interactions.

values are considerably greater than the distances of typical Ge–N and Ge–O single bonds, at 1.85 and 1.80 Å, respectively (*22*–*25*). The elongation strongly suggests that the Ge atom does not have substantial bonding interactions with any of the cryptand atoms and that, to a first approximation, compound **2** is a cryptand-protected salt of Ge^{2+} with two triflate anions.

To gain a deeper understanding of the electronic structure of compound **2**, we performed a natural bond orbital (NBO) analysis (*26*) of the (Ge·cryptand[2.2.2])$^{2+}$ complex at the experimental solid-state D_3 geometry using the PBE1PBE density functional (*27*, *28*) and the 6-311+G(2d,p) basis set. The NBO method (*26*) determines the best possible Lewis-type structure for a given molecule by identifying all core orbitals, localized two-electron two-center bonds, one-center nonbonding orbitals (lone pairs), and other conventional covalency effects. The results of our NBO calculations (*29*, *30*) indicate that the Ge atom does not participate in any covalent bonding interactions. The most direct evidence of this is the fact that the valence NBO on the germanium center is a pure 4s nonbonding lone electron pair (Fig. 2). Donor interactions of the valence electrons of germanium with the cryptand moiety were also found to be negligible: The second-order energy lowering (*31*) $\Delta E^{(2)}$ does not exceed 1.5 kJ/mol for any interaction between the occupied lone pair on Ge and the virtual orbitals of the heteroatoms. At the same time, the Ge^{2+} cation must be a strong Lewis acid capable of accepting some electron density from the cryptand heteroatoms. The NBO analysis, in fact, predicts relatively large noncovalent interactions between the N and O lone electron pairs and the virtual orbitals of Ge [with $\Delta E^{(2)}$ values of up to 90 kJ/mol]. We have also considered the possibility that the Ge center is involved in three-centered bonds with the heteroatoms, but no such bonds have been found by the NBO method. Natural population analysis (*32*) of the (Ge·cryptand[2.2.2.])$^{2+}$ complex at the PBE1PBE/6-311+G(2d,p) level reveals a relatively high residual charge of +1.38 on Ge, which suggests that much of the cationic charge remains on the encapsulated Ge atom despite the donor/acceptor interactions with the cryptand. The Wiberg bond indices (*33*, *34*) calculated using the natural atomic orbital basis for the Ge–N and Ge–O interactions were found to be 0.11 and 0.10, respectively. These values are both much smaller than the standard 1.00 bond index predicted for a classical single bond.

On the basis of the position of germanium in the periodic table, an unprotected germanium dication is expected to be highly electrophilic. Undoubtedly, the encapsulating cryptand will moderate the reactivity of the cation. As previously noted, the cryptand effectively prevents interaction with the triflate counterions. Furthermore, because crystals of the salt can be grown from acetonitrile, the cryptand is able to prevent reaction with this weakly Lewis basic solvent. In the related germylium ion, $(Me^tBu_2Si)_3Ge^+$, the bulky silyl substituents are unable to prevent the coordination of acetonitrile to the electrophilic germanium center (*5*). In preliminary experiments, we have demonstrated that the central germanium dication is accessible to anionic nucleophiles. The addition of potassium *tert*-butoxide and 1,3-diisopropyl-4,5-dimethylimidazol-2-ylidene to **2** suspended in THF gave the known NHC-stabilized Ge(O-^{t}Bu)$_2$ (*15*). Further work is required to assess the scope of the reactivity of **2**.

We have synthesized a germanium(II) dication encapsulated within a cryptand. Given the large number of cryptands available to accommodate cations of different size, we anticipate that cationic species of other nonmetallic elements will be isolated in the future. Furthermore, because compound **2** can be easily formed in high yield, it has the potential to be a unique precursor for functionalized germanium compounds.

References and Notes

1. K.-C. Kim *et al.*, *Science* **297**, 825 (2002).
2. P. P. Gaspar, *Science* **297**, 785 (2002).
3. A. Sekiguchi, M. Tsukamoto, M. Ichinohe, *Science* **275**, 60 (1997).
4. P. von Ragué Schleyer, *Science* **275**, 39 (1997).
5. A. Sekiguchi, T. Fukawa, V. Y. Lee, M. Nakamoto, M. Ichinohe, *Angew. Chem. Int. Ed.* **42**, 1143 (2003).
6. I. Krossing, I. Raabe, *Angew. Chem. Int. Ed.* **43**, 2066 (2004).
7. V. Y. Lee, A. Sekiguchi, *Acc. Chem. Res.* **40**, 410 (2007).
8. T. Müller, *Adv. Organomet. Chem.* **53**, 155 (2005).
9. P. Jutzi *et al.*, *Science* **305**, 849 (2004).
10. G. Bertrand, *Science* **305**, 783 (2004).
11. P. Jutzi, N. Burford, *Chem. Rev.* **99**, 969 (1999).
12. C. Douvris, O. V. Ozerov, *Science* **321**, 1188 (2008).
13. P. P. Gaspar, in *Organosilicon Chemistry VI: From Molecules to Materials*, vol. 1, N. Auner, J. Weis, Eds. (Wiley-VCH, Weinheim, Germany, 2005), pp. 10–24.
14. P. A. Rupar, M. C. Jennings, P. J. Ragogna, K. M. Baines, *Organometallics* **26**, 4109 (2007).
15. P. A. Rupar, M. C. Jennings, K. M. Baines, *Organometallics* **27**, 5043 (2008).
16. P. A. Rupar, V. N. Staroverov, P. J. Ragogna, K. M. Baines, *J. Am. Chem. Soc.* **129**, 15138 (2007).
17. B. Dietrich, in *Comprehensive Supramolecular Chemistry*, vol. 1, J. L. Atwood, J.-M. Lehn, Eds. (Pergamon, New York, 1996), pp. 153–211.
18. There are structurally characterized examples of stable Pb salts complexed by cryptand [2.2.2], see (*19*, *20*).
19. A. N. Chekhlov, *J. Struct. Chem.* **47**, 352 (2006).
20. A. N. Chekhlov, *Russ. J. Coord. Chem.* **32**, 552 (2006).
21. Materials and methods are available as supporting material on *Science* Online.
22. K. M. Baines, W. G. Stibbs, *Coord. Chem. Rev.* **145**, 157 (1995).
23. Ge–N bond lengths in N-heterocyclic Ge(II) cationic compounds are ~1.9 Å. For selected examples, see (*24*, *25*).
24. M. Stender, A. D. Phillips, P. P. Power, *Inorg. Chem.* **40**, 5314 (2001).
25. H. V. R. Dias, Z. Wang, *J. Am. Chem. Soc.* **119**, 4650 (1997).
26. F. Weinhold, in *Encyclopedia of Computational Chemistry*, vol. 3, P. von Ragué Schleyer *et al.*, Eds. (Wiley, Chichester, UK, 1998), pp. 1792–1811.
27. M. Ernzerhof, G. E. Scuseria, *J. Chem. Phys.* **110**, 5029 (1999).
28. C. Adamo, V. Barone, *J. Chem. Phys.* **110**, 6158 (1999).
29. All NBO calculations were carried out using the Gaussian 03 program (*30*).
30. Gaussian 03, Revision C.02, M. J. Frisch *et al.* (Gaussian, Wallingford, CT, 2004).
31. A. E. Reed, L. A. Curtiss, F. Weinhold, *Chem. Rev.* **88**, 899 (1988).
32. A. E. Reed, R. B. Weinstock, F. Weinhold, *J. Chem. Phys.* **83**, 735 (1985).
33. K. B. Wiberg, *Tetrahedron* **24**, 1083 (1968).

34. I. Mayer, *Chem. Phys. Lett.* **97**, 270 (1983).
35. Funding was provided by the Natural Sciences and Engineering Research Council of Canada and the University of Western Ontario. Computational resources were provided by the facilities of the Shared Hierarchical Academic Research Computing Network (www.sharcnet.ca). X-ray diffraction data were collected by R. McDonald at the X-Ray Crystallography Laboratory of the Department of Chemistry, University of Alberta. EDX spectra were collected by T. Simpson of the Nanofabrication Laboratory at the University of Western Ontario. We thank Teck Cominco for a donation of $GeCl_4$, D. Hairsine for acquisition of mass spectral data, and M. C. Jennings for helpful discussions. CCDC 704541 contains the supplementary crystallographic data for this paper. These data can be obtained free of charge from The Cambridge Crystallographic Data Centre (www.ccdc.cam.ac.uk/data_request/cif).

Supporting Online Material
www.sciencemag.org/cgi/content/full/322/5906/1360/DC1
SOM Text
Figs. S1 to S3
Tables S1 and S2
References

10 July 2008; accepted 16 October 2008
10.1126/science.1163033

Carbonatite Melts and Electrical Conductivity in the Asthenosphere

Fabrice Gaillard,[1]* Mohammed Malki,[2,3] Giada Iacono-Marziano,[1,4] Michel Pichavant,[1] Bruno Scaillet[1]

Electrically conductive regions in Earth's mantle have been interpreted to reflect the presence of either silicate melt or water dissolved in olivine. On the basis of laboratory measurements, we show that molten carbonates have electrical conductivities that are three orders of magnitude higher than those of molten silicate and five orders of magnitude higher than those of hydrated olivine. High conductivities in the asthenosphere probably indicate the presence of small amounts of carbonate melt in peridotite and can therefore be interpreted in terms of carbon concentration in the upper mantle. We show that the conductivity of the oceanic asthenosphere can be explained by 0.1 volume percent of carbonatite melts on average, which agrees with the carbon dioxide content of mid-ocean ridge basalts.

Laboratory measurements on anhydrous peridotite and olivine single crystals indicate that the electrical conductivity of the upper mantle, if dry, should be ~10^{-4} to 10^{-2} S m^{-1}, with the higher values reflecting high mantle temperatures (*1*, *2*) (Fig. 1). Deep magnetotelluric data, however, indicate that the electrical conductivity of some mantle regions exceeds these values (*3*–*5*). In the Pacific Ocean mantle, for example, conductivities of >10^{-1} S m^{-1} have been measured at depths of >60 km (*4*, *5*). Such zones require the presence of conductive phases; silicate melts or hydrated olivine crystals are commonly considered (*3*, *5*–*8*). Silicate melts have electrical conductivities of 10^{-2} to 10 S m^{-1} (*6*, *7*, *9*, *10*) (Fig. 1) but peridotite melting requires high temperatures or high water content (*11*). The high mantle conductivities have therefore usually been interpreted as indicating trace amounts of hydrogen in olivine (*4*, *5*, *8*, *12*). Direct measurements in mantle xenoliths provide compelling evidence for hydrated mantle olivine (*13*). However, the magnitude of the effect of water on olivine conductivity remains under debate (*14*, *15*) (Fig. 1). Furthermore, it is unclear how hydrated olivine can produce high electrical anisotropy measured in the asthenospheric mantle (*15*). We present here experimental data showing that molten carbonates (i.e., carbonatites) can potentially explain high mantle conductivities.

The carbon dioxide content of mantle-derived magmas is a few hundred parts per million by weight (ppmw) in mid-ocean ridge basalts (MORBs) and can reach a few thousand ppmw in specific settings (*16*, *17*), which constrains the CO_2 content of the mantle source to a few tens to hundreds ppmw (*16*–*18*). Under most of the pressure-temperature-oxygen fugacity conditions prevailing in the upper mantle, carbon is likely to be present in the form of molten carbonates (*19*–*22*). Such carbonatite melts have exceedingly large wetting properties (*23*): They form interconnected liquid networks at olivine grain boundaries even at very low-volume fractions (*23*, *24*) and could therefore contribute to the electrical conductivity of the mantle. The available data on the electrical conductivity of molten carbonates cover Li-rich compositions of industrial interest (*25*). However, mantle carbonatites are particularly Li-poor and Mg, Ca-rich and have variable K and Na (*26*). We measured the electrical conductivity of molten Li-free and Ca-rich carbon-

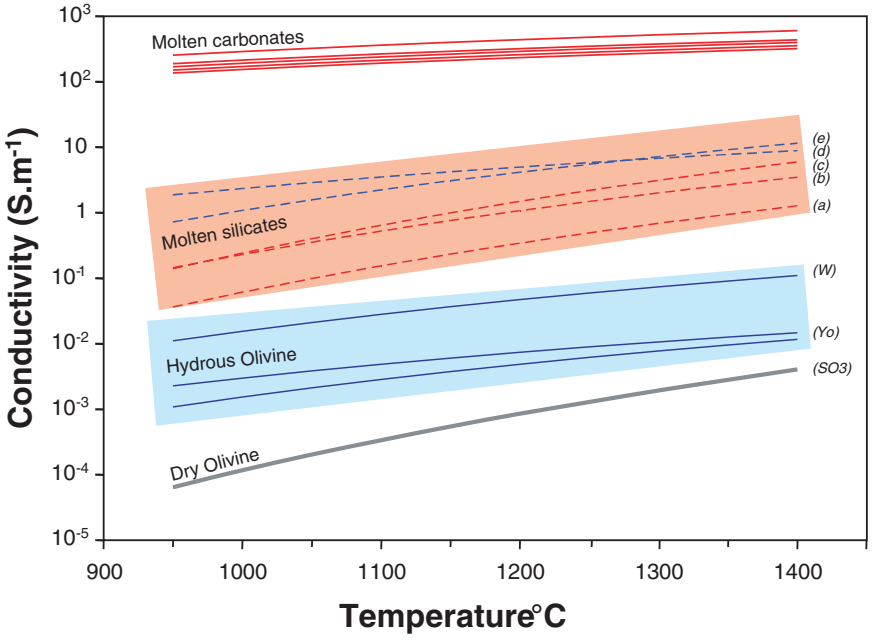

Fig. 1. Electrical conductivity versus temperature for the most important mantle phases (dry and hydrous olivine, molten silicates, and molten carbonates). SO3 refers to anhydrous olivine conductivity (*2*). For hydrous olivine, we show experimental data sets of (*14*, *15*). The two curves labeled Yo, which exhibit the lowest conductivity in the hydrous olivine field, are on oriented single olivine crystals containing 100 to 150 ppmw water (*15*). Each curve corresponds to crystallographic axes yielding the fastest and the slowest conduction. The upper curve labeled W refers to olivine aggregates with 100 ppmw water dissolved in olivine (*14*). For silicate melts, anhydrous results are shown in red and hydrous in blue. From the less to the more conductive, results for (a) a dry MORB at 2 GPa (*7*), (b) a dry MORB at 1 bar (*7*), (c) a dry alkali basalt at 1 bar (*6*, *10*), (d) a hydrous silica-rich melt at 1 bar (*9*), and (e) a hydrous alkali basalt at 1 bar (*10*) are shown. In the upper part of the diagram, the conductivities of molten carbonates are presented, extrapolated from our experiments at 400 to 1000°C using Eq. 1 (see fig. S8). From the less to the more conductive, we show $(KCa_{0.5})_2(CO_3)_2$, $(NaKCa_{0.5})_2(CO_3)_3$, $(NaKCa)(CO_3)_2$, $(NaK)_2(CO_3)_2$, and $(LiNaK)_2(CO_3)_3$.

[1]Centre National de la Recherche Scientifique (CNRS), Institut National des Sciences de l'Univers (INSU), Université d'Orléans, Université François Rabelais–Tours, Institut des Sciences de la Terre d'Orléans, UMR 6113, Campus Géosciences, 1A, Rue de la Férollerie, 41071 Orléans cedex 2, France. [2]Conditions Extrêmes et Matériaux: Haute Température et Irradiation (CEMHTI), CNRS, UPR3079, 1D Avenue de la Recherche Scientifique, 45071 Orléans cedex 2, France. [3]Ecole Polytechnique de l'Université d'Orléans, 8 Rue Léonard de Vinci, 45072 Orléans cedex 2, France. [4]Istituto Nazionale di Geofisica e Vulcanologia, Sezione di Palermo, Via Ugo La Malfa 153, 90146 Palermo, Italy.

*To whom correspondence should be addressed. E-mail: gaillard@cnrs-orleans.fr

ates. Our measurements were performed at 1 atmosphere (atm) of CO_2 pressure using a four-electrode experimental method adapted to greatly conductive molten materials (*27*, *28*). No magnesium carbonate was included in our material because Mg-bearing molten carbonates are not stable at 1 atm pressure. The high conductivities of carbonate melts shown below make it challenging to measure conductivity with conventional setup at high pressure. Pressure effects are probably minor, as discussed below.

Our data show that the electrical conductivity of molten carbonate increases from 50 to 200 S m^{-1} as temperature increases from 400 to 1000°C (Fig. 1, fig. S8, and Table 1). Such conductivity values are comparable to those reported on Li-rich molten carbonates (*25*, *28*). Molten carbonates at 1000°C are 1000 times as conductive as molten silicates (*6*, *7*, *9*, *10*) at the same temperature and at least 100,000 times as conductive as hydrous and dry olivine single crystals (*2*, *14*, *15*). In our measurements, the electrical conductivity of molten carbonates varied slightly with chemical composition. Calcium-free carbonates containing 30 mole % Li_2CO_3 were about two to three times as conductive as a Li-free melt containing 50 mole % $CaCO_3$ (Fig. 1, fig. S8, and Table 1). Another feature of molten carbonate conductivities is their small temperature dependence. The temperature dependence of molten carbonate electrical conductivities (σ) can be adequately fitted using an Arrhenius law

$$\sigma = \sigma_0 \times \exp[-E_a/(RT)] \quad (1)$$

where R is the universal gas constant, 8.314 J K^{-1} mol^{-1}, and T is the temperature in kelvin.

The derived pre-exponential terms (σ_0) and the activation energies (E_a) for each investigated composition are in Table 1. Activation energies are 30 to 35 kJ/mol, which is about one-third of the average E_a for natural molten silicates [70 to 150 kJ/mol (*6*, *7*, *9*, *10*)] and one-tenth of those for dry olivine [200 to 300 kJ/mol (*2*)]. Such low activation energies are similar to those (38 kJ/mol) reported for the viscosity of synthetic molten carbonates of composition $(K_2Ca)(CO_3)_2$ (*29*). Furthermore, we calculated (table S1) that the diffusing process responsible for the electrical conductivity and the viscosity of molten $(K_2Ca)(CO_3)_2$ are similar (~10^{-9} m^2 s^{-1} at 1000°C). This suggests that, unlike silicate melts (*9*, *10*), both viscosity and electrical conductivity of carbonate melts entail similar transport mechanisms. Extrapolation to mantle conditions requires an evaluation of the effect of $MgCO_3$ on the conductivity of molten carbonates, because mantle carbonatites should contain 5 to 15 weight % MgO at equilibrium with mantle minerals (*26*), and of the effect of pressure. In view of the similarities between conductivity and viscosity, both effects can be deduced from the effect of $MgCO_3$ and pressure on the viscosity of molten carbonates. Magnesium-bearing molten carbonates are slightly less viscous than those that are Mg free (*29*). We therefore expect that the conductivities of Mg-bearing carbonatites are slightly higher than those of Mg-free molten carbonates. Experimental data (*29*) and molecular dynamics calculations (*30*) indicate that pressure has little effect on the viscosity of molten carbonates up to mantle pressures. We thus conclude that mantle carbonatites should preserve the high conductivity we determined at 1 bar (*28*). The electrical conductivity of mantle carbonatites can therefore reasonably be described by the Arrhenius equation given in Table 1.

Molten carbonates are therefore by far the most conductive phase of Earth's upper mantle. High electrical conductivity globally observed in the asthenosphere (*3*) could therefore reveal small amounts of carbonatite melts hosted in the mantle. As an example of application of these data, we focus on the asthenosphere below the Pacific Oceanic ridge. This region of the mantle has been relatively well studied by geophysical imaging (*4*, *5*), and petrological evidence suggests that small quantities of carbonatite liquids are formed in such asthenospheric mantle at depths of up to ~300 km (*19*, *20*). The geophysical surveys imaged a resistive body ($\sigma \sim 10^{-2}$ to 10^{-3} S m^{-1}) consistent with anhydrous peridotite in the upper 60 km of the mantle (*4*, *5*), which corresponds to the oceanic lithosphere. A conductive structure ($\sigma \sim 1$ to 10^{-1} S m^{-1}) extends down to 200 km below the ridge axis (*5*). A structure of nearly comparable conductivity ($\sigma \sim 10^{-1}$ to 10^{-2} S m^{-1}) extends

Table 1. Summary of experimentally defined parameter values for electrical conductivity of molten carbonates (Eq. 1).

Compositions	σ° S m^{-1} (±800)	E_a J mol^{-1} (±350)	σ at 1000°C S m^{-1} (±15)
$(LiNaK)_2(CO_3)_3$	6590	32,500	305
$(NaK)_2(CO_3)_2$	4177	31,427	214
$(NaKCa_{0.5})_2(CO_3)_3$	4144	32,500	192
$(NaKCa)(CO_3)_2$	2504	30,307	143
$(KCa_{0.5})_2(CO_3)_2$	3149	34,489	121
Mantle carbonatites	3440	31,900	169

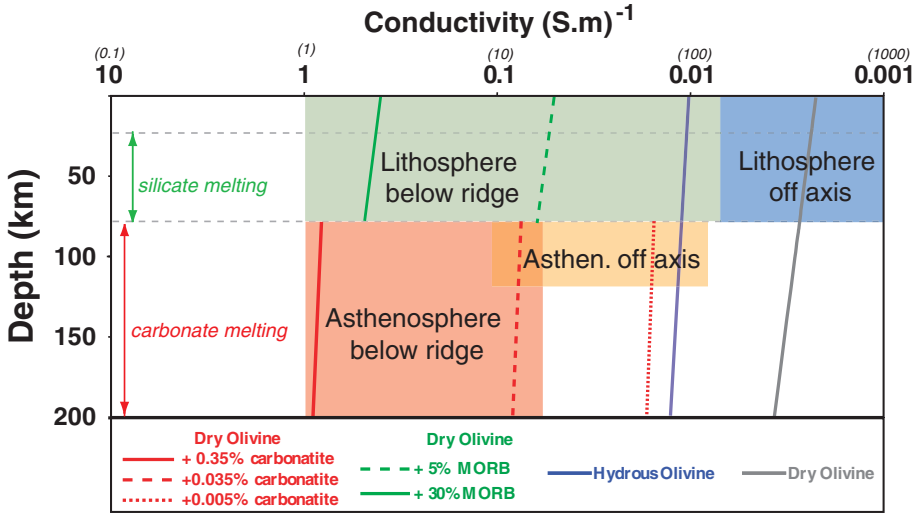

Fig. 2. Electrical conductivity (and resistivity in brackets) versus depth calculated assuming adiabatic temperature changes (*19*) (i.e., $T_{300\ km}$ ~ 1420°C) for dry olivine (gray line), hydrous olivine (blue line), dry olivine with 5 and 30 volume % of basalt (green lines), and dry olivine with 0.005, 0.035, and 0.35 volume % of carbonatite melt (red lines). For the calculation of electrical conductivity of mixtures, we assume a Hashin-Shtrikman upper bound that implies an interconnected melt between olivine grains (*6*). Dry olivine conductivity is calculated from (*2*), and the hydrous olivine is calculated after (*15*) for crystals containing ~150 ppmw water (average between fast and slow crystallographic orientation). The olivine + 5 volume % basalt is calculated by taking the conductivity of dry basalt at 1 bar (*7*); increasing pressure would decrease the conductivity of such a mixture, but the magnitude of the pressure effect differs between different laboratory studies (*7*, *9*, *10*). The olivine-carbonatite mixtures are calculated after the conductivity of mantle carbonatite given in Table 1. The asthenosphere conductivity below the Pacific ridge (*5*) (red box) is best explained by olivine with 0.035 to 0.35 volume % of carbonatite melts. The top of the asthenosphere extending 350 km east of the ridge (*4*, *5*) (orange box) is best explained by the presence of 0.005 to 0.035 volume % of carbonatite. The resistive lithosphere (*4*, *5*) (blue box) matches the conductivity of dry olivine, whereas the lithosphere below the ridge axis is characterized by a broad range of conductivities, with the highest range probably reflecting the contributions of the rising MORB. The expected depth of carbonate melting (*19*, *20*) and the one of silicate melting (*11*, *19*) are shown by the arrows on the left of the figure.

in the direction perpendicular to the ridge axis on the east side of the ridge at depths between 70 and 120 km (*4*, *5*). Such structure was not observed on the west side of the axis (*4*, *5*). Both conductive structures show strong anisotropy that cannot be accounted for by hydrated olivine crystals (*15*). An additional conductive component is therefore needed, and the presence of silicate melt has been suggested (*15*).

Figure 2 shows in a conductivity-depth plot the different electrical structures of the Pacific Ocean mantle described above. We also show electrical conductivities calculated for different model mantles consisting of dry and hydrous olivine, dry olivine with 5 to 30 volume % of MORB and dry olivine with variable amounts of carbonatite melt. All calculated conductivities vary with depth following an adiabatic path (*19*, *20*). The deep conductive asthenosphere (70 to 200 km) under the ridge axis can be explained considering olivine mixed with between 0.035 and 0.35 volume % of carbonatite. Olivine with more than 5 volume % of basalt could alternatively account for the high conductivity of this region, but an elevated degree of peridotite melting is precluded at such depth (*11*, *19*). Hydrous olivine is unable to account for such a high conductivity domain (*14*, *15*). The presence of a small amount of carbonatite is therefore the best explanation for the high conductivity of this region. Furthermore, the range 0.035 to 0.35 volume % of carbonatite corresponds (*31*) on average to ~300 ppmw of CO_2 stored in the asthenosphere, in reasonable agreement with the variable estimates of CO_2 concentrations in the source region of MORBs (*16*–*18*, *32*). The off-axis conductive asthenosphere (depths of 70 to 120 km in Fig.2) can not be explained by olivine with a few percent of basalt, because it extends at depths inconsistent with silicate melting (*11*). Hydrous olivine may account for its lowermost conductivity but not for the upper range of values. From our results, the off-axis asthenosphere can be interpreted as olivine with ~0.005 to 0.035 volume % of carbonatite melts.

It has been shown that the off-axis conductive zone joins the deep asthenosphere under the ridge (*5*). Carbonatite melts under the ridge derive from the decompression melting initiating at depths of 300 km (*20*), whereas their presence extending 350 km eastward of the ridge at depths of 70 to 120 km might result from their lateral migration. Based on conductivities shown in Fig. 2, we suggest that about one-tenth of the carbonatite melt produced in the asthenosphere under the ridge may flow laterally in the mantle. The rest would migrate upward and be incorporated in the silicate melts deriving from peridotite melting at depths ~70 to 80 km below the ridge. The CO_2 contents in MORBs and their heterogeneity (*16*–*18*) would therefore originate from the incorporation of small amount of carbonatite melts by basaltic melts.

References and Notes

1. Y. Xu, T. J. Shankland, B. T. Poe, *J. Geophys. Res.* **105**, 27865 (2000).
2. S. Constable, *Geophys. J. Int.* **166**, 435 (2006).
3. A. G. Jones, *Lithos* **48**, 57 (1999).
4. R. L. Evans *et al.*, *Nature* **437**, 249 (2005).
5. K. Baba *et al.*, *J. Geophys. Res.* **111**, B02101 (2006).
6. F. Gaillard, G. I. Marziano, *J. Geophys. Res.* **110**, B06204 (2005).
7. J. A. Tyburczy, H. S. Waff, *J. Geophys. Res.* **88**, 2413 (1983).
8. S.-I. Karato, in *Water in Nominally Anhydrous Minerals, Book Series: Reviews in Mineralogy and Geochemistry*, H. Keppler, J. R. Smyth, Eds. (Mineralogical Society of America, Chantilly, VA, 2006), vol. 62, chap.15.
9. F. Gaillard, *Earth Planet. Sci. Lett.* **218**, 215 (2004).
10. A. Pommier, F. Gaillard, M. Pichavant, B. Scaillet, *J. Geophys. Res.* **113**, B05205 (2008).
11. C. Aubaud, E. H. Hauri, M. M. Hirschmann, *Geophys. Res. Lett.* **31**, L20611 (2004).
12. P. Tarits, S. Hautot, F. Perrier, *Geophys. Res. Lett.* **31**, L06612 (2004).
13. S. Demouchy, S. D. Jacobsen, F. Gaillard, C. R. Stern, *Geology* **34**, 429 (2006).
14. D. J. Wang, M. Mookherjee, Y. S. Xu, S.-I. Karato, *Nature* **443**, 977 (2006).
15. T. Yoshino, T. Matsuzaki, S. Yamashita, T. Katsura, *Nature* **443**, 973 (2006).
16. A. E. Saal, E. H. Hauri, C. H. Langmuir, M. R. Perfit, *Nature* **419**, 451 (2002).
17. P. Cartigny, F. Pineau, C. Aubaud, M. Javoy, *Earth Planet. Sci. Lett.* **265**, 672 (2008).
18. B. Marty, I. N. Tolstikhin, *Chem. Geol.* **145**, 233 (1998).
19. R. Dasgupta, M. M. Hirschmann, N. D. Smith, *Geology* **35**, 135 (2007).
20. R. Dasgupta, M. M. Hirschmann, *Nature* **440**, 659 (2006).
21. D. J. Frost, C. A. McCammon, *Annu. Rev. Earth Planet. Sci.* **36**, 389 (2008).
22. S. S. Shcheka, M. Wiedenbeck, D. J. Frost, H. Keppler, *Earth Planet. Sci. Lett.* **245**, 730 (2006).
23. W. G. Minarik, E. B. Watson, *Earth Planet. Sci. Lett.* **133**, 423 (1995).
24. T. Hammouda, D. Laporte, *Geology* **28**, 283 (2000).
25. T. Kojima, Y. Miyazaki, K. Nomura, K. Tanimoto, *J. Electrochem. Soc.* **155**, F150 (2008).
26. R. J. Sweeney, *Earth Planet. Sci. Lett.* **128**, 259 (1994).
27. C. Simonnet, J. Phalippou, M. Malki, A. Grandjean, *Rev. Sci. Instrum.* **74**, 2805 (2003).
28. Materials and methods are available as supporting material on *Science* Online.
29. D. P. Dobson *et al.*, *Earth Planet. Sci. Lett.* **143**, 207 (1996).
30. M. J. Genge, G. D. Price, A. P. Jones, *Earth Planet. Sci. Lett.* **131**, 225 (1995).
31. Q. Liu, R. A. Lange, *Contrib. Mineral. Petrol.* **146**, 370 (2003).
32. A mantle peridotite with 0.35 volume % of carbonatite melts yields a conductivity of 1 S m^{-1}, which matches the highest value detected by geophysicists at a depth of 150 km (*5*). Such value, however, designates the conductivity in the direction parallel to the ridge axis, whereas the conductivity in the perpendicular direction is lower by a factor of 10 (*5*). We do not incorporate such anisotropic effects in our interpretation, which implies that on average 0.1 volume % of carbonatite melts (300 ± 200 ppmw CO_2) would be needed to explain such mantle conductivities.

33. We thank an INSU grant and the Electrovolc project, which is funded by the French national agency for research (ANR): contract JC05-42707 allocated to F.G. We also thank two anonymous reviewers.

Supporting Online Material

www.sciencemag.org/cgi/content/full/322/5906/1363/DC1
Materials and Methods
Figs. S1 to S8
Table S1
References

8 August 2008; accepted 17 October 2008
10.1126/science.1164446

Tight Regulation of Unstructured Proteins: From Transcript Synthesis to Protein Degradation

Jörg Gsponer,[1]* Matthias E. Futschik,[1,2,3] Sarah A. Teichmann,[1] M. Madan Babu[1]*

Altered abundance of several intrinsically unstructured proteins (IUPs) has been associated with perturbed cellular signaling that may lead to pathological conditions such as cancer. Therefore, it is important to understand how cells precisely regulate the availability of IUPs. We observed that regulation of transcript clearance, proteolytic degradation, and translational rate contribute to controlling the abundance of IUPs, some of which are present in low amounts and for short periods of time. Abundant phosphorylation and low stochasticity in transcription and translation indicate that the availability of IUPs can be finely tuned. Fidelity in signaling may require that most IUPs be available in appropriate amounts and not present longer than needed.

Up to one third of all eukaryotic proteins have large segments that are unstructured and are commonly referred to as intrinsically IUPs. These proteins lack a unique structure, either entirely or in parts, when alone in solution (*1*). The lack of structure is thought to provide several advantages, such as (i) an increased interaction surface area, (ii) conformational flexibility to interact with several targets, (iii) the presence of molecular recognition elements that fold upon binding, (iv) accessible posttranslational modification sites, and (v) the availability of short linear interaction motifs (*2*–*5*). These and other properties are ideal for proteins that mediate signaling and coordinate regulatory events, and indeed proteins that participate in regulatory and signaling functions are enriched in unstructured segments (*6*–*8*) [supporting online material (SOM) text S1]. Because of their unusual structural and important functional properties, the presence of IUPs in a cell may need to be carefully monitored. In fact, altered abundance of IUPs is associated with several disease conditions. For instance, overexpression of thyroid cancer 1 (TC-1) (*9*) or underexpression of adenosine

[1]Medical Research Council (MRC) Laboratory of Molecular Biology, Hills Road, Cambridge CB2 0QH, UK. [2]Institute for Theoretical Biology, Charité, Humboldt-University, Berlin 10115, Germany. [3]Institute for Biotechnology and Bioengineering Centre for Molecular and Structural Biomedicine, University of Algarve, Faro 8005-139, Portugal.

*To whom correspondence should be addressed. E-mail: madanm@mrc-lmb.cam.ac.uk (M.M.B.); jgsponer@mrc-lmb.cam.ac.uk (J.G.)

5′-diphosphate (ADP) ribosylation factor (Arf) (*10*) and p27 (*11*) has been linked with various types of cancer. Similarly, overexpression of α-synuclein and tau proteins increases the risk of aggregate formation and has been linked to Parkinson's disease and Alzheimer's disease (*12*, *13*). We therefore tested whether specific control mechanisms affect the availability of IUPs (that is, their abundance and residence time) within a cell.

Using the Disopred2 software (*6*), which reports unstructured residues based on the protein sequence, we computed the fraction of the polypeptide that is predicted to be unstructured for every protein in *Saccharomyces cerevisiae* (*14*). This allowed us to categorize 1971 sequences as highly structured ("S"; 0 to 10% of the total length is unstructured), 2711 sequences as moderately unstructured ("M"; 10 to 30% of the protein is unstructured), and 2020 sequences as highly unstructured ("U"; 30 to 100% of the protein is unstructured) (Fig. 1). This information was integrated with different genome-scale datasets that describe most of the regulatory steps that influence protein synthesis or degradation (table S1 and fig. S1), and we compared the distributions of the values for the proteins in the U and S groups with statistical tests (*14*).

We compared the transcription of genes encoding highly unstructured proteins with that of genes encoding more structured proteins. Because the steady-state amount of mRNA could be affected by the rate at which the transcripts are produced or degraded, we investigated whether the transcriptional rate or the degradation rate were different for the transcripts that encode highly structured and unstructured proteins. The number of transcription factors (TFs) that regulate a gene was comparable between the two groups ($P = 0.55$, Wilcoxon test) (Fig. 2A). However, mRNAs encoding highly unstructured proteins were generally less abundant than transcripts encoding more structured proteins ($P = 1 \times 10^{-6}$, Wilcoxon test) (Fig. 2B). The mRNA half-lives of the transcripts that encode highly unstructured proteins were lower than transcripts that encode more structured proteins ($P < 10^{-16}$, Wilcoxon test) (Fig. 2C) and a comparison of the distribution of transcriptional rates showed that the difference between the two groups was less significant ($P = 1 \times 10^{-8}$, Wilcoxon test) (table S3). Thus, differences in decay rates appear to be a major factor leading to differences in mRNA abundance (SOM text S5).

We analyzed polyadenylate [poly(A)] tail length because the two major pathways of mRNA decay are initiated by removal of the poly(A) tail. A significantly larger fraction of the unstructured proteins had a short poly(A) tail (table S1) than did structured proteins ($P < 10^{-16}$, Fisher's exact test) (Fig. 2D). Analysis of transcript binding by Puf family RNA-binding proteins, which affect transcript stability, showed that Puf5p binding was enriched for transcripts that encode highly unstructured proteins. In fact, 108 of the 224 transcripts bound by Puf5p encode highly unstructured proteins, a much greater number than expected by chance, which was 68 transcripts (z score = 5.3; $P = 5 \times 10^{-10}$) (*14*). Thus, poly(A) tail length and interaction with specific RNA-binding proteins may modulate the stability of transcripts encoding IUPs (SOM text S5).

Unstructured proteins tend to be less abundant than structured proteins ($P < 10^{-16}$; Wilcoxon test) (Fig. 2F, fig. S2, and SOM text S2 and S5). The rate of protein synthesis was significantly lower ($P < 10^{-16}$, Wilcoxon test) (Fig. 2E) and protein half-life was shorter ($P = 1 \times 10^{-15}$, Wilcoxon test) (Fig. 2G and SOM text S5) for highly unstructured than for more structured proteins. Two pathways that mediate ubquitin proteasome–dependent degradation are the N-end–rule pathway and PEST–mediated degradation pathway. Although the distribution of N-end residues was not significantly different (SOM text S3 and figs. S3 and S4), a significantly greater fraction of the unstructured proteins contained PEST motifs (regions rich in proline, glutamic acid, serine, and threonine) ($P < 10^{-16}$, Fisher's exact test) (Fig. 2H and SOM text S5) as previously observed (*1*, *15*). Therefore, it appears that the availability of many IUPs is regulated via proteolytic degradation and a reduced translational rate.

For certain IUPs (for example, p27), post-translational modifications such as phosphorylation (*11*, *16*) can affect their abundance or half-life in a cell. In fact, recent computational studies using phosphorylation site–prediction methods have suggested that unstructured regions are enriched for sites that can be posttranslationally modified (*17*). We analyzed the experimentally determined yeast kinase-substrate network and found that highly unstructured proteins are on average substrates of twice as many kinases as are structured proteins ($P = 1 \times 10^{-12}$, Wilcoxon test) (SOM text S4 and fig. S5). On average, 51 ± 19% (SD) of all substrates of the kinases are highly unstructured, whereas only 19 ± 13% (SD) are highly structured [the remaining 30 ± 14% (SD) of all substrates are moderately unstructured]. This is a significant bias as compared with the expected genomewide distribution of ~30% highly unstructured and ~30% structured proteins based on our categorization ($P < 10^{-16}$, Fisher's exact test) (*14*). We found that 85% of the kinases for which more than 50% of their substrates are highly unstructured (table S2) are either regulated in a cell cycle–dependent manner (for example, Cdc28) or activated upon exposure to particular stimuli (for example, Fus3) or stress (for example, Atg1). This suggests that posttranslational modification of IUPs through phosphorylation may be an important mechanism in fine-tuning their function and possibly their availability under different conditions.

We investigated whether genes that encode highly unstructured proteins display low stochasticity in their expression levels among individuals in a population of genetically homogeneous cells. An important source of such stochasticity in cellular systems is random noise in transcription and translation, which results in very different amounts of transcripts and protein products. We used the presence of a TATA box in the promoter region to infer genes that might be more subjected to noise in gene expression (*18*) and found that genes encoding highly unstructured proteins are less likely to have a TATA box than those that encode structured proteins ($P = 8 \times 10^{-7}$, Fisher's exact test) (Fig. 2I). At the protein level, analysis of direct experimental data revealed that unstructured proteins have lower noise levels than do structured proteins ($P = 3 \times 10^{-11}$, Wilcoxon test) (Fig. 2J). These results indicate that highly unstructured proteins may display less noise in transcription and translation than more structured proteins.

To assess regulation of IUPs in other organisms, we analyzed datasets (table S1) for *Schizosaccharomyces pombe* and *Homo sapiens*. Similar trends to those observed for *S. cerevisiae* were evident in these organisms (Fig. 3 and tables S3

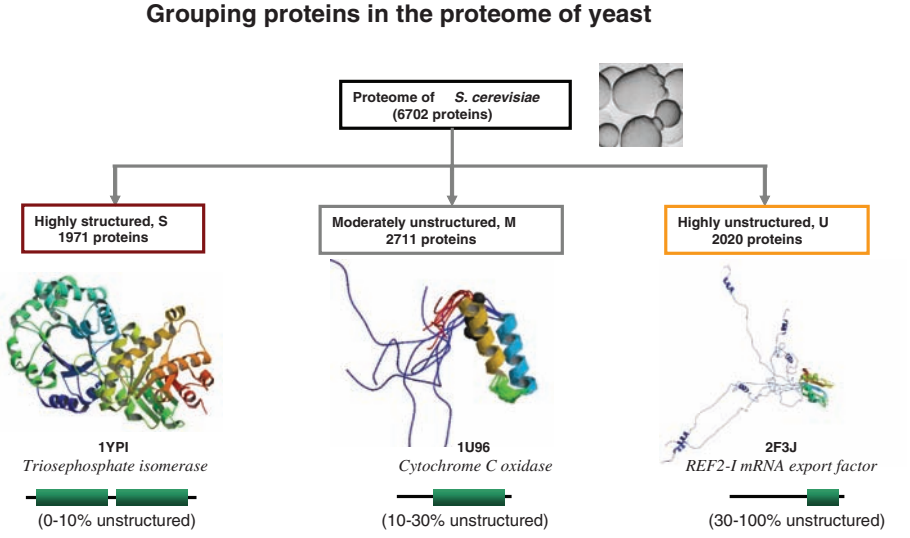

Fig. 1. The *S. cerevisiae* proteome was grouped into three categories, highly structured (S), moderately unstructured (M), and highly unstructured (U), based on the fraction of unstructured residues over the entire protein length.

and S4). Thus, both unicellular and multicellular organisms appear to regulate the availability of IUPs. The observed differences between structured and unstructured proteins were independent of the IUP prediction method used, protein length, localization within the major subcellular compartments, different grouping of proteins, or the number of interaction partners per protein (tables S6 to S11). Though the distributions of the values for the proteins in the structured and unstructured groups are broad and overlap, the differences reported here are consistently statistically significant with two independent statistical tests, the Wilcoxon rank-sum test and the Kolmogorov-Smirnov test (tables S3 to S5) (*14*). Thus, the reported trends appear to be attributable to the intrinsically unstructured nature of the proteins. Of all the IUPs, those that contain polyglutamine [poly(Q)] or polyasparagine [poly(N)] stretches seem to be more tightly controlled (table S3 and S4).

Proteins with unstructured regions predominantly have signaling or regulatory roles and are often reused in multiple pathways to produce different physiological outcomes (*2*, *6*–*8*). Accordingly, increased abundance of IUPs can result in undesirable interactions (for example, titration of unrelated proteins by inappropriate interaction through exposed peptide motifs), thereby disturbing the fine balance of the signaling networks leading to dampened or inappropriate activities (*19*). Spatial and temporal segregation of signaling proteins as well as an increased signaling complexity may contribute to fidelity in regulation (SOM text S5 and fig. S6). In addition, tight regulation of signaling and regulatory IUPs could minimize the potentially harmful effects of ectopic interactions and may provide robustness to signaling processes by ensuring that such proteins are present in appropriate amounts and time periods. Indeed, free IκB [an IUP that interacts with and inhibits the nuclear factor κB (NF-κB) transcription factor] must be continuously degraded to allow for rapid and robust NF-κB activation and to make the pathway sensitive for a signaling input (*20*, *21*). In contrast, stabilization of free IκB by removal of the PEST motif reduces NF-κB activation (*20*, *21*). In mammalian cells exposed to mild endoplasmic reticulum stress, survival is favored as a direct consequence of the intrinsic instability of mRNAs and of proteins that drive apoptosis (such as Chop, an IUP) as compared with that of proteins that promote adaptation and cell longevity (for example, the chaperone protein BiP, a structured protein) (*22*).

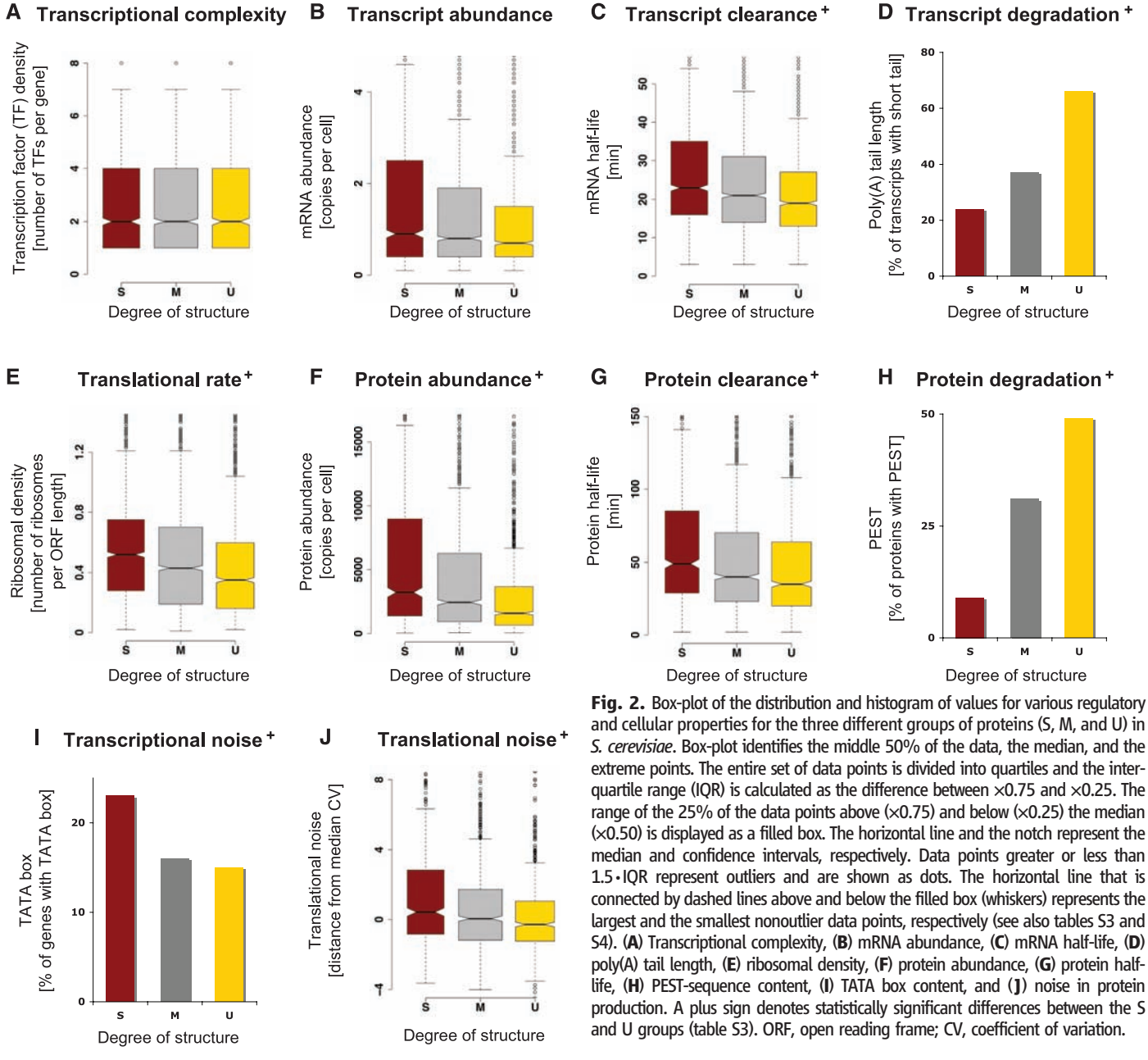

Fig. 2. Box-plot of the distribution and histogram of values for various regulatory and cellular properties for the three different groups of proteins (S, M, and U) in *S. cerevisiae*. Box-plot identifies the middle 50% of the data, the median, and the extreme points. The entire set of data points is divided into quartiles and the interquartile range (IQR) is calculated as the difference between ×0.75 and ×0.25. The range of the 25% of the data points above (×0.75) and below (×0.25) the median (×0.50) is displayed as a filled box. The horizontal line and the notch represent the median and confidence intervals, respectively. Data points greater or less than 1.5 • IQR represent outliers and are shown as dots. The horizontal line that is connected by dashed lines above and below the filled box (whiskers) represents the largest and the smallest nonoutlier data points, respectively (see also tables S3 and S4). (**A**) Transcriptional complexity, (**B**) mRNA abundance, (**C**) mRNA half-life, (**D**) poly(A) tail length, (**E**) ribosomal density, (**F**) protein abundance, (**G**) protein half-life, (**H**) PEST-sequence content, (**I**) TATA box content, and (**J**) noise in protein production. A plus sign denotes statistically significant differences between the S and U groups (table S3). ORF, open reading frame; CV, coefficient of variation.

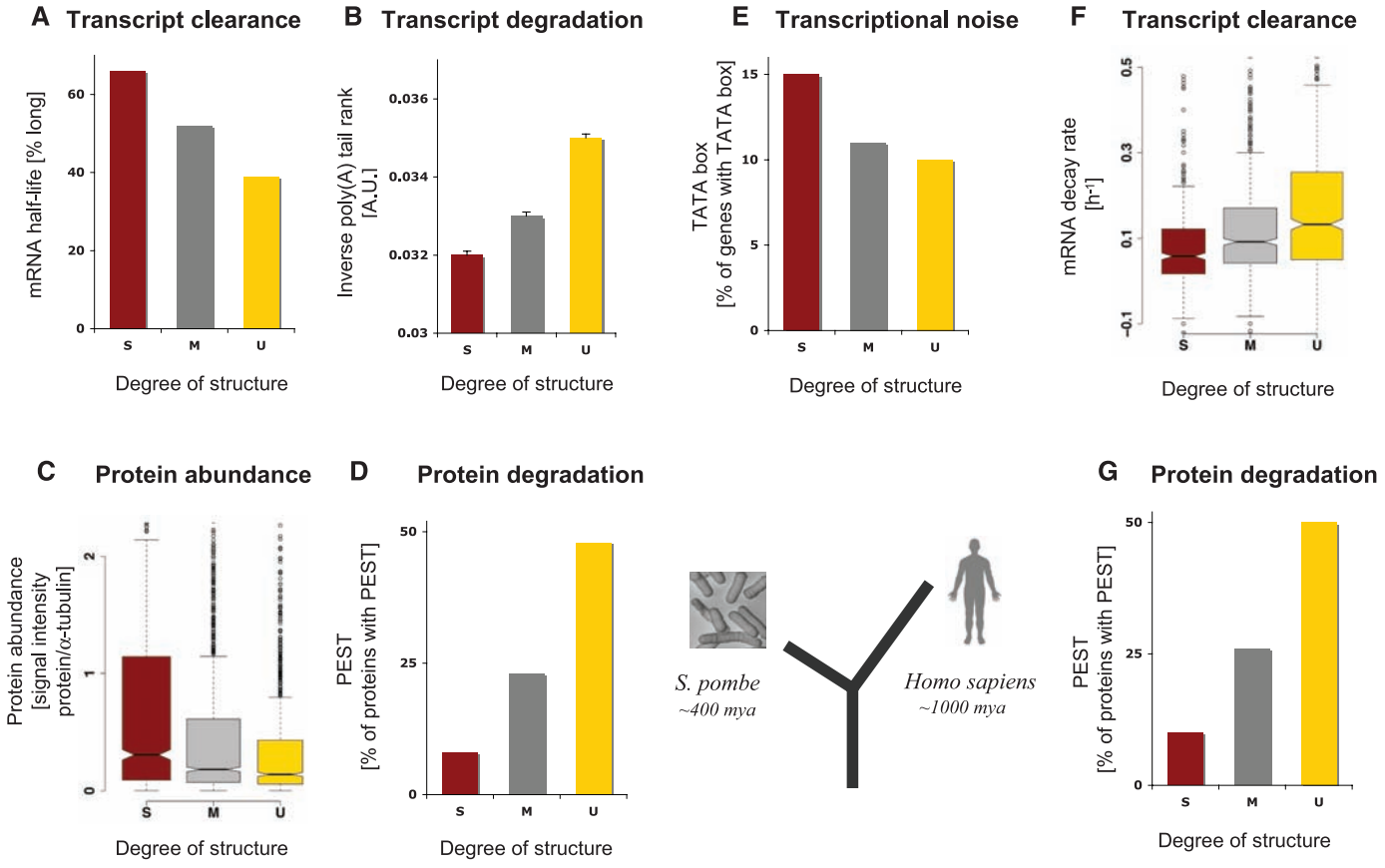

Fig. 3. Box-plot of the distribution and histogram of values for various regulatory and cellular parameters for the three groups of proteins (S, M, and U) in *S. pombe* (**A** to **D**) and humans (**E** to **G**). All reported differences are statistically significant (table S4). A.U., arbitrary units; mya, million years ago.

Although the abundance of many IUPs is strictly controlled, certain IUPs are present in cells in large amounts or for long periods of time. In fact, in some cases (for example, the fibrous muscle protein titin), large amounts may be required throughout the lifetime of a cell. Fine-tuning of IUP availability can be achieved with posttranslational modifications and interactions with other factors (*1*, *3*, *11*, *16*). Both mechanisms can promote increased abundance or longer half-life through changes in cellular localization or by protection from the degradation machinery (for example, certain phosphorylated forms of the cyclin-dependent kinase inhibitory protein $p27^{kip1}$ and the spinocerebellar ataxia type 1 protein ataxin-1) (*23*, *24*). Although association with other proteins may increase their stability, free IUPs are likely to be rapidly degraded by the 20*S* proteasome via degradation by default (*25*), as shown for the unbound forms of $p21^{cip1}$ (*26*), $p27^{kip1}$ (*27*), α-synuclein (*28*), and tau (*29*). Certain posttranslational modifications may promote regulated degradation (for example, that of $p27^{Kip1}$) (*11*, *16*). In this context, our finding that many IUPs tend to be phosphorylated by multiple kinases and display low noise in transcription and translation suggests that their abundance and half-lives may be finely tuned in cells (SOM text S5).

Our studies reveal an evolutionarily conserved tight control of synthesis and clearance of most IUPs. The discovery was made possible by integrating multiple large-scale datasets that describe control mechanisms during transcription, translation, and post-translational modification with structural information on proteins. Besides the elucidation of general trends, the framework describing multiple levels of regulation introduced here may facilitate investigation of how individual IUPs are fine-tuned in different cell types and how perturbations to this tight control might influence disease conditions (*30*).

References and Notes

1. A. K. Dunker *et al.*, *J. Mol. Graph. Model.* **19**, 26 (2001).
2. P. E. Wright, H. J. Dyson, *J. Mol. Biol.* **293**, 321 (1999).
3. R. W. Kriwacki, L. Hengst, L. Tennant, S. I. Reed, P. E. Wright, *Proc. Natl. Acad. Sci. U.S.A.* **93**, 11504 (1996).
4. P. Tompa, *FEBS Lett.* **579**, 3346 (2005).
5. C. J. Oldfield *et al.*, *Biochemistry* **44**, 12454 (2005).
6. J. J. Ward, J. S. Sodhi, L. J. McGuffin, B. F. Buxton, D. T. Jones, *J. Mol. Biol.* **337**, 635 (2004).
7. J. Liu *et al.*, *Biochemistry* **45**, 6873 (2006).
8. L. M. Iakoucheva, C. J. Brown, J. D. Lawson, Z. Obradovic, A. K. Dunker, *J. Mol. Biol.* **323**, 573 (2002).
9. M. Sunde *et al.*, *Cancer Res.* **64**, 2766 (2004).
10. C. J. Sherr, *Nat. Rev. Cancer* **6**, 663 (2006).
11. M. Grimmler *et al.*, *Cell* **128**, 269 (2007).
12. F. Chiti, C. M. Dobson, *Annu. Rev. Biochem.* **75**, 333 (2006).
13. M. Goedert, *Nat. Rev. Neurosci.* **2**, 492 (2001).
14. Materials and methods are available as supporting material on *Science* Online.
15. P. Tompa, J. Prilusky, I. Silman, J. L. Sussman, *Proteins* **71**, 903 (2007).
16. I. Chu *et al.*, *Cell* **128**, 281 (2007).
17. L. M. Iakoucheva *et al.*, *Nucleic Acids Res.* **32**, 1037 (2004).
18. J. M. Raser, E. K. O'Shea, *Science* **304**, 1811 (2004).
19. T. Pawson, N. Warner, *Oncogene* **26**, 1268 (2007).
20. E. Mathes, E. L. O'Dea, A. Hoffmann, G. Ghosh, *EMBO J.* **27**, 1421 (2008).
21. E. L. O'Dea *et al.*, *Mol. Syst. Biol.* **3**, 111 (2007).
22. D. T. Rutkowski *et al.*, *PLoS Biol.* **4**, e374 (2006).
23. H. K. Chen *et al.*, *Cell* **113**, 457 (2003).
24. I. M. Chu, L. Hengst, J. M. Slingerland, *Nat. Rev. Cancer* **8**, 253 (2008).
25. G. Asher, N. Reuven, Y. Shaul, *Bioessays* **28**, 844 (2006).
26. X. Li *et al.*, *Mol. Cell* **26**, 831 (2007).
27. W. S. Tambyrajah, L. D. Bowler, C. Medina-Palazon, A. J. Sinclair, *Arch. Biochem. Biophys.* **466**, 186 (2007).
28. G. K. Tofaris, R. Layfield, M. G. Spillantini, *FEBS Lett.* **509**, 22 (2001).
29. D. C. David *et al.*, *J. Neurochem.* **83**, 176 (2002).
30. W. E. Balch, R. I. Morimoto, A. Dillin, J. W. Kelly, *Science* **319**, 916 (2008).

31. The authors acknowledge MRC for funding and thank the two anonymous referees, the editor, A. Bertolotti, A. Tzakos, A. Wuster, C. Brockmann, C. Chothia, D. Finley, D. Rubinsztein, E. Levy, H. McMahon, I. Schafer, J. Bui, K. Weber, M. Goedert, R. Janky, S. Michnick, and S. Sarkar for providing helpful comments. We apologize for, because of lack of space, not citing the work that describes the datasets and other references. Many can be found in the SOM. M.M.B. acknowledges Darwin College and Schlumberger Ltd, and M.M.B. and M.E.F. acknowledge the Royal Society for support. J.G. is funded by an MRC Special Training Fellowship in computational biology.

Supporting Online Material

www.sciencemag.org/cgi/content/full/322/5906/1365/DC1
Materials and Methods
SOM Text S1 to S5
Figs. S1 to S6
Tables S1 to S12
References

22 July 2008; accepted 9 October 2008
10.1126/science.1163581

Structural Evidence for Common Ancestry of the Nuclear Pore Complex and Vesicle Coats

Stephen G. Brohawn,[1]* Nina C. Leksa,[1]* Eric D. Spear,[1]
Kanagalaghatta R. Rajashankar,[2] Thomas U. Schwartz[1]†

Nuclear pore complexes (NPCs) facilitate nucleocytoplasmic transport. These massive assemblies comprise an eightfold symmetric scaffold of architectural proteins and central-channel phenylalanine-glycine-repeat proteins forming the transport barrier. We determined the nucleoporin 85 (Nup85)•Seh1 structure, a module in the heptameric Nup84 complex, at 3.5 angstroms resolution. Structural, biochemical, and genetic analyses position the Nup84 complex in two peripheral NPC rings. We establish a conserved tripartite element, the ancestral coatomer element ACE1, that reoccurs in several nucleoporins and vesicle coat proteins, providing structural evidence of coevolution from a common ancestor. We identified interactions that define the organization of the Nup84 complex on the basis of comparison with vesicle coats and confirmed the sites by mutagenesis. We propose that the NPC scaffold, like vesicle coats, is composed of polygons with vertices and edges forming a membrane-proximal lattice that provides docking sites for additional nucleoporins.

Exchange of macromolecules across the nuclear envelope is exclusively mediated by NPCs (*1*–*3*). Whereas much progress has been made understanding the soluble factors mediating nucleocytoplasmic transport, the structure of the ~40- to 60-MD NPC itself is still largely enigmatic. Cryo-electron tomography (cryo-ET) and cryo-electron microscopy (cryo-EM) have established the NPC structure at low resolution (*4*–*6*). Crystal structures of scaffold NPC components are emerging (*7*–*10*), but the resolution gap still precludes fitting into the cryo-ET structure. Overall, the NPC has eightfold rotational symmetry with an outer diameter of ~100 nm and a core scaffold ring ~30 nm wide. The central FG repeat containing transport channel measures ~40 nm in diameter, defining the maximum size of substrates (*11*).

The modularity of the NPC assembly suggests a path toward a high-resolution structure (*12*). Of the ~30 bona fide nucleoporins (Nups) that compose the NPC, only a core subset is stably attached (*13*). In *Saccharomyces cerevisiae*, this core includes two essential complexes: the heptameric Nup84 complex and the heteromeric Nic96-containing complex (hereafter called the Nic96 complex; unless noted, all proteins are from *S. cerevisiae*). The Nup84 complex is composed of one copy each of Nup84, Nup85, Nup120, Nup133, Nup145C, Sec13, and Seh1. It self-assembles from recombinant proteins in vitro and forms a branched Y-shaped structure (*14*). Deletion or depletion of individual components of the Nup84 complex leads to severe assembly defects in many organisms (*15*–*17*). The Nic96 complex is less well characterized but appears to contain the architectural nucleoporins Nup157/170, Nup188, Nup192, Nup53, and Nup59 (*18*–*20*). β propellers and stacked α-helical domains form the building blocks of the constituents of Nup84 and Nic96 complexes (*12*, *21*). Because vesicle coats [including coat protein complex I (COPI), COPII, and clathrin] share similar elements, a common ancestry has been hypothesized despite very low sequence homology and the absence of experimental structural evidence (*22*).

A recent computer-generated model of the NPC based on a plethora of primary data from different sources placed the Nup84 complex at the NPC periphery, sandwiching the Nic96 complex in the center (*23*). In contrast, a model solely based on the structure of the Nup145C•Sec13 heterodimer and crystal packing interactions was proposed that is inconsistent with the computer model (*9*).

We solved the structure of a complex of Nup85 residues 1 to 564 (of 744) and intact Seh1 (referred to as Nup85•Seh1) at 3.5 Å (table S1). Seh1 and Nup85 form distinct units in a tightly associated complex (Fig. 1 and fig. S1). Seh1 folds into an open six-bladed β-propeller structure. The blades fan out consecutively around a central axis, typical for canonical β-propeller structures (*24*). Between blades 1 and 6, the N terminus of Nup85 is inserted and forms a three-stranded blade that completes the Seh1 propeller in trans. Following its N-terminal insertion blade, Nup85 forms a compact cuboid structure composed of 20 helices, with two distinct modules, referred to as "crown" and "trunk." Helices α1 to α3 (residues 100 to 200) meander along one side of the trunk; the other side is formed by helices α12 to α19 (residues 362 to 509) running in the opposite direction in an antiparallel zigzag to the C terminus. The trunk elements are separated by an intervening crown composed of helices α4 to α11 (residues 201 to 361) that form a distinct bundle that caps one end of the trunk. Helices α5 to α10 in the crown module are almost perpendicular to the helices in the trunk.

In the asymmetric unit of the crystal, two heterodimers are aligned along a noncrystallographic dyad, generating patches of contacts (fig. S2). This interaction is unlikely to be functionally meaningful because the contact residues are poorly conserved in orthologs. Moreover, analysis of Nup85•Seh1 by analytical ultracentrifugation (AUC) showed a single species of ~104 kD with a hydrodynamic radius of 4.4 nm (fig. S3). This hydrodynamic radius is

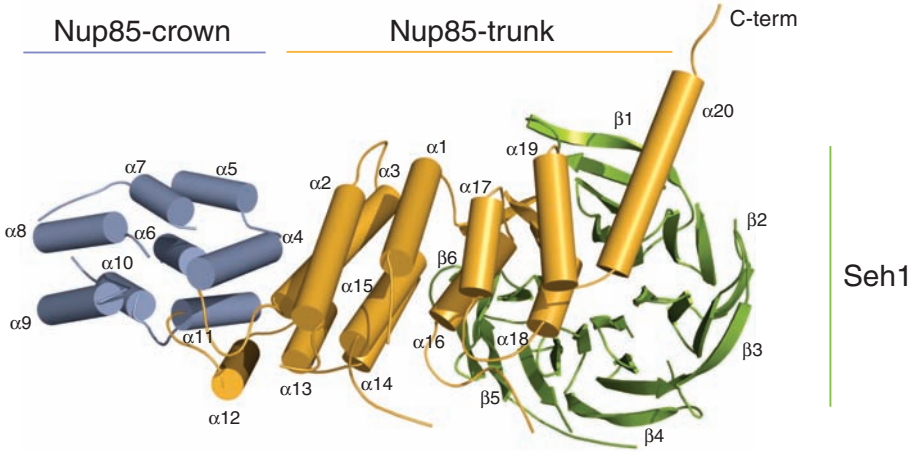

Fig. 1. Structure of the Nup85•Seh1 complex. The structure of the heterodimeric Nup85•Seh1 complex is shown. Nup85 has a trunk (orange, helices α1 to α3 and α12 to α20) and a crown (blue, helices α4 to α11) module. The β strands at the extreme N terminus of Nup85 form an insertion blade, which complete the Seh1 (green) β propeller.

[1]Department of Biology, Massachusetts Institute of Technology, 77 Massachusetts Avenue, Cambridge, MA 02139, USA. [2]Northeastern Collaborative Access Team, Building 436, Argonne National Laboratory, Argonne, IL 60439, USA.

*These authors contributed equally to this work.
†To whom correspondence should be addressed. E-mail: tus@mit.edu

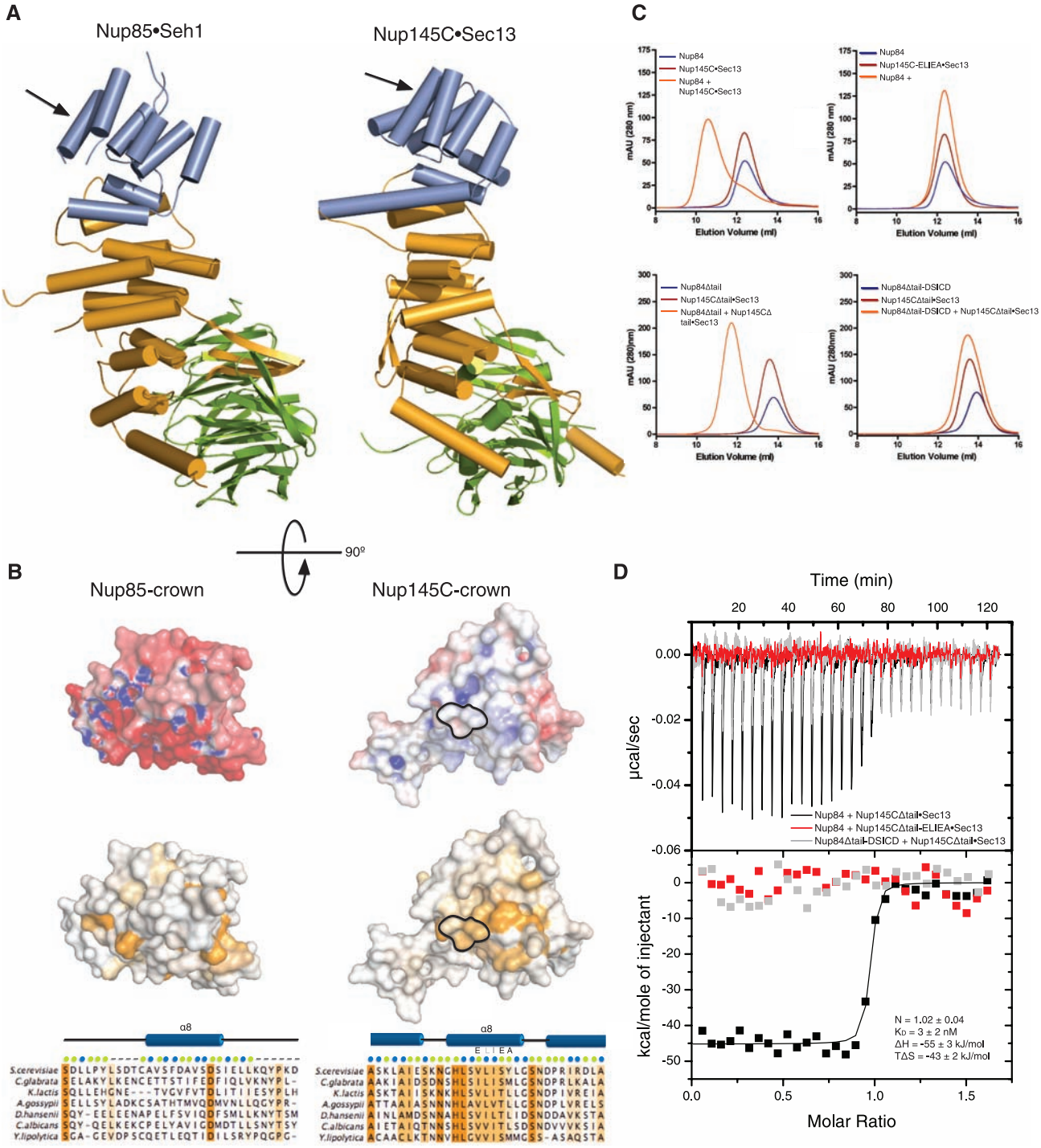

Fig. 2. Comparison of Nup85•Seh1 and Nup145C•Sec13 and identification of the Nup84•Nup145C crown-crown binding interface. (**A**) The topologies of the Nup85•Seh1 (left) and Nup145C•Sec13 [right, PDB code 3BG1 (*9*)] complexes are shown, illustrating an overall similarity with three shared structural elements: trunk, crown, and β propeller. Colors are assigned as in Fig. 1. (**B**) Surface representations of the crowns of Nup85 and Nup145C are shown colored according to electrostatic surface potentials (top) and sequence conservation (bottom) in a view rotated 90° from (A). Sequence conservation has its basis in the phylogenetic tree of budding yeasts (*40*) and is colored from white (not conserved) to orange (conserved). A partial sequence alignment of helix α8 [indicated by arrows in (A)] is also shown, with surface-exposed residues indicated by green dots, residues buried in the hydrophobic core by blue dots, and residues not modeled in the structure by dashes (*26*). Mutations made in this helix in Nup145C are shown above the sequence alignment, and the corresponding residues are outlined in the surface representations of Nup145C. (**C**) In the top graphs, gel filtration data of Nup84 alone, Nup145C•Sec13 (wild type or -ELIEA mutant) alone, and Nup84 plus Nup145C•Sec13 (wild type or -ELIEA mutant) are shown. The shift in the Nup84 plus wild-type Nup145C•Sec13 chromatogram indicates complex formation and is absent in the case of the -ELIEA mutant. In the bottom graphs, gel filtration data of Nup145C•Sec13 alone, Nup84 alone (wild type or -DSICD mutant) alone, and Nup145C•Sec13 plus Nup84 (wild type or -DSICD mutant) are shown. The shift in the Nup145C•Sec13 plus wild-type Nup84 chromatogram indicates complex formation and is absent in the case of the -DSICD mutant. (**D**) ITC data illustrating high-affinity binding for wild-type Nup145C•Sec13 and Nup84 (black). Experimental values for N, K_d, enthalpy ΔH, and entropy $T\Delta S$ are shown. In contrast, binding is lost for both crown-surface mutants Nup84-DSICD (gray) and Nup145C-ELIEA (red).

close to the theoretical value calculated from the atomic coordinates with use of HYDROPRO (*25*) and reflects the elongated shape of the 103-kD Nup85•Seh1 complex (a spherical protein of 220 kD would have the same radius). Gel filtration also showed that Nup85•Seh1 is a single 103-kD heterodimer at concentrations up to 20 mg/ml (fig. S4). Hence, we restrict our analysis to this heterodimer.

The connectivity and topology of secondary structure elements and the three-dimensional folds of Nup85•Seh1 and Nup145C•Sec13 (*9*) are remarkably similar (Fig. 2A), despite very low sequence identity between Nup85 and Nup145C (10%) and moderate identity between Seh1 and Sec13 (32%). Like Nup85, Nup145C has an N-terminal three-stranded β sheet that provides a seventh blade to close the open β propeller of Sec13. The trunk and crown modules of Nup145C are also similar to those in Nup85, although their relative orientation is modestly different in the two proteins.

The most conserved regions of Nup85 are involved in the interaction with Seh1. The corresponding interface between Nup145C and Sec13 is also well conserved, but Nup145C has an additional highly conserved surface on the crown module around helix α8 that is not observed in Nup85 (Fig. 2B). This region is reasonably polar and poorly conserved in Nup85 but highly conserved and distinctly hydrophobic in Nup145C, suggesting a protein-protein interaction site. Nup84 and Nup120 bind to roughly opposite sides of Nup145C•Sec13 in the Y-shaped complex (*14*), and the C-terminal helical region of Nup145C is necessary for binding Nup120 (fig. S5). Thus, we hypothesized that the α8 crown surface of Nup145C is the binding site for Nup84.

To test this hypothesis, we mutated the Nup145C sequence VLISY (*26*) in α8 to ELIEA, introducing two negative charges and eliminating a conserved aromatic side chain on the crown surface (Fig. 2B). The overall structure of Nup145C did not appear to be perturbed by this modification: (i) Nup145C-ELIEA•Sec13 bound to Nup120 to form a 1:1 complex indistinguishable from one formed with Nup145C•Sec13 in gel-filtration experiments (fig. S6); Nup145C•Sec13 and Nup145C-ELIEA•Sec13 complexes (ii) had comparable thermostability (fig. S7) and (iii) showed identical behavior in gel filtration (Fig. 2C). The ELIEA mutation completely eliminated Nup84 binding. In isothermal-titration calorimetry (ITC) experiments, Nup84 bound wild-type Nup145C•Sec13 tightly [dissociation constant (K_d) = 3 ± 2 nM; 1:1 stoichiometry] but not Nup145C-ELIEA•Sec13 (Fig. 2D). Similarly, Nup84 formed a stable complex with Nup145C•Sec13 but not with Nup145C-ELIEA•Sec13 in gel filtration (Fig. 2C). We conclude that the Nup84 binding site on Nup145C includes the exposed surface of helix α8.

To determine the consequences of abolishing the Nup84 binding site on Nup145C in vivo, we introduced the Nup145C-ELIEA mutation into the *NUP145* gene in yeast. Strains carrying *NUP145-ELIEA* in a Δ*NUP145*/*NUP84-GFP* or Δ*NUP145*/*NUP133-GFP* background displayed a marked defect in incorporating Nup84–green fluorescent protein (GFP) and Nup133-GFP into the NPC (Fig. 3 and fig. S8). Compared with wild type, a significantly larger fraction of GFP-tagged proteins was found in the cytoplasm, indicating that the Nup84 binding interface on Nup145C is crucial in recruiting both Nup133 and Nup84 to the NPC (fig. S10). In addition, nuclear pores were clustered into discrete foci on the nuclear envelope of the strains expressing Nup145C-ELIEA, indicative of severe NPC assembly defects and similar to Nup84 and Nup133 null strains (*27*, *28*). Cells expressing wild-type Nup145C demonstrated the expected punctate nuclear rim staining in both Nup84-GFP and Nup133-GFP strains. Thus, disruption of the Nup84 binding site on Nup145C affects NPC assembly and function and causes loss of Nup84 and Nup133 from pores. The loss of Nup133 can be rationalized because it is attached to the Y-shaped Nup84 complex through a binary interaction with Nup84 (*8*, *14*). Some Nup84 and Nup133 proteins remain associated with nuclear pores in the Nup145C-ELIEA expressing strains, arguing for the existence of additional weaker attachment sites for both proteins in the NPC. It has been shown that an ALPS membrane-binding motif is present in Nup133 (*29*). Because Nup133 and Nup84 are tightly associated (*8*), the ALPS motif might be weakly functional in recruiting Nup133•Nup84 to the NPC even when the Nup84•Nup145C interaction is compromised.

On the basis of lattice packing observed in crystals of Nup145C•Sec13, Hsia *et al*. (*9*) proposed that Nup145C•Sec13 and Nup85•Seh1 each form heterooctameric poles that span the entire NPC in a "concentric cylinder" model of NPC structure. However, the Nup145C•Sec13 lattice contacts involved in the putative heterooctamer overlap with the crown surface of Nup145C shown here to be the Nup84-binding site. Additionally, Nup145C•Sec13 and Nup85•Seh1 behave nearly identically during gel filtration, indicative of heterodimers when their large hydrodynamic radii are taken into account (Fig. 2 and fig. S4). AUC experiments confirmed that Nup85•Seh1 is a heterodimer in solution (fig. S3). Thus, the heterooctameric pole model (*9*) is inconsistent with our results.

The structural similarity between Nup85 and Nup145C extends to at least three other proteins (Fig. 4 and fig. S11). First, the architectural nucleoporin Nic96 (*10*) shares a common structural core (fig. S11) but has a distinct N terminus (Fig. 4). The shared cores mutually superimpose with a root mean square deviation of 3.0 to 3.5 Å. Nic96 has a trunk module (α1 to α3 and α12 to α19), a crown module (α4 to α11), and an N-terminal coiled-coil extension (instead of the insertion blade of Nup145C and Nup85) that tethers it to the FG-containing Nsp1 complex (*30*). Apart from the N-terminal differences, the three proteins differ mainly in the relative orientation of the crown and trunk modules. Although a previous comparison of Nup145C to the COPII coat component Sec31 did not reveal a strong similarity (*9*), comparison with Nup85, Nup145C, and Nic96 shows that Sec31 has corresponding trunk (α1 to α3 and α12 to α18) and crown (α4 to α11) modules. Sec31 homodimerizes to create an "edge element" in the COPII coat by an internal domain swap between two crown modules (*31*). This domain swap results in a mixed crown module that is identical in topology to the unmixed crowns in Nup85, Nup145C, and Nic96 (*31*). Structural prediction using Phyre (*32*) also places Nup84 in the group containing Nic96, Nup85, Nup145C, and Sec31. Similarity extends beyond the trunk and crown modules to a "tail" module that has been structurally characterized in the C-terminal domain of human Nup107 (homolog of yNup84) and in Nic96 (*8*, *10*) (fig. S11C). The

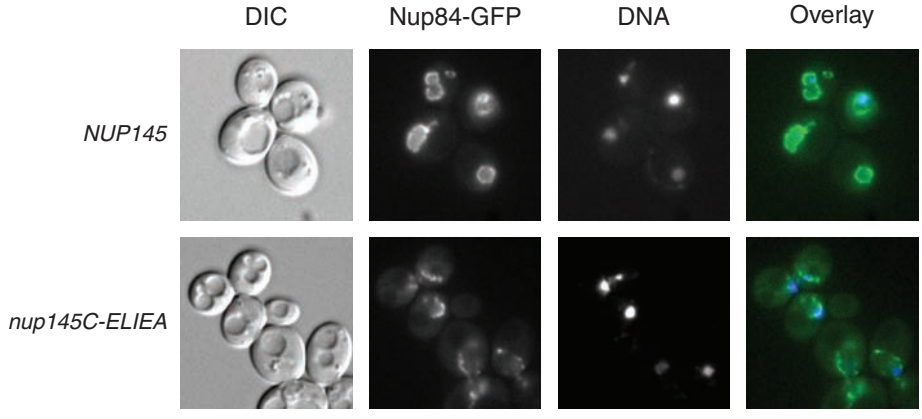

Fig. 3. Elimination of the Nup84 binding site on Nup145C results in nuclear pore assembly defects in vivo. *NUP145/NUP84-GFP* and *NUP145-ELIEA/NUP84-GFP* were grown at 24°C and visualized by fluorescence microscopy. Differential interference contrast, GFP-fluorescence, DNA (visualized with Hoechst dye), and false-colored overlay (GFP fluorescence is green, DNA blue) images of the same field are shown in columns from left to right.

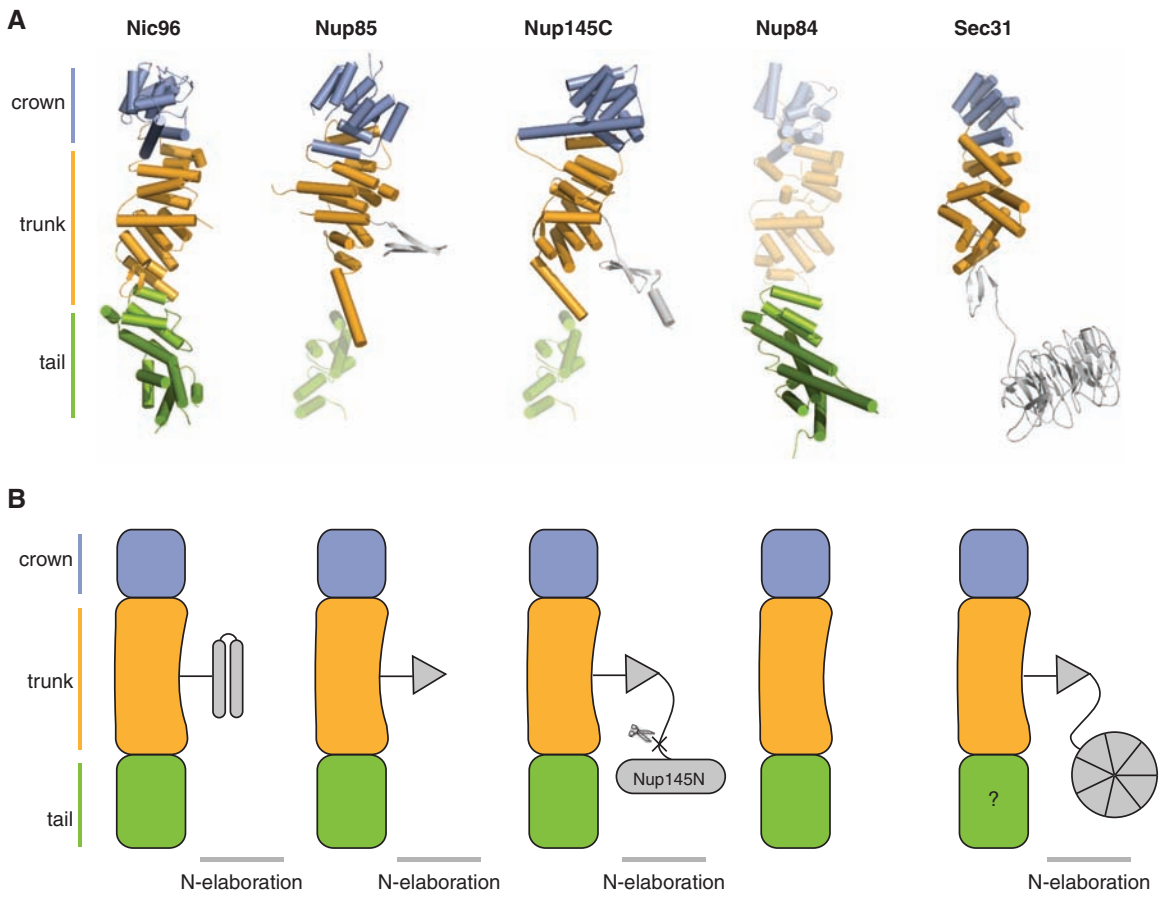

Fig. 4. Architecture of ACE1. (**A**) ACE1 containing proteins are shown as cylinders and sheets. Crowns are shown in blue, trunks in orange, tails in green, and other domains in gray. Modules with predicted structures are shown half-transparent. [PDB codes are 2QX5 for Nic96; 3BG1, Nup145C; 3CQC, Nup107 (Nup84 homolog); and 2PM6, Sec31] (**B**) Cartoons illustrating the similarity and modular nature of the ACE1 element. The N-terminal elaborations are, for Nic96, a coiled-coil domain that interacts with the Nsp1 complex; for Nup85, the Seh1-interacting insertion blade; for Nup145C, the Sec13-interacting insertion blade preceded by an autocatalytic cleavage domain and Nup145N; and, for Sec31, the Sec13-interacting insertion blade is preceded by its own N-terminal seven-bladed β propeller. Sec31 has a unique proline-rich insertion C-terminal to its trunk module followed by a conserved region predicted to be α-helical.

last three helices in the tail module of Nup107 form the interaction site with Nup133 (*8*). In Nic96, this region is predicted to be a protein binding site as well (*10*). Because we find this characteristic tripartite structural element of crown, trunk, and tail in architectural proteins of the NPC and the COPII coat, we term it the ancestral coatomer element 1 (ACE1).

Can we predict ACE1 functional sites from established interactions? Analogy to Sec31 monomers in the COPII edge element suggests that Nup145C and Nup84 might interact crown to crown. On the basis of the Phyre model and structural alignment, we constructed a surface point mutant, replacing two conserved hydrophobic residues on helix α8 of the Nup84 crown with aspartate [Nup84-ISICM to Nup84-DSICD (*26*)] (figs. S7 and S12). Nup84-DSICD disrupts Nup145C binding in a manner analogous to that of Nup145C-ELIEA, severing Nup84 binding as shown by gel filtration and ITC (Fig. 2, C and D). Thus, the Nup84•Nup145C interface is a crown-crown interaction involving α8 helices as in Sec31 homodimerization. Additionally, we found that the tail modules of Nup145C and Nup85 are necessary for interaction with Nup120 in a manner analogous to the human Nup107 interaction site for human Nup133 (*8*) (figs. S5 and S6).

Here, we have shown that ACE1 is abundant in the two main scaffolding subcomplexes of the NPC. To date, Nic96 is the only ACE1 protein in which all three modules (crown, trunk, and tail) are structurally defined. In Nic96, the three modules form a continuous, rigid hydrophobic core (*10*, *33*). In the other four experimental structures, only a subset of the modules are present. We speculate that the three modules within ACE1 can allow hinge movements, used to different extents in specific family members.

ACE1 is different from regular α-helical repeat structures, including HEAT repeats and TPR repeats [as discussed in (*10*)]. The α-helical modules that compose ACE1 are distinctly irregular, most notably with elements that fold back onto themselves, forming a U-turn within the crown module. The trunk is composed of two zigzagging helical units running in opposite directions. We propose that this architecture confers rigidity to the trunk and thus distinguishes it from regular helical repeat structures that are often inherently flexible (*34*). As a consequence of the specific arrangement of the helices in ACE1, several helices in trunk and crown are encased by neighboring helices and thus have a characteristic hydrophobic character (typically helices α6 and α10). This pattern of hydrophobic helices may help to find additional ACE1 proteins. Several sequence elements, notably in the crown and at the predicted hinge regions, distinguish ACE1 from other α-helical domains (*10*). Nevertheless, these characteristics are subtle enough to remain undetected in typical primary sequence (i.e., BLAST) searches, and candidate proteins need to be examined using all available tools, including phylogeny and secondary and tertiary structure analysis.

On the basis of distance constraints and stoichiometric considerations, the heptameric Y-shaped Nup84 complex has been placed in two concentric eight-membered rings on the nucleoplasmic and cytoplasmic faces of the NPC (*23*). But how is it oriented, and how is it connected to the inner ring of the scaffold? Nup133 is anchored to the structural scaffold by its interaction with Nup84, positioning it at the periphery of the pore (*8*). Nup84 is the link between Nup133 and Nup145C. Thus, we position the extended arm of the Y composed of Nup145C•Sec13, Nup84, and Nup133 facing outward (Fig. 5). Excluding the Nup133•Nup84 pair, the remaining pentamer forms a roughly symmetrical triskelion that conceptually resembles the vertex elements that form polygonal cages in vesicle coats. EM analysis showed that the triskelion measures about 20 nm between the tips (*14*). An eight-membered ring of the

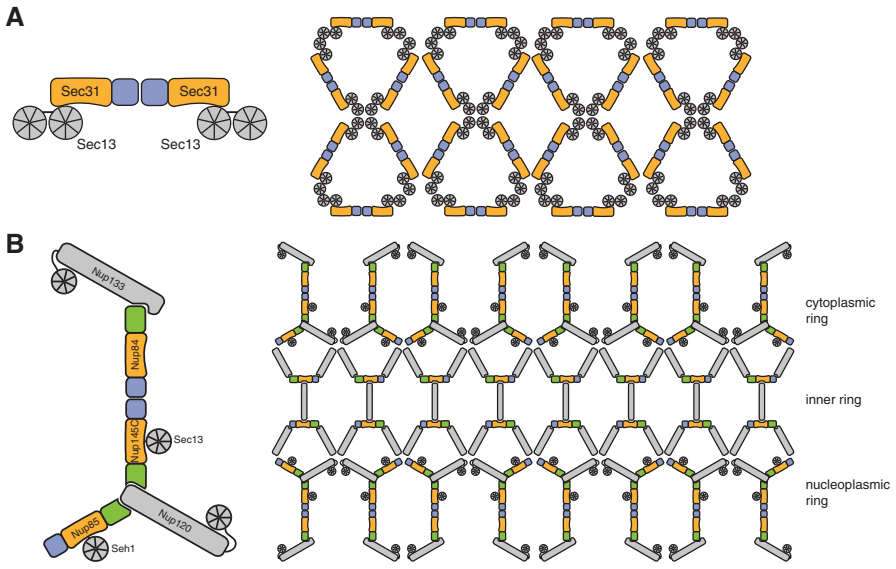

Fig. 5. Lattice model for the Nup84 complex and the structural scaffold of the NPC. The ACE1 proteins Nup85, Nup145C, Nup84, Sec31, and Nic96 are colored according to Fig. 4. (**A**) Schematic diagram of COPII outer coat organization. The Sec31•Sec13 cuboctahedron composed of 24 edge elements (Sec31•Sec13 heterotetramers) is shown unwrapped and laid flat in two dimensions. The Sec31•Sec31 crown-crown interactions make edge elements, whereas propeller-propeller interactions are vertex elements (*31*). (**B**) Schematic diagram of the predicted latticelike organization of the structural scaffold of the NPC. The entire scaffold (eight spokes) is illustrated unwrapped and laid flat in two dimensions. The Nup84 complex comprises the nuclear and cytoplasmic rings, whereas the Nic96-containing complex makes up the inner ring. The relative position and interactions between the seven proteins in the Nup84 complex are shown with Sec13, Seh1, Nup133, and Nup120 colored in gray. The remainder of the Nic96 complex (Nup157/170, Nup188, and Nup192) is illustrated in gray. The illustration is not meant to predict relative positions of proteins or structure of the inner ring per se but shows the latticelike organization of the structural scaffold that is similar to vesicle coating complexes.

Y complex around the central transport channel has an ~50-nm diameter if the edges were to touch at the tips. Alternatively, the Y complexes might connect through a yet-unidentified adaptor protein.

Two of the three interface types observed in the outer COPII coat are also found in the NPC coat (Fig. 5). Nup145C and Nup84 heterodimerize via their crown modules similar to Sec31 homodimerization, and the insertion of a seventh blade into an incomplete propeller domain is a recurring theme in Sec31•Sec13, Nup145C•Sec13, and Nup85•Seh1. Because Nic96 shares an ACE1 element, we predict that the inner scaffold ring is branched and latticelike, as are the peripheral rings. We postulate that the Nup84 and Nic96 complexes are both vertex elements in the assembly of the NPC structural scaffold. This would generate a latticelike NPC coat similar to clathrin and COP coats (*31*, *35*) (Fig. 5B). This model explains how the relatively small mass of Nup subcomplexes fills the large volume observed for the scaffold structure of the NPC (*23*) and is generally consistent with low-resolution images of NPCs (*4*, *6*). Notably, COP and clathrin cages do not directly contact membranes but use adaptor protein (AP) complexes to span the ~10-nm gap between the surfaces (*36*). Consistent with a related architecture, a similar sized gap has been observed between the scaffold ring and membrane surface in intact NPCs (*4*).

The modular nature of COP and clathrin coats enables the construction of assemblies varying in composition and size (*37*, *38*) because the polygonal elements can be arranged in different ways. If the same principle applies to the NPC, it could explain the existence of a subset of NPCs that do not obey eightfold rotational symmetry (*39*) or further allow for the assembly of NPCs of distinct composition, possibly tailored to more-specific tasks. These possibilities are now testable and will bring us closer to fully understanding the many functions of the NPC.

References and Notes

1. E. J. Tran, S. R. Wente, *Cell* **125**, 1041 (2006).
2. K. Weis, *Cell* **112**, 441 (2003).
3. M. A. D'Angelo, M. W. Hetzer, *Trends Cell Biol.* **18**, 456 (2008).
4. M. Beck, V. Lucic, F. Forster, W. Baumeister, O. Medalia, *Nature* **449**, 611 (2007).
5. S. P. Drummond, S. A. Rutherford, H. S. Sanderson, T. D. Allen, *Can. J. Physiol. Pharmacol.* **84**, 423 (2006).
6. D. Stoffler *et al.*, *J. Mol. Biol.* **328**, 119 (2003).
7. I. C. Berke, T. Boehmer, G. Blobel, T. U. Schwartz, *J. Cell Biol.* **167**, 591 (2004).
8. T. Boehmer, S. Jeudy, I. C. Berke, T. U. Schwartz, *Mol. Cell* **30**, 721 (2008).
9. K. C. Hsia, P. Stavropoulos, G. Blobel, A. Hoelz, *Cell* **131**, 1313 (2007).
10. S. Jeudy, T. U. Schwartz, *J. Biol. Chem.* **282**, 34904 (2007).
11. N. Pante, M. Kann, *Mol. Biol. Cell* **13**, 425 (2002).
12. T. U. Schwartz, *Curr. Opin. Struct. Biol.* **15**, 221 (2005).
13. G. Rabut, V. Doye, J. Ellenberg, *Nat. Cell Biol.* **6**, 1114 (2004).
14. M. Lutzmann, R. Kunze, A. Buerer, U. Aebi, E. Hurt, *EMBO J.* **21**, 387 (2002).
15. E. Fabre, E. Hurt, *Annu. Rev. Genet.* **31**, 277 (1997).
16. V. Galy, I. W. Mattaj, P. Askjaer, *Mol. Biol. Cell* **14**, 5104 (2003).
17. A. Harel *et al.*, *Mol. Cell* **11**, 853 (2003).
18. C. P. Lusk, T. Makhnevych, M. Marelli, J. D. Aitchison, R. W. Wozniak, *J. Cell Biol.* **159**, 267 (2002).
19. M. Marelli, J. D. Aitchison, R. W. Wozniak, *J. Cell Biol.* **143**, 1813 (1998).
20. U. Zabel *et al.*, *J. Cell Biol.* **133**, 1141 (1996).
21. D. Devos *et al.*, *Proc. Natl. Acad. Sci. U.S.A.* **103**, 2172 (2006).
22. D. Devos *et al.*, *PLoS Biol.* **2**, e380 (2004).
23. F. Alber *et al.*, *Nature* **450**, 695 (2007).
24. I. Chaudhuri, J. Soding, A. N. Lupas, *Proteins* **71**, 795 (2008).
25. J. Garcia De La Torre, M. L. Huertas, B. Carrasco, *Biophys. J.* **78**, 719 (2000).
26. Single-letter abbreviations for the amino acid residues are as follows: A, Ala; C, Cys; D, Asp; E, Glu; F, Phe; G, Gly; H, His; I, Ile; K, Lys; L, Leu; M, Met; N, Asn; P, Pro; Q, Gln; R, Arg; S, Ser; T, Thr; V, Val; W, Trp; and Y, Tyr.
27. V. Doye, R. Wepf, E. C. Hurt, *EMBO J.* **13**, 6062 (1994).
28. S. Siniossoglou *et al.*, *Cell* **84**, 265 (1996).
29. G. Drin *et al.*, *Nat. Struct. Mol. Biol.* **14**, 138 (2007).
30. P. Grandi, N. Schlaich, H. Tekotte, E. C. Hurt, *EMBO J.* **14**, 76 (1995).
31. S. Fath, J. D. Mancias, X. Bi, J. Goldberg, *Cell* **129**, 1325 (2007).
32. R. M. Bennett-Lovsey, A. D. Herbert, M. J. Sternberg, L. A. Kelley, *Proteins* **70**, 611 (2008).
33. N. Schrader *et al.*, *Mol. Cell* **29**, 46 (2008).
34. E. Conti, C. W. Muller, M. Stewart, *Curr. Opin. Struct. Biol.* **16**, 237 (2006).
35. A. Fotin *et al.*, *Nature* **432**, 573 (2004).
36. D. J. Owen, B. M. Collins, P. R. Evans, *Annu. Rev. Cell Dev. Biol.* **20**, 153 (2004).
37. S. M. Stagg *et al.*, *Cell* **134**, 474 (2008).
38. Y. Cheng, W. Boll, T. Kirchhausen, S. C. Harrison, T. Walz, *J. Mol. Biol.* **365**, 892 (2007).
39. J. E. Hinshaw, R. A. Milligan, *J. Struct. Biol.* **141**, 259 (2003).
40. B. Dujon, *Trends Genet.* **22**, 375 (2006).

41. We thank staff at beamlines 24-ID-C/-E at Argonne National Laboratory and X6A at National Synchrotron Light Source for excellent assistance with data collection, R. Sauer and T. Baker for critically reading the manuscript, G. Wink for contributions, members of the Schwartz laboratory for discussions, and the Biophysical Instrumentation Facility for the Study of Complex Macromolecular Systems (NSF-0070319 and NIH GM68762) for providing instrumentation. Supported by NIH grant GM77537 (T.U.S.), a Pew Scholar Award (T.U.S.), a Koch Fellowship Award (S.G.B.), and a Vertex Scholarship (S.G.B.). Coordinates and structure factors of the Nup85•Seh1 crystal structure have been deposited in the Protein Data Bank (PDB) with accession code 3EWE.

Supporting Online Material

www.sciencemag.org/cgi/content/full/1165886/DC1
Materials and Methods
Figs. S1 to S13
Tables S1 and S2
References

15 September 2008; accepted 16 October 2008
Published online 30 October 2008;
10.1126/science.1165886
Include this information when citing this paper.

The Widespread Threat of Calcium Decline in Fresh Waters

Adam Jeziorski,[1] Norman D. Yan,[2,3] Andrew M. Paterson,[3] Anna M. DeSellas,[1,3] Michael A. Turner,[4] Dean S. Jeffries,[5] Bill Keller,[6] Russ C. Weeber,[7] Don K. McNicol,[7] Michelle E. Palmer,[2] Kyle McIver,[1] Kristina Arseneau,[1] Brian K. Ginn,[1] Brian F. Cumming,[1] John P. Smol[1]*

Calcium concentrations are now commonly declining in softwater boreal lakes. Although the mechanisms leading to these declines are generally well known, the consequences for the aquatic biota have not yet been reported. By examining crustacean zooplankton remains preserved in lake sediment cores, we document near extirpations of calcium-rich *Daphnia* species, which are keystone herbivores in pelagic food webs, concurrent with declining lake-water calcium. A large proportion (62%, 47 to 81% by region) of the Canadian Shield lakes we examined has a calcium concentration approaching or below the threshold at which laboratory *Daphnia* populations suffer reduced survival and fecundity. The ecological impacts of environmental calcium loss are likely to be both widespread and pronounced.

Lake-water calcium concentrations are currently falling in softwater lakes in many boreal regions (*1*–*3*). Declining calcium is part of an expected concentration trajectory (*4*) that is linked to a reduction in the exchangeable calcium concentration of catchment soils (*5*). Although such reduction is part of the natural, long-term process of soil acidification, it is accelerated by other factors that vary regionally in importance [for example, acidic deposition (*1*, *6*), reduction in atmospheric calcium inputs (*7*), calcium loss from forest biomass harvesting, and regrowth after multiple timber harvesting cycles (*2*, *8*)]. Acidic deposition plays an especially complex role because it initially increases soil leaching of calcium and surface-water calcium concentrations. However, in watersheds with thin soils underlain by weathering resistant bedrock, the leaching rate typically exceeds the replenishment rate from weathering and atmospheric deposition (*9*) so that decades of acidic deposition result in the depletion of soil base saturation (*1*, *6*). Depleted base saturation necessarily results in reduced calcium concentrations in runoff, and reduced acidic deposition further accentuates this trend (*7*). Surface-water calcium concentrations may even fall below pre-acidification levels (*4*). Watershed geochemists recognize the importance of soil calcium depletion as a factor confounding the recovery of lakes from acidification (*1*).

Whereas the biogeochemical dynamics that underpin calcium decline are largely understood, little is known regarding the direct effects of declining calcium concentrations on the biota of softwater lakes, and clear evidence of such biological damage does not currently exist. We investigated the consequences of calcium decline for *Daphnia* in Precambrian Shield lakes that have aqueous calcium concentrations near or below 1.5 mg L^{-1}. This is the threshold concentration that has been experimentally demonstrated to reduce *Daphnia pulex* survival and to delay reproduction and reduce fecundity (*10*). First, using dated lake sediment cores, we examined temporal changes in calcium-rich *Daphnia* species (keystone pelagic herbivores). Second, we used a regional paleolimnological survey to compare the abundances of modern-day and preindustrial daphniid subfossil remains in 43 lakes. Finally, to assess the current prevalence of the threat of aquatic calcium loss, we analyzed changes in pH and calcium in 770 lakes from the 1980s to the 2000s .

Although many calcium-rich organisms may be directly affected by declining aqueous calcium concentrations, we focused on the crustacean zooplankton because they leave identifiable remains of individuals in lake sediments that allow the reconstruction of detailed paleoecological records (*11*). Because they are important phytoplankton grazers and the principal prey of predatory macroinvertebrates and small, planktivorous fish in pelagic ecosystems, changes in the crustacean zooplankton community will profoundly influence aquatic ecosystems (*12*, *13*). Partial life cycle bioassays with *D. pulex* (a species common to softwater lakes) indicate that calcium reductions below 1.5 mg L^{-1} delay reproduction and reduce clutch sizes, substantially reducing intrinsic rates of population growth (*10*). Furthermore, daphniids (Daphnidae, Anomopoda, Crustacea) have much higher calcium concentrations than other crustacean zooplankton taxa [2 to 8% of dry body weight compared with 0.2 to 0.4% for non-daphniid competitors (*14*)] and thus are probably more sensitive to calcium decline.

Because the stressors that have led to calcium decline pre-date water chemistry monitoring programs in most regions (*15*), a paleolimnological analysis of calcium-rich daphniid remains, using standard methods (*16*), was performed for Plastic Lake (45° 11′N, 78° 50′W)—a 32-ha dimictic, softwater [specific conductivity = 17 μS cm^{-1}

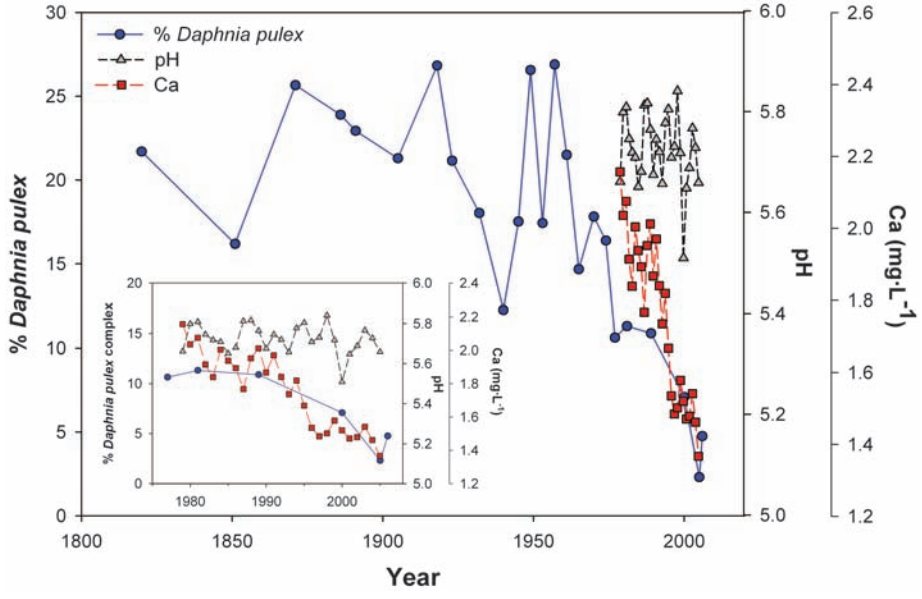

Fig. 1. Changes in the relative abundance of remains from the *D. pulex* complex relative to other sedimentary cladoceran remains, ice-free whole-lake calcium, and the pH of Plastic Lake, Ontario, Canada. (Inset) Changes in these same three variables since 1976.

[1]Paleoecological Environmental Assessment and Research Lab, Department of Biology, Queen's University, Kingston, ON, Canada, K7L 3N6. [2]Department of Biology, York University, 4700 Keele Street, Toronto, ON, Canada, M3J 1P3. [3]Ontario Ministry of the Environment, Dorset Environmental Science Centre, 1026 Bellwood Acres Road, Post Office Box 39, Dorset, ON Canada, P0A 1E0. [4]Experimental Lakes Area, Fisheries and Oceans Canada, 501 University Crescent, Winnipeg, MB, Canada, R3T 2N6. [5]Environment Canada, National Water Research Institute, Post Office Box 5050, Burlington, ON, Canada, L7R 4A6. [6]Ontario Ministry of the Environment, Cooperative Freshwater Ecology Unit, Laurentian University, Sudbury, ON, Canada, P3E 2C6. [7]Canadian Wildlife Service (Ontario), Environment Canada, 335 River Road, Ottawa, ON, Canada, K1A 0H3.

*To whom correspondence should be addressed. E-mail: smolj@queensu.ca

(where 1S = 1A/v) 2000 to 2005 average] lake in south-central Ontario, Canada. Measured twice a month, the ice-free mean pH of the lake has been quite stable since the late 1970s at ~5.8 (Fig. 1), a value that has not changed much from a diatom-inferred (*17*) pH of 5.7 that pre-dates the onset of modern human influence (*18*). However, calcium concentrations have fallen from ~2.2 mg L^{-1} in 1980 to ~1.4 mg L^{-1} in 2006, with a period of steep decline occurring after 1991 (Fig. 1). Correlating with the decline in calcium, there has also been a decrease in the relative abundance of daphniid sedimentary remains (Pearson product moment correlation between percent of *Daphnia* and calcium = 0.95, $P < 0.05$) (Fig. 1).

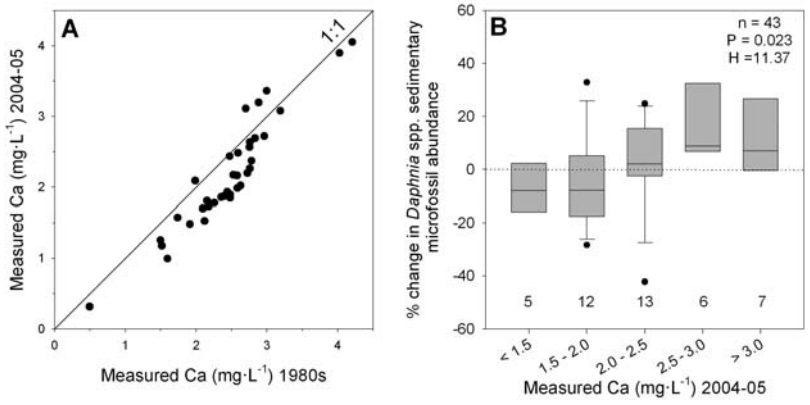

Fig. 2. Changes in ice-free season average lake-water calcium concentration and *Daphnia* spp. remains over time. (**A**) Changes in aqueous calcium from the 1980s to 2004 or 2005 of 36 softwater lakes from the Muskoka region of the Canadian Shield in Ontario (calcium declined in all but four lakes). (**B**) Change in the relative abundance of *Daphnia* spp. sedimentary remains since preindustrial times for 43 Muskoka lakes sorted by present-day calcium (Kruskal-Wallis nonparametric analysis of variance for all five classes, $P = 0.023$, $H = 11.37$, $df = 4$; inset values denote sample size within each calcium class). Error bars indicate the 10th (lower line) and 90th (upper line) percentiles.

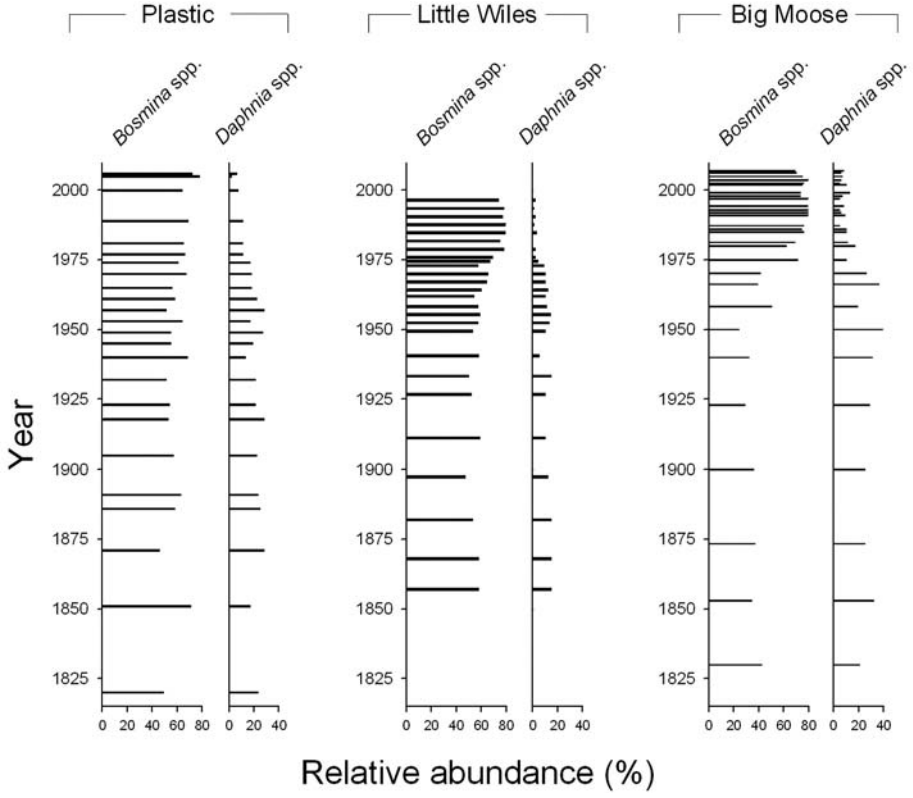

Fig. 3. Cladoceran relative abundances over time from lake sediment cores of three geographically distant North American lakes. Changes in the relative abundance of the two dominant pelagic cladoceran zooplankton groups (calcium-poor *Bosmina* spp. and calcium-rich *Daphnia* spp.) among sedimentary zooplankton assemblages from Plastic Lake (Ontario, Canada), Little Wiles Lake (Nova Scotia, Canada), and Big Moose Lake (New York, U.S.) are shown. The *y* axis denotes sediment age as estimated by ^{210}Pb analysis.

Between 1985 and 2005, a mean calcium decline of 13% was observed in 36 lakes from the Muskoka region of the southern Canadian Shield in Ontario, concurrent with an increase in their average pH from 5.9 to 6.2 (Fig. 2A). During the 1980s, only 1 of the lakes had a calcium concentration <1.5 mg L^{-1}; now 5 of the 36 lakes are below this threshold. We compared recent sedimentary cladoceran remains and those deposited before European settlement (~1850) (*19*) from an additional set of 43 Muskoka lakes (including Plastic Lake). The relative abundances of all daphniids have decreased in 60% of the lakes having a present-day calcium concentration <1.5 mg L^{-1} and in 67% of the lakes with calcium concentration between 1.5 and <2.0 mg L^{-1} (Fig. 2B). These changes contrast with increases in *Daphnia* spp. relative abundances in all the lakes with calcium concentrations >2.5 mg L^{-1} (Fig. 2B).

We also identified long-term declines in the abundance of calcium-rich *Daphnia* spp. relative to increases in calcium-poor *Bosmina* spp. (*14*) in paleolimnological records from two other eastern North American lakes (Fig. 3). These lakes have calcium concentrations near 1.5 mg L^{-1} but have different acidification histories. Little Wiles Lake (44° 24′N, 64° 39′W; Nova Scotia, Canada; see inset map in Fig. 4) is naturally acidic (pH ~ 5.6) (*20*) and has experienced declining calcium concentration (*21*), whereas diatom profiles indicate that the pH remained stable (like Plastic Lake) during the period of maximum acid deposition in the 1970s (*22*). In contrast, Big Moose Lake (43° 49′N, 74° 51′W; New York, U.S.) has experienced a steady calcium decline throughout a period of acidification in the 1950s (to pH 4.6) (*23*) and a subsequent recovery in pH (current pH is >5.5) (*24*). Daphniid relative abundance dropped to trace levels in Little Wiles Lake during the mid-1970s (Fig. 3). Declines in daphniid populations were also detected in Big Moose Lake, and populations remain substantially below their pre-impact abundances despite a recovery of pH (Fig. 3). Hence, calcium decline may be preventing daphniid recovery from lake acidification in Big Moose Lake and perhaps other acidified lakes in eastern North America.

Concurrent changes in other limnological variables have often accompanied the regional aqueous calcium decline—notably an increase in pH (Fig. 4), a decrease in total phosphorus concentration (*18*, *25*), and an increase in occurrences of predatory bass, *Micropterus* (*26*). The loss of daphniids in the low-calcium lakes cannot be attributed to these trends, which should favor the large, highly visible, calcium-rich daphniids

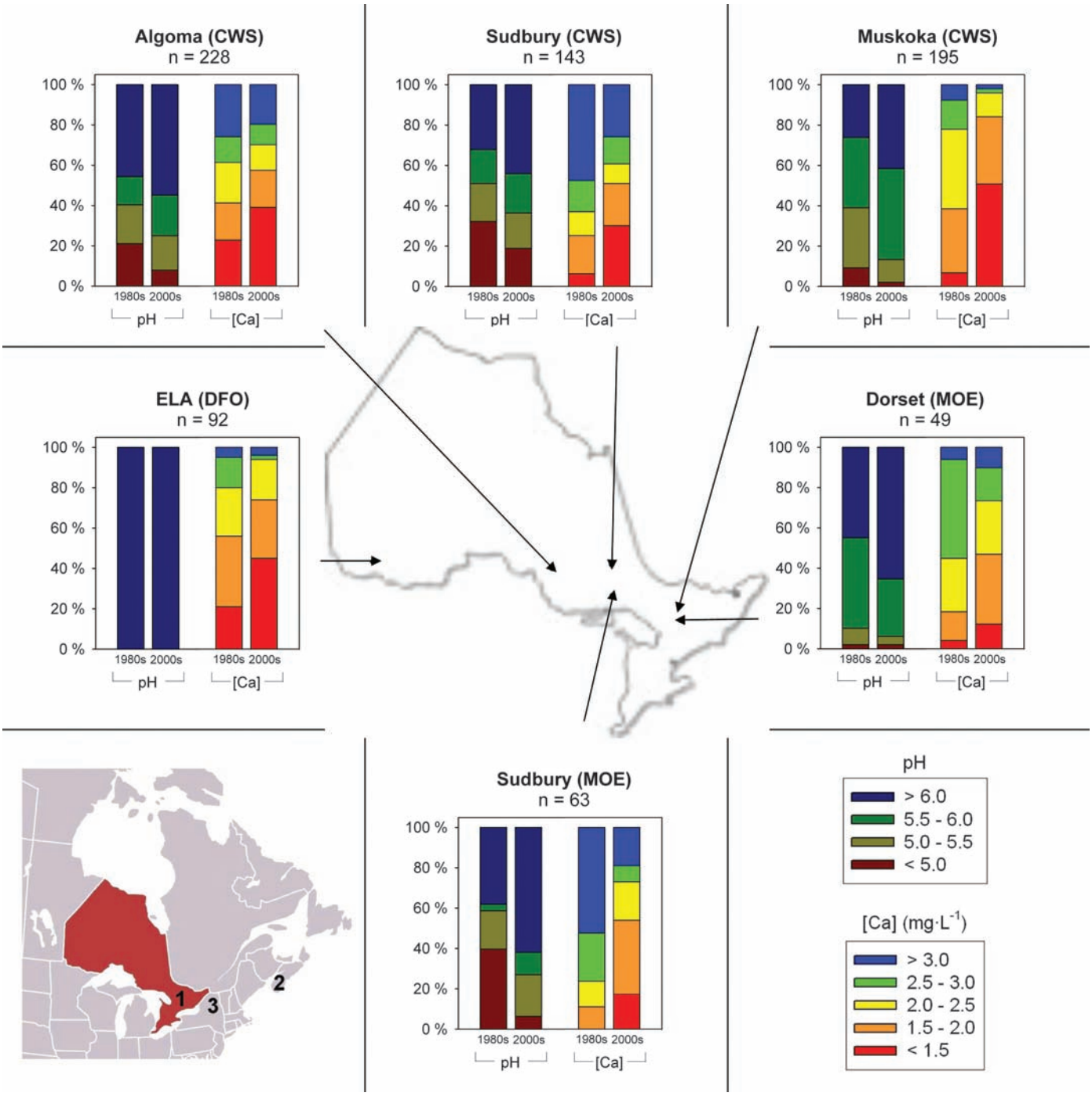

Fig. 4. Regional changes in lake-water pH and calcium concentration across Ontario, Canada. The map shows changes in the proportion of lakes by broad pH and calcium categories between the 1980s and 2000s for 770 lakes (see supporting online material text) spread across six study regions of Ontario, Canada. Data sets include: Dorset (Ontario Ministry of the Environment); Sudbury (Ontario Ministry of the Environment); Experimental Lakes Area (ELA; Fisheries and Oceans, Canada); and Algoma, Muskoka, and Sudbury surveys that were conducted by the Canadian Wildlife Service (CWS). (Inset at Bottom Left) Location of Ontario within eastern North America and locations of Plastic (1), Little Wiles (2), and Big Moose (3) lakes. *n*, number of lakes in subset; DFO, Fisheries and Oceans, Canada; MOE, Ontario Ministry of the Environment.

over their smaller, less visible, calcium-poor competitors (*25*, *27*, *28*). We did see increases in daphniids in our survey, perhaps driven by these trends, but only in those lakes with calcium concentrations >2.5 mg L^{-1} (Fig. 2B); when calcium concentrations were lower, daphniid populations fell.

It remains unclear what proportion of European and northeastern North American lakes has fallen below 1.5 mg L^{-1} calcium. We have examined the extent of calcium decline throughout Ontario using several long-term monitoring data sets (Fig. 4). Currently, 35% (12 to 51% among regions) of the 770 lakes have calcium concentrations <1.5 mg L^{-1}, and 62% (47 to 81%) are below 2.0 mg L^{-1} (particularly those among the small lakes sampled by the Canadian Wildlife Service). It is also apparent that calcium decline is occurring in lakes with relatively low acid inputs—for instance, in the Experimental Lakes Area of northwestern Ontario, Canada (Fig. 4).

Aqueous calcium concentrations are already either below or near experimentally defined thresholds of population fitness for calcium-rich crustacean zooplankton in a large proportion of lakes on the southeastern Canadian Shield, and additional declines are predicted for the next half century (*29*). The declining calcium trend we have observed is not restricted to Ontario; similar patterns have been observed in many other softwater regions of Europe and North America (*1*–*3*, *30*). Thus, we predict a similar threat to the abundances of calcium-rich zooplankton in other lake districts with historically high acid-deposition rates. Calcium-rich daphniids are some of the most abundant zooplankton in many lake systems, and their loss will substantially affect food webs. Furthermore, it is likely that the calcium decline will influence other aquatic biota, not just daphniids. The ecological effects may transcend aquatic boundaries to affect a variety of calcium-rich biota.

References and Notes

1. J. L. Stoddard *et al*., *Nature* **401**, 575 (1999).
2. S. A. Watmough, J. Aherne, P. J. Dillon, *Can. J. Fish. Aquat. Sci.* **60**, 1095 (2003).
3. B. L. Skjelkvåle *et al*., *Environ. Pollut.* **137**, 165 (2005).
4. S. A. Norton, J. Veselý, in *Treatise on Geochemistry*, vol. 9, H. D. Holland, K. K. Turekian, Eds. (Elsevier-Pergamon, Oxford, 2003), pp. 367–406.
5. D. Houle, R. Ouimet, S. Couture, C. Gagnon, *Can. J. Fish. Aquat. Sci.* **63**, 471 (2006).
6. J. W. Kirchner, E. Lydersen, *Environ. Sci. Technol.* **29**, 1953 (1995).
7. G. E. Likens, C. T. Driscoll, D. C. Buso, *Science* **272**, 244 (1996).
8. T. G. Huntington *et al*., *Soil Sci. Soc. Am. J.* **64**, 1845 (2000).
9. S. A. Watmough *et al*., *Environ. Monit. Assess.* **109**, 1 (2005).
10. D. Ashforth, N. D. Yan, *Limnol. Oceanogr.* **53**, 420 (2008).
11. J. P. Smol, *Pollution of Lakes and Rivers: A Paleoenvironmental Perspective* (Blackwell, Oxford, ed. 2, 2008).
12. M. A. Leibold, *Am. Nat.* **134**, 922 (1989).
13. H. Cyr, J. M. Curtis, *Oecologia* **118**, 306 (1999).
14. A. Jeziorski, N. D. Yan, *Can. J. Fish. Aquat. Sci.* **63**, 1007 (2006).
15. W. Keller, S. S. Dixit, J. Heneberry, *Can. J. Fish. Aquat. Sci.* **58**, 2011 (2001).
16. A. Korhola, M. Rautio, in *Tracking Environmental Change Using Lake Sediments*, vol. 4, J. P. Smol, H. J. B. Birks, W. M. Last, Eds. (Kluwer Academic, Dordrecht, Netherlands, 2001), pp. 4–41.
17. R. W. Battarbee, D. F. Charles, S. S. Dixit, I. Renberg, in *The Diatoms: Applications for the Environmental and Earth Sciences*, E. F. Stoermer, J. P. Smol, Eds. (Cambridge Univ. Press, Cambridge, 1999), pp. 85–127.
18. R. I. Hall, J. P. Smol, *Can. J. Fish. Aquat. Sci.* **53**, 1 (1996).
19. A. M. DeSellas, A. M. Paterson, J. N. Sweetman, J. P. Smol, *Hydrobiologia* **600**, 105 (2008).
20. B. K. Ginn, B. F. Cumming, J. P. Smol, *Can. J. Fish. Aquat. Sci.* **64**, 1043 (2007).
21. T. A. Clair, T. Pollock, G. Brun, A. Ouellet, D. Lockerbie, *Environment Canada's Acid Precipitation Monitoring Networks in Atlantic Canada: Occasional Report No. 16* (Environment Canada, Ottawa, Canada, 2001).
22. C. Chan, thesis, Queen's University (2004).
23. D. F. Charles *et al*., *Biogeochemistry* **3**, 267 (1987).
24. C. T. Driscoll, K. M. Driscoll, K. M. Roy, M. J. Mitchell, *Environ. Sci. Technol.* **37**, 2036 (2003).
25. N. D. Yan *et al*., *Can. J. Fish. Aquat. Sci.* **65**, 862 (2008).
26. P. S. D. MacRae, D. A. Jackson, *Can. J. Fish. Aquat. Sci.* **58**, 342 (2001).
27. K. E. Havens, N. D. Yan, W. Keller, *Environ. Sci. Technol.* **27**, 1621 (1993).
28. Z. M. Gliwicz, *Nature* **343**, 638 (1990).
29. S. A. Watmough, J. Aherne, *Can. J. Fish. Aquat. Sci.* **65**, 821 (2008).
30. D. S. Jeffries, D. K. McNicol, R. C. Weeber, Eds., *2004 Canadian Acid Deposition Science Assessment. Chapter 6: Effects on Aquatic Chemistry and Biology* (Environment Canada, Ottawa, Canada, 2004).

31. This work was primarily supported by grants from the Natural Sciences and Engineering Research Council of Canada, as well as funding from the Ontario Ministry of the Environment, Environment Canada, and Fisheries and Oceans Canada. We thank the latter three agencies for the data used to develop Fig. 4. N.D.Y. thanks the School of Environmental Systems Engineering from the University of Western Australia for their support. We would also like to thank D. Schindler and S. Watmough for their valuable comments on this manuscript.

Supporting Online Material

www.sciencemag.org/cgi/content/full/322/5906/1374/DC1
SOM Text

21 August 2008; accepted 15 October 2008
10.1126/science.1164949

Genomic Analysis of the Clonal Origins of Relapsed Acute Lymphoblastic Leukemia

Charles G. Mullighan,[1] Letha A. Phillips,[1] Xiaoping Su,[1] Jing Ma,[2] Christopher B. Miller,[1] Sheila A. Shurtleff,[1] James R. Downing[1]*

Most children with acute lymphoblastic leukemia (ALL) can be cured, but the prognosis is dismal for the minority of patients who relapse after treatment. To explore the genetic basis of relapse, we performed genome-wide DNA copy number analyses on matched diagnosis and relapse samples from 61 pediatric patients with ALL. The diagnosis and relapse samples typically showed different patterns of genomic copy number abnormalities (CNAs), with the CNAs acquired at relapse preferentially affecting genes implicated in cell cycle regulation and B cell development. Most relapse samples lacked some of the CNAs present at diagnosis, which suggests that the cells responsible for relapse are ancestral to the primary leukemia cells. Backtracking studies revealed that cells corresponding to the relapse clone were often present as minor subpopulations at diagnosis. These data suggest that genomic abnormalities contributing to ALL relapse are selected for during treatment, and they point to new targets for therapeutic intervention.

Despite cure rates for pediatric ALL exceeding 80% (*1*), treatment failure remains a formidable problem. Relapsed ALL ranks as the fourth most common childhood malignancy and has an overall survival rate of only 30% (*2*, *3*). Important biological and clinical differences have been identified between diagnostic and relapsed leukemic cells, including the acquisition of new chromosomal abnormalities, gene mutations, and reduced responsiveness to chemotherapeutic agents (*4*–*7*). However, many questions remain about the molecular abnormalities responsible for relapse, as well as the relationship between the cells giving rise to the primary and recurrent leukemias in individual patients.

[1]Department of Pathology, St. Jude Children's Research Hospital, Memphis, TN 38105, USA. [2]Hartwell Center for Bioinformatics and Biotechnology, St. Jude Children's Research Hospital, Memphis, TN 38105, USA.

*To whom correspondence should be addressed. E-mail: james.downing@stjude.org

Single-nucleotide polymorphism (SNP) arrays have enabled genome-wide analyses of DNA CNAs and loss of heterozygosity (LOH) in cancer and have provided important insights into the pathogenesis of newly diagnosed ALL. We previously reported multiple recurring somatic CNAs in genes encoding transcription factors, cell cycle regulators, apoptosis mediators, lymphoid signaling molecules, and drug receptors in B-progenitor and T-lineage ALL (B-ALL and T-ALL) (*8*, *9*). To gain insights into the molecular lesions responsible for ALL relapse, we have now performed genome-wide CNA and LOH analyses on matched diagnostic and relapse bone marrow samples from 61 pediatric ALL patients (table S1). These samples included 47 B-ALL and 14 T-ALL cases (*10*). Samples were flow-sorted to ensure at least 80% tumor cell purity before DNA extraction (fig. S1). DNA copy number and LOH data were obtained using Affymetrix SNP 6.0 (47 diagnosis-relapse pairs) or 500K arrays (14 pairs). Remission bone marrow samples were also analyzed for 48 patients (table S1).

These analyses identified a mean of 10.8 somatic CNAs per B-ALL case and 7.1 CNAs per T-ALL case at diagnosis (table S4 and figs. S2 and S4). Of the B-ALL cases at diagnosis, 48.9% had CNAs in genes known to regulate B-lymphoid development, including *PAX5* ($N = 12$), *IKZF1* ($N = 12$), *EBF1* ($N = 2$), and *RAG1/2* ($N = 2$) (tables S5, S6, and S9). Deletion of *CDKN2A/B* was present in 36.2% of B-ALL and 71.4% T-ALL cases, and deletion

of *ETV6* was present in 11 B-ALL cases. We also identified novel CNAs involving *ARID2*, which encodes a member of a chromatin-remodeling complex (*11*); the cyclic adenosine monophosphate–regulated phosphoprotein *ARPP-21*; the cytokine receptor genes *IL3RA* and *CSF2RA* (fig. S3); and the Wnt/β-catenin pathway genes *CTNNB1*, *WNT9B*, and *CREBBP* (tables S5 and S6).

Although evidence for clonal evolution and/or selection at relapse has been reported (*4*, *6*, *7*, *12*–*21*), we observed a striking degree of change in the number, extent, and nature of CNAs between diagnosis and relapse in paired samples of ALL. A significant increase in the mean number of CNAs per case was observed in relapse B-ALL samples (10.8 at diagnosis versus 14.0 at relapse, $P = 0.0005$), with the majority being additional regions of deletion (6.8 deletions per case at diagnosis versus 9.2 deletions per case at relapse, $P = 0.0006$; 4.0 gains per case at diagnosis versus 4.8 gains per case at relapse, $P = 0.03$; table S4 and fig. S4). By contrast, no significant changes in lesion frequency were observed in T-ALL (table S4).

The majority (88.5%) of relapse samples harbored at least some of the CNAs present in the matched diagnosis sample, indicating a common clonal origin (table S5 and fig. S5); however, 91.8% exhibited a change in the pattern of CNAs from diagnosis to relapse (table S7). Of these, 34% acquired new CNAs, 12% showed loss of lesions present at diagnosis, and 46% both acquired new lesions and lost lesions present at diagnosis. In 11% of relapsed samples (three B-ALL and four T-ALL cases), all CNAs present at diagnosis were lost at relapse, raising the possibility that the relapse represents the emergence of a second unrelated leukemia. One case (BCR-ABL-SNP-15) retained the same translocation at relapse, indicating a common clonal origin. In four cases, lack of similarity of the patterns of deletion at immunoglobulin (Ig) and T cell antigen receptor (TCR) gene loci, or lack of deletions at these loci, suggested that relapse represented the emergence of a distinct leukemia (see below and figs. S6 and S7). For all other relapse cases (86%), analysis of Ig and TCR deletions demonstrated a clonal relationship between diagnostic and relapse samples (table S21 and fig. S6).

The genes most frequently affected by CNAs acquired at relapse were *CDKN2A/B*, *ETV6*, and regulators of B cell development (Table 1, Fig. 1, tables S8 to S18, and fig. S8). Sixteen B-ALL and two T-ALL cases acquired new CNAs of *CDKN2A/B*, 10 of which lacked *CDKN2A/B* deletions at diagnosis (Fig. 1, A and B, and tables S17 and S18). The *CDKN2A/B* deletions acquired at relapse were biallelic in 70% of cases, resulting in a complete loss of expression of all three encoded proteins: INK4A (p16), ARF (p14), and INK4B (p15). Deletion of *ETV6*, a frequent abnormality at diagnosis in *ETV6-RUNX1* B-ALL (*8*, *19*), was also common in relapsed ALL, being identified in 11 cases (10 B-ALLs and one T-ALL) with only one case *ETV6-RUNX1*–positive (fig. S8). Mutations of genes regulating B cell development are common at

Table 1. Targets of relapse-acquired CNAs in ALL, ranked in order of frequency.

Lesion		B-progenitor ALL	T-lineage ALL
Deletion	*CDKN2A*	16	2
	ETV6	10	1
	IKZF1	5	2
	NR3C1	4	0
	TCF3	3	0
	DMD	2	0
	ARPP-21	2	0
	BTLA/CD200	2	1
	RAG1/2	2	0
	IKZF2	1	1
	ADD3	1	0
	C20orf94	1	0
	TBL1XR1	1	0
	IKZF3	1	0
Gain	*MYB*	0	2
	DMD	1	0

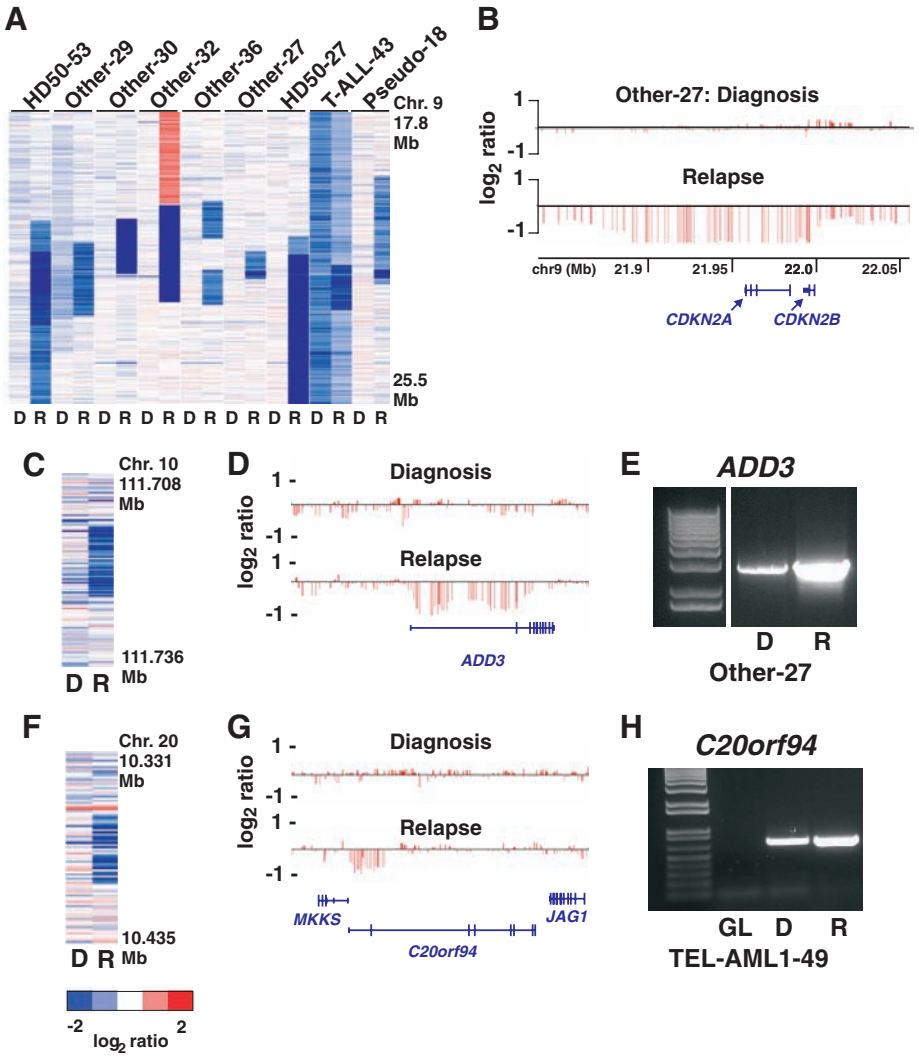

Fig. 1. Deletions of *CDKN2A/B* and lesion-specific backtracking in relapsed ALL. (**A**) Log_2 ratio Affymetrix SNP 6.0 copy number data (median smoothed with a window of five markers; blue is deletion and red is gain) of chromosome 9p flanking *CDKN2A/B* for nine representative cases showing new or more extensive deletions at this locus at relapse. Deletions in selected cases were confirmed by quantitative genomic PCR (table S17). (**B**) Coverage of the locus for one case. Each vertical red line represents the genomic position and log_2 ratio copy number of an individual marker. This case has acquired a homozygous deletion involving exon 2 of *CDKN2B* and all of *CDKN2A* at relapse. (**C** to **H**) Backtracking of CNAs by lesion-specific genomic PCR assays in ALL [(C) to (E), *ADD3*; (F) to (H), *C20orf94*]. Log_2 ratio copy number heat maps for diagnosis and relapse samples are shown in (C) and (F); genomic locations of SNP probes and regions of deletion are shown in (D) and (G). In (E) and (H), PCR for each lesion was performed for diagnosis, relapse, and (where available) germline DNA samples. In each case, a CNA-specific PCR product was observed at diagnosis as well as relapse, indicating that each CNA was present at diagnosis.

diagnosis in B-ALL (*8*), and additional lesions in this pathway were observed at relapse, with a number of cases acquiring multiple hits within the pathway (table S9). Four cases lacked CNAs in this pathway at diagnosis but acquired deletions in *PAX5* ($N = 1$), *IKZF1* ($N = 2$), or *TCF3* ($N = 1$) at relapse. Eleven cases with CNAs in this pathway at diagnosis acquired additional lesions at relapse, most commonly *IKZF1* (five cases), *IKZF2* (two cases), and *IKZF3* (one case) (figs. S9 and S10). New CNAs were also observed in *PAX5* ($N = 3$), *TCF3* ($N = 3$), *RAG1/2* ($N = 2$; figs. S9 and S10), and *EBF1* ($N = 1$; fig. S9). CNAs involving genes that encode regulators of lymphoid development were also observed in four T-ALL relapse samples, but these involved the early lymphoid regulators *IKZF1* ($N = 2$), *IKZF2* ($N = 1$), and *LEF1* ($N = 2$; table S9), rather than B lineage–specific genes such as *PAX5* and *EBF1*.

A number of other less frequent CNAs previously detected in diagnostic ALL samples (*8*) were also observed as new lesions at relapse, including CNAs of *ADD3*, *ARPP-21*, *ATM*, *BTG1*, *CD200/BTLA*, *FHIT*, *KRAS*, *IL3RA/CSF2RA*, *NF1*, *PTCH*, *TBL1XR1*, *TOX*, *WT1*, *NR3C1*, and *DMD* (table S8 and fig. S11). Progression of intrachromosomal amplification of chromosome 21, a poor prognostic marker in childhood ALL (*22*), was also observed in two B-ALL cases (fig. S12). In addition, relapsed T-ALL was remarkable for the loss and acquisition of sentinel lesions, including the loss of *NUP214-ABL1* in one case, and the acquisition of *NUP214-ABL1*, *LMO2*, and *MYB* amplification (one case each) at relapse (*8*, *23*–*25*) (table S8 and fig. S13).

In addition to defining CNAs, we performed an analysis of regions of copy-neutral LOH (CN-LOH) that can signify mutated, reduplicated genes. CN-LOH acquired at relapse was identified in only 15 B-ALL and three T-ALL cases (table S19). The most common region involved was chromosome 9p ($N = 8$), which in each case contained a homozygous *CDKN2A/B* deletion consistent with reduplication of a hemizygous *CDKN2A/B* deletion.

To determine which biologic pathways were most frequently targeted by relapse-acquired CNAs, we categorized each gene contained within altered genomic regions into one or more of 148 biologic pathways. The pathways were then assessed for their frequency of involvement by CNAs across the data set with the use of Fisher's exact test (*10*). This analysis identified cell cycle regulation and B cell development as the most common pathways targeted at relapse (table S20).

There was a clear clonal relationship between the diagnosis and relapse ALL samples in most cases (93.6% of B-ALL and 71.4% of T-ALL cases). This suggests that the relapse-associated CNAs either (i) were present at low levels at diagnosis and selected for at relapse, or (ii) were acquired as new genomic alterations after initial therapy. To explore these possibilities, we mapped the genomic breakpoints of several CNAs acquired at relapse (*ADD3*, *C20orf94*, *DMD*, *ETV6*, *IKZF2*, and *IKZF3*) and developed lesion-specific polymerase chain reaction (PCR) assays. Evidence of the relapse clone was detected in 7 of 10 diagnosis samples analyzed (Fig. 1, C to H, and figs. S14 and S15). Thus, the relapse clone is frequently present as a minor subpopulation at diagnosis.

By carefully analyzing the changes in CNAs between matched diagnostic and relapse samples, we were able to map their evolutionary relationship (Fig. 2). In a minority of cases, "relapse" is a misnomer, as no CNAs were shared by the diagnostic and relapse clones. The recurrent disease in these cases represents either a secondary leukemia or a leukemia arising from an ancestral clone that lacks any of the CNAs present in the diagnosis leukemia. In 8% of the cases, there were no differences in CNAs between the diagnostic and relapse clones, whereas in 34% of the cases, relapse represented clonal evolution of the diagnosis leukemic populations. Remarkably, in about half of the cases, the relapse clone was derived from an ancestral, prediagnosis leukemic precursor cell and not from the clone predominating at diagnosis. One illustrative case (Other-SNP-29) had two relapse-acquired deletions (*ETV6* and *DMD*), only one of which was present in the diagnostic sample as a minor clone (*ETV6*, fig. S15), indicating that these lesions were acquired at different stages of evolution of the relapse clone. This case provides unequivocal evidence of a common ancestral clone that gave rise to the major clone at diagnosis, and to a second clone that was present as a minor population at diagnosis but acquired different genetic alterations before emerging as the relapse clone.

These results complement those of previous studies examining individual genetic loci in relapsed ALL (*6*, *14*, *16*, *20*, *21*, *26*–*28*) and provide important insights into the spectrum of genetic lesions that underlie this process. Although our data are limited to a single class of mutations (CNAs), they show that no single genetic lesion or alteration of a single pathway is responsible for relapse. Moreover, global genomic instability does not appear to be a prevalent mechanism. Instead, a diversity of mutations appear to contribute to relapse, with the most common alterations targeting key regulators of tumor suppression, cell cycle control, and lymphoid/B cell development. Notably, few lesions involved genes with roles in drug import, metabolism, export, and/or response (an exception being the glucocorticoid receptor gene *NR3C1*), which suggests that the mechanism of relapse is more complex than simple "drug resistance."

The diversity of genes that are targeted by relapse-associated CNAs, coupled with the presence of the relapse clone as a minor subpopulation at diagnosis that escapes drug-induced killing, represent formidable challenges to the development of effective therapy for relapsed ALL. Nonetheless, our study has identified several common pathways that may contain rational

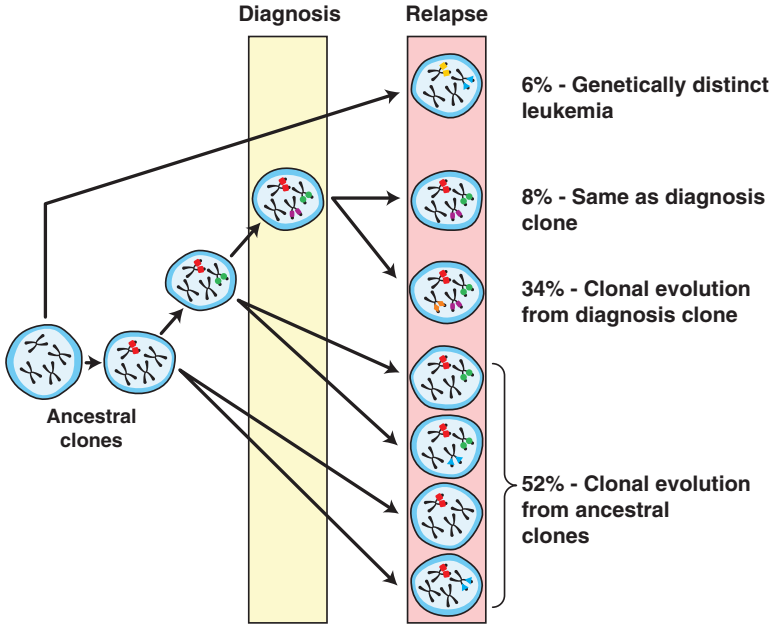

Fig. 2. Clonal relationship of diagnosis and relapse samples in ALL. The majority of relapse cases have a clear relationship to the diagnosis leukemic clone, either arising through the acquisition of additional genetic lesions or, more commonly, arising from an ancestral (prediagnosis) clone. In the latter scenario, the relapse clone acquires new lesions while retaining some but not all of the lesions found in the diagnostic sample. Lesion-specific backtracking studies revealed that in most cases the relapse clone exists as a minor subclone within the diagnostic sample before the initiation of therapy. In only a minority of ALL cases does the relapse clone represent the emergence of a genetically distinct and thus unrelated second leukemia.

targets against which novel therapeutic agents can be developed.

References and Notes

1. C. H. Pui, L. L. Robison, A. T. Look, *Lancet* **371**, 1030 (2008).
2. H. G. Einsiedel *et al.*, *J. Clin. Oncol.* **23**, 7942 (2005).
3. G. K. Rivera *et al.*, *Cancer* **103**, 368 (2005).
4. S. C. Raimondi, C. H. Pui, D. R. Head, G. K. Rivera, F. G. Behm, *Blood* **82**, 576 (1993).
5. E. Klumper *et al.*, *Blood* **86**, 3861 (1995).
6. K. W. Maloney, L. McGavran, L. F. Odom, S. P. Hunger, *Blood* **93**, 2380 (1999).
7. J. A. Irving *et al.*, *Cancer Res.* **65**, 3053 (2005).
8. C. G. Mullighan *et al.*, *Nature* **446**, 758 (2007).
9. C. G. Mullighan *et al.*, *Nature* **453**, 110 (2008).
10. See supporting material on *Science* Online.
11. Z. Yan *et al.*, *Genes Dev.* **19**, 1662 (2005).
12. J. J. Taylor *et al.*, *Leukemia* **8**, 60 (1994).
13. G. M. Marshall *et al.*, *Leukemia* **9**, 1847 (1995).
14. F. Davi, C. Gocke, S. Smith, J. Sklar, *Blood* **88**, 609 (1996).
15. R. Rosenquist *et al.*, *Eur. J. Haematol.* **63**, 171 (1999).
16. A. M. Ford *et al.*, *Blood* **98**, 558 (2001).
17. G. Germano *et al.*, *Leukemia* **17**, 1573 (2003).
18. S. Takeuchi *et al.*, *Oncogene* **22**, 6970 (2003).
19. J. Zuna *et al.*, *Clin. Cancer Res.* **10**, 5355 (2004).
20. E. R. Panzer-Grumayer *et al.*, *Clin. Cancer Res.* **11**, 7720 (2005).
21. S. Choi *et al.*, *Blood* **110**, 632 (2007).
22. A. V. Moorman *et al.*, *Blood* **109**, 2327 (2007).
23. C. Graux *et al.*, *Nat. Genet.* **36**, 1084 (2004).
24. I. Lahortiga *et al.*, *Nat. Genet.* **39**, 593 (2007).
25. E. Clappier *et al.*, *Blood* **110**, 1251 (2007).
26. A. Beishuizen *et al.*, *Blood* **83**, 2238 (1994).
27. M. Peham *et al.*, *Genes Chromosomes Cancer* **39**, 156 (2004).
28. M. Konrad *et al.*, *Blood* **101**, 3635 (2003).

29. We thank R. Ashmun and the St. Jude Flow Cytometry and Cell Sorting Shared Resource for flow sorting of leukemia samples, the St. Jude Clinical Applications Core Technology Laboratory for performing SNP arrays, L. Kiedrowski for lesion mapping and backtracking assays, and J. Stokes for assistance with artwork. Supported by the American Lebanese Syrian Associated Charities of St. Jude Children's Research Hospital and by the National Health and Medical Research Council of Australia (C.G.M.). Primary SNP array data are available from the authors upon request. J.R.D. has participated in gene expression profiling research sponsored by Roche. C.G.M. and J.R.D. have filed a patent application related to this work.

Supporting Online Material

www.sciencemag.org/cgi/content/full/322/5906/1377/DC1
Materials and Methods
SOM Text
Figs. S1 to S15
Tables S1 to S21
References

6 August 2008; accepted 27 October 2008
10.1126/science.1164266

A Genetic Framework for the Control of Cell Division and Differentiation in the Root Meristem

Raffaele Dello Ioio,[1] Kinu Nakamura,[2]* Laila Moubayidin,[1]* Serena Perilli,[1]* Masatoshi Taniguchi,[2] Miyo T. Morita,[3] Takashi Aoyama,[2] Paolo Costantino,[1] Sabrina Sabatini[1]†

Plant growth and development are sustained by meristems. Meristem activity is controlled by auxin and cytokinin, two hormones whose interactions in determining a specific developmental output are still poorly understood. By means of a comprehensive genetic and molecular analysis in *Arabidopsis*, we show that a primary cytokinin-response transcription factor, ARR1, activates the gene *SHY2/IAA3* (*SHY2*), a repressor of auxin signaling that negatively regulates the *PIN* auxin transport facilitator genes: thereby, cytokinin causes auxin redistribution, prompting cell differentiation. Conversely, auxin mediates degradation of the SHY2 protein, sustaining PIN activities and cell division. Thus, the cell differentiation and division balance necessary for controlling root meristem size and root growth is the result of the interaction between cytokinin and auxin through a simple regulatory circuit converging on the *SHY2* gene.

Postembryonic root growth is sustained by the root meristem. Stem cells in the root meristem generate transit-amplifying cells, which undergo additional division in the proximal meristem, and differentiate at the meristem transition zone that encompasses the boundary between dividing and expanding cells in the different cell files (Fig. 1A). For meristem maintenance, the rate of cell differentiation must equal the rate of generation of new cells: How this balance is achieved is a central question in plant development.

Classic plant tissue culture experiments showed that auxin and cytokinin are key signaling molecules controlling meristems activity because they antagonistically affect, in vitro, shoot and root organogenesis (*1*, *2*). Recently, the in vivo importance of the cytokinin and auxin antagonistic interaction has been proven during *Arabidopsis* root meristem size determination (*3*) and for embryonic root stem cell niche specification (*4*), but the genetic and molecular basis of this interaction remains to be clarified.

The expression domains of the genes encoding the two-component cytokinin signaling pathway, the AHK3 receptor kinase and the ARR1 and ARR12 transcription factors, and the root meristem phenotype of *ahk3*, *arr1*, and *arr12* mutants demonstrate that cytokinin acts at the transition zone to control cell differentiation rate (*3*, *5*, *6*). Furthermore, the expression patterns of cytokinin biosynthesis genes (*7*) and experiments of tissue- and spatial-specific cytokinin depletion in the root meristem showed that cytokinin specifically acts at the vascular tissue transition zone, where it controls the differentiation rate of all the other root cells by antagonizing a non–cell-autonomous signal that we suggested may be auxin (*3*). On the other hand, experiments of exogenous application of auxin and the effects of mutations in the PIN auxin efflux facilitators are consistent with a role of auxin in controlling cell division (*3*, *8*). Thus, the size of the root meristem may be established by a balance between the antagonistic effects of cytokinin, which mediates cell differentiation, and auxin, which mediates cell division.

In order to dissect the cytokinin-auxin interaction in the root meristem, we sought to identify the gene(s) immediately responsive to cytokinin signaling. Cytokinin control of root meristem size is mediated by both ARR1 and the ARR12 transcription factors, specifically expressed at the root transition zone and acting, respectively, early and late during meristem development (*3*). Whereas the root meristems of *arr12* mutants were larger than those of wild type but eventually stopped growing, *arr1* mutant meristems kept increasing in size over time (*3*). ARR1 seems therefore to have a critical role in determining root meristem size, and thus we set to verify whether this transcription factor alone would be sufficient to control cell differentiation and root meristem size. To this aim, we checked the root phenotype of plants harboring a glucocorticoid-inducible construct of ARR1 (*35S::ARR1ΔDDK:GR*) (*9*). As in the case of exogenous cytokinin applications (*3*), root meristems of *35S::ARR1ΔDDK:GR* plants were significantly reduced after 8 hours of dexamethasone (a glucocorticoid derivative) induction, suggesting that ARR1 is capable alone of controlling root meristem size (fig. S1, A and B).

The same *35S::ARR1ΔDDK:GR* construct had been previously used to identify a number of putative direct-target genes of the ARR1 transcription factor (*10*). Among the 23 putative targets of ARR1 (*10*), there is notably *SHY2*, a member of the auxin/indole-3-acetic acid inducible (*Aux/IAA*) family of genes (*11*) that act as auxin-response inhibitors by forming heterodimers with the ARF (auxin response factor) transcription factors, thereby preventing activation of auxin-responsive genes (among which are the *Aux/IAA* genes) by these latter (*12*, *13*). Auxin causes the

[1]Dipartimento di Genetica e Biologia Molecolare, Laboratorio di Genomica e proteomica funzionale dei sistemi modello (FGPL), Università La Sapienza - Piazzale Aldo Moro 5, 00185 Rome, Italy. [2]Institute for Chemical Research, Kyoto University, Uji, Kyoto 611-0011, Japan. [3]Graduate School of Biological Sciences, Nara Institute of Science and Technology, Ikoma, 630-0101, Japan.

*These authors contributed equally to this work.
†To whom correspondence should be addressed. E-mail: sabrina.sabatini@uniroma1.it

degradation of the Aux/IAA proteins via the SKIP-CULLIN-FBOX and transport inhibitor response 1 (SCF^{TIR1}) ubiquitin-ligase complex, thus releasing the ARFs from inhibition (*13*). Degradation of the Aux/IAA proteins and consequent ARF activity depend on auxin concentration: High concentration of auxin causes Aux/IAA degradation, whereas at low auxin concentration these proteins are stable and interact with the ARFs (*13*).

The presence of *SHY2* among the putative targets of ARR1 suggests that, in determining root meristem size, cytokinin antagonizes auxin by modulating auxin signaling.

To verify this hypothesis, we analyzed the root-meristem phenotype of *shy2* gain- and loss-of-function mutants (*14*, *15*). The *shy2-2* gain-of-function mutant allele displayed a shorter root (*14*, *15*) (fig. S1D) and a reduced root meristem size already 2 days after germination (Fig. 1, C and D), which phenocopied the effects of application of cytokinin and of induction of *35S::ARR1ΔDDK:GR*. On the contrary, the *shy2-31* loss-of-function mutant allele (*15*) showed an increased number of meristematic cells and kept accumulating cells in the meristem 5 days after germination, vastly exceeding the fixed number of cells of wild-type meristems (Fig. 1, B and D). The increased size of the root meristem correlated with an enhanced rate of root growth and resulted in a longer root (fig. S1D). Because the *shy2-31* roots closely resembled *arr1* mutant roots, we constructed and analyzed *arr1,shy2-2* and *arr1,shy2-31* double mutant plants. The root meristem sizes of both *arr1,shy2-2* and *arr1,shy2-31* double mutants were indistinguishable from that of the *arr1* mutant (fig. S1E), supporting the notion that the SHY2 protein may act downstream of the ARR1 transcription factor.

To substantiate the suggested regulatory role of ARR1 on the *SHY2* gene, we compared the expression of this gene in wild-type and *arr1* mutant roots by using a *SHY2::GUS* promoter fusion (*11*, *16*). In wild-type root meristems, the activity of this fusion was specifically detected at the vascular tissue transition zone (*16*) (Fig. 1E and fig. S4J) and was strongly induced by cytokinin treatment (Fig. 1F). This induction of *SHY2* promoter activity was matched by a corresponding accumulation of the SHY2 protein, as visualized by Western blot analysis of a transgenic line harboring a Myc-epitope–tagged SHY2 protein (*16*) (fig. S3A). In contrast, in the *arr1* mutant background SHY2::GUS activity was hardly detectable and did not show any increase upon cytokinin treatment (Fig. 1G), confirming that activation of the *SHY2* promoter in roots depends on ARR1.

To assess whether *SHY2* is necessary and sufficient to mediate the cytokinin control of root meristem size, we analyzed the root phenotype of the *shy2-31* loss-of-function mutant harboring the *35S::ARR1ΔDDK:GR* construct. The *shy2-31*, *35S::ARR1ΔDDK:GR* roots did not show any reduction in size after 8 hours of dexamethasone induction (fig. S1, A to C), suggesting that *SHY2* alone mediates the effect of ARR1 in response to cytokinin to control root meristem size.

The genetic evidence provided establishes a regulatory interaction between ARR1 and *SHY2*. To confirm the physical interaction between the ARR1 protein and the *SHY2* promoter in vivo, we

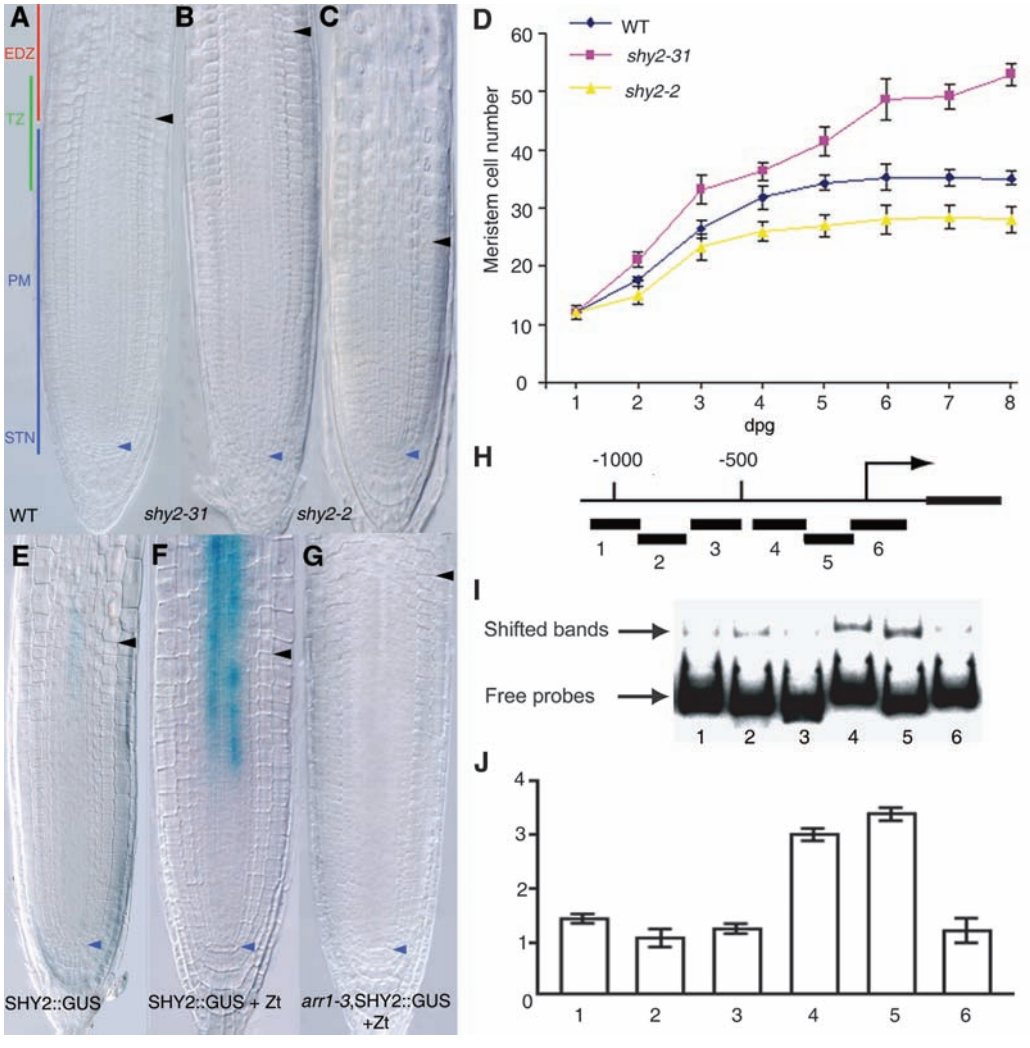

Fig. 1. The *SHY2* gene controls root meristem size and is a direct regulatory target of ARR1. (**A** to **C**) Five-days-postgermination (dpg) root meristems of wild-type (A), *shy2-31* loss-of-function mutant (B), and *shy2-2* gain-of-function mutant (C). Root meristem size is expressed as the number of cortex cells in a file extending from the quiescent center (blue arrowheads) to the first elongated cortex cell (black arrowheads). STN indicates stem cell niche, PM, proximal meristem; EDZ, elongation-differentiation zone; and TZ, transition zone. The transition zone is different for each cell type, giving a jagged shape to the boundary between dividing and expanding cells. (**D**) Root meristem cell number of wild-type, *shy2-2*, and *shy2-31* mutants depicted in (A) to (C), measured over time. (**E** to **G**) Expression of the SHY2::GUS construct in wild-type roots (E), in roots treated 3 hours with 5 μM transzeatin (Zt) and stained for 6 hours (F), and in the *arr1-3* mutant treated 3 hours with 5 μM Zt and stained for 6 hours (G). (**H**) Schematic representation of the *SHY2* promoter region. Thick and thin lines correspond to coding and noncoding regions, respectively. The bent arrow indicates the transcription start site. Bars with numbers illustrate the DNA fragments used in both ChIP (J) and gel mobility shift analyses (I). (**I**) Gel mobility shift analysis. Labeled DNA fragments were subjected to gel mobility shift analysis with a fusion protein consisting of GST and ARR1 DNA binding domain. (**J**) ChIP analysis. Chromatin preparations from ARR1:GFP and wild-type (negative control) roots were coimmunoprecipitated with anti-GFP antibody. An enrichment fold of each fragment was obtained by normalizing the recovery rate for the ARR1:GFP preparation against that for the negative control preparation (*24*). Error bars indicate SE.

performed chromatin immunoprecipitation (ChIP) assays using roots expressing an ARR1:GFP (green fluorescent protein) fusion protein under the control of the *ARR1* promoter. Two DNA fragments in the *SHY2* promoter region (fragments 4 and 5 in Fig. 1, H and J) but not those in the promoter of a negative control gene, *TUA4* (fig. S2, A and B), were significantly enriched by co-immunoprecipitation with anti-GFP using fragmented chromatin prepared from ARR1:GFP roots as compared with the preparation from wild-type roots. As in the case of the promoter region of *ARR6*, a direct target-gene of ARR1 (*9*), the enrichment of DNA fragments was correlated with the binding affinity of the fragments to the ARR1 DNA binding domain in an in vitro gel mobility shift analysis (Fig. 1, I and J, and fig. S2, C and D), supporting the evidence that ARR1 specifically bound to the *SHY2* promoter in vivo. The interaction was confirmed to be sequence-specific by gel mobility shift analysis with specific and nonspecific competitors and deoxyribonuclease (DNase) I footprinting analysis (fig. S2, E to G).

These data confirm that *SHY2* is a direct regulatory target of the ARR1 transcription factor and provide support for the suggestion that cytokinin antagonizes auxin at the vascular tissue transition zone by modulating auxin signaling and thus determines root meristem size.

The existence of a positive feedback loop between auxin and the PIN auxin-transport facilitators had been established (*17*), and we had previously reported that cytokinin, acting from the vascular tissue transition zone, requires polar auxin transport to determine the transition zone of all other tissues (*3*). Thus, we asked whether *SHY2* activation by cytokinin, and the resulting reduction of auxin response at the vascular tissue transition zone, would interfere with the activity of the *PIN* genes in order to control root meristem size.

We first monitored the effect of application of exogenous cytokinin on the expression of the *PIN1*, *PIN3*, and *PIN7* genes. These particular *PIN* genes were chosen because they are expressed in the vascular tissue transition zone (*17*) and because a role for these genes in controlling root meristem size has already been established (*3*, *7*); in fact, the triple *pin1,pin3,pin7* mutant displays a short root meristem (*7*) and is cytokinin-resistant (fig. S3B). Real-time quantitative reverse transcription polymerase chain reaction (qRT-PCR) showed that 4 hours of cytokinin treatment were sufficient to significantly reduce expression of *PIN1*, *PIN3*, and *PIN7* (Fig. 2J), whereas cytokinin-mediated reduction in root meristem size was first detectable only after 12 hours of exposure to cytokinin (fig. S3B). Notably, as visualized by PIN:GFP translational reporter fusions (*8*, *18*), down-regulation of *PIN* genes was particularly evident in the vascular tissue transition zone (Fig. 2, B, E, and H).

To assess whether this cytokinin-dependent down-regulation of the *PIN1*, *PIN3*, and *PIN7* genes was mediated by the AHK3/ARR1 sig-

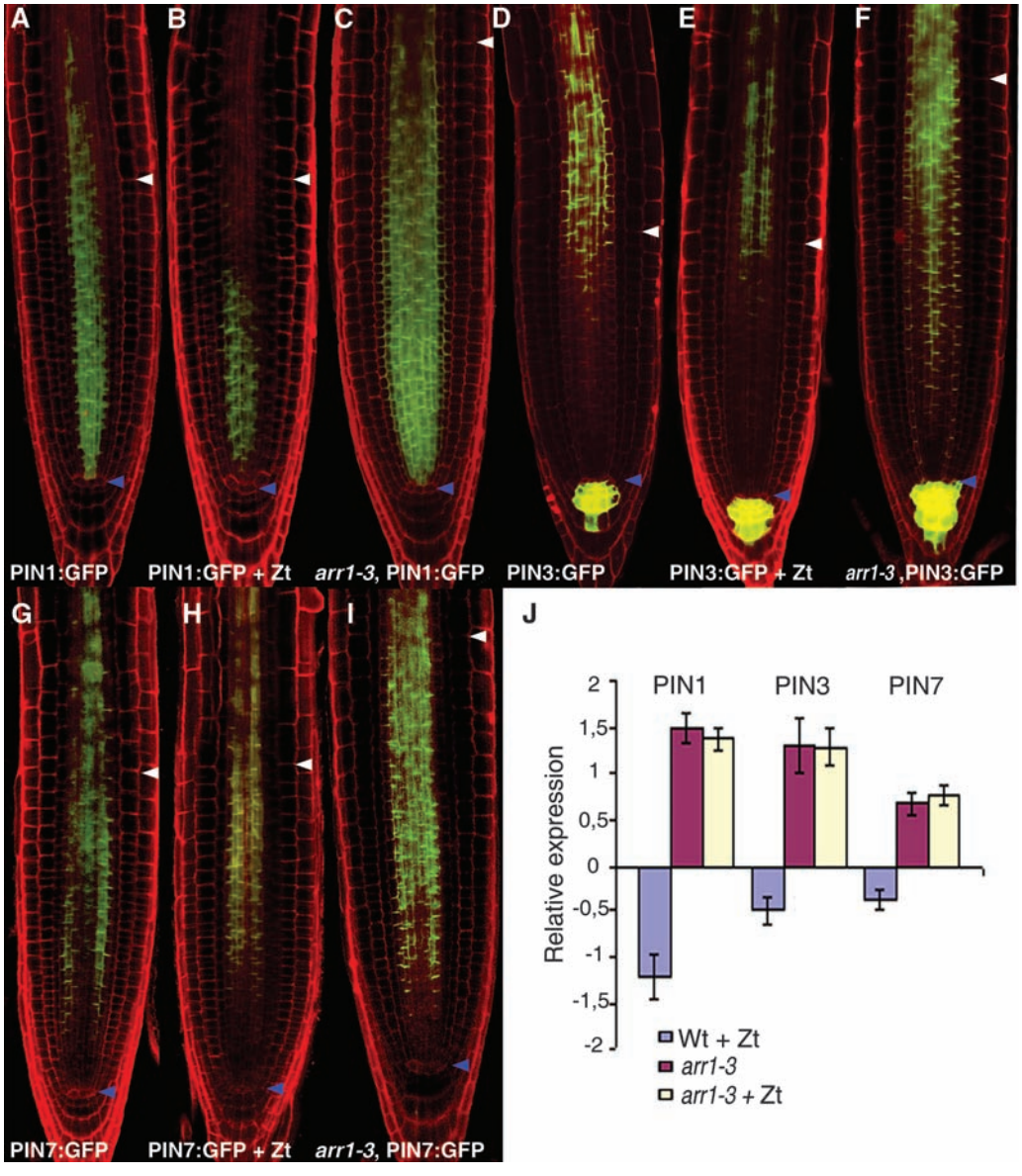

Fig. 2. Cytokinin perception at the vascular tissue transition zone controls root meristem size restricting PIN1, PIN3, and PIN7 expression domain. (**A**, **D**, and **G**) Five-dpg wild-type root meristems expressing, respectively, PIN1:GFP, PIN3:GFP, and PIN7:GFP. (**B**, **E**, and **H**) Reduction of PIN expression in cytokinin-treated roots (5 μM Zt, 6 hours) expressing, respectively, PIN1:GFP, PIN3:GFP, and PIN7:GFP. No reduction in root meristem size is still detectable. (**C**, **F**, and **I**) PIN expression in the *arr1-3* mutant root meristem expressing, respectively, PIN1:GFP, PIN3:GFP, and PIN7:GFP. In the *arr1-3* mutant, the PIN expression domain at the vascular tissue transition zone is expanded (white arrowheads). Blue arrowheads indicate quiescent center cells; white arrowheads indicate cortex transition zone. (**J**) qRT-PCR confirm *PINs* gene mRNA down-regulation after 4 hours of cytokinin treatment (5 μM Zt) in wild-type roots, up-regulation in the *arr1-3* mutant background, and no down-regulation in the *arr1-3* mutant upon cytokinin treatment. Relative expression is normalized to *ACTIN*, and 0 corresponds to *PINs* mRNA amount in untreated wild-type roots. Error bars, SD; $P < 0.5$; Student's *t* test; $n = 3$.

naling pathway, we monitored the expression and distribution of *PIN* mRNAs in the *ahk3* and *arr1* mutant backgrounds. The expression of the three *PIN* mRNAs was higher in the *ahk3* and *arr1* mutants (Fig. 2J and fig. S4K) and the PIN expression domains in the vascular tissue transition zone were expanded as compared with the wild type (Fig. 2, C, F, and I, and fig. S4, B, E, and H). Furthermore, no reduction in root meristem size (fig. S3B) and no down-regulation of *PIN1*, *PIN3*, and *PIN7* were observed in the *ahk3* and *arr1* mutant backgrounds in response to cytokinin treatment (Fig. 2J and fig. S4, C, F, I, and K). Thus, perception of cytokinin at the root vascular tissue transition zone, mediated by the AHK3/ARR1 signaling pathway, down-regulates the *PIN1*, *PIN3*, and *PIN7* genes and restricts their expression domain.

To assess whether this *PIN* down-regulation depended on *SHY2* activation by cytokinin, we monitored the expression and distribution of *PIN1*, *PIN3*, and *PIN7* mRNAs in the *shy2-31* loss-of-function mutant background. PIN::GFP fusion analysis (Fig. 3, B, E, and H) and real-time qRT-PCR (Fig. 3J) showed that, as in the case of the *ahk3* and *arr1* mutants described above, the expression of *PIN1*, *PIN3*, and *PIN7* in the *shy2-31* mutant was increased and expression domains expanded at the vascular tissue transition zone as compared with the expression of wild type. Furthermore, no down-regulation of the *PIN* genes and no root meristem reduction were observed in the *shy2-31* mutant in response to cytokinin (Fig. 3, C, F, I, and J, and fig. S3B). On the contrary, the expression of *PIN1*, *PIN3*, and *PIN7* mRNAs was lower in the *shy2-2* gain-of-function mutant (fig. S5H).

To further substantiate the regulatory role of the SHY2 protein on the expression of the *PIN* genes, we transiently expressed a nondegradable version of the SHY2 protein under a heat-shock promoter (*HS::shy2-6*) (*15*) and recorded changes in *PIN1*, *PIN3*, and *PIN7* gene expression by real-time qRT-PCR. Induction of *HS::shy2-6* for 1 hour was sufficient to reduce the expression of *PIN1*, *PIN3*, and *PIN7* (Fig. 3K), and the consequent reduction of root meristem size was observed after 3 hours (fig. S5, E to G). These data suggest that the activation of *SHY2* by cytokinin at the vascular tissue transition zone restricts the expression of *PIN1*, *PIN3*, and *PIN7* to the vascular tissue transition zone and that this is necessary to position the transition zone of all other tissues of the root.

It had been shown that auxin controls root meristem size, sustaining the activity of the *PIN* genes as well as cell division (*3*, *8*). Accordingly, exogenous application of auxin to wild-type roots during growth caused an increase in meristem size detectable after 24 hours of exposure to auxin (fig. S5, A, B, and G), whereas 12 hours of auxin treatment were sufficient to induce the expression of *PIN1*, *PIN3*, and *PIN7* (fig. S5H).

We then asked whether this up-regulation was the result of the auxin-dependent SHY2 protein degradation via the SCF^{TIR1} ubiquitin-ligase complex (fig. S3A) (*13*, *19*). No up-regulation of the *PIN* genes and no increase of meristem size (i.e., cell division) upon application of auxin were

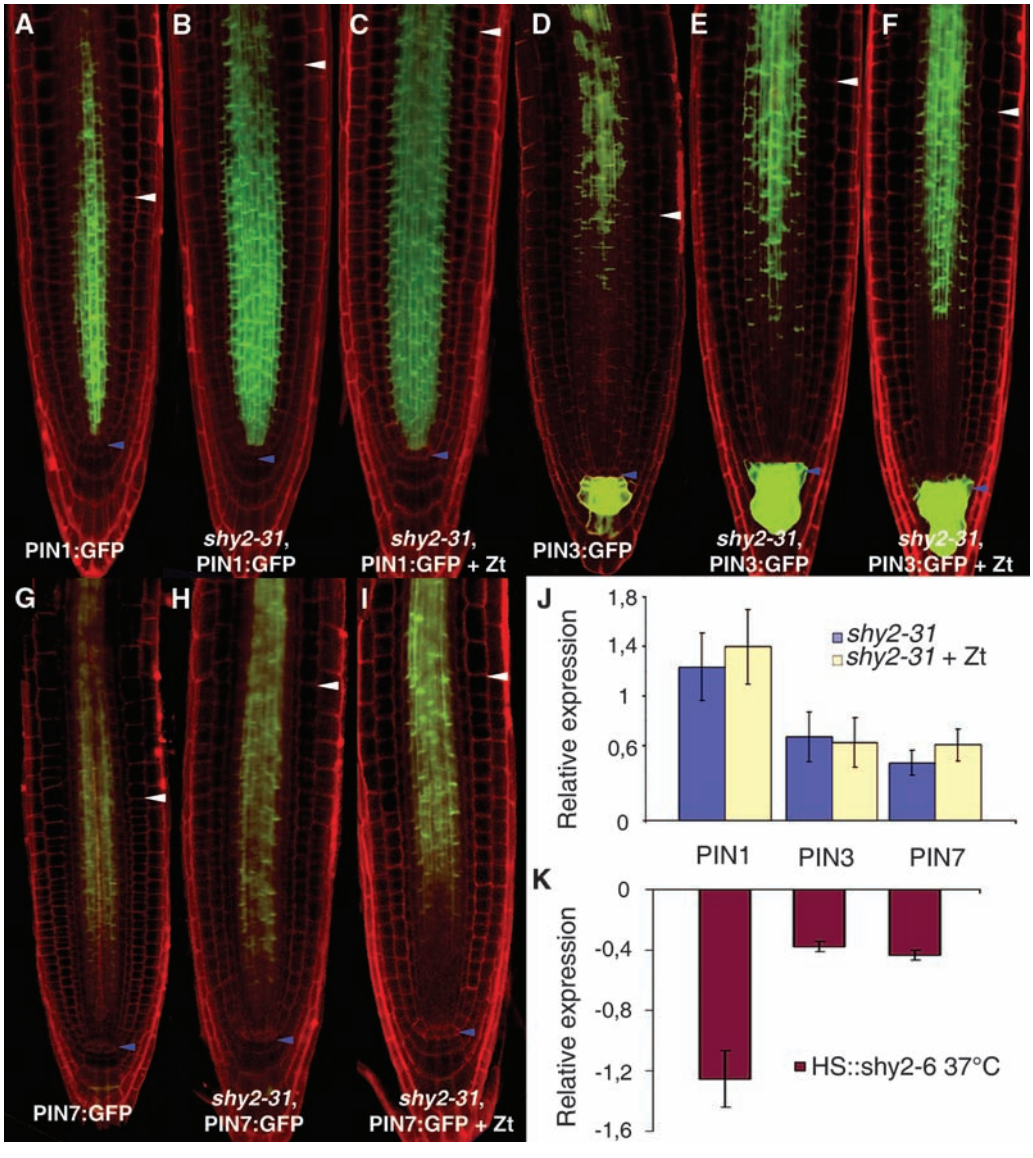

Fig. 3. Cytokinin-mediated *SHY2* gene induction at the vascular tissue transition zone controls root meristem size restricting the PIN1, PIN3, and PIN7 expression domain. (**A**, **D**, and **G**) Five-dpg wild-type root meristem expressing, respectively, PIN1:GFP, PIN3:GFP, and PIN7:GFP. (**B**, **E**, and **H**) Five-dpg *shy2-31* root meristems expressing, respectively, PIN1:GFP, PIN3:GFP, and PIN7:GFP. PIN expression domain at the vascular tissue transition zone is expanded (white arrowheads). (**C**, **F**, and **I**) No change in PIN expression in cytokinin-treated *shy2-31* mutant root meristem (5 μM Zt, 12 hours) expressing, respectively, PIN1:GFP, PIN3:GFP, and PIN7:GFP. No changes in root meristem size are detectable. Blue arrowheads indicate quiescent center cells; white arrowheads indicate cortex transition zone. (**J**) qRT-PCR confirms up-regulation of the *PIN* gene mRNAs in the *shy2-31* mutant and no down-regulation in the *shy2-31* mutant upon cytokinin treatment (5 μM Zt, 12 hours). Relative expression is normalized to *ACTIN*, and 0 corresponds to *PIN* mRNA levels in untreated wild-type roots. Error bars, SD; $P < 0.5$; Student's *t* test; $n = 3$. (**K**) qRT-PCR showing *PIN* down-regulation in root of *HS::shy2-6* plants induced at 37°C for 1 hour. Relative expression is normalized to *ACTIN*, and 0 corresponds to *PIN* mRNA amounts in wild-type roots kept for 1 hour at 37°C. Error bars, SD; $P < 0.5$; Student's *t* test; $n = 3$.

observed in the gain-of-function mutant *shy2-2* in which the interaction of SHY2 with the F-box protein TIR1 is affected (*19*) (fig. S5, C, D, G, and H).

The cytokinin biosynthetic gene adenosine triphosphate/adenosine diphosphate isopentenyltransferase 5 (AtIPT5), involved in controlling root meristem size (*3*) and specifically expressed in the columella and at the vascular tissue transition zone (*7*) (fig. S6, A to E), is rapidly induced by auxin (*7*). To establish whether the control of auxin on cytokinin biosynthesis is mediated by *SHY2*, we analyzed the expression of an IPT5::GUS promoter fusion (*7*) in the *shy2-2* gain-of-function mutant and in the *shy2-31* loss-of-function mutant. Although IPT5::GUS activity was higher and more sensitive to auxin in the *shy2-31* mutant than in the wild type, auxin-dependent IPT5::GUS activity was totally lost in the *shy2-2* gain-of-function mutant (fig. S6, A to E).

We propose a model where cytokinin and auxin antagonistically interact at the vascular tissue transition zone to balance cell differentiation with cell division, thus determining root meristem size, by controlling in opposite ways the abundance of the SHY2 protein. Cytokinin reduces auxin response by activating, via the AHK3/ARR1 two-component signaling pathway, transcription of the *SHY2* gene; the SHY2 protein in turn regulates negatively the expression of the *PIN* genes (fig. S7). The resulting redistribution of auxin leads to cell differentiation of all the other tissues, thus reducing root meristem size. Conversely, auxin controls root meristem growth by directing degradation of the SHY2 protein, thus sustaining the activity of the *PIN* genes and cell division (fig. S7). The SHY2 protein negatively controls auxin transport on the one hand and cytokinin biosynthesis on the other, thus conferring robustness to the feedback loop we propose.

This model is consistent with the low concentration of auxin at the transition zone observed by other authors (*20*) and with our previous demonstration that the vascular tissue transition zone is the developmental domain of cytokinin action (*3*).

It is tempting to hypothesize that in root meristem size determination the PLETHORA (PLT) (*21*) proteins mediate the effect of cytokinin by responding to changes in polar auxin transport caused by cytokinin. It has been shown that the gradient of auxin in the root meristem creates a gradient of PLT proteins that direct different outputs in response to auxin in different regions of the meristem (*22*). Changes in PIN proteins activity affect the gradient distribution of auxin and of the PLT proteins (*8*, *23*). Interestingly, we observed that the *PLT1* and *PLT2* genes are down-regulated by cytokinin (fig. S6F).

References and Notes

1. F. Skoog, C. O. Miller, *Symp. Soc. Exp. Biol.* **11**, 118 (1957).
2. H. J. Klee, M. B. Lanahan, *Plant Hormones: Physiology, Biochemistry and Molecular Biology*, P. J. Davies, Ed. (Kluwer, Dordrecht, Netherlands, 1995), pp. 340–353.
3. R. Dello Ioio *et al*., *Curr. Biol.* **17**, 678 (2007).
4. B. Müller, J. Sheen, *Nature* **453**, 1094 (2008).
5. R. Dello Ioio, F. S. Linhares, S. Sabatini, *Curr. Opin. Plant Biol.* **11**, 23 (2008).
6. B. Müller, J. Sheen, *Science* **318**, 68 (2007).
7. K. Miyawaki, M. Matsumoto-Kitano, T. Kakimoto, *Plant J.* **37**, 128 (2004).
8. I. Blilou *et al*., *Nature* **433**, 39 (2005).
9. H. Sakai *et al*., *Science* **294**, 1519 (2001); published online 1 November 2001 (10.1126/science.1065201).
10. M. Taniguchi, N. Sasaki, T. Tsuge, T. Aoyama, A. Oka, *Plant Cell Physiol.* **48**, 263 (2007).
11. Q. Tian, N. J. Uhlir, J. W. Reed, *Plant Cell* **14**, 301 (2002).
12. T. J. Guilfoyle, G. Hagen, *Curr. Opin. Plant Biol.* **10**, 453 (2007).
13. K. Mockaitis, M. Estelle, *Annu. Rev. Cell Dev. Biol.* **10**, 453 (2008).
14. Q. Tian, J. W. Reed, *Development* **126**, 711 (1999).
15. K. Knox, C. S. Grierson, O. Leyser, *Development* **130**, 5769 (2003).
16. D. Weijers *et al*., *EMBO J.* **24**, 1874 (2005).
17. A. Vieten *et al*., *Development* **132**, 4521 (2005).
18. E. Benková *et al*., *Cell* **115**, 591 (2003).
19. Q. Tian, P. Nagpal, J. W. Reed, *Plant J.* **36**, 643 (2003).
20. K. Ljung *et al*., *Plant Cell* **17**, 1090 (2005).
21. M. Aida *et al*., *Cell* **119**, 109 (2004).
22. C. Galinha *et al*., *Nature* **449**, 1053 (2007).
23. V. A. Grieneisen *et al*., *Nature* **449**, 1008 (2007).
24. Materials and methods are available as supporting material on *Science* Online.

25. We thank B. Scheres, O. Leyser, J. Reed, and G. Jurgens for providing material and all members of the FGPL for indispensable and helpful technical support. This work was supported by a Giovanni Armenise-Harvard Foundation career development grant (to S.S.) and by Istituto Pasteur-Fondazione Cenci Bolognetti, Ministero dell'Istruzione, dell'Università e della Ricerca (MIUR) progetti di Ricerca di Interesse Nazionale, and MIUR Fondo per gli Investimenti della Ricerca di Base European Research Area-Plant Genomics (to P.C.).

Supporting Online Material

www.sciencemag.org/cgi/content/full/322/5906/1380/DC1
Materials and Methods
Figs. S1 to S7
References

4 August 2008; accepted 28 October 2008
10.1126/science.1164147

Chromosome Alignment and Transvection Are Antagonized by Condensin II

Tom A. Hartl, Helen F. Smith, Giovanni Bosco*

Polytene chromosome structure is a characteristic of some polyploid cells where several to thousands of chromatids are closely associated with perfect alignment of homologous DNA sequences. Here, we show that *Drosophila* condensin II promotes disassembly of polytene structure into chromosomal components. Condensin II also negatively regulates transvection, a process whereby certain alleles are influenced transcriptionally via interallelic physical associations. We propose that condensin II restricts trans-chromosomal interactions that affect transcription through its ability to spatially separate aligned interphase chromosomes.

Interphase chromosomal trans-interactions occur in many species and impact chromosome structure and gene expression (*1*–*4*). As evidenced in *Drosophila*, trans-interactions can lead to polytene chromosomes, where all maternal and paternal chromatids are aligned in precise register (*5*). The *Drosophila* ovarian nurse cells disassemble their polytene chromosomes into unpaired homologs and chromatid fibers during mid-oogenesis (Fig. 1A and fig. S1) (*6*). We used this system to isolate two noncomplementing mutations in a predicted condensin II subunit, *Cap-H2* (*7*–*9*), that cause failure in nurse cell polytene disassembly. Polyteny instead persists in the trans-heterozygous combinations of $Cap\text{-}H2^{Z3\text{-}0019}/Cap\text{-}H2^{Z3\text{-}5163}$ (Fig. 1B and fig. S2A) and when either allele is in trans to a deletion of its genomic locus (Fig. 1, C and D). This was corroborated through fluorescence in situ hybridization (FISH) labeling to a specific locus in stage 7 egg chambers, where wild-type polytenes disassembled, yet 92.9% of mutant nuclei had all maternal and paternal chromatids aligned in register (fig. S3) (*7*). Polytene persistence in *Cap-H2* mutants likely does not occur indirectly through altered cell cycle progression or DNA replication patterns because neither the length of S phase nor ploidy were detectably different in homozygous polytene mutants versus heterozygous controls (figs. S4 and S5) (*7*). This result instead suggests that Cap-H2 function is necessary to disassemble nurse cell polytene chromosomes.

Metazoa have two condensin complexes that are referred to as condensin I and II. Each uses the adenosine triphosphatases SMC2 and SMC4, but forms complexes with different non-SMC subunits Cap-H, Cap-G, and Cap-D2 or Cap-H2, Cap-G2, and Cap-D3, respectively (*10*, *11*). Condensins function in the condensation of chromosomes, facilitate proper anaphase segregation, and

Department of Molecular and Cellular Biology, University of Arizona, 1007 East Lowell Street, Tucson, AZ 85721–0106, USA.

*To whom correspondence should be addressed. E-mail: gbosco@email.arizona.edu

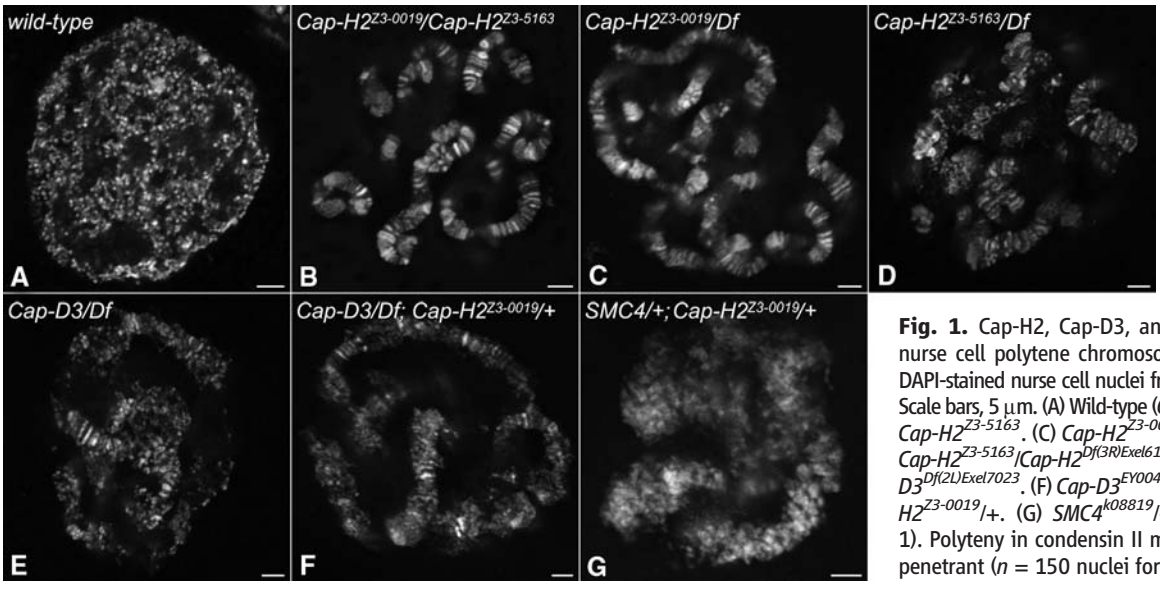

Fig. 1. Cap-H2, Cap-D3, and SMC4 are necessary for nurse cell polytene chromosome disassembly. (**A** to **G**) DAPI-stained nurse cell nuclei from stage 10 egg chambers. Scale bars, 5 μm. (A) Wild-type (*Oregon R*). (B) *Cap-H2*$^{Z3\text{-}0019}$/*Cap-H2*$^{Z3\text{-}5163}$. (C) *Cap-H2*$^{Z3\text{-}0019}$/*Cap-H2*$^{Df(3R)Exel6159}$. (D) *Cap-H2*$^{Z3\text{-}5163}$/*Cap-H2*$^{Df(3R)Exel6159}$. (E) *Cap-D3*^{EY00456}/*Cap-D3*$^{Df(2L)Exel7023}$. (F) *Cap-D3*^{EY00456}/*Cap-D3*$^{Df(2L)Exel7023}$; *Cap-H2*$^{Z3\text{-}0019}$/+. (G) *SMC4*^{k08819}/+; *Cap-H2*$^{Z3\text{-}0019}$/+ (Table 1). Polyteny in condensin II mutant nurse cells is highly penetrant (n = 150 nuclei for each genotype).

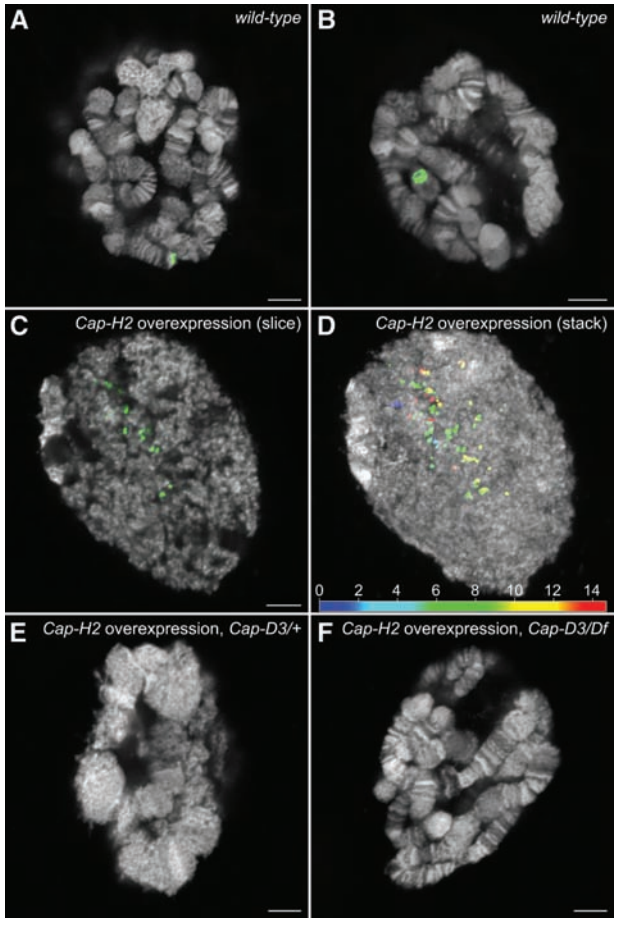

Fig. 2. *Cap-H2* is sufficient to disassemble salivary gland polytene chromosomes and cooperates with *Cap-D3*. (**A** and **B**) Wild-type controls not overexpressing *Cap-H2*. (**C**) Nucleus overexpressing *Cap-H2*. (**D**) Stacked *z* series of the same nucleus shown in (C) to demonstrate the full extent of polytene disassembly. Color scale is in microns of the *z* axis. (**E**) *Cap-D3*^{EY00456}/+ control overexpressing *Cap-H2*. (**F**) *Cap-D3*^{EY00456}/*Cap-D3*$^{Df(2L)Exel7023}$ mutant overexpressing *Cap-H2*. In comparison with (E), note *Cap-D3*'s ability to rescue *Cap-H2*–induced polytene disassembly. Scale bars, 5 μm.

in vitro induce and trap DNA positive supercoiling (*9*, *12*, *13*). Supercoiling has been proposed to gather chromatin into domains that are then further ordered to assemble metaphase chromosomes (*12*). Cap-H2 likely acts within a condensin II complex, as other predicted condensin II subunits also regulate nurse cell polytene dispersal. *Cap-D3* mutants (fig. S2B) exhibited nurse cell polytene persistence (Fig. 1E) that was enhanced through the introduction of one mutant *Cap-H2* copy (Fig. 1F). Furthermore, *SMC4/Cap-H2* double-heterozygotes had a loosened, but clear, polytene morphology (Fig. 1G) (*7*). Consistent with a polytene disassembly function, Cap-H2 protein first becomes enriched within posterior stage 5 and 6 egg chambers, where disassembly is initiated (*6*), and Cap-H2 is detected in all stage 7 to 10 nuclei (figs. S6 and S7) (*7*).

Unlike nurse cells, polyteny is persistent in the nuclei of the larval salivary glands (Fig. 2, A and B). *Cap-H2* overexpression induced drastic separation of salivary gland polytene chromosomal components, as visualized through green fluorescent protein (GFP) labeling of a second chromosome locus (Fig. 2, C and D, and figs. S8 to S10, movies S1 and S2). In the wild-type, the GFP locus had a width 15.9 ± 1.6% (SEM) of the nuclear radius (Fig. 2, A and B), yet individual foci reached distances 110.8 ± 9.1% (SEM) of the nuclear radius after *Cap-H2* induction (Fig. 2, C and D, and fig. S9) (*7*).

In the salivary gland, Cap-H2–induced polytene disassembly occurs only 6 hours after *Cap-H2* overexpression in fully developed late larvae (fig. S10), which makes it unlikely that disassembly is an indirect consequence of altered larval development. It is also improbable that disassembly occurs through the creation of large-scale chromosomal breaks, because this was not detected after *Cap-H2* overexpression, and that the creation of DNA breaks with γ-radiation did not alter polytene alignment (fig. S11) (*7*). Rather, the ability of *Cap-H2* overexpression to induce polytene disassembly indicates that polytene alignment of chromatids is constrained with wild-type Cap-H2 levels. Providing excess Cap-H2 may induce polytene disassembly because its dosage is limiting to other condensin II subunits in salivary glands and/or it acts as a catalytic subunit that promotes condensin II activity. Cap-H2 does rely on Cap-D3 to induce polytene disassembly as all salivary gland nuclei from a *Cap-D3* mutant background overexpressing *Cap-H2* had polytenes that appeared like the wild-type (n = 195 nuclei). This contrasted to *Cap-D3* heterozygous controls, where only 24.1 ± 8.5% (SEM) nuclei per gland con-

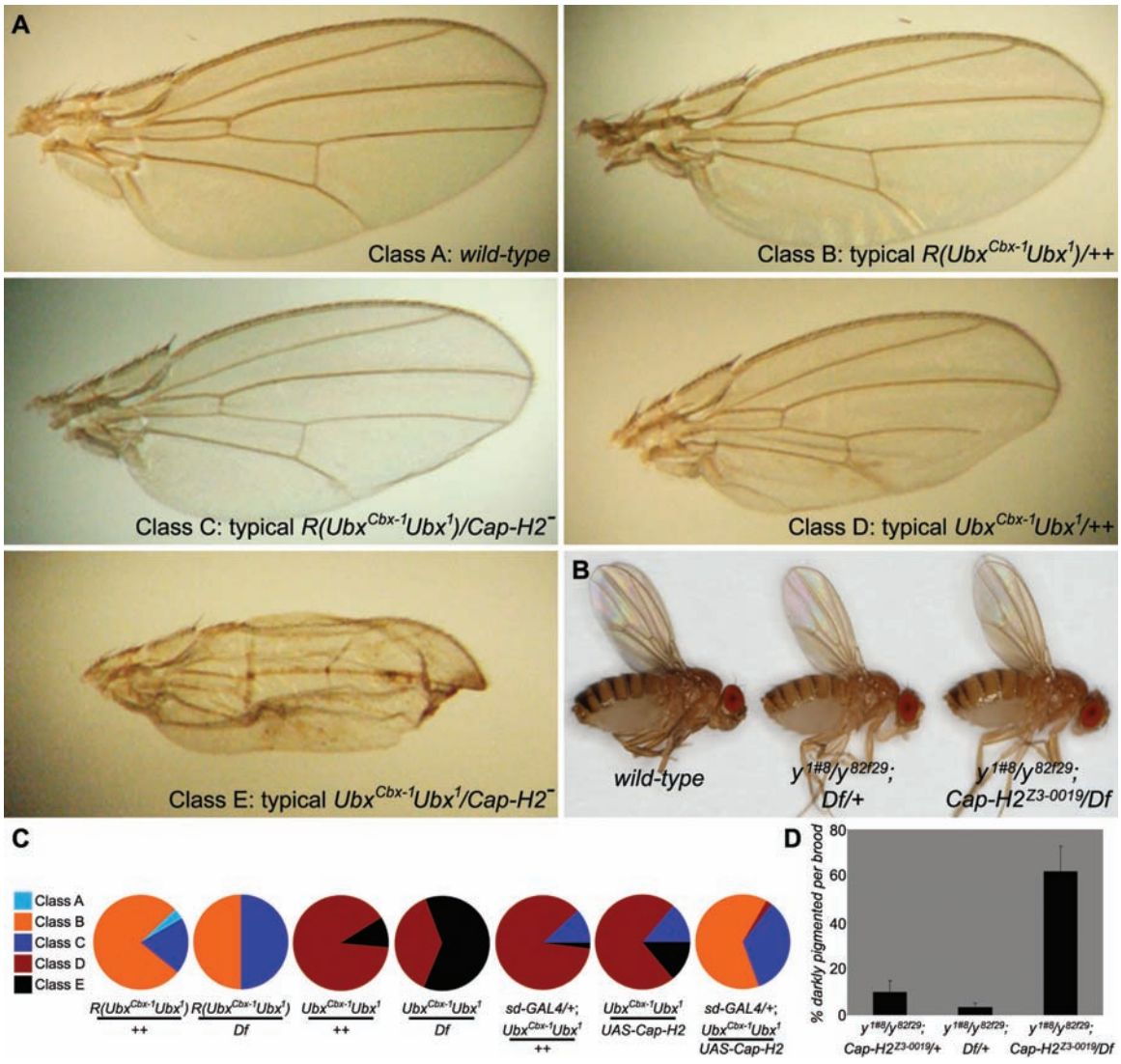

Fig. 3. *Cap-H2* negatively regulates transvection at *Ubx* and *yellow* loci. (**A**) Wing phenotypes depicting *Cap-H2* modification to $Ubx^{Cbx\text{-}1}$ Ubx^{1} transvection. Class A: wild-type. Class B: typical $R(Ubx^{Cbx\text{-}1}\ Ubx^{1})/++$ wing. Notice slight loss of tissue at the posterior. Class C: enhancement of the $R(Ubx^{Cbx\text{-}1}\ Ubx^{1})/++$ wing phenotype found through introduction of a *Cap-H2* mutation. Notice withering at the posterior. Class D: typical $Ubx^{Cbx\text{-}1}\ Ubx^{1}/++$ wing. Class E: enhancement of the $Ubx^{Cbx\text{-}1}\ Ubx^{1}$ wing phenotype through introduction of a *Cap-H2* mutation. (**B**) Flies depicting *Cap-H2* enhancement of $y^{1\#8}/y^{82f29}$ transvection. (Left) Wild-type. (Middle) $y^{1\#8}/y^{82f29}$; $Cap\text{-}H2^{Z3\text{-}0019}/+$ control illustrating "light" stripes. (Right) $y^{1\#8}/y^{82f29}$; $Cap\text{-}H2^{Z3\text{-}0019}/Cap\text{-}H2^{Df(3R)Exel6159}$ with "dark" stripes. (**C**) $Ubx^{Cbx\text{-}1}\ Ubx^{1}$ transvection data (n = 50 wings) (see tables S1 to S5 for complete data set). (**D**) Quantification of $y^{1\#8}/y^{82f29}$ transvection enhancement by *Cap-H2* mutants. Darker stripes were consistently found for $y^{1\#8}/y^{82f29}$; $Cap\text{-}H2^{Z3\text{-}0019}/Cap\text{-}H2^{Df(3R)Exel6159}$ flies relative to the two heterozygous controls (bars indicate SEM, n = 97, 95 (controls), and 43 (trans-heterozygote) flies, $P < 0.005$, two-tailed t test assuming unequal variances).

Table 1. Percentage of polytene nurse cells in condensin II mutant backgrounds. The number of polytene nurse cells per stage 10 egg chamber was quantified (n = 10 egg chambers and 150 total nuclei) (±SEM).

Genotype	% Polytene nurse cells
Wild-type (*Oregon R*)	0.0
$Cap\text{-}H2^{Z3\text{-}0019}/+$	6.0 ± 2.7
$Cap\text{-}H2^{Z3\text{-}0019}/Cap\text{-}H2^{Z3\text{-}5163}$	100.0
$Cap\text{-}H2^{Z3\text{-}0019}/Cap\text{-}H2^{Df(3R)Exel6159}$	100.0
$Cap\text{-}H2^{Z3\text{-}5163}/Cap\text{-}H2^{Df(3R)Exel6159}$	100.0
$SMC4^{k08819}/+$	0.0
$SMC4^{k08819}/+$; $Cap\text{-}H2^{Z3\text{-}0019}/+$	77.3 ± 9.1
$Cap\text{-}D3^{Df(2L)Exel7023}/+$	6.0 ± 3.2
$Cap\text{-}D3^{EY00456}/Cap\text{-}D3^{Df(2L)Exel7023}$	91.3 ± 2.3
$Cap\text{-}D3^{EY00456}/Cap\text{-}D3^{Df(2L)Exel7023}$; $Cap\text{-}H2^{Z3\text{-}0019}/+$	100.0

tained wild-type polytenes (n = 182) (Fig. 2, E and F) (*7*).

Because of Cap-H2's ability to transform aligned polytene structure into chromosomal components, we predicted it would function in a similar manner to disrupt aligned loci within diploid somatic cells. We therefore investigated whether it regulates diploid trans-chromosomal interactions by studying its role in transvection, a phenomenon whereby certain mutant alleles are influenced transcriptionally via association with their homologous locus (*1*). It is inferred from transvection phenomena that somatic homolog pairing also plays a role in regulating wild-type loci.

The first transvection system we utilized involves the gain-of-function mutation $Ubx^{Cbx\text{-}1}$, which causes misexpression of *Ubx* in the imaginal wing disc and leads to a partial wing-to-haltere transformation (*14*–*16*). A wing transformation occurs even in flies where *Ubx* of the $Ubx^{Cbx\text{-}1}$ allele is rendered null through the introduction of a second mutation ($Ubx^{Cbx\text{-}1}\ Ubx^{1}$) (Fig. 3A, compare class A with class D). This $Ubx^{Cbx\text{-}1}\ Ubx^{1}/++$ phenotype suggested that the Cbx^{1} lesion is capable of transcriptionally activating the wild-type *Ubx* on the homologous chromosome through a trans physical association (*14*, *17*). This was supported by the ability of chromosomal rearrangements (*R*) that disrupt homolog pairing at *Ubx* to suppress transvection (Fig. 3A, compare class D

with class B) (*14*, *17*, *18*). Consistent with a role for Cap-H2 in antagonizing homolog pairing, the $Ubx^{Cbx\text{-}1}$ Ubx^{1}/++ phenotype was dominantly enhanced by *Cap-H2* mutations [(Fig. 3A), compare class D with class E (Fig. 3C and table S1)]. Conversely, *Cap-H2* overexpression suppressed the $Ubx^{Cbx\text{-}1}$ Ubx^{1}/++ wing phenotype closer to wild-type [Fig. 3A, compare class D with class B (Fig. 3C and tables S3 to S5)].

Cap-H2 mutant enhancement of the $Ubx^{Cbx\text{-}1}$ Ubx^{1} phenotype was suppressed in a chromosomal rearrangement background [$R(Ubx^{Cbx\text{-}1}$ $Ubx^{1})$/++] that is thought to disrupt allelic associations between $Ubx^{Cbx\text{-}1}$ Ubx^{1} and wild-type *Ubx* [(Fig. 3A), compare class E with class C (Fig. 3C, table S2)] (*7*). The $Ubx^{Cbx\text{-}1}$ Ubx^{1}/*Cap-H2*$^{-}$ and $R(Ubx^{Cbx\text{-}1}$ $Ubx^{1})$/*Cap-H2*$^{-}$ flies only vary by the reciprocal translocation that moves 3*R* bearing $Ubx^{Cbx\text{-}1}$ Ubx^{1} to 2*R* and vice versa. This suggests that *Cap-H2* enhancement of the $Ubx^{Cbx\text{-}1}$ Ubx^{1} phenotype is through increasing the association of homologous loci. Alternatively, Cap-H2 function may follow trans-chromosomal interactions, for example, acting locally to enable enhancer interactions in trans or as a general transcriptional repressor. Although either is formally possible, *Cap-H2*'s ability to globally disrupt aligned polytene structure suggests it carries out a related function in diploid cells to antagonize trans-chromosomal interactions.

Cap-H2 was tested in a second transvection system involving mutant alleles of the gene *yellow* (*y*). In y^{82f29}/y^{82f29} and $y^{1\#8}/y^{1\#8}$ flies, there is minimal cuticle pigmentation, yet when placed in trans to one another ($y^{82f29}/y^{1\#8}$) complementation occurs with partial restoration of pigment nearer to wild-type levels. The $y^{1\#8}$ allele is a deletion of the *yellow* promoter and the y^{82f29} allele a deletion of upstream enhancer elements. It is thought that partial complementation occurs in $y^{82f29}/y^{1\#8}$ through the ability of $y^{1\#8}$'s enhancers to act in trans, to associate with the intact promoter of y^{82f29}, and then to activate *yellow* transcription (*19*, *20*). As are $Ubx^{Cbx\text{-}1}$ Ubx^{1}, transvection of $y^{82f29}/y^{1\#8}$ is enhanced in a *Cap-H2* mutant background, which leads to darker pigmentation of the abdominal stripes relative to controls (Fig. 3, B and D) (*7*).

Transvection can be enhanced by slowing the rate of cell division (*21*). The percent of *Cap-H2* homozygous mutant cells specifically in mitosis was cytologically found to be greater relative to heterozygous controls, but this was statistically insignificant [1.37% (n = 1318) versus 0.95% (n = 3375), $P > 0.05$ (χ^2)]. Furthermore, with flow cytometry, homozygotes and heterozygotes did not vary significantly in the percentage of cells in G_1, S, and G_2/M (fig. S12). Although these data do not rule out a cell cycle delay leading to enhanced transvection, they also do not support a major regulatory role for Cap-H2 in cell cycle progression. Cap-H2's ability to disassemble the aligned structure of polytene chromosomes instead suggests that it antagonizes transvection by inhibiting homology-dependent chromosomal interactions in diploid somatic cells.

Just as condensin-mediated supercoiling has been proposed to initiate chromosome condensation (*12*), we speculate that supercoiling activity also exists in interphase nuclei and can disrupt chromosome alignment. This may be through providing a force that physically disrupts interchromosomal associations and/or favors intrachromosomal higher-order structures that make inaccessible regions prone to trans-associate (fig. S13). This condensin activity may be a crucial aspect of gene regulation by disrupting trans-communication of allelic regulatory elements.

References and Notes

1. I. W. Duncan, *Annu. Rev. Genet.* **36**, 521 (2002).
2. F. Savarese, R. Grosschedl, *Cell* **126**, 248 (2006).
3. F. Bantignies, C. Grimaud, S. Lavrov, M. Gabut, G. Cavalli, *Genes Dev.* **17**, 2406 (2003).
4. J. Vazquez, M. Muller, V. Pirrotta, J. W. Sedat, *Mol. Biol. Cell* **17**, 2158 (2006).
5. B. A. Edgar, T. L. Orr-Weaver, *Cell* **105**, 297 (2001).
6. K. J. Dej, A. C. Spradling, *Development* **126**, 293 (1999).
7. Materials and methods are available as supporting material on *Science* Online.
8. A. Schleiffer *et al.*, *Mol. Cell* **11**, 571 (2003).
9. T. Hirano, *Curr. Biol.* **15**, R265 (2005).
10. T. Ono *et al.*, *Cell* **115**, 109 (2003).
11. F. M. Yeong *et al.*, *Curr. Biol.* **13**, 2058 (2003).
12. T. Hirano, *Nat. Rev. Mol. Cell Biol.* **7**, 311 (2006).
13. K. Kimura, T. Hirano, *Cell* **90**, 625 (1997).
14. E. B. Lewis, *Am. Nat.* **89**, 73 (1955).
15. C. V. Cabrera, J. Botas, A. Garcia-Bellido, *Nature* **318**, 569 (1985).
16. R. A. H. White, M. Akam, *Nature* **318**, 567 (1985).
17. J. E. Castelli-Gair, J. L. Micol, A. Garcia-Bellido, *Genetics* **126**, 177 (1990).
18. M. J. Gemkow, P. J. Verveer, D. J. Arndt-Jovin, *Development* **125**, 4541 (1998).
19. J. R. Morris, J. L. Chen, P. K. Geyer, C. T. Wu, *Proc. Natl. Acad. Sci. U.S.A.* **95**, 10740 (1998).
20. P. K. Geyer, M. M. Green, V. G. Corces, *EMBO J.* **9**, 2247 (1990).
21. M. M. Golic, K. G. Golic, *Genetics* **143**, 385 (1996).

22. We acknowledge T. Orr-Weaver for supporting the initial screen. We are grateful to the following individuals: C. Boswell (microscopy), V. Lien (UAS–Cap-H2–mCherry transgenics), M. Hart (mitotic index), P. Jansma (fly imaging), and J. Blumenstiel (FISH). We thank S. Hawley, T. Orr-Weaver, M. Lilly, E. Kelleher, and the JMST student forum for critical reading of the manuscript and, especially, C.-T. Wu for exceptional guidance with transvection studies. We are grateful to J. Sedat, J. Vazquez, C. Zuker, P. O'Farrell, and C.-T. Wu for fly stocks. Support was from NIH (GM069462) grant to G.B., and T.H. was funded by the University of Arizona NSF-IGERT (Integrative Graduate Education and Research Traineeships) Program in Genomics and NIH Grant for Graduate Training in Biochemistry and Molecular Biology.

Supporting Online Material

www.sciencemag.org/cgi/content/full/322/5906/1384/DC1
Materials and Methods
SOM Text
Figs. S1 to S13
Tables S1 to S5
References
Movies S1 and S2

12 August 2008; accepted 2 October 2008
10.1126/science.1164216

An Epigenetic Role for Maternally Inherited piRNAs in Transposon Silencing

Julius Brennecke,[1]* Colin D. Malone,[1]* Alexei A. Aravin,[1] Ravi Sachidanandam,[1]† Alexander Stark,[2,3] Gregory J. Hannon[1]‡

In plants and mammals, small RNAs indirectly mediate epigenetic inheritance by specifying cytosine methylation. We found that small RNAs themselves serve as vectors for epigenetic information. Crosses between *Drosophila* strains that differ in the presence of a particular transposon can produce sterile progeny, a phenomenon called hybrid dysgenesis. This phenotype manifests itself only if the transposon is paternally inherited, suggesting maternal transmission of a factor that maintains fertility. In both *P*- and *I*-element–mediated hybrid dysgenesis models, daughters show a markedly different content of Piwi-interacting RNAs (piRNAs) targeting each element, depending on their parents of origin. Such differences persist from fertilization through adulthood. This indicates that maternally deposited piRNAs are important for mounting an effective silencing response and that a lack of maternal piRNA inheritance underlies hybrid dysgenesis.

In *Drosophila melanogaster*, the progeny of intercrosses between wild-caught males and laboratory-strain females are sterile because of defects in gametogenesis, whereas the genetically identical progeny of wild-caught females and laboratory-strain males remain fertile (*1*–*3*). This phenomenon, known as hybrid dysgenesis, was attributed to the mobilization in dysgenic progeny of *P*-element or *I*-element transposons, which were present in wild-caught flies but absent from laboratory strains (*4*–*9*). The disparity in outcomes, depending on the parent of transposon origin, indicated the existence of cytoplasmically inherited determinants of the phenotype, which must be transmitted through the maternal germ line (*8*, *9*).

The control of mobile elements in germ cells depends heavily on a small RNA-based immune system, composed of Piwi-family proteins (Piwi, Aubergine, and AGO3) and piRNAs (*10*, *11*).

Both Piwi and Aubergine (Aub) are deposited into developing oocytes and accumulate in the pole plasm (*12*, *13*), implying possible transfer of maternal piRNAs into the germ lines of their progeny. We therefore asked whether maternally deposited small RNAs might affect transposon suppression in a heritable fashion and whether piRNAs might be the maternal suppressor of hybrid dysgenesis.

We first focused on *I*-element–induced hybrid dysgenesis (*14*). A cross of inducer males carrying active *I*-elements (designated "I" in Fig. 1) to reactive females devoid of active *I*-elements (designated "R") yielded dysgenic daughters (termed SF; Fig. 1 and fig. S1) (*5*, *6*, *8*, *15*). These were sterile, despite normal ovarian morphology. Sterility correlated with *I*-element expression in SF ovaries (Fig. 1B) (*16*). The reciprocal cross of inducer females to reactive males yielded fertile progeny (termed RSF; Fig. 1 and fig. S1).

[1]Watson School of Biological Sciences, Howard Hughes Medical Institute, Cold Spring Harbor Laboratory (CSHL), 1 Bungtown Road, Cold Spring Harbor, NY 11724, USA. [2]Broad Institute of Massachusetts Institute of Techonology and Harvard University, Cambridge, MA 02141, USA. [3]Computer Science and Artificial Intelligence Laboratory, Massachusetts Institute of Technology, Cambridge, MA 02139, USA.

*These authors contributed equally to this work.
†Present address: Department of Genetics and Genomic Sciences, Mount Sinai School of Medicine, New York, NY 10029, USA.
‡To whom correspondence should be addressed. E-mail: hannon@cshl.edu

We sequenced 18- to 29-nucleotide RNAs from the ovaries of inducer (w^{1118}) and reactive (w^{k}) strains, 0- to 2-hour embryos from dysgenic and nondysgenic crosses, and ovaries from SF and RSF daughters (Fig. 1A and fig. S1A). Both parental ovary and early embryo libraries contained similarly complex small RNA populations (fig. S1A). This indicates that small RNAs were maternally deposited, because the zygotic genome remains inactive during most of the period that we analyzed.

In *Drosophila*, piRNAs loaded into the Piwi, Aub, and AGO3 proteins exhibit distinctive features (*17*, *18*). piRNAs occupying Piwi and Aub are predominantly antisense to transposons and contain a 5′ terminal uridine residue (1U; fig. S2A). In contrast, AGO3 harbors mainly sense piRNAs with a strong bias for adenosine at position 10 (10A; fig. S2B). On the basis of these characteristics, we could infer the binding partner(s) for many small RNAs within our sequenced populations. A comparison of small RNAs in mothers and embryos indicated robust maternal inheritance for the Aub/Piwi pool and substantial but weaker deposition of AGO3-bound piRNAs (fig S2, A and B). This observation is consistent with the degree of maternal deposition of the corresponding Piwi-family proteins (figs. S3 and S4) (*12*, *13*).

Patterns of ovarian piRNAs targeting individual *D. melanogaster* transposons showed marked similarity between inducer and reactive strains (Fig. 2A). However, there were notable differences (Fig. 2, B and C). The *I*-element exhibited the lowest piRNA count in the reactive strain and the greatest disparity (21-fold) between strains (Fig. 2, B and C, and fig. S5A). Less pronounced differences were noted for *tirant* and *gypsy12*, which were more heavily targeted in the inducer strain, and for *1731* and *micropia*, which were more heavily targeted in the reactive strain (Fig. 2, B and C). These differences were mirrored in corresponding embryonic libraries, with reactive mothers depositing 12-fold fewer *I*-element piRNAs than inducer mothers (Fig. 2B). This supports the hypothesis that piRNAs correspond to the maternally transmitted phenotypic determinant noted in many studies of hybrid dysgenesis.

The outcome of an inducer-reactive (I-R) dysgenic cross manifests itself not in embryos but in adults. We therefore asked whether differences in maternally deposited piRNAs continued to influence adult piRNA profiles 2 weeks after fertilization. Consistent with their being genetically identical, SF and RSF daughters had virtually identical piRNA levels targeting nearly all transposons (Fig. 2, B and C). Thus, piRNA profiles for many elements had adjusted to a stable equilibrium during the course of germline development. As an example, for *1731* a ninefold difference in piRNA levels between mothers had equalized in progeny (fig. S5B). In RSF females, *I*-element piRNAs dropped twofold as compared

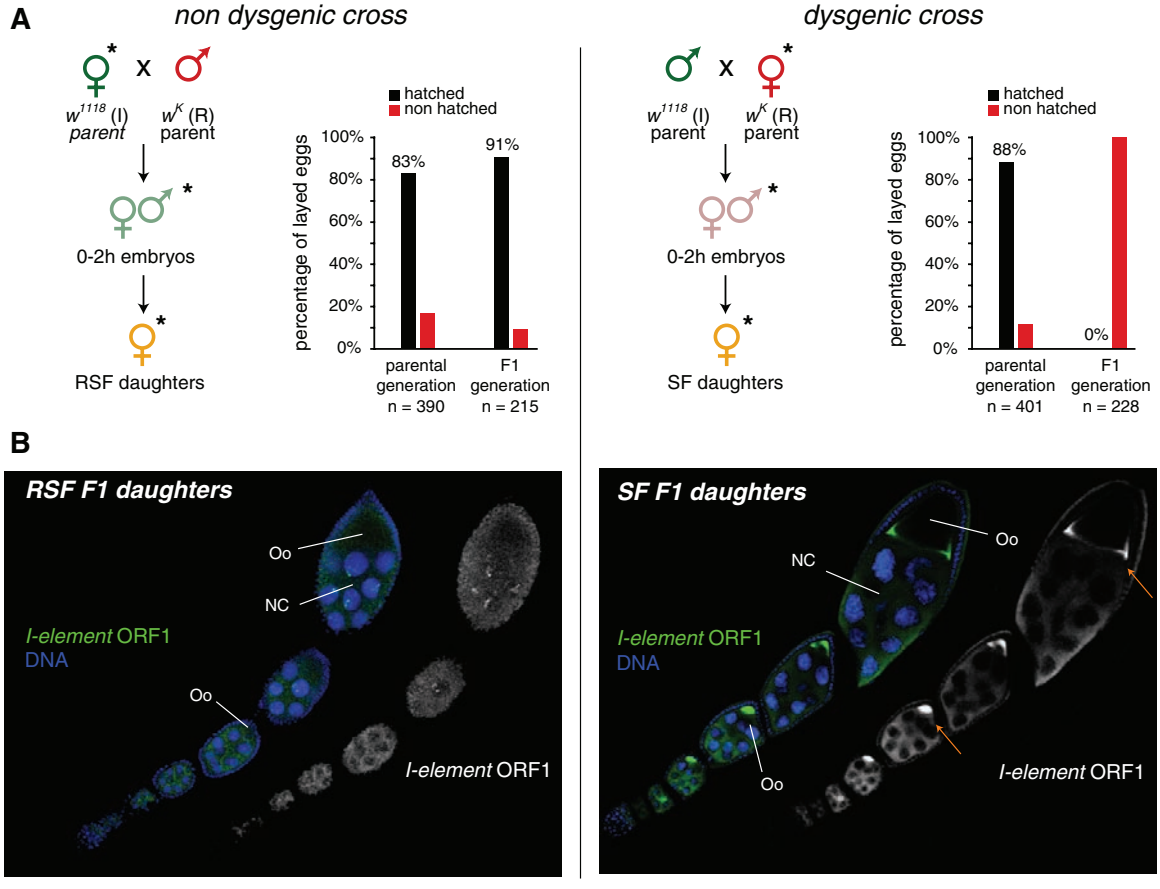

Fig. 1. The I-R hybrid dysgenesis system. (**A**) Crossing scheme to generate nondysgenic (left) and dysgenic (right) progeny. Small RNA libraries were made from flies indicated by asterisks. Bar diagrams indicate fertility analysis of parental and F1 females on the basis of egg hatching rates. *n*, number of counted eggs. (**B**) Immunofluorescence for *I*-element ORF1 (green) is shown for nondysgenic (RSF) and dysgenic (SF) daughters. Oo, oocyte; NC, nurse cells.

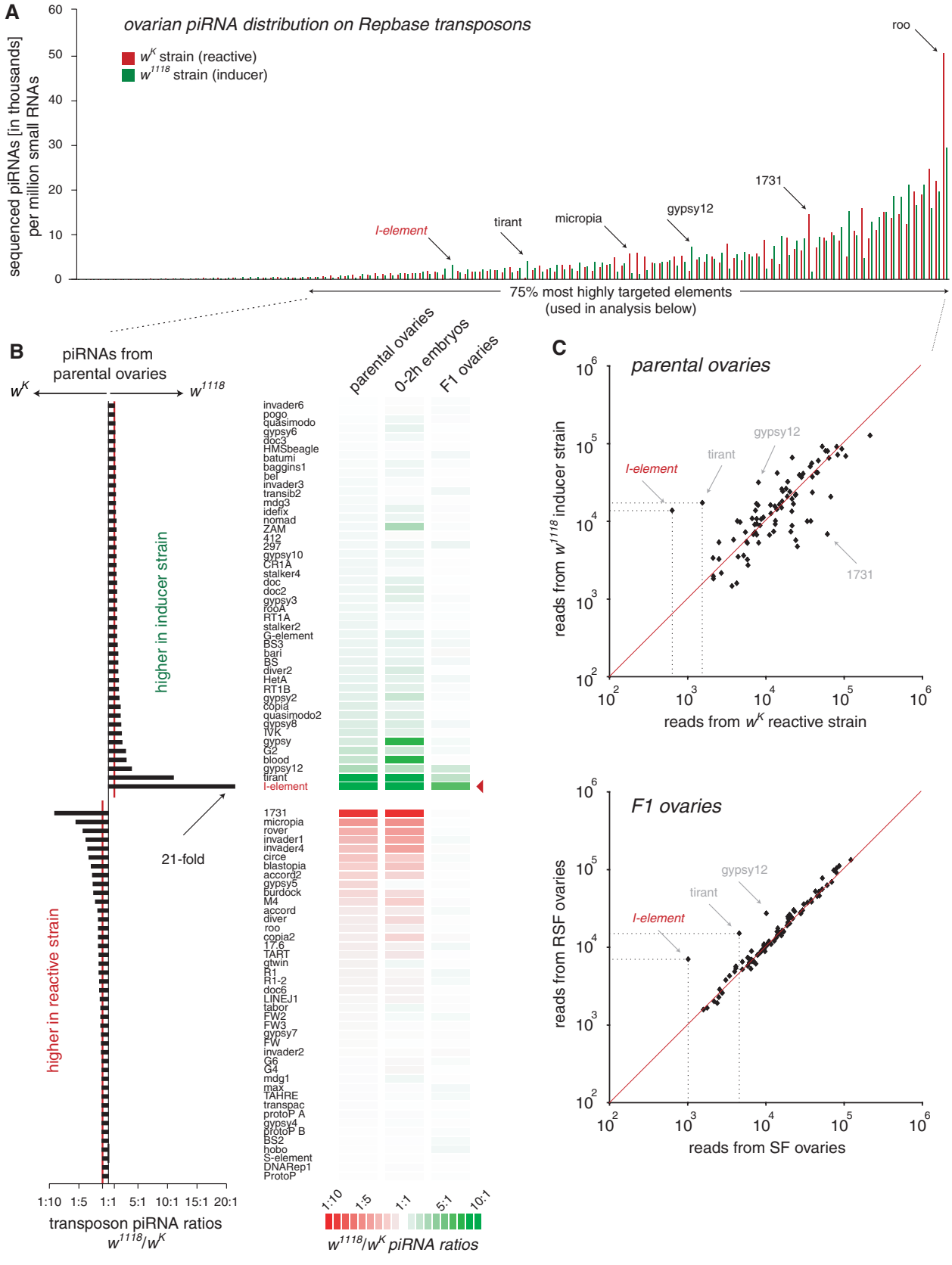

Fig. 2. I-R hybrid dysgenesis correlates with maternal piRNA inheritance. (**A**) Normalized piRNA counts for Repbase transposons are plotted for w^{1118} inducer and w^{K} reactive ovaries. (**B**) (Left) Fold differences in piRNA counts comparing w^{1118} and w^{K} mothers are shown (red line indicates a 1:1 ratio). (Right) Transposon piRNA ratios for mothers, embryos, and F1 progeny (SF: RSF ratio) are shown as a heat map. (**C**) Scatter plots indicating transposon piRNA correlations between w^{1118} and w^{K} mothers (top) and their respective intercross progeny (bottom).

with their inducer mothers (fig. S5B). This paralleled the overall reduction in active *I*-element load as the inducer genome was diluted by that of the reactive strain. However, limits on the adaptability of the system are seen in SF daughters for the *I*-element and, to a lesser degree, for *tirant* and *gypsy12* (Fig. 2, B and C, and fig. S5). Though SF daughters contained ~1.6-fold more *I*-element piRNAs than their reactive mothers, these were still sevenfold less abundant than in RSF daughters. This deficit ultimately results in de-repression of the paternally inherited, active *I*-elements and in sterility (Fig. 1, A and B).

Though active *I*-elements are confined to inducer strains, all *D. melanogaster* strains contain ancestral *I*-related fragments, (*6*, *19*–*21*). These are typically found in heterochromatin and exhibit 80 to 95% identity to the modern *I*-element. Such fragments have been proposed to mediate adaptation to and suppression of *I*-elements in inducer strains (*15*, *22*–*24*). To understand the lack of adaptation to *I*-elements in SF daughters, we probed the nature of interaction between active and ancestral *I*-element sequences.

The ping-pong model of piRNA biogenesis and silencing describes a Slicer-dependent amplification cycle between active transposons and

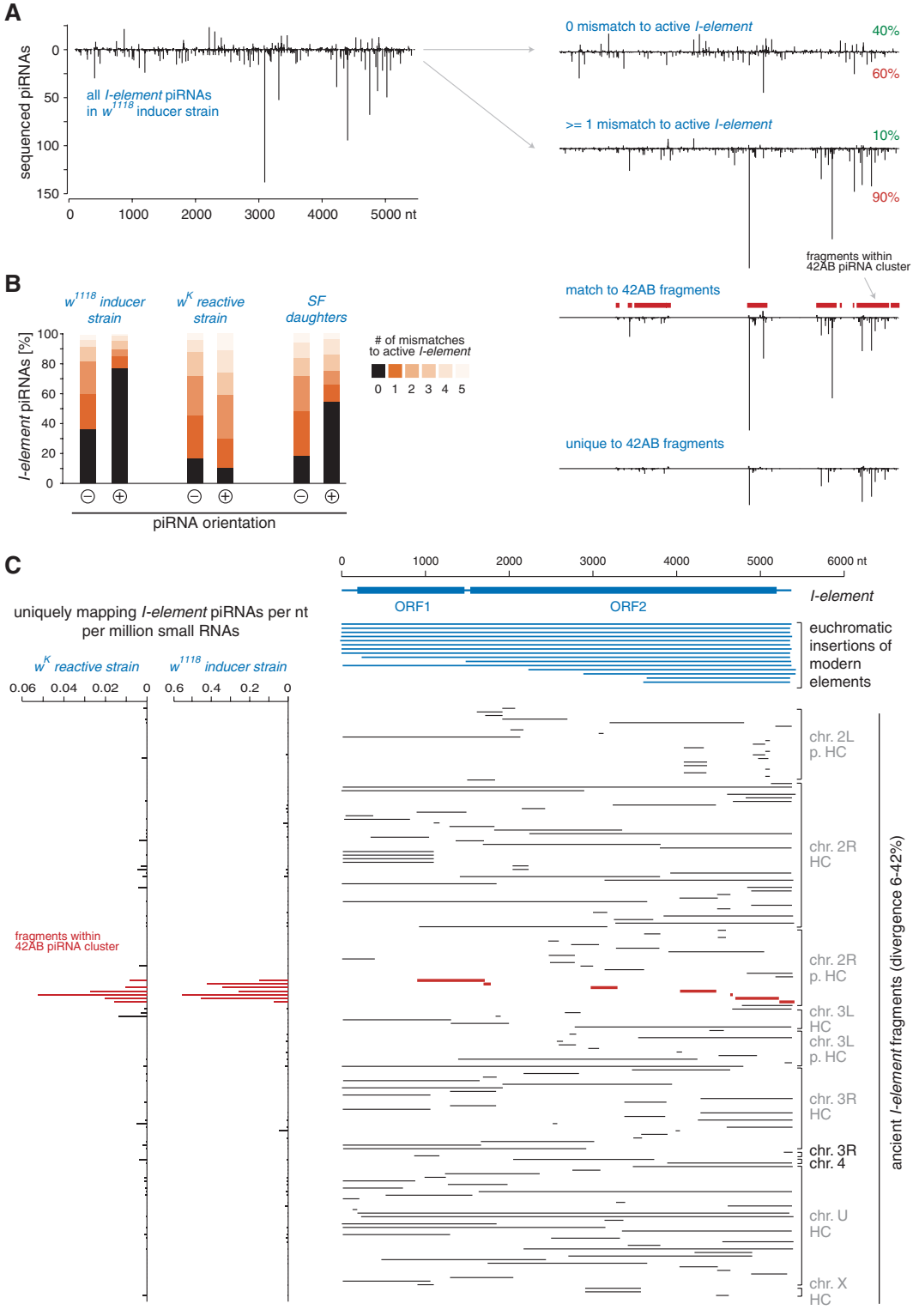

Fig. 3. A piRNA amplification loop between active *I*-elements and ancestral fragments. (**A**) Density profile of piRNAs matching the *I*-element with up to five mismatches (left) and profiles for those species with zero (top right) or at least one mismatch (below) to the active element (sense/antisense fractions in red and green) are shown. Profiles below indicate species that have the potential (upper) or must (lower) derive from the 42AB piRNA cluster. *I*-element fragments contained within the 42AB cluster are indicated in red. (**B**) Shown are fractions of *I*-element piRNAs from w^{1118}, w^{K} mothers, and SF daughters (right) that match the active sequence with the indicated number of mismatches, split into sense (+) and antisense (–). (**C**) (Right) All *I*-element fragments in the Release 5 genome sequence [split into modern insertions (blue) and ancestral fragments (black) and sorted by chromosomal position] are shown (gray coloring indicates heterochromatic; HC, heterochromatin; p. HC, pericentromeric HC). Red fragments map to the 42AB piRNA cluster. (Left) Bar diagrams indicate the density of piRNAs mapping uniquely to the ancestral fragments shown at right (42AB fragments in red). As fragments with high piRNA density were not more divergent overall, clustering in 42AB is not an artifact of analysis (fig. S7).

transposon fragments resident in piRNA clusters (*17*, *18*). Sequence features fitting this model were obvious in piRNAs from the inducer strain (fig. S6). More than half of all *I*-element piRNAs deviated from the modern sequence and, therefore, must have originated from ancestral fragments (Fig. 3A). Of those piRNAs, the overwhelming majority (90%) were antisense. As a whole, sense-oriented species showed a strong tendency (~78%) to originate from modern active *I*-element copies (Fig. 3B), whereas 63% of antisense species must have originated from heterochromatic fragments.

Because the reactive strain lacks active *I*-element copies, no ping-pong amplification occurred, and piRNAs mapping to the sense or antisense strand showed no distinguishing pattern of matching to the active element (Fig. 3B). Despite the lack of an efficient silencing response in SF daughters, we still observed a clear trend for sense piRNAs to originate from active *I*-element copies, which were paternally transmitted (Fig. 3B). This is consistent with the adaptive system having begun to mount a response in SF daughters, although they ultimately failed to silence the element.

In both reactive and inducer strains, the 42AB cluster represents a major source of piRNAs targeting a variety of mobile elements (fig. S8) (*17*). Of all heterochromatic *I*-fragments present in the sequenced *melanogaster* strain, seven lie within 42AB, and we verified the existence of all in both our reactive and inducer strains (fig. S9). None of the other heterochromatic *I*-fragments lie within the remaining 19 most active clusters. In the inducer strain, the majority of heterochromatin-derived *I*-element piRNAs arose from ancestral fragments within 42AB, including many of the most abundant species (Fig. 3, A and C). Despite

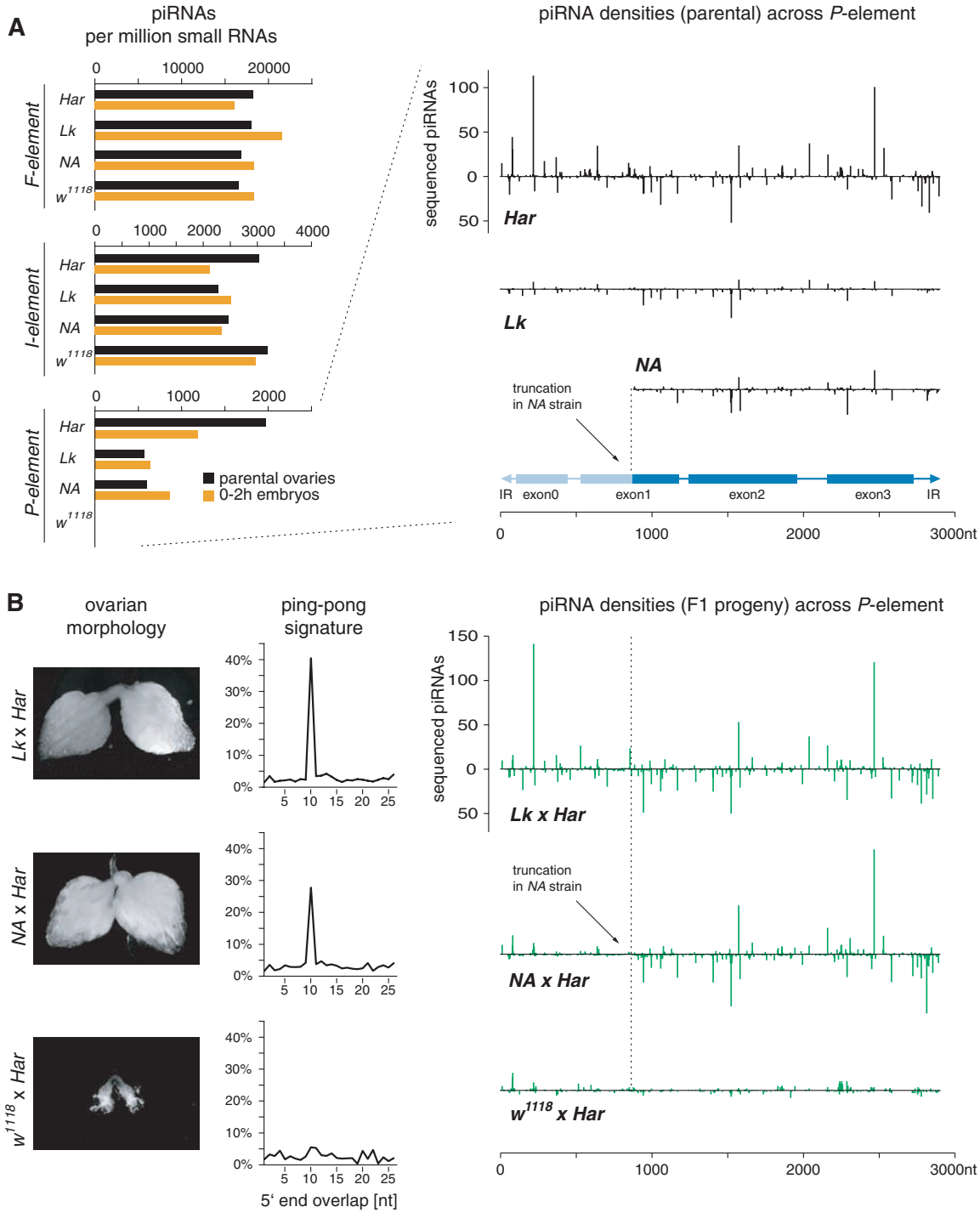

Fig. 4. Suppression of P-M hybrid dysgenesis correlates with maternally deposited piRNAs. (**A**) Normalized number of ovarian (black) and early embryonic (orange) piRNAs from the indicated strains mapping to the *F*-, *I*-, and *P*-elements with up to three (*F* and *I*) or with one (*P*) mismatch(es). To the right (sense, upper; antisense, lower), densities of piRNAs are displayed over the *P*-element in parental ovaries of the *Har*, *LK*, and *NA* strains. The extent of the truncation of the telomeric *P*-insertion in the *NA* strain is indicated. The intron-exon structure of the *P*-element is shown below. (**B**) F1 ovarian morphology, ping-pong signature, and piRNA densities from nondysgenic (*LK* × *Har* and *NA* × *Har*) and dysgenic (w^{1118} × *Har*) F1 progeny are shown.

a more than 20-fold difference in their relative levels, *I*-element piRNAs matching heterochromatic fragments were also derived from 42AB in the reactive strain (Fig. 3C).

We sought to test whether the role of maternally inherited small RNAs in transposon silencing was general. In P-strain/M-strain (P-M) hybrid dysgenesis, crosses between males containing *P*-elements (P-strains) and females devoid of such elements (M-strains) yield sterile progeny with severe gonadal atrophy (GD sterility) (*3*, *9*). We examined small RNAs from *Harwich* (*Har*), a P-strain containing 30 to 50 *P*-element copies, and w^{1118}, here serving as an M-strain. *Harwich* showed strong maternal deposition of *P*-element piRNAs, whereas both M-strain mothers and their 0- to 2-hour embryos lacked such species (Fig. 4A). This contrasted with *I*- and *F*-element piRNAs, which were abundant in parents and embryos from both strains. Crosses between *Harwich* males and w^{1118} females yielded dysgenic (GD) progeny. Because of the impact of severe gonadal atrophy (Fig. 4B and table S1), we normalized the daughter library using piRNAs targeting the *F*-element, a transposon exhibiting consistent profiles in all strains examined. Clearly, dysgenic daughters lacked prominent *P*-element piRNAs and signatures of the ping-pong amplification cycle (Fig. 4B).

Lerik-P(1A) (designated *Lk*) contains two *P*-elements in the X-TAS piRNA cluster, and *Nasr'Allah-P(1A)* (designated *NA*) contains a single 5′ truncated insertion at the same locus (*25*, *26*). *Lk* and *NA* both produce and maternally deposit *P*-element piRNAs (Fig. 4A), with these species in the *NA* strain precisely corresponding to the extent of its only *P*-fragment (Fig. 4A) (*25*). Unlike w^{1118}, *Lk* and *NA* mothers were able to produce fertile offspring with *Harwich*. This result correlated with robust piRNA production in daughter ovaries and with a strong signature of the ping-pong amplification cycle.

The 5′ end of the *P*-element largely lacked piRNAs, particularly antisense species, in both dysgenic flies and fertile *NA-Harwich* progeny (Fig. 4B). *NA* does not deposit maternal piRNAs corresponding to this region, because of the truncation of its *P*-element in X-TAS. Thus, maternal piRNAs are important for potent piRNA generation in daughters, even when the *P*-element is being effectively silenced by piRNAs matching other parts of the transposon.

piRNA clusters have been envisioned as a genetic reservoir of transposon resistance, with immunity being determined by the content of these loci (*17*). Our data indicate that the content of piRNA clusters alone is insufficient to provide resistance to at least some elements within a single generation. Instead, maternally inherited small RNAs appear to be essential to prime the resistance system at each generation to achieve full immunity (see also *27*).

In the I-R system, environmental factors influence the severity of the phenotype in a dysgenic cross (*28*) in a manner linked to the expression level of ancestral *I*-fragments (*29*). Rearing of reactive mothers at elevated temperature or increases in maternal age raise the proportion of fertile progeny. These observations suggest that the experience of the mother translates into a dominant effect on progeny. Our data suggest that this experience may be transmitted through variations in maternally deposited small RNA populations. Thus, transmission of instructive piRNA populations, shaped by both genetic and environmental factors, may provide a previously unknown mechanism for epigenetic inheritance.

References and Notes

1. G. Picard, P. L'Heritier, *Drosophila Inf. Serv.* **46**, 54 (1971).
2. G. Picard, *Genetics* **83**, 107 (1976).
3. M. G. Kidwell, J. F. Kidwell, J. A. Sved, *Genetics* **86**, 813 (1977).
4. G. M. Rubin, M. G. Kidwell, P. M. Bingham, *Cell* **29**, 987 (1982).
5. A. Pelisson, *Mol. Gen. Genet.* **183**, 123 (1981).
6. A. Bucheton, R. Paro, H. M. Sang, A. Pelisson, D. J. Finnegan, *Cell* **38**, 153 (1984).
7. M. G. Kidwell, *Proc. Natl. Acad. Sci. U.S.A.* **80**, 1655 (1983).
8. S. Chambeyron, A. Bucheton, *Cytogenet. Genome Res.* **110**, 215 (2005).
9. J. P. Castro, C. M. Carareto, *Genetica* **121**, 107 (2004).
10. A. A. Aravin, G. J. Hannon, J. Brennecke, *Science* **318**, 761 (2007).
11. C. Klattenhoff, W. Theurkauf, *Development* **135**, 3 (2008).
12. H. B. Megosh, D. N. Cox, C. Campbell, H. Lin, *Curr. Biol.* **16**, 1884 (2006).
13. A. N. Harris, P. M. Macdonald, *Development* **128**, 2823 (2001).
14. Materials and methods are available as supporting material on *Science* Online.
15. S. Jensen, L. Cavarec, M. P. Gassama, T. Heidmann, *Mol. Gen. Genet.* **248**, 381 (1995).
16. M. C. Seleme, I. Busseau, S. Malinsky, A. Bucheton, D. Teninges, *Genetics* **151**, 761 (1999).
17. J. Brennecke *et al.*, *Cell* **128**, 1089 (2007).
18. L. S. Gunawardane *et al.*, *Science* **315**, 1587 (2007), published online 21 February 2007 (10.1126/science.1140494).
19. P. Dimitri, A. Bucheton, *Cytogenet. Genome Res.* **110**, 160 (2005).
20. M. Crozatier, C. Vaury, I. Busseau, A. Pelisson, A. Bucheton, *Nucleic Acids Res.* **16**, 9199 (1988).
21. C. Vaury, P. Abad, A. Pelisson, A. Lenoir, A. Bucheton, *J. Mol. Evol.* **31**, 424 (1990).
22. S. Jensen, M. P. Gassama, X. Dramard, T. Heidmann, *Genetics* **162**, 1197 (2002).
23. S. Jensen, M. P. Gassama, T. Heidmann, *Nat. Genet.* **21**, 209 (1999).
24. S. Malinsky, A. Bucheton, I. Busseau, *Genetics* **156**, 1147 (2000).
25. L. Marin *et al.*, *Genetics* **155**, 1841 (2000).
26. S. Ronsseray, M. Lehmann, D. Anxolabehere, *Genetics* **129**, 501 (1991).
27. J. P. Blumenstiel, D. L. Hartl, *Proc. Natl. Acad. Sci. U.S.A.* **102**, 15965 (2005).
28. A. Bucheton, *Heredity* **41**, 357 (1978).
29. X. Dramard, T. Heidmann, S. Jensen, *PLoS One* **2**, e304 (2007).

30. We thank M. Rooks and D. McCombie (CSHL) for help with deep sequencing, S. Jensen and S. Ronsseray for fly stocks and helpful discussions, and D. Finnegan for the *I*-element ORF-1 antibody. J.B. is supported by a fellowship from The Ernst Schering Foundation, C.D.M. is a Beckman fellow of the Watson School of Biological Sciences and is supported by an NSF Graduate Research Fellowship, and A.S. is supported by a Human Frontier Science Program fellowship. This work was supported by grants from NIH to G.J.H. and A.A.A. and a kind gift from K. W. Davis (to G.J.H.). Small RNA libraries are deposited at Gene Expression Omnibus (accession no. GSE13081, data sets GSM327620 to GSM327634).

Supporting Online Material

www.sciencemag.org/cgi/content/full/322/5906/1387/DC1
Materials and Methods
Figs. S1 to S9
Tables S1 to S3
References

26 August 2008; accepted 27 October 2008
10.1126/science.1165171

PA-824 Kills Nonreplicating *Mycobacterium tuberculosis* by Intracellular NO Release

Ramandeep Singh,[1]* Ujjini Manjunatha,[1,2]* Helena I. M. Boshoff,[1] Young Hwan Ha,[1] Pornwaratt Niyomrattanakit,[2] Richard Ledwidge,[1] Cynthia S. Dowd,[1] Ill Young Lee,[1] Pilho Kim,[1] Liang Zhang,[1] Sunhee Kang,[1] Thomas H. Keller,[2] Jan Jiricek,[2] Clifton E. Barry 3rd[1]†

Bicyclic nitroimidazoles, including PA-824, are exciting candidates for the treatment of tuberculosis. These prodrugs require intracellular activation for their biological function. We found that Rv3547 is a deazaflavin-dependent nitroreductase (Ddn) that converts PA-824 into three primary metabolites; the major one is the corresponding des-nitroimidazole (des-nitro). When derivatives of PA-824 were used, the amount of des-nitro metabolite formed was highly correlated with anaerobic killing of *Mycobacterium tuberculosis* (Mtb). Des-nitro metabolite formation generated reactive nitrogen species, including nitric oxide (NO), which are the major effectors of the anaerobic activity of these compounds. Furthermore, NO scavengers protected the bacilli from the lethal effects of the drug. Thus, these compounds may act as intracellular NO donors and could augment a killing mechanism intrinsic to the innate immune system.

Drug-resistant tuberculosis (TB) has emerged as a major threat to global health (*1*). Promising new candidate drugs are the bicyclic nitroimidazoles, including PA-824 and OPC-67683, which are currently in human clinical trials (*2*, *3*). These molecules are active not only against actively replicating bacteria, but also against bacteria that are nonreplicating by

virtue of hypoxia (*4*). These nonreplicating cells are thought to be particularly difficult to eradicate and may be a major determinant of the extended treatment periods (6 to 8 months) necessary to cure a patient and to avoid disease relapse (*5*). In addition, such nonreplicating bacteria have been proposed to be responsible for latent tuberculosis, a condition that affects one-third of the entire human population (*6*).

The mechanism of cell killing by these prodrugs is complex. Treatment with PA-824 or OPC-67683 disrupts the formation of mycolic acids, major constituents of the cell envelope of Mtb (*4*, *7*). However, this effect seemed unlikely to be responsible for cell killing under nonreplicating conditions, because the bacilli do not extensively remodel mycolic acids under anaerobic conditions (*8*). The deazaflavin cofactor F_{420} and the nonessential F_{420}-dependent glucose-6-phosphate dehydrogenase Fgd1 are both essential for the activation of bicyclic nitroimidazoles, and loss of either confers high-level resistance to PA-824 (*4*, *9*, *10*). We recently identified a rare third class of mutants that had lesions in Rv3547, a member of a large family of proteins in Actinobacteria of unknown function (fig. S1) (*11*). We speculated that Rv3547 was a deazaflavin (F_{420})-dependent nitroreductase and renamed it Ddn (*12*).

To test this, purified F_{420} was reduced by the use of recombinant Mtb Fgd1 and glucose-6-phosphate (*12*). Recombinant Ddn was capable of reoxidizing this cofactor in a time- and enzyme-dependent fashion in the presence of PA-824 (Fig. 1, A and B). To test the specificity of this reaction, the opposite enantiomer of PA-824 (which has the *R* configuration at the 6-position and is about 1/100th as active against whole cells of Mtb) was tested and found to be a poor substrate for Ddn (Fig. 1B).

We next studied the chemical structures of the products of PA-824 reduction by Ddn. By titrating the enzyme with $F_{420}H_2$ and analyzing an aliquot by liquid chromatography–mass spectrometry (LC-MS), we characterized three reduction products (Fig. 1C). The major product had a molecular mass of 315 and was labeled metabolite 1. The formation of this metabolite was mostly complete after addition of a single equivalent of $F_{420}H_2$, as was formation of a minor peak showing a mass/charge ratio (*m/z*) of 331 (metabolite 2). Additional $F_{420}H_2$ equivalents increased mainly metabolite 3 (mass 291), and an unstable intermediate with a molecular mass of 346 (triangles in Fig. 1C). This intermediate (compound C in Figs. 1C and 2) was not stable enough

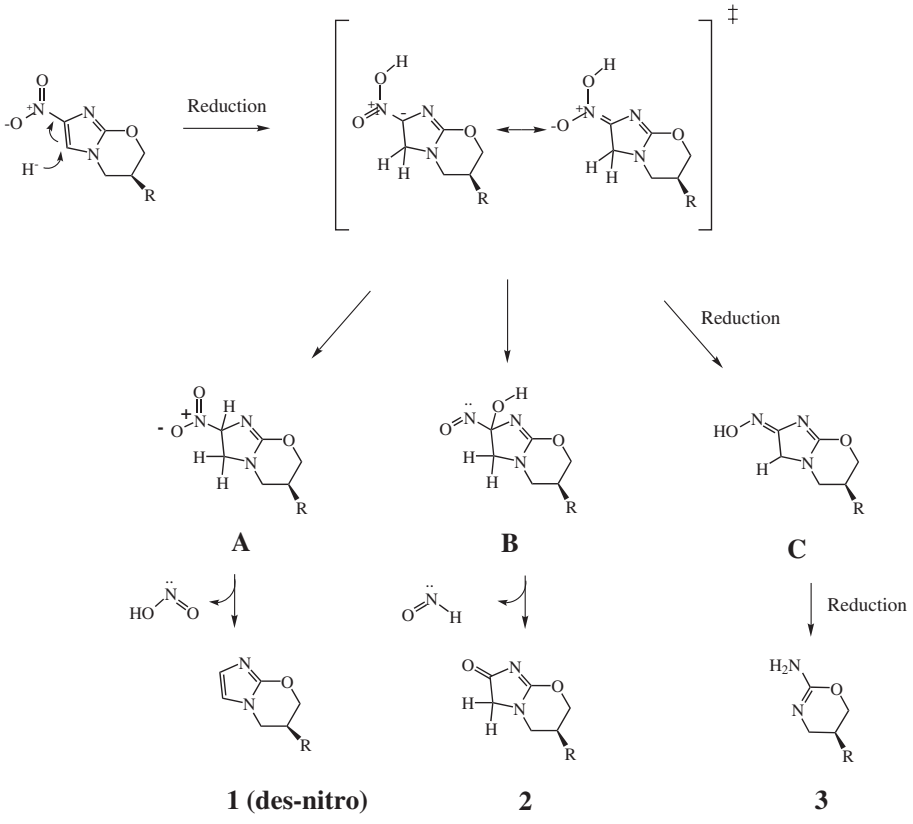

Fig. 2. Mechanism of nitroimidazole reduction by Ddn. Initial hydride addition to C-3 of the bicyclic nitroimidazole results in formation of an intermediate that gives rise to all three observed stable products through the two resonance forms shown. Protonation of the C-2 position by solvent to give (**A**) followed by the elimination of nitrous acid to give **1**. Hydrolysis gives (**B**) which leads to another loss of a reactive nitrogen species in an "enzymatic Nef reaction" to produce **2**. Further reduction of the intermediate produces the unstable hydroxylamine (**C**) which decomposes to **3**.

[1]Tuberculosis Research Section, Laboratory of Clinical Infectious Diseases, National Institute of Allergy and Infectious Diseases, NIH, Bethesda, MD 20892, USA. [2]Novartis Institute for Tropical Diseases, 138670 Singapore.

*These authors contributed equally to this work.
†To whom correspondence should be addressed. E-mail: cbarry@mail.nih.gov

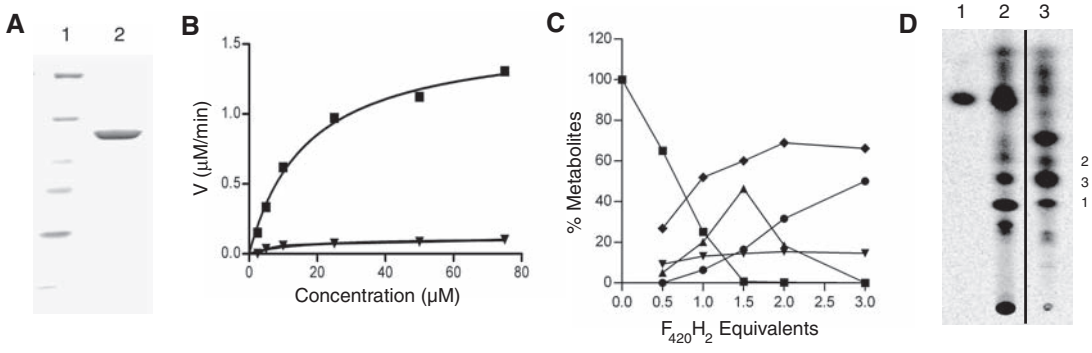

Fig. 1. Ddn-mediated activation of PA-824. (**A**) Ddn was expressed as a maltose-binding protein fusion in *E. coli* and purified on an amylose resin column. (**B**) Ddn-catalyzed oxidation of $F_{420}H_2$ using PA-824 as substrate (squares, the maximum number of substrate molecules an enzyme can turn over per unit of time, k_{cat}/K_m = 0.145 min^{-1} μM^{-1}, or the enantiomer of PA-824 (inverted triangles k_{cat}/K_m = 0.016 min^{-1} μM^{-1}). (**C**) Reaction was initiated by the addition of the indicated amount of $F_{420}H_2$, followed by incubation and analysis of aliquots by LC-MS. Squares, PA-824 (*m/z* 360); diamonds, des-nitro PA-824 (**1**, *m/z* 315); circles, metabolite **3** (*m/z* 291); inverted triangles, metabolite **2** (*m/z* 331); triangles, *m/z* 346, an unstable intermediate (**C**) quickly converted to **3**. (**D**) Thin-layer chromatography (TLC) analysis of the conversion of [^{14}C]PA-824 (lane 1) by whole cells of Mtb (lane 2) or by purified Ddn using 25 μM $F_{420}H_2$ (lane 3). The numbered spots in (D) were shown to comigrate with the numbered metabolites from (C) by collecting HPLC peaks from (C) and analyzing by TLC.

to isolate, and it decomposed quickly and cleanly to metabolite 3. Comparing the metabolites produced from radioactive PA-824 in vitro by using purified Ddn with those produced in whole cells of Mtb revealed only slight differences in the proportion of products formed (Fig. 1D).

On the basis of these results and the previous report that the major metabolite formed from OPC-67683 by whole cells of Mtb was the des-nitro form of this compound (*7*), we proposed the structures for these metabolites shown in Fig. 2. The structures and retention times on high-performance liquid chromatography (HPLC) of all three compounds were confirmed by chemical synthesis and complete analytical characterization (fig. S2). Using synthetic material, we showed that neither the des-nitro nor either of the other two stable metabolites formed by Ddn-mediated reduction of PA-824 had any detectable activity against Mtb, which suggested that the bactericidal event occurred during the process of reduction.

Unlike flavoproteins that perform nitroreduction by single-electron chemistry, F_{420} is an obligate two-electron, or hydride, donor resembling the nicotinamide cofactors (*13*). To explore the chemical mechanism for this unusual reduction, we performed the analogous chemical reduction of PA-824 by sodium borohydride (fig. S2). Des-nitro PA-824, although not the major product, was also produced by borohydride-mediated reduction of PA-824. We unambiguously assigned H-2 (δ6.68 ppm) and H-3 (δ6.48 ppm) of des-nitro PA-824 by observing a nuclear Overhauser effect (NOE) between the two protons at C-5 on the oxazine ring (δ4.01 ppm) and the imidazole proton at C-3 (δ6.48 ppm) (fig. S3). By performing the reduction with sodium borohydride in deuterated methanol and sodium borodeuteride in normal methanol, the proton at the C-3 position of des-nitro PA-824 was shown to be derived from reductant, whereas the proton at the C-2 position was derived from solvent (fig. S4).

Thus, we hypothesized that des-nitro PA-824 was formed by hydride transfer from $F_{420}H_2$ to C-3 of the imidazole ring followed by protonation of the resulting nitronic acid to give **A**, which can eliminate nitrous acid (Fig. 2). This is also observed in bacterial enzymes involved in bioremediation of 2,4,6-trinitrotoluene (TNT), at least one of which has been shown to be F_{420}-dependent (*14*, *15*). An electrochemical study of the sequential single-electron reduction of PA-824 by a radical mechanism supports the novel reduction of the imidazole ring preferentially to the nitro group (*16*). The nitrous acid released would be unstable and quickly disproportionate into nitric oxide (NO) and other reactive nitrogen intermediates (*17*). This same nitronic acid intermediate (or its tautomer) could instead be quenched by water giving **B**, followed by elimination of hyponitrous acid (HNO) to give product **2**, the biochemical equivalent of the Nef reaction that typically requires strongly acidic conditions (*18*). Biological Nef reactions have previously been limited to nitroalkane dioxygenases that utilize flavins and molecular oxygen to convert an alkyl nitro group to a carbonyl (*19*). Although this is a minor product with PA-824, certain bicyclic nitroimidazoles (e.g., compound **7** in Table 1) show this as the major product. Further reduction of the nitronic

Table 1. Structures of bicyclic nitroimidazoles and their aerobic MIC (minimum inhibitory concentration), anaerobic MAC (minimum anaerobicidal concentration), and the apparent V_{max}/K_m for in vivo NO release. MIC values represent the micromolar concentration that will inhibit 99% of the growth of an inoculum of Mtb. MAC values represent the micromolar concentration that will cause a 1 log reduction in bacterial numbers after a 1-week exposure to a compound of hypoxia-adapted Mtb. V_{max}/K_m ratio (RFU hr $^{-1}$ μM^{-1}) values represent the in vivo NO release in *M. bovis* BCG cells. NS, no significant NO release observed; ND, not determined.

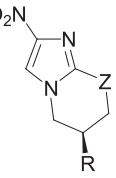

	R	Z	MIC	MAC	V_{max}/K_m
1	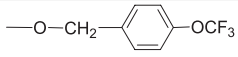	O	0.80	12	12.5
2	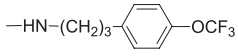	O	0.08	3.1	60.1
3	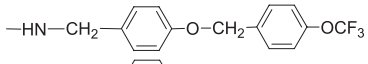	O	0.16	2.1	76.9
4	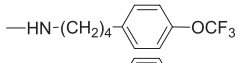	O	0.04	8.1	71.6
5	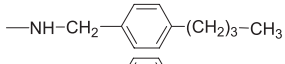	O	0.78	75	4.7
6	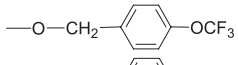	S	1.2	25	NS
7	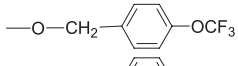	NH	0.80	130	4.8
8	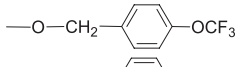	NCHO	6.3	31	ND
9	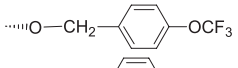	O	110	250	NS
10	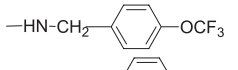	O	0.40	8.0	10.1
11	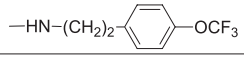	O	0.04	2.0	28.7

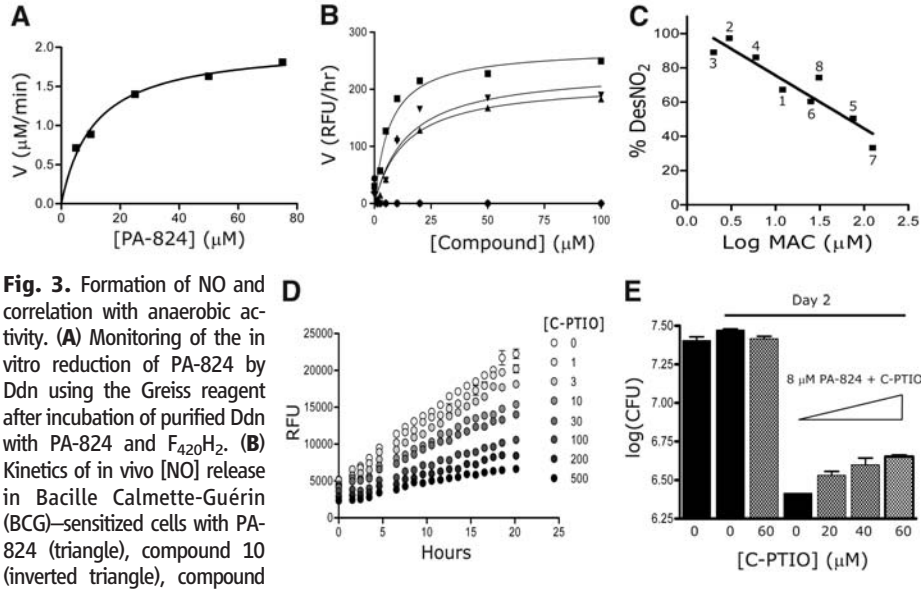

Fig. 3. Formation of NO and correlation with anaerobic activity. (**A**) Monitoring of the in vitro reduction of PA-824 by Ddn using the Greiss reagent after incubation of purified Ddn with PA-824 and $F_{420}H_2$. (**B**) Kinetics of in vivo [NO] release in Bacille Calmette-Guérin (BCG)–sensitized cells with PA-824 (triangle), compound 10 (inverted triangle), compound 11 (square), isoniazid (diamond), and metronidazole (circle) by using DAF-FM diacetate. RFU, relative fluorescence units. (**C**) Correlation between anaerobic killing and the percentage of des-nitro metabolite formed by 8 bicyclic nitroimidazoles (Table 1). (**D**) In vivo [NO] release in BCG cells with 20 μM PA-824 in the presence of increasing C-PTIO [2-(4-carboxyphenyl)-4,4,5,5-tetramethylimidazoline-1-oxyl-3-oxide] concentration. (**E**) Protection of PA-824–mediated killing of nonreplicating hypoxic cells by C-PTIO. Error bars are SD of three independent replicates.

acid intermediate produces the aromatic hydroxylamine metabolite **C**, which, upon further reduction and fragmentation, produces **3** (fig. S5) (*20*).

To test the hypothesis that reduction of PA-824 by Ddn resulted in the release of reactive nitrogen species, we used the Griess reagent to directly detect nitrous acid. A PA-824–dependent production of HNO_2 by Ddn was consistently observed in the presence of $F_{420}H_2$ (Fig. 3A). NO could also be detected in PA-824–treated whole cells, under both aerobic (Fig. 3B) and hypoxic nonreplicating conditions (fig. S6), by preloading cells with diaminofluorescein (DAF-FM) diacetate, a probe that fluoresces specifically in the presence of NO (*21*, *22*).

To correlate NO release with anaerobic killing, we selected a series of eight derivatives that had a broad range (from 2 to 125 μM, Table 1) of minimum anaerobicidal concentration (MAC) values (the aerobic potency of these compounds ranges from 0.04 to 6 μM). These derivatives revealed a strong correlation between the amount of the corresponding des-nitro product formed and anaerobic killing activity (Fig. 3C). Des-nitro formation did not correlate with aerobic activity, nor did any other metabolite correlate with either aerobic or anaerobic activity (fig. S7). The rate of NO release [an apparent V_{max}/K_m as RFU per hour divided by substrate affinity (the Michaelis constant) measured intracellularly] also correlated with anaerobic killing activity (Table 1). Finally, the effect of PA-824 on cells could be abrogated by a scavenger of NO, C-PTIO, which showed a dose-dependent decrease in NO production (Fig. 3D) and partially rescued hypoxic cells from killing by PA-824 (Fig. 3E). This effect was muted by both toxicity and poor cell penetrating ability of C-PTIO. Mtb mutants hypersensitive to NO, such as proteasome mutants, also display increased anaerobic sensitivity to PA-824 (fig. S8). The simplest interpretation of these data is that reactive nitrogen species are dominant in anaerobic activity but under aerobic conditions this is augmented by other effects.

Reactive nitrogen species play a major role in mammalian defense against mycobacterial infections, and mice deficient in the ability to produce NO are hypersusceptible to infection with Mtb (*23*). PA-824–resistant mutants in F_{420} biosynthesis have also been shown to be hypersensitive to killing by NO (*24*). Nitrite and NO both react with cytochromes and cytochrome c oxidase to interfere with electron flow and to cripple the coupling of respiration to reduction of oxygen. Thus, bicyclic nitroimidazoles may function as highly specific NO donors requiring activation by a powerful deazaflavin cofactor (F_{420}) that is unique to a small group of microorganisms and extremophiles, which makes cross-activation by mammalian enzymes highly unlikely. This unusual mechanism for nitroimidazole reduction avoids the single-electron–reduced nitrogen species typical of oxygen-sensitive, flavin-dependent enzymes and defines the chemistry of a class of F_{420}-dependent enzymatic nitroreductases.

NO-donating drugs have been shown to have potential for a wide variety of human diseases including cardiovascular disease, asthma, hypoxic-ischemic brain injury, glaucoma, and Alzheimer's disease (*25*). Indeed, it may be possible to more generally co-opt bacterial nitroreductases to reduce other nitro-containing heterocycles as an avenue for developing anti-infectives. It is noteworthy that the two candidate molecules in phase 2 trials (PA-824 and OPC-67683) were both optimized only for whole-cell aerobic activity and, as a result, have fairly modest anaerobic activity. Thus, these results have the potential to enable structure-based design of a drug specific for the treatment of latent tuberculosis.

References and Notes

1. A. Matteelli *et al.*, *Expert Rev. Anti Infect. Ther.* **5**, 857 (2007).
2. C. E. Barry 3rd, H. I. Boshoff, C. S. Dowd, *Curr. Pharm. Des.* **10**, 3239 (2004).
3. StopTB Working Group on New Drugs; www.stoptb.org/wg/new_drugs/assets/documents/2007GlobalPipeline.pdf (2008).
4. C. K. Stover *et al.*, *Nature* **405**, 962 (2000).
5. H. I. Boshoff, C. E. Barry 3rd, *Nat. Rev. Microbiol.* **3**, 70 (2005).
6. J. E. Gomez, J. D. McKinney, *Tuberculosis (Edinburgh)* **84**, 29 (2004).
7. M. Matsumoto *et al.*, *PLoS Med.* **3**, e466 (2006).
8. H. I. Boshoff, C. E. Barry 3rd, *Drug Discov. Today Dis. Mech.* **3**, 237 (2006).
9. K. P. Choi, T. B. Bair, Y. M. Bae, L. Daniels, *J. Bacteriol.* **183**, 7058 (2001).
10. K. P. Choi, N. Kendrick, L. Daniels, *J. Bacteriol.* **184**, 2420 (2002).
11. Materials and methods are available as supporting material on *Science* Online.
12. U. H. Manjunatha *et al.*, *Proc. Natl. Acad. Sci. U.S.A.* **103**, 431 (2006).
13. C. Walsh, *Acc. Chem. Res.* **19**, 216 (1986).
14. B. F. Smets, H. Yin, A. Esteve-Nunez, *Appl. Microbiol. Biotechnol.* **76**, 267 (2007).
15. K. W. Hofmann, H. J. Knackmuss, G. Heiss, *Appl. Environ. Microbiol.* **70**, 2854 (2004).
16. R. F. Anderson *et al.*, *Org. Biomol. Chem.* **6**, 1973 (2008).
17. J. O. Lundberg, E. Weitzberg, M. T. Gladwin, *Nat. Rev. Drug Discov.* **7**, 156 (2008).
18. R. Ballini, M. Petrini, *Tetrahedron* **60**, 1017 (2004).
19. P. F. Fitzpatrick, A. M. Orville, A. Nagpal, M. P. Valley, *Arch. Biochem. Biophys.* **433**, 157 (2005).
20. B. B. Beaulieu, M. A. Mclafferty, R. L. Koch, P. Goldman, *Antimicrob. Agents Chemother.* **20**, 410 (1981).
21. H. Kojima *et al.*, *Anal. Chem.* **70**, 2446 (1998).
22. H. I. Boshoff *et al.*, *J. Biol. Chem.* **279**, 40174 (2004).
23. J. D. MacMicking *et al.*, *Proc. Natl. Acad. Sci. U.S.A.* **94**, 5243 (1997).
24. K. H. Darwin, S. Ehrt, J. C. Gutierrez-Ramos, N. Weich, C. F. Nathan, *Science* **302**, 1963 (2003).
25. B. Rigas, J. L. Williams, *Nitric Oxide* **19**, 199 (2008).

26. We thank C. Nathan (Cornell University) and T. P. Begley (Cornell University) for insightful comments, S. Ehrt (Cornell University) for proteosome mutants, L. Daniels (Texas A&M University) for F_{420} and M. Goodwin (Tuberculosis Research Section) for analytical support. This work was funded (in part) by the intramural research program of National Institute of Allergy and Infectious Diseases, NIH, and (in part) by a grant from the Bill and Melinda Gates Foundation and the Wellcome Trust through the Grand Challenges in Global Health Initiative. This work was also supported by the Korea Foundation for International Cooperation of Science and Technology (KICOS) through a grant provided by the Korean Ministry of Education, Science and Technology (MEST) (No. K20501000001).

Supporting Online Material

www.sciencemag.org/cgi/content/full/322/5906/1392/DC1
Materials and Methods
Figs. S1 to S8
References

12 August 2008; accepted 2 October 2008
10.1126/science.1164571

Absence of the SRC-2 Coactivator Results in a Glycogenopathy Resembling Von Gierke's Disease

Atul R. Chopra,[1]* Jean-Francois Louet,[1]* Pradip Saha,[1] Jie An,[4] Franco DeMayo,[1] Jianming Xu,[1] Brian York,[1] Saul Karpen,[1,2] Milton Finegold,[3] David Moore,[1] Lawrence Chan,[1] Christopher B. Newgard,[4] Bert W. O'Malley[1]†

Hepatic glucose production is critical for basal brain function and survival when dietary glucose is unavailable. Glucose-6-phosphatase (G6Pase) is an essential, rate-limiting enzyme that serves as a terminal gatekeeper for hepatic glucose release into the plasma. Mutations in *G6Pase* result in Von Gierke's disease (glycogen storage disease–1a), a potentially fatal genetic disorder. We have identified the transcriptional coactivator SRC-2 as a regulator of fasting hepatic glucose release, a function that SRC-2 performs by controlling the expression of hepatic *G6Pase*. SRC-2 modulates *G6Pase* expression directly by acting as a coactivator with the orphan nuclear receptor RORα. In addition, SRC-2 ablation, in both a whole-body and liver-specific manner, resulted in a Von Gierke's disease phenotype in mice. Our results position SRC-2 as a critical regulator of mammalian glucose production.

In mammals, when exogenous glucose is not available, between meals and during fasting, the liver produces glucose from substrates such as glycogen, lactate, pyruvate, glycerol, and amino acids (*1*). During fasting, the liver contributes about 85 to 90% of the glucose load, and the remainder is contributed by the kidney (*1*, *2*). This function of the liver is vital for basal brain function, and thus for the survival of the fasting organism (*1*, *3*).

Glucose-6-phosphatase (G6Pase) is an essential, rate-limiting enzyme that catalyzes the terminal reaction that produces glucose during fasting

(*2*, *4*, *5*). This reaction is common to glycogenolysis and gluconeogenesis, the two processes that provide the body with glucose when the organism is subjected to a fast. This metabolic location, at the crossroad between glycogenolysis and gluconeogenesis, allows G6Pase to control both the short-term and longer-term responses to fasting (*2*, *4*, *5*). G6Pase is present at the membrane of the endoplasmic reticulum in the liver and kidney, where it dephosphorylates glucose-6-phosphate to produce free glucose (*2*, *4*, *5*). Without dephosphorylation, glucose remains trapped in the liver, because the glucose transporters that shuttle it into the plasma cannot transport the phosphorylated form (*2*, *4*, *5*). Loss-of-function mutations in *G6Pase* result in Von Gierke's disease (glycogen storage disorder–1a), an autosomal recessive disorder with an incidence of 1 in 100,000 live births (*6*). Von Gierke's disease is clinically characterized by impaired growth, fasting hypoglycemia, and an increase in concentrations of triglycerides, cholesterol, free fatty acids, ketone bodies, uric acid, and lactic acid in the plasma of fasting animals. Increased liver glycogen stores and hepatic steatosis also occur (*6*).

Steroid receptor coactivator 2 (SRC-2), a member of the p160 family of transcriptional coactivators, has been implicated in a number of physiological processes, from reproduction, mammary morphogenesis, and uterine function to energy metabolism in adipose tissue via regulation of adaptive thermogenesis (*7*–*10*). Its role in liver-mediated glucose homeostasis, however, is unknown. Because fasting is a powerful inducer of the glycogenolytic and gluconeogenic response through increased transcription of the *G6Pase* gene, we tested the role of SRC-2 in fasting modulation of *G6Pase* expression. In the absence of SRC-2 in mice, there was a deficit in fasting *G6Pase* expression in both the liver and the kidney (Fig. 1A). This deficit in expression was accompanied by a deficiency in the catalytic activity of hepatic G6Pase.

Because *G6Pase* expression is enhanced by fasting and suppressed by feeding, we tested the effect of a lack of SRC-2 in those settings. SRC-2 was critical for both basal as well as induced expression of *G6Pase* (Fig. 1B). The fasting expression of other genes involved in the control of gluconeogenic activity such as *phosphoenolpyruvate carboxykinase* (*PEPCK*), *fructose-1,6-bisphosphatase 1* (*FBP1*), *peroxisome proliferator-activated receptor gamma, coactivator 1 alpha* (*PGC-1a*), and *Glucose-6-phosphate translocase* (*G6P translocase*) was essentially unaffected by the absence of SRC-2 (Fig. 1C). Of 21 other genes that are important for fasting glucose homeostasis, in the glycogenolysis, glycogenesis, β-oxidation, ketogenesis, and hexose monophosphate shunt pathways, expression of none of these genes was significantly decreased in mice lacking SRC-2 (table S1). To determine whether other p160 coactivator family members (SRC-1 and SRC-3) function in *G6Pase* regulation during fasting, we determined *G6Pase* expression in the livers of SRC-1 and SRC-3 null animals that were fasted for 24 hours. The absence of SRC-1 and SRC-3 did not affect the expression of *G6Pase*, suggesting an SRC-2–specific effect on the regulation of fasting hepatic *G6Pase* expression (fig. S10).

It was possible that the expression deficit of *G6Pase* that we observed in SRC-2 null animals was due to an indirect systemic effect. To rule out this possibility we isolated primary hepatocytes from wild-type (WT) mice and depleted SRC-2 using RNA interference (RNAi). RNAi-mediated knockdown of SRC-2 resulted in a down-regulation of *G6Pase* expression, suggesting a cell-autonomous effect (Fig. 1D). *G6Pase* is positively regulated, at the transcriptional level, by fasting-associated hormones such as glucagon, catecholamines, and glucocorticoids. We exposed primary hepatocytes from WT and SRC-2 null animals to dexamethasone to stimulate the glucocorticoid receptor or forskolin to simulate hormonal stimulation of adenylyl cyclase. Ablation of SRC-2 decreased both control and hormone-mediated transcription of *G6Pase* (fig. S6, A and B).

The primary manifestations of Von Gierke's disease, which occur as a result of mutations in the *G6Pase* gene, are diminished growth; fasting hypoglycemia; increased concentrations of triglycerides, cholesterol, free fatty acids, ketone bodies, uric acid, and lactic acid in the plasma; increased liver glycogen stores; and hepatic steatosis (*6*). SRC-2 null mice showed fasting hypoglycemia, although the animals maintained normoglycemia in the fed state (Fig. 2A). Considered along with the observation of fasting hypoinsulinemia (Fig. 2B), this suggests a defect in liver function. Further plasma analysis demonstrated increased concentrations of triglycerides, cholesterol, free fatty acids (FFAs), and ketone bodies in SRC-2$^{-/-}$ animals that were fasted for 24 hours (Fig. 2C). Histologically, liver morphology was distorted with a char-

[1]Department of Molecular and Cellular Biology, Baylor College of Medicine, 1 Baylor Plaza, Houston, TX 77030, USA. [2]Department of Pediatrics, Baylor College of Medicine, Houston, TX 77030, USA. [3]Department of Pathology, Baylor College of Medicine, Houston, TX 77030, USA. [4]Sarah W. Stedman Nutrition and Metabolism Center, Duke University Medical Center, Durham, NC 27710, USA.

*These authors contributed equally to this work.
†To whom correspondence should be addressed. E-mail: berto@bcm.tmc.edu

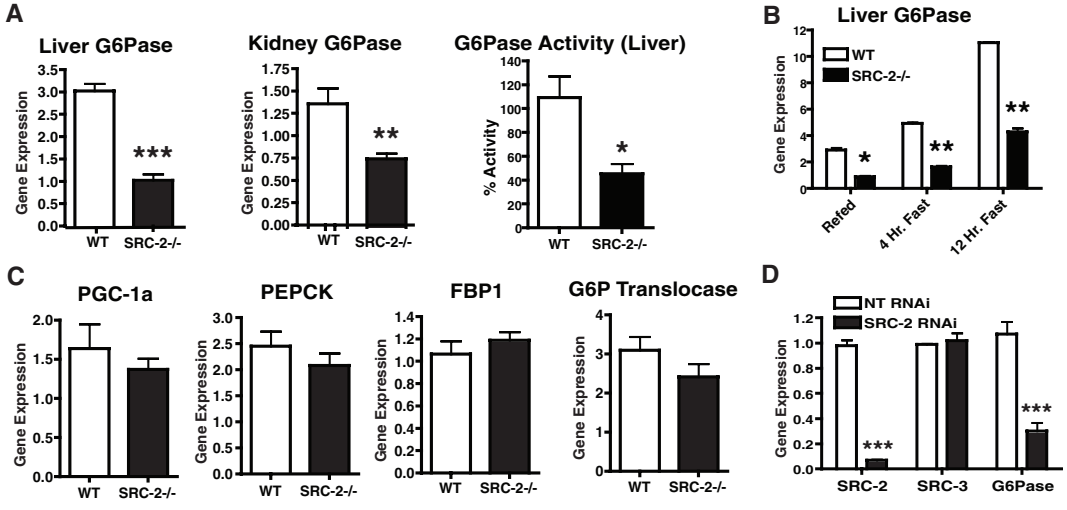

Fig. 1. Role of SRC-2 in *G6Pase* expression in the mouse liver and kidney. (**A**) Diminished expression and activity of G6Pase in the liver and kidney of SRC-2$^{-/-}$ mice. *G6Pase* expression was measured via relative quantitation by quantitative polymerase chain reaction (QPCR) in the liver and kidney of SRC-2 null mice and WT littermates upon 24 hours of fasting (n = 5 mice per group). For G6Pase activity analysis, the first value (WT#1) was fixed at 100, and the rest of the values were compared relative to that (n = 5 mice per group). (**B**) Role of SRC-2 in basal as well as induced hepatic *G6Pase* expression. *G6Pase* expression was measured via relative quantitation by QPCR in the liver of WT and SRC-2 null mice that were refed for 2 hours after a 4-hour fast, fasted for 4 hours, or fasted for 12 hours (n = 3 to 4 mice per group). (**C**) SRC-2 does not regulate the expression of other rate-limiting genes in the gluconeogenesis program. Expression of *G6P translocase*, *PEPCK*, *FBP1*, and *PGC-1a* was measured via relative quantitation by QPCR in the liver of SRC-2 null mice and WT littermates upon 24 hours of fasting (n = 5 mice per group). (**D**) SRC-2 regulates *G6Pase* expression in a cell-autonomous manner. RNAi to SRC-2 results in down-regulation of G6Pase mRNA levels compared with nontargeting (NT) RNAi, as determined via relative quantitation by QPCR. SRC-3 expression level is used as a control for specificity of SRC-2 knockdown. Data are represented as the mean ± SEM. Unpaired student's t test was used for evaluation of statistical significance. *P < 0.05, **P < 0.01, and ***P < 0.001.

acteristic mosaic pattern like that of patients with Von Gierke's disease (Fig. 2D) (*11*). Periodic acid–Schiff staining, Oil Red O staining, and electron microscopy (EM) revealed heavy accumulation of glycogen and triglycerides in the liver of fasted SRC-2 null animals (Fig. 2, E through G). Livers of 24-hour fasted SRC-2 null animals contained about twice as much glycogen and about three times as much triglycerides as did livers from WT animals (Fig. 2H). This was accompanied by increased concentrations of circulating glucagon and catecholamine in SRC-2 null animals,

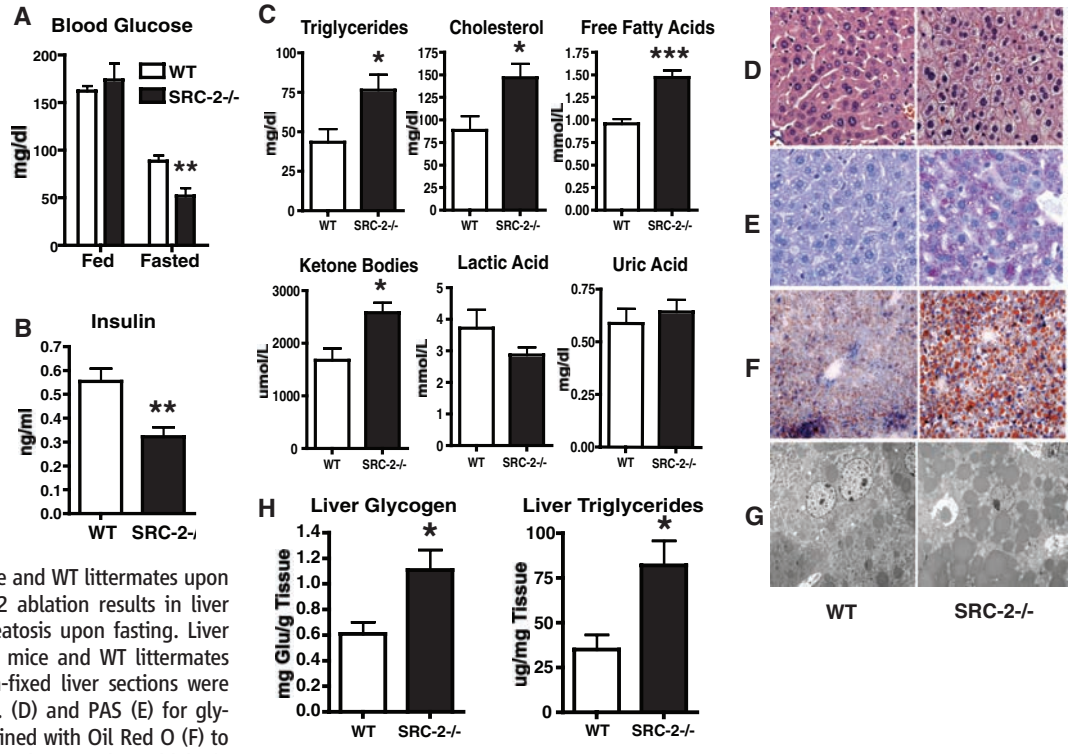

Fig. 2. Lack of SRC-2 results in features like those of Von Gierke's disease (glycogen storage disorder–1a). (**A**) SRC-2 ablation results in fasting hypoglycemia. Blood glucose concentrations were determined in mice upon ad libitum feeding and after 24 hours of fasting ($n = 5$ mice per group), by means of a hand-held glucometer. (**B**) Insulin concentrations were determined in plasma isolated from SRC-2 null mice and WT littermates upon 24 hours of fasting ($n = 5$ mice per group). (**C**) SRC-2 ablation results in increased concentrations of triglycerides, cholesterol, FFAs, and ketone bodies in the plasma upon fasting. Plasma concentrations of triglycerides, cholesterol, FFAs, ketone bodies, uric acid, and lactic acid were determined from plasma isolated from SRC-2 null mice and WT littermates upon 24 hours of fasting. (**D** to **G**) SRC-2 ablation results in liver glycogen accumulation and liver steatosis upon fasting. Liver tissue was isolated from SRC-2 null mice and WT littermates upon 24 hours of fasting. Formalin-fixed liver sections were stained with hematoxylin and eosin. (D) and PAS (E) for glycogen. Frozen liver sections were stained with Oil Red O (F) to demonstrate neutral lipids. Sections fixed in 2% gluteraldehyde and viewed by EM (G) demonstrated the abundance of lipid. (**H**) Measurement of hepatic glycogen and triglyceride content in mice fasted 24 hours. Data are represented as the mean ± SEM. Unpaired student's *t* test was used for evaluation of statistical significance. $^{*}P < 0.05$, $^{**}P < 0.01$, and $^{***}P < 0.001$.

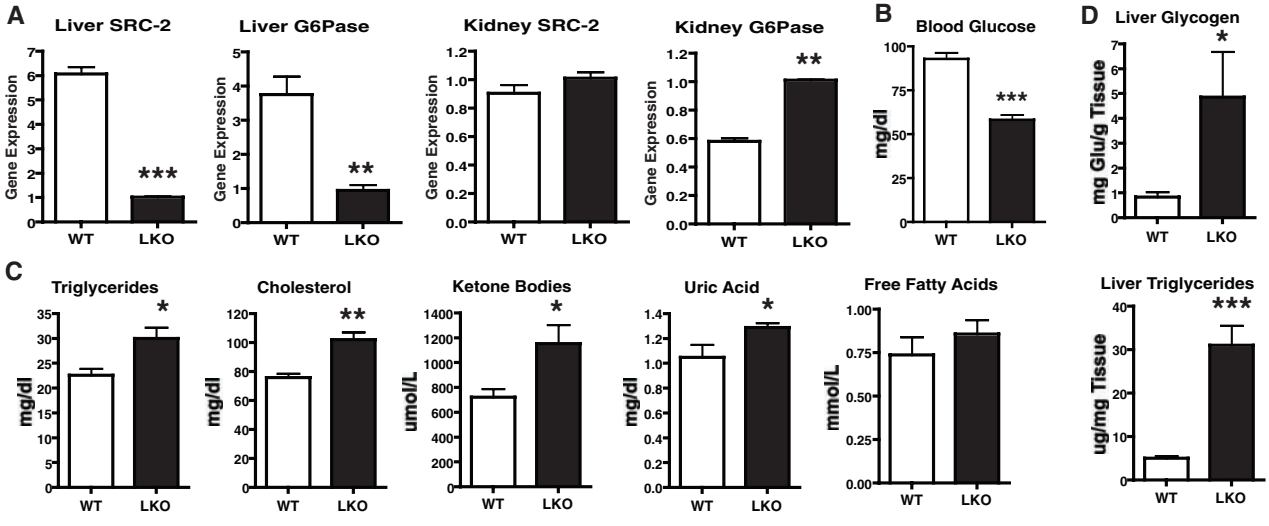

Fig. 3. Liver-selective ablation of SRC-2 results in development of the Von Gierke's disease phenotype. (**A**) Liver-selective SRC-2 ablation results in decreased expression of hepatic *G6Pase* and increased expression of renal *G6Pase*. SRC-2 F/F mice exposed to adenoviral CRE (liver knockout, LKO) were compared with SRC-2 F/F mice exposed to empty adenovirus (WT) by means of tail-vein infusion. Mice fasted for 24 hours were killed, and then plasma and various organs were isolated. Gene expression was measured via relative quantitation by QPCR. (**B**) Fasting hypoglycemia. Blood glucose concentrations were determined in mice fasted for 24 hours by means of a hand-held glucometer. (**C**) Concentrations of triglycerides, cholesterol, ketone bodies, and uric acid in plasma. Plasma concentrations of triglycerides, cholesterol, FFAs, ketone bodies and uric acid were determined from plasma isolated from mice fasted for 24 hours. (**D**) Hepatic steatosis and accumulation of liver glycogen. Measurement of hepatic glycogen and triglyceride content was done in mice fasted for 24 hours ($n = 7$ mice per group). Data are represented as the mean ± SEM. Unpaired student's *t* test was used for evaluation of statistical significance. $^{*}P < 0.05$, $^{**}P < 0.01$, and $^{***}P < 0.001$.

suggesting a compensatory attempt to mobilize liver glycogen (fig. S1). The growth deficit that accompanies the lack of SRC-2 has been described (*12*).

To unequivocally assess the effect of SRC-2 ablation on fasting (basal) liver glucose production, we measured hepatic glucose production using radiolabeled glucose in awake SRC-2 null animals and WT littermates that had been fasted overnight. Basal hepatic glucose production in SRC-2 null animals was depressed compared with that of WT littermates (fig. S3A). In vitro glucose production from gluconeogenic precursors lactate and pyruvate, by primary hepatocytes subjected to RNAi-mediated knockdown of SRC-2, was one-half that by control cells (fig. S3B).

Given that glucose homeostasis in fasting animals is primarily a function of the liver, we tested whether SRC-2 ablation, specifically in the liver, would reproduce the features of Von Gierke's disease. We infused adenovirus carrying the CRE recombinase gene into the tail veins of homozygous SRC-2 floxed (F/F) mice and exposed control SRC-2 F/F mice to empty adenovirus. This approach produces liver-selective transgenesis, because most of the adenoviral load is localized in the liver (*13*–*15*). Liver-selective depletion of SRC-2 resulted in decreased abundance of G6Pase mRNA in the liver of fasting animals (Fig. 3A). *G6Pase* expression in the kidney was increased, possibly as a compensatory response (Fig. 3A). By contrast, the results in fasted SRC-2 (whole-body) knockout mice showed decreased renal *G6Pase* expression, and thus exemplifies the critical nature of SRC-2's influence over *G6Pase* expression (Fig. 1A). Liver-selective depletion of SRC-2 in fasted animals resulted in hypoglycemia (Fig. 3B), along with increased concentrations of triglycerides, cholesterol, ketone bodies, and uric acid in the plasma (Fig. 3C). This plasma profile was accompanied by an accumulation of hepatic glycogen and triglycerides in fasted liver-selective SRC-2 null animals (Fig. 3D), thereby reproducing the phenotypic characteristics of Von Gierke's disease.

Because SRC-2 is a "coactivator" and lacks specific DNA binding activity, it is presumably recruited to a gene promoter by a transcription factor in order to function. Although transcriptional coactivators often function at multiple genes, our results indicated that SRC-2 might regulate the expression of just one gene in the gluconeogenesis and glycogenolysis pathways—*G6Pase* (Fig. 1, A and B, and table S1). We therefore searched the *G6Pase* promoter sequence for transcription factor response elements that might explain such selectivity. We found an evolutionarily conserved retinoid-related orphan receptor α (RORα) response element (RORE) close to the transcriptional start site (fig. S11). SRC-2 and RORα have been reported to bind and synergize in reporter assays (*16*). Consequently, we tested the human WT *G6Pase* promoter (−1227, +57) by coexpressing it with expression plasmids carrying SRC-2 and RORα. SRC-2 and RORα, when expressed together, synergized strongly to produce *G6Pase* promoter activation (Fig. 4A). This synergism (coactivation) was completely abolished upon specific mutation of the RORE (Fig. 4A). We also tested other transcription factors that bind SRC-2 and are important for regulation of fasting glucose homeostasis such as the glucocorticoid receptor and orphan nuclear receptor Nurr77, and found that SRC-2 did not synergize with them in this context (fig. S7C).

To demonstrate the effect of RORα on transactivation of *G6Pase* in the correct chromatin context, we transduced primary hepatocytes with adenoviral RORα. This resulted in increased expression of the endogenous *G6Pase* gene, without affecting the expression of other key genes involved in the gluconeogenic pathway such as *PEPCK*, *FBP1*, *PGC-1a* and *G6P translocase* (Fig. 4B). The RORα-mediated increase in *G6Pase* transactivation was abolished in a SRC-2 null background (fig. S4B). Furthermore, RNAi-mediated depletion of RORα in primary hepatocytes resulted in decreased expression of *G6Pase* (fig. S4). To assess whether RORα affects *G6Pase* regulation mediated by fasting hormones, we treated primary hepatocytes that had been exposed to RNAi-mediated depletion of RORα with dexamethasone or forskolin. Depletion of RORα diminished the effect of dexamethasone and forskolin stimulation of *G6Pase* gene expression (fig. S6C), although forskolin retained a strong activating effect. We also tested the effects of the promoter-proximal RORE on mediation of the signal from dexamethasone and forskolin (fig.S6D). Basal activity of the *G6Pase* promoter and that induced by a combination of dexamethasone and forskolin was inhibited upon mutation of the RORE, suggesting that this response element functions in the signaling from fasting hormones that results in *G6Pase* promoter activation. In vivo chromatin immunoprecipitation (ChIP) experiments showed that both SRC-2 and RORα proteins bound to the *G6Pase* promoter, selectively in the region of the RORE (Fig. 4C). To further substantiate that SRC-2 was recruited to the *G6Pase* promoter by RORα, we overexpressed RORα in primary hepatocytes. This resulted in increased promoter occupancy of RORα, which in turn increased the promoter occupancy of SRC-2, suggesting that RORα could indeed recruit SRC-2 to the *G6Pase* promoter (Fig. S5A). Conversely, SRC-2 promoter occupancy was abolished in cells depleted of RORα (Fig. S5B). These results suggest that RORα is necessary and sufficient to recruit SRC-2 to the *G6Pase* promoter.

The phenotype and the gene-expression profile of SRC-2 null animals suggests that the perturbation of glucose homeostasis is due to a deficiency in *G6Pase* expression. However, the

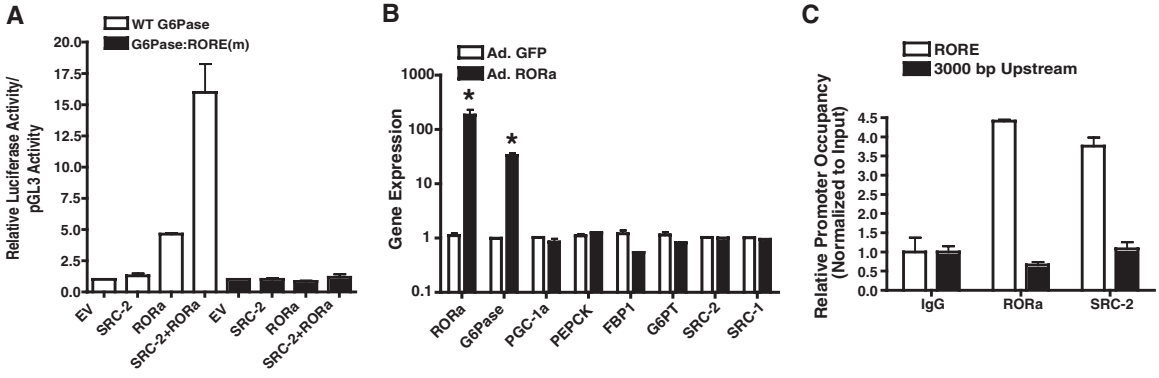

Fig. 4. Cooperation of SRC-2 with orphan nuclear receptor RORα for transactivation of the *G6Pase* promoter. (**A**) Synergism of SRC-2 with RORα in producing transactivation of the *G6Pase* promoter. HeLa cells were transfected with a reporter-gene plasmid driven by the WT human *G6Pase* promoter (−1227, +57) and the same promoter with the four central residues mutated in the hexameric RORE, together with expression plasmids for SRC-2 and RORα. Reporter-gene expression levels were determined 48 hours after transfection. The empty vector (EV) value was fixed at 1, and the rest of the values are compared relative to that. (**B**) RORα regulates *G6Pase* expression in a cell-autonomous manner. Adenoviral overexpression of RORα in mouse primary hepatocytes results in up-regulation of *G6Pase* expression as determined via relative quantitation by QPCR. (**C**) In vivo ChIP: In the mouse liver, SRC-2 and RORα bind the *G6Pase* promoter in the region containing the RORE. ChIP assays were performed with 150 to 200–base pair (bp) amplicons flanking the region containing the RORE and an irrelevant region 3000 bp upstream of the transcription start site. Sybr-Green QPCR (normalized to input) was used to assess SRC-2 and RORα occupancy of the *G6Pase* promoter upon ChIP, with SRC-2– and RORα-specific antibodies. Data are represented as the mean ± SEM. **P* < 0.05, ***P* < 0.01, and ****P* < 0.001.

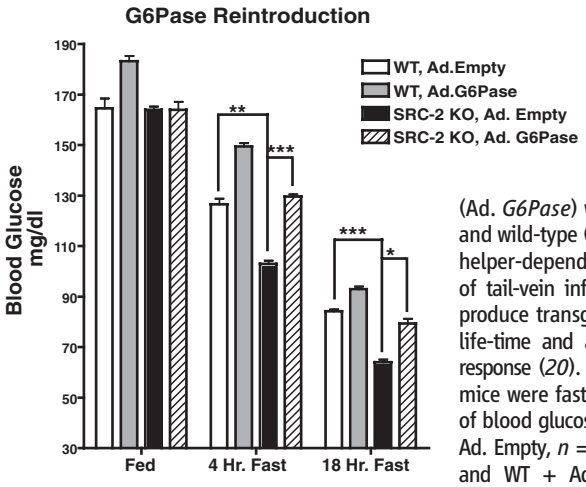

Fig. 5. Correction of hypoglycemia in SRC-2$^{-/-}$ mice by overexpression of *G6Pase*. Adenoviral reintroduction of *G6Pase* in SRC-2 null mice and WT littermates. SRC-2 null mice (KO) exposed to canine helper-dependent adenoviral *G6Pase* (Ad. *G6Pase*) were compared with SRC-2 null (KO) and wild-type (WT) littermate mice exposed to empty helper-dependent adenovirus (Ad. Empty) by means of tail-vein infusion. Helper-dependent adenoviruses produce transgenesis for the duration of the mouse life-time and are associated with little inflammatory response (*20*). Thirty days after adenoviral infusion, mice were fasted for 24 hours before determination of blood glucose (KO + Ad. *G6Pase*, $n = 5$ mice; KO + Ad. Empty, $n = 6$ mice; WT + Ad. Empty, $n = 5$ mice; and WT + Ad. *G6Pase*, $n = 4$ mice). Data are represented as the mean ± SEM. Unpaired student's *t* test was used for evaluation of statistical significance. $^*P < 0.05$, $^{**}P < 0.01$, and $^{***}P < 0.001$. Statistical comparison between WT + Ad. Empty group and WT + Ad. *G6Pase* group achieved significance in the 4-hour fasted animals and in the 18-hour fasted animals. For clarity, this is not indicated in the figure.

possibility that SRC-2 might regulate another gene that might contribute to the phenotype cannot be ruled out. Therefore, we reintroduced G6Pase into SRC-2 null mice by infusion of a recombinant adenovirus containing *G6Pase* cDNA, or an adenovirus containing no cDNA insert. We measured blood glucose concentration in three independent feeding states—fed, fasted for 4 hours, and fasted for 18 hours. Fasting hypoglycemia caused by lack of SRC-2 was diminished in animals that received the G6Pase adenovirus compared to that in animals that were exposed to an empty adenovirus (Fig. 5). This result is consistent with the possibility that some of the glucose homeostasis deficit observed in fasted SRC-2 null animals results from a deficiency in *G6Pase* expression.

Glycogenolysis is the primary process of endogenous glucose production in the first 4 hours after a meal and is followed by the transition to gluconeogenesis upon prolonged fasting (*2*, *4*, *5*). During glycogenolysis, there is no requirement for the activation of PEPCK and FBP1, enzymes that are limited to the process of gluconeogenesis (*1*). We report the identification of two transcriptional entities, SRC-2 and RORα, that regulate *G6Pase* without regulating *PEPCK* and *FBP1*. Unlike systems in which transcriptional coactivators exert control over multiple downstream target genes to modulate physiology (*17*–*19*), SRC-2 appears to control glucose availability through the regulation of one key mediator (Fig. 1, A and B, and table S1). This study unmasks a biological entity, other than mutations in the *G6Pase* gene itself, that might contribute to cases of glycogen storage disorders and unexplained hypoglycemia. Accordingly, SRC-2 and RORα may represent new therapeutic targets against these diseases.

References and Notes

1. R. C. Nordlie, J. D. Foster, A. J. Lange, *Annu. Rev. Nutr.* **19**, 379 (1999).
2. E. van Schaftingen, I. Gerin, *Biochem. J.* **362**, 513 (2002).
3. A. J. Liedtke, *J. Mol. Cell. Cardiol.* **29**, 1073 (1997).
4. R. C. Nordlie, *Curr. Top. Cell. Regul.* **8**, 33 (1974).
5. R. C. Nordlie, *Life Sci.* **24**, 2397 (1979).
6. K. J. Lei *et al.*, *Nat. Genet.* **13**, 203 (1996).
7. J. W. Jeong *et al.*, *Endocrinology* **148**, 4238 (2007).
8. F. Picard *et al.*, *Cell* **111**, 931 (2002).
9. A. Mukherjee *et al.*, *Mol. Cell. Biol.* **26**, 6571 (2006).
10. A. Mukherjee, P. Amato, D. C. Allred, F. J. DeMayo, J. P. Lydon, *Nucl. Recept. Signal.* **5**, e011 (2007).
11. S. Gogus *et al.*, *Pediatr. Dev. Pathol.* **5**, 299 (2002).
12. M. Gehin *et al.*, *Mol. Cell. Biol.* **22**, 5923 (2002).
13. F. Li *et al.*, *Cancer Res.* **66**, 5608 (2006).
14. D. Phaneuf, A. D. Moscioni, C. LeClair, S. E. Raper, J. M. Wilson, *DNA Cell Biol.* **23**, 592 (2004).
15. D. E. Stec, R. L. Davisson, R. E. Haskell, B. L. Davidson, C. D. Sigmund, *J. Biol. Chem.* **274**, 21285 (1999).
16. G. B. Atkins *et al.*, *Mol. Endocrinol.* **13**, 1550 (1999).
17. J. C. Yoon *et al.*, *Nature* **413**, 131 (2001).
18. C. Yu *et al.*, *Mol. Cell* **25**, 765 (2007).
19. J. St-Pierre *et al.*, *Cell* **127**, 397 (2006).
20. D. D. Koeberl *et al.*, *Mol. Ther.* **15**, 1253 (2007).
21. We thank O. McGuinness for help with assessment of liver glycogen and triglyceride content; D. White for help with primary hepatocyte isolation; S. Zhou and J. Song for help with animal breeding; J. Barish for performing the electron microscopy; J. Lin for the RORα adenovirus; J. Lydon for the SRC-2 F/F mice and M. Stallcup for the SRC-2 activation domain mutants; R. Lanz for help with QPCR setup and analysis; M. Muehlbauer for help with plasma analysis of various metabolites; H. Klein and S. Greene for help with figure and model construction; and J. Sagen and C. Foulds for helpful discussion and critical reading of the manuscript. F.D. is supported by the National Institute of Diabetes and Digestive and Kidney Diseases (NIDDK) (grant PO1 DK59820). L.C. is supported by the NIH (grant HL51586). J.X. is supported by the NIH (DK58242). C.B.N. is supported by the NIH (grant PO1 DK58398). B.W.O. is supported by the NIDDK (grant PO1 DK59820), Nuclear Receptor Signaling Atlas (NURSA) (U19 DK062434), and a grant from the Welch Foundation.

Supporting Online Material

www.sciencemag.org/cgi/content/full/322/5906/1395/DC1
Methods
Figs. S1 to S11
Table S1
References

19 August 2008; accepted 22 October 2008
10.1126/science.1164847

New Products

3D Microscope Software

The 3D Measurement module of AxioVision software permits quantitative three-dimensional (3D) evaluation of microscope photos. In combination with the Inside4D module, the new software is used for the segmentation of objects in the 3D volume model, including a 3D view and the generation of a binary image. The latter can be edited using the 3D binary image editor. In addition, the module permits the user to measure interactively by clicking on individual objects in the 3D view or to automatically measure the entire image stack.

Carl Zeiss
For information +49-(0)-3641/642770
www.zeiss.de/mikro

Metagenomic DNA

The Metagenomic DNA Isolation Kit for Water offers an alternative to traditional, time-consuming DNA isolation for metagenomic library production. The kit eliminates the need for agarose plugs, random shearing, and size-selection by pulse-field electrophoresis. The kit isolates DNA from culturable and unculturable microbes in water samples, including gram-positive bacteria. The isolated DNA can be used immediately for end repair and cloning into a suitable vector.

Epicentre Biotechnologies
For information 800-284-8474
www.EpiBio.com

Genomic Analysis Platform

A new Small RNA Expression Analysis Kit, which runs on the Solid System high-throughput platform for DNA sequencing and genomic analysis, enables scientists to rapidly discover and profile novel small RNA molecules without prior knowledge of sequence information. The system includes a new multiplexing technology that enables the simultaneous analysis of up to 256 samples in a single sequencing run. The kit is designed to reduce the experimental variability associated with small RNA library preparation. The kit converts total RNA into a library suitable for input into the Solid System workflow for high throughput applications such as studying the function of small RNA molecules, validation of whole genome association results, targeted resequencing, chromatin immunoprecipitation, rare and somatic mutation detection, and epigenetic studies.

Applied Biosystems
For information 800-327-3002
www.appliedbiosystems.com

Chiral Method Development

The Chiral Methods Development Kit for capillary electrophoresis analysis on the P/ACE MDQ System features highly sulfated cyclodextrins, a family of three chiral reagents that deliver excellent performance in the separation of most neutral, basic, and weakly acidic compounds of pharmaceutical and biological interest. Capillary electrophoresis uses significantly less sample and reagent than high-performance liquid chromatography for chiral separations, while providing broad selectivity and fast results.

Beckman Coulter
For information 714-993-8736
www.beckman.com

Affinity Chromatography Resin

Strep-Tactin Superflow high capacity is an affinity chromatography resin for purification of recombinant Strep-tag proteins. The resin has improved binding capacity but the same high-protein purity as standard Strep-Tactin Superflow. The resin combines outstanding flow characteristics with superior mechanical stability. It is suitable for high flow rates and useful for purification of large protein complexes.

IBA
For information +49-551-50672-114
www.strep-tag.com

Fluorescence Difference Gel Electrophoresis

The 2D Fluorescence Difference Gel Electrophoresis (DIGE) offers significant cost and time savings in comparison with traditional two-dimensional (2D) electrophoresis. Protein mixtures are labeled prior to electrophoresis with size-matched and charge-matched, spectrally resolvable CyDye fluoroflores, allowing the simultaneous separation and comparative analysis of up to three samples on a single 2D gel. Following 2D electrophoresis, the results can be scanned with the Typhoon Variable Mode Imager or the Ettan DIGE Imager. DeCyder Differential Analysis Software automatically locates and analyzes protein spots, assigning statistical confidence to every difference between the samples. The system ensures that each protein spot has its own internal standard, eliminating gel variation issues and increasing accuracy and reproducibility.

GE Healthcare
For information 732-457-8149
www.gelifesciences.com/trydige

Oxidative Stress Kit

The OxyELISA Oxidized Protein Quantitation kit provides all the reagents necessary for quantitative, high throughput detection of modified proteins in cells undergoing oxidative stress. By providing a fast and sensitive assay for oxidation, the kit can help researchers, especially neuroscientists, understand the mechanisms of cellular aging. As a result of oxidative stress, oxygen-free radicals and other reactive species introduce carbonyl groups into proteins in the cell. The OxyELISA kit detects these carbonyl groups. The kit makes use of a direct-labeled monoclonal antibody that is readily detected without a secondary antibody.

Millipore
For information 800-548-7853
www.millipore.com

Electronically submit your new product description or product literature information! Go to **www.sciencemag.org/products/newproducts.dtl** for more information.

Newly offered instrumentation, apparatus, and laboratory materials of interest to researchers in all disciplines in academic, industrial, and governmental organizations are featured in this space. Emphasis is given to purpose, chief characteristics, and availabilty of products and materials. Endorsement by *Science* or AAAS of any products or materials mentioned is not implied. Additional information may be obtained from the manufacturer or supplier.

POSITIONS OPEN

INSTITUTE DIRECTOR POSITION

Shanghai Institutes for Biological Science (SIBS) is recruiting a highly motivated full-time Director of the Institute of Biochemistry and Cell Biology (IBCB), an institute conducting basic research relevant to human health with expertise in biochemistry, molecular biology, and cell biology. There are over 700 research staff in 50 research groups, including 11 members of the Chinese Academy of Sciences and the Chinese Academy of Engineering. Research at the Institute is divided into two major areas; in the field of biochemistry and molecular biology, the research focuses on protein science including proteomics, protein complexes, structural biology, gene expression regulation including epigenetics and noncoding RNAs, and male reproductive biology. In the field of cell biology, the research focuses on signal-transduction networks, stem-cell biology, immunology, developmental biology, and cancer biology. IBCB is also actively involved in translational research using animal models of human diseases and drug discovery-related small molecule screening.

SIBS is the largest life science research organization in the Chinese Academy of Sciences. There are eight research institutes, including Institute of Biochemistry and Cell Biology, Institute of Neuroscience, Institute of Materia Medica, Institute of Plant Physiology and Ecology, Institute of Health Sciences, Institute for Nutritional Sciences, Institut Pasteur of Shanghai, and CAS-MPG Partner Institute for Computational Biology.

Qualified candidates must have a Ph.D., M.D./Ph.D., or equivalent graduate degree, outstanding academic credentials, and established leadership. Applicants should be at the tenured **FULL PROFESSOR** rank and are less than 50 years old. The successful candidate will be provided with a competitive startup package and is expected to develop a strong research program in addition to excellent leadership to IBCB. Attractive salary and other personal benefits are available.

Interested applicants should forward curriculum vitae, a brief description of research interests, a publication list, reprints of five selected papers published in the last five years, three reference letters, a copy of Ph.D. diploma, and other relevant certificates before January 15, 2009, to:

Mr. Weijun Wang
Shanghai Institutes for Biological Sciences
Chinese Academy of Sciences
320 Yue Yang Road, Shanghai, 200031, China
Fax: 0086-21-54920078; telephone: 0086-21-54920027; e-mail: wjwang@sibs.ac.cn

For more information, please visit **website: http://www.sibs.ac.cn.**

Funded by the European Commission grant, Marie Curie Development Host Fellowship, the Institute for Bioprocessing and Analytical Measurement Techniques has established a project team comprising of experienced scientists. The starting date was December 1, 2006.

To expand the project team, the position of an experienced scientist is available. The successful candidate holds a Ph.D. and has at least four years of experiences in biophysics, physics, or (micro) engineering.

Starting as soon as possible the position will be funded for two years. The candidate will investigate microsystems to apply electrokinetic principles for biology, biotechnology, and biomedicine and will establish laboratory prototypes. Please send your application as soon as possible to the head of the Institute:

Prof. Beckmann
Institute for Bioprocessing and Analytical Measurement Techniques, Rosenhof
D-37308 Heilbad Heiligenstadt Germany
Telephone:+49 0 3603-671-100
Fax:+49 03603-671-200
E-mail: dieter.beckmann@iba-heiligenstadt.de
Website: http://www.iba-heiligenstadt.de/

Equal opportunities, particularly between women and men, are given.

POSITIONS OPEN

University of Maryland
CENTER FOR ENVIRONMENTAL SCIENCE

FACULTY and POSTDOCTORAL POSITIONS
Chesapeake Biological Laboratory

The University of Maryland Center for Environmental Science, Chesapeake Biological Laboratory announces openings to enhance our research and teaching programs and contribute to our strategic direction. The growing multidisciplinary environmental research programs focus on environmental issues of both international concern and local relevance to the Chesapeake Bay ecosystem **(website: http://www.cbl.umces.edu).** We seek scientists with interdisciplinary interests in environmental research, graduate level training, and in scientific integration and application. Applications are invited in the following areas:

Organic geochemistry in coastal environments with interests in the impact of regional climate change on land-sea interactions of organic materials or the cycling of anthropogenic compounds of emerging concern in coastal systems. A strong analytical focus is desirable.

Ecological forecasting with interests in how coastal and estuarine ecosystems respond to natural or anthropogenic perturbation such as eutrophication and/or regional climate change. Candidates that link empirical approaches with strong quantitative skills in ecosystem modeling or spatial and temporal dynamics are particularly encouraged.

Fishery economics with interests in stock assessment and fisheries management. Candidates that link economics, policy, and fishery science including the use and critical analysis of quantitative methods and models are particularly encouraged.

For the Faculty positions, Junior Faculty ranks with postdoctoral experience or outstanding Senior Scientists with interests in programmatic development will be considered. Full participation in our Graduate Program **(website: http://www.mees.umd.edu)** is expected. For Postdoctoral positions, we seek applications from researchers who have completed their Ph.D.

Application process: Only electronic applications will be accepted. Applicants should send: (1) a cover letter including the names and contact details for three references (2) curriculum vitae; (3) a statement of research and teaching experience and interests; and (4) electronic (PDF) files of up to five reprints. Letters should be addressed to: **Dr. Margaret A. Palmer, Director, Chesapeake Biological Laboratory,** and all materials sent to **e-mail: facultysearch@cbl.umces.edu.** Applications received by December 31, 2008, will be given strong preference.

Salary and benefits are competitive and dependent on qualifications. Ph.D. is required of successful candidate at time of appointment. The applicant must be able to generate external research funding and participate in graduate teaching and training. *UMCES is an Affirmative Action/Equal Opportunity Employer. We promote excellence through diversity and encourage women and minorities to apply.*

FACULTY POSITION
Plant Molecular Ecology
The University of Queensland
Brisbane, Australia

The School of Integrative Biology together with the Queensland Herbarium invites applications for a five-year, fixed-term **LECTURER LEVEL B** position **(ASSISTANT PROFESSOR)** to develop a vibrant, externally funded research program in plant molecular ecology, systematics, and conservation. A competitive startup package will be negotiated with the successful applicant. Closing date is 5 January 2009. To apply please visit **website: http://www.jobsatuq.net** to obtain a copy of the position description and application process, or contact **Prof. Hugh Possingham** at **e-mail: h.possingham@uq.edu.au** for more information.

NIAAA
National Institute on Alcohol Abuse and Alcoholism

Tenure-Track Investigator Position Available

The National Institute on Alcohol Abuse and Alcoholism (NIAAA), a major research component of the National Institutes of Health (NIH) and the Department of Health and Human Services (HHS), is recruiting for a tenure-track scientist to establish an independent research program in the area of human physiology and pharmacokinetics within the Laboratory of Clinical and Translational Studies (LCTS), Division of Intramural Clinical and Biological Research (DICBR), NIAAA. Individuals with interest in the pharmacology of alcohol in humans and experience employing an integrative approach to evaluate the genetic and environmental determinants of the pharmacokinetics and pharmacodynamics of psychoactive agents are encouraged to apply.

Candidates must hold a Ph.D., M.D., Pharm D or equivalent degree and have at least 3 years of postdoctoral experience. The selected candidate will be expected to establish an independent program to develop model laboratory paradigms to screen novel potential treatments for alcoholism and to evaluate genetic and environmental determinants of variability in the pharmacokinetics and CNS pharmacodynamics of alcohol in humans. Criteria for selection will include: a strong publication record, demonstrated expertise in clinical pharmacology, including advanced pharmacokinetic modeling skills, demonstrated success in leading and mentoring research staff at various levels (i.e., postdoctoral fellows, research associates, technicians, etc.), and demonstrated success in establishing, facilitating and maintaining collaborations. Resources provided to the selected candidate include laboratory and office space, personnel and an operating budget sufficient to develop this independent research program.

Interested candidates wishing to be considered for this position may submit a curriculum vitae, bibliography, the names and addresses of three references, and a brief proposal that reflects the applicant's research interests/goals and an approach for establishing an independent research program, by the closing date to: **Chair, Search Committee, NIAAA, National Institute on Alcohol Abuse & Alcoholism (NIAAA), NIH, c/o Ms. Patricia Scullion, 5635 Fishers Lane, Room 3061, Bethesda, MD 20892 **For Federal Express delivery, Rockville, MD 20852. OR Submit Via Secure Email: LCTSRecruit@mail.nih.gov.**

NOTE: The closing date for receipt of applications is **January 28, 2009**

NIAAA
National Institute on Alcohol Abuse and Alcoholism

Tenure-Track Investigator Position Available

The National Institute on Alcohol Abuse and Alcoholism (NIAAA), a major research component of the National Institutes of Health (NIH) and the Department of Health and Human Services (HHS), is recruiting for a tenure-track Investigator to establish and direct an independent research program in the area of comparative behavioral genomics in the Laboratory of Neurogenetics (LNG), Division of Intramural Clinical and Biological Research (DICBR), NIAAA.

The selected candidate will be expected to establish an independent research program that examines how genetic and environmental factors relate to intra- and inter-specific variation in traits that, in humans, are known risk factors for alcohol use disorders (e.g., stress reactivity, behavioral dyscontrol, reward seeking/sensitivity). Candidates must hold a Ph.D., M.D. or equivalent degree. Criteria for selection will include: a strong publication record in the field of genetics/genomics, demonstrated experience using animal models of human psychiatric disorders or addictions, demonstrated success in establishing and maintaining collaborations and demonstrated success in leading and mentoring research staff at various levels (e.g., postdoctoral fellows, research associates, and/or technicians).

Resources provided to the selected candidate include laboratory and core laboratory facilities, office space, personnel and an operating budget sufficient to develop this independent research program.

Interested candidates wishing to be considered for this position may submit a curriculum vitae, bibliography, the names and addresses of three references, and a brief proposal that reflects the applicant's research interests/goals and an approach for establishing an independent research program, by the closing date to Ms. Patricia Scullion at address below. *Note – we encourage you to submit your complete application electronically so that we may confirm receipt of your materials. **Chair, Search Committee, c/o Ms. Patricia Scullion, National Institute on Alcohol Abuse & Alcoholism (NIAAA), NIH, c/o Ms. Patricia Scullion, 5635 Fishers Lane, Room 2023, Bethesda, MD 20892, **For Federal Express delivery, Rockville, MD 20852. OR Submit Via Secure Email to: LNGRecruit@mail.nih.gov**. The closing date for receipt of applications is **January 28, 2009.**

Staff Scientist
Signaling Transduction Abnormalities in Cancer

The Staudt laboratory of the Metabolism Branch, Center for Cancer Research, National Cancer Institute seeks applications for a Staff Scientist position to lead the laboratory's analysis of pathological signaling pathways in lymphoid malignancies. This 5-year renewable position in the National Cancer Institute is an outstanding opportunity for a scientist who wishes to study the molecular pathogenesis of cancer in a stimulating and well-supported environment. The laboratory is using RNA interference genetic screens to identify genes that are required for the proliferation and survival of cancer cells (Ngo et al. Nature 2006 441:106; Shaffer et al. Nature 2008 454:226; Bidere et al. Nature 2008, in press). These screens have revealed constitutive activation of anti-apoptotic signaling pathways in lymphoid malignancies, leading to the discovery of oncogenic activating mutations affecting signal transduction molecules (Lenz et al. Science 2008 319:1676). The Staff Scientist will investigate the aberrant signaling networks in lymphoid malignancies and devise therapeutic strategies to capitalize on these insights, using biochemical, molecular biological and genomic methodologies. This is a key leadership position in the Staudt laboratory, which consists of 16 highly collaborative researchers. The successful candidate will have an M.D. and/or Ph.D. degree, at least 3 years of post-doctoral research, and a strong publication record in the field of signal transduction. United States citizenship is not required but proficiency in English is essential. Please submit curriculum vitae and 3 letters of reference to:

Louis M. Staudt, M. D., Ph.D., Deputy Chief, Metabolism Branch, CCR, NCI, Bldg. 10, Rm. 4N114, NIH, 9000 Rockville Pike, Bethesda, MD 20892.

NIDDK | NATIONAL INSTITUTE OF DIABETES AND DIGESTIVE AND KIDNEY DISEASES

POSTDOCTORAL FELLOWSHIPS IN MOLECULAR AND CELL BIOLOGY AT THE NIH

We are a group of molecular and cell biologists on the main intramural campus of the National Institutes of Health (NIH) in Bethesda, Maryland, a 20-minute ride from Washington, D.C. The intramural program of the NIH offers an outstanding research environment and many opportunities for collaborations. Applications are invited from individuals of the highest caliber with Ph.D., M.D., or M.D./Ph.D. degrees. The current research interests of the group include:

- Mechanisms of protein secretion in pathogenic and non-pathogenic bacteria. Our group uses a combination of biochemical, biophysical and genetic methods to study protein secretion via both the classical Sec and autotransporter (type V) pathways. For recent work see Proc. Nat. Acad. Sci. (2005) 102: 221; Mol. Cell (2006) 22: 587; EMBO J. (2007) 26: 1942; Nat. Struct. Mol. Biol. (2007) 14: 1214; Mol. Microbiol. (2008) 67: 188 (**Harris Bernstein**: harris_bernstein@nih.gov).

- Biochemistry and molecular biology of double-strand break repair and homologous recombination. Current interests include mouse and human meiosis (Dev. Cell (2003) **4**: 497; Nat. Struct. Mol. Biol. (2005) **12**: 449; J. Cell Science (2005) **118**: 3233; J. Biol. Chem. (2006) 281: 18426; Genes Dev. (2007) **21**: 1758) and evolutionary genomics (Nature Genet. (2004) **36**: 642; Nature Genet. (2005) **37**: 3; Trends in Genet. (2005) **21**: 3). (**Dan Camerini-Otero**)

- Molecular Mechanisms of DNA Mismatch Repair. Our focus is on the role of repair proteins in the cellular response to DNA damage involving checkpoint activation and apoptosis and molecular mechanisms of post-replication repair and mutation avoidance. (Mol. Cell (2006) **22**:501; J. Cell. Bioch. (2008) **105**:245). (**Peggy Hsieh**: ph52x@nih.gov).

Interested candidates should submit a cover letter and a curriculum vitae/bibliography, and arrange to have three letters of recommendation sent to one of the investigators above, or to be considered for more than one lab to **Dan Camerini-Otero (camerini@ncifcrf.gov) at: Bldg. 5, Rm 201, 5 Memorial Dr, MSC 0538, National Institutes of Health, Bethesda, MD 20892-0538.**

WWW.NIH.GOV

Department of Health and Human Services
National Institutes of Health
National Cancer Institute
Center for Cancer Research

Senior Tenured or Tenure-Track Investigator Position

The Mouse Cancer Genetics Program (MCGP), Center for Cancer Research (CCR), National Cancer Institute (NCI), National Institutes of Health (NIH), Department of Health and Human Services (DHHS) is accepting applications for the position of a Senior Tenured or Tenure-Track Investigator to develop an independent research program focused on mechanistic analysis in cancer biology. The current MCGP labs directed by Dr. Terry Van Dyke focus on the in vivo analysis of complex biological problems, with expertise in the areas of cell cycle regulation, apoptosis, genome stability, receptor tyrosine kinase signaling in development and cancer, angiogenesis, stem cell regulation and complex genetics.

In addition, the newly established NCI Center for Advanced Preclinical Research (CAPR) provides a unique opportunity to translate basic discovery into preclinical and clinical application using an extensive infrastructure that incorporates the use of genetically engineered cancer models with modern analytical technologies and therapeutic/diagnostic development. Candidate will develop/sustain a laboratory that is focused on complex cancer-related biological processes, building on the existing strengths of MCGP. Areas of emphasis for recruitment include metastasis, cancer-propagating (stem) cells and mechanisms, the cancer microenvironment (particularly the role of the immune system), and mechanisms of resistance.

Candidates are expected to establish or continue highly competitive research programs in one or more of these areas. Utilization of comparative genomics, proteomics, and/or complex genetics in the approach to these problems is desired, but not required. Candidates must have strong written and oral communication skills; record of high quality publications showing significant contributions to the conceptual understanding of cancer mechanisms; have strong analytical skills and a demonstrated ability for collaborative or team science; and must be sufficiently experienced to function independently, both in the development of their own research efforts and (in the case of established investigators) in the mentoring and supervision of junior investigators.

Applicant will be provided sufficient space, equipment and supply budget. Salary is competitive and commensurate with research experience and accomplishments and a full Civil Service package of benefits (including retirement, health insurance, life insurance, and a Thrift Savings Plan). Candidates may be eligible for the NIH Loan Repayment Program. This position is not restricted to U.S. citizens but candidates must have a Ph.D. and/or M.D. degree.

Interested individuals should send a cover letter, curriculum vitae, a brief summary of research experience, accomplishments and research interests and goals, copies of three publications or reprints, and have at least three letters of reference sent to: **Ms. Elizabeth Brawner, Administrative Officer, NCI-Frederick, PO Box B, Bldg. 578, Frederick, Maryland, 21702-1201, Tel. 301-846-1066, FAX 301-846-6053, E-mail: brawnere@mail.nih.gov**, by **January 2, 2009**. PDF files are encouraged.

National Institute of Mental Health
Division of Intramural Research Programs
Scientific Core for Mental Health Services, Economics, and Public Health
Core Director

The Division of Intramural Research Programs (DIRP), National Institute of Mental Health (NIMH), National Institutes of Health (NIH), seeks an accomplished Staff Scientist to be the Director of the Scientific Core for Mental Health Services, Economics, and Public Health; to conduct research and analyses that enable NIMH to address key scientific and policy issues relating to mental health services and intervention research in a proactive way, in service of NIMH's strategic objective of strengthening the public health impact of NIMH-supported research. The Core Director has full responsibility for the policy, planning, scientific and fiscal management, analysis, and operational aspects of the Core. The position comes with a budget and staff. The strong scientific environment and outstanding resources at NIMH make this a unique opportunity for a high-achieving scientist. The position also offers unparalleled opportunities for inter-disciplinary collaboration with scientists throughout the NIH. The successful candidate will be expected to complement and strengthen the current NIMH Division of Intramural Research Program, the Extramural Research Program and other divisions and offices within NIMH, and at the level of the NIMH Director's Office.

Applicants should have a Ph.D. or equivalent degree in economics or health services research, and a minimum of ten years of experience conducting policy-relevant health economics and health services research, with particular focus on research relating to the development and dissemination of evidence-based mental health practice, including financing issues; and experience engaging and working with key stakeholder groups, such as large employers and public and private health plans.

The ideal candidate must have a record of high scientific achievement and should also have leadership experience, including oversight of team members. Finally, applicants should have experience directly administering a research program. These achievements should be nationally and/or internationally recognized. Salary is commensurate with experience and accomplishments, and a full Civil Service package of benefits (including retirement, health, life, and long-term care insurance, as well as a Thrift Savings Plan, etc.) is available.

NIMH is a major research component of the National Institutes of Health and the Department of Health and Human Services, which have nationwide responsibility for improving the health and well-being of all Americans. Interested applicants should send curriculum vitae, bibliography, statement of research interests, accomplishments and experience with research administration, and goals, written statement with perspective on the needs and opportunities necessary to move from having clinically efficacious interventions to achieving large-scale use of such interventions and resulting public health benefits. Statement should indicate how the applicant's particular expertise and background could contribute to this transition. Applicant should also send three letters of reference to: **Dr. Richard Frank, Chair, Search Committee for Scientific Core, NIMH, NIH, 9000 Rockville Pike, Bethesda, MD 20892; or e-mail to: Steyerm@mail.nih.gov**. Application deadline: **January 5th, 2009**.

UNIVERSITY of NEW HAMPSHIRE

Director, Institute for the Study of Earth, Oceans and Space

The University of New Hampshire (UNH) invites nominations and letters of application for the position of Director, Institute for the Study of Earth, Oceans, and Space (EOS). The EOS Director will provide dynamic leadership for formulating and implementing a compelling shared vision to advance Earth systems and space science research at UNH within an international context. As one of nine dean-level positions reporting directly to the Provost, the EOS Director is a senior academic and research officer with specific responsibility for advancing research, outreach, engagement and academic integration activities for EOS. The University actively promotes a dynamic research and learning environment in which qualified individuals of differing perspectives, life experiences, and cultural backgrounds pursue academic goals with mutual respect and shared inquiry.

UNH is a major research institution, providing comprehensive, high-quality undergraduate and graduate programs. UNH offers students the living and learning environment of a New England liberal arts college with the breadth, spirit of discovery, and civic commitment of a land-, sea-, and space-grant research university. UNH is located in Durham on a 188-acre campus, 60 miles north of Boston, 8 miles from the Atlantic coast, and is convenient to New Hampshire's lakes and mountains. The total enrollment at UNH is 14,000 students. The full-time faculty of over 650 offers more than 90 undergraduate and 70 graduate programs.

EOS is currently the largest research unit at UNH, expending approximately $38 million in annual external funding. Research areas include Earth systems studies with a focus on environmental change and human interactions with that change; climate records in snow, ice, and other proxies; atmospheric chemistry and dynamics; field and modeling studies of ecosystem ecology and biogeochemistry; large scale hydrology; and physical, chemical, and biological oceanography. Remote sensing and geographic information systems are central themes, bridging many Earth systems investigations. Space system studies include heliophysics, high energy astrophysics as well as theoretical space and plasma physics. In depth information about EOS, its programs and faculty can be found at: **http://www.eos.unh.edu**.

The successful candidate will be an internationally prominent leader, addressing policy and research issues of compelling interest to the Earth systems and space science research community. Further, the successful candidate will have a deep intellectual curiosity and an understanding of and appreciation for the breadth of faculty research activity within EOS and across UNH. A strong record of accomplishment in scholarly research appropriate for appointment as a tenured Full Professor is required; as is a record of success in assisting faculty in the advancement of their research. Strong communication skills, demonstrated ability to work collaboratively with other administrative units, and a demonstrated success in leadership, including the ability to work collaboratively with diverse constituents are necessary. A position profile is available at **http://www.eos.unh.edu**.

The confidential review of nominations and applications will begin now and continue until the position is filled. Starting date is negotiable, but soon after July 1, 2009, is preferred. Successful nominations and applications will include a letter of interest, curriculum vitae, and full contact information for five references. These should be sent by email only (in pdf or Word.doc format) to: **eos.search@unh.edu**. References will not be contacted without permission of the applicant.

The University seeks excellence through diversity among its administrators, faculty, staff, and students. The university prohibits discrimination on the basis of race, color, religion, sex, age, national origin, sexual orientation, gender identity or expression, disability, veteran status, or marital status. Application by members of all underrepresented groups is encouraged. We welcome the opportunity to work with candidates to identify suitable employment opportunities for spouses or partners.

UMASS.

FACULTY POSITION
UNIVERSITY OF MASSACHUSETTS MEDICAL SCHOOL

The Program in Molecular Medicine at the University of Massachusetts Medical School invites applications for a **SENIOR TENURED** or **JUNIOR TENURE-TRACK** faculty position. The Program consists of basic scientists and physician scientists representing a broad range of disciplines in the biomedical sciences, and operates as an academic department in the Medical School. The Program occupies a modern research building of approximately 80,000 square feet on an expanding Medical School campus. Core facilities for deep sequencing, proteomics, genotyping, fluorescence-activated cell sorting, digital imaging/confocal microscopy, genomics/bioinformatics, transgenic/knockout mice, and mouse metabolic phenotyping are available. The position will be highly competitive with regard to start-up funds, laboratory space and salary. The Program seeks an individual of outstanding research potential in any of the broadly defined areas of cell, developmental, molecular or structural biology; pathophysiology and translation; genomics/proteomics and bioinformatics; chemical and structural biology.

Applicants should send curriculum vitae, statement of research interests, and names and addresses of three references to:

Dr. Roger Davis, Search Committee Chair,
or Dr. Michael P. Czech, Director
Program in Molecular Medicine
University of Massachusetts Medical School
373 Plantation Street
Worcester, MA 01605

Website (http://umassmed.edu/pmm/)

As an Equal Opportunity and Affirmative Action Employer, UMMS recognizes the power of a diverse community and encourages applications from individuals with varied experiences, perspectives, and backgrounds.

UMASS.

FACULTY POSITIONS
UNIVERSITY OF MASSACHUSETTS MEDICAL SCHOOL
Developmental Biology
Cell Biology

The Program in Cell and Developmental Dynamics and the Program in Molecular Medicine at the University of Massachusetts Medical School have an opening for a **SENIOR TENURED** or **JUNIOR TENURE-TRACK** faculty member. The Program in Cell and Developmental Dynamics is an interdepartmental program housed in state of the art laboratories with access to core facilities for deep sequencing, genotyping, protein chemistry and proteomics, fluorescence-activated cell sorting, digital imaging and confocal microscopy, shRNA knock down, genomics and mouse transgenics/gene knock out. The successful applicant will have a primary appointment in the Program in Molecular Medicine, which consists of basic scientists and physician scientists representing the full spectrum of disciplines in the biomedical sciences.

The positions will be highly competitive with regard to start-up funds, laboratory space and salary. The Program seeks individuals of outstanding research potential in the broadly defined areas of cell and developmental biology. Applicants with research interests that complement new institutional initiatives in stem cell biology and RNAi therapeutics are encouraged.

Applicants should send curriculum vitae, statement of research interests, and names and addresses of three references to:

Dr. William Theurkauf
Program in Cell and Developmental Dynamics
University of Massachusetts Medical School
377 Plantation Street
Worcester, MA 01605

As an Equal Opportunity and Affirmative Action Employer, UMMS recognizes the power of a diverse community and encourages applications from individuals with varied experience, perspectives, and backgrounds.

Wellcome Trust/DBT India Alliance

Biomedical Research Careers Programme for India

The Department of Biotechnology, Ministry of Science and Technology, India, and the Wellcome Trust, UK, have established an Alliance to fund biomedical research fellowships in India.

These fellowships will provide opportunities for support at key career stages and will fund science across the full spectrum of biomedical research, from fundamental molecular and cellular studies through to clinical and public health research.

Intermediate Fellowships for Researchers in India

For excellent scientists who wish to undertake high-quality research and to establish themselves as independent researchers in India.

The Fellowship provides five years' funding to support the Fellow's salary and research expenses. Fellows may spend up to 12 months outside their host institution either in other laboratories in India or elsewhere.

Candidates should have between three and six years' postdoctoral (or equivalent clinical) research experience at submission of a full application.

Deadlines

Preliminary applications must be received no later than **2 February 2009**.

Full applications will be invited by 2 March 2009.

Awards can be taken up from September 2009.

Early Career Fellowships for Researchers in India

For the most promising newly qualified postdoctoral researchers to make an early start in launching their independent research careers, working in the best laboratories in India.

The Fellowship provides four years' funding to support the Fellow's salary and research expenses. Fellows may spend up to 12 months outside their host institution either in other laboratories in India or elsewhere.

Candidates should:

- be Indian nationals, but do not have to be resident in India during the application process
- have no more than 12 months' postdoctoral (or equivalent clinical) experience at submission of a full application.

Deadlines

Preliminary applications must be received no later than **30 April 2009**.

Full applications will be invited by 1 June 2009.

Awards can be taken up from December 2009.

Further information and preliminary application forms are available at **www.wellcomedbt.org**

wellcome trust

Department of Biotechnology
Ministry of Science and Technology

Scientist/Senior Scientist High Content Screening

The High Throughput Drug Screening Facility (HTDSF) uses a combination of robotics, computational tools and small molecule libraries to study biological pathways and to discover novel probes which potentially could be developed as therapies for cancer, infectious diseases, immunology and virology. The Facility develops, validates and performs both chemical (ChemScan) and genomewide (GeneScan) screening on biological assays submitted by the MSKCC investigators.

We are seeking a highly-motivated, multi-discipline trained scientist to join our group to implement all aspects of cell based assay development and screening. This position requires expert knowledge of cell biology and will work closely with MSKCC investigators to develop and validate cell-based assays for high-throughput screening of small molecules and/or siRNAs. The candidate should have experience in signal transduction, phenotypic screens, and/or functional genomics. This position offers a unique opportunity for a talented scientist to work in a dynamic and innovative environment at the heart of basic research and drug discovery and development.

A minimum of 2-4 years of biotech/pharmaceutical experience with an emphasis in cell based assay development and high content screening (we will also consider academics with a strong performance record in similar scientific disciplines). Solid background in the development, troubleshooting of cell-based assays, automated imaging and screening data acquisition and analysis is highly desirable. Candidates should have excellent communication skills, computer skills, meticulous lab technique and recording of findings and must be able to work in a highly collaborative manner.

Interested candidates should send their CV and three letters of references to **djaballh@mskcc.org** EOE/AA.

Memorial Sloan-Kettering Cancer Center
www.mskcc.org

Max-Planck-Institut für Plasmaphysik

The Technische Universität Berlin intends to fill the post of

University professor in experimental plasma physics, W2 (Ref. No. II-776),

in its Centre for Astronomy and Astrophysics. The post is a joint appointment *(S-Professur)* within the framework of a co-operation agreement between the Technische Universität Berlin and the Max-Planck-Institut für Plasmaphysik (Garching and Greifswald).

The focus of the appointment lies in the area of experimental plasma astrophysics (laboratory astrophysics, high temperature plasmas, cold plasmas, spectroscopy). It is expected that the successful candidate will represent the descipline in research and be active in acquiring contract funding. He or she will also be involved in the Bachelor and Masters teaching programme of the Centre for Astronomy and Astrophysics. The teaching duties involve five hours a week *(5 SWS)*.

Candidates must fulfill the requirements for professional appointments according to § 100 of the Berliner Hochschulgesetz (BerlHG), and should have teaching experience and an outstanding research record in the area of experimental plasma physics.

Written applications (**quoting the reference number II-776**) with the usual documentation should be sent to the **President of the Technische Universität Berlin, Fakultät II Mathematik und Naturwissenschaften – Geschäftsstelle Physik – Sekretariat EW 2-1, Hardenbergstraße 36, 10623 Berlin by 31.01.2009.**

The Technische Universität Berlin wishes to ensure equal opportunities for men and women; it therefore specifically invites women with the above qualifications to apply for this post.

Seriously handicapped persons with equal qualifications will be given preference.

FACULTY POSITION IN CANCER GENETICS

The Human Genetics Program at the Fox Chase Cancer Center seeks an outstanding investigator for a tenure track faculty position. Applicants with research experience in kidney cancer will be given special consideration. Applications for either an Assistant Professor or more senior level appointments are welcomed. The Human Genetics Program is focused on understanding genetic aspects of cancer predisposition and tumor progression. The successful applicant will receive a generous start-up package, including funds for equipment, technical assistance, and operating expenses, and will be expected to lead a productive, independent research program.

The Fox Chase Cancer Center is an NCI-designated Comprehensive Cancer Center with strong clinical and basic science programs. The Center provides an exceptional, highly interactive research environment supported by state-of-the-art core facilities, extramural and intramural postdoctoral training grants, endowed fellowships, and an outstanding funding record for investigator-initiated grant applications.

To apply, please send CV, a description of research accomplishments and plans, and 3 letters of recommendation to: **Joseph R. Testa, Ph.D., Director, Human Genetics Program, Fox Chase Cancer Center, 333 Cottman Avenue, Philadelphia, PA 19111. Joseph.Testa@fccc.edu.** Equal Opportunity Employer.

FOX CHASE CANCER CENTER

Stanford University and Veterans Affairs Palo Alto Health Care System
Director, VA Rehabilitation R & D Center

The Department of Orthopaedic Surgery and the Department of Mechanical Engineering at Stanford University in conjunction with the Veterans Affairs Palo Alto Health Care System (VA) seek applicants for the position of Associate or Full Professor (Research). This is a joint academic appointment between the Schools of Medicine and Engineering at Stanford University. The individual selected will hold the position of Director of the Rehabilitation Research and Development (RR&D) Bone and Joint Center of the Palo Alto VA. Employees of the VA must be U.S. citizens. This is intended to be a broad based search and may encompass individuals with a wide range of expertise.

The RR&D Bone and Joint Center is a major national laboratory focusing on basic and clinical musculoskeletal research at scales that range from the cell to whole body movement. The successful applicant will have a well-established history of research on topics related to the Center's focus, demonstrated the ability to collaborate with both clinical and basic scientists, the proven capacity to attract federal research funding and will be expected to have leadership and administrative abilities in a multidisciplinary environment. Preferred research interests include regenerative medicine, biomaterials, cell or molecular engineering, or musculoskeletal bioengineering. The candidate will be expected to serve as a research supervisor for doctoral candidates, mentor post-doctoral fellows, lecture in Orthopaedic Surgery and interact with students and faculty at all levels.

The application should include a brief research plan, a resume, and the names and addresses of at least five references, which should be sent to: **William J. Maloney, MD, Professor and Chair, Department of Orthopaedic Surgery, 300 Pasteur Drive, Edwards R109, Stanford, CA 94305-5335**. You may also submit your application via email to: **ksjoblom@stanford.edu**.

Stanford University and the Veterans Affairs Palo Alto Health Care System are Equal Opportunity Employers and are committed to increasing the diversity of their faculty. They welcome nominations of and applications from women and members of minority groups, as well as others who would bring additional dimensions to the university's research, teaching and clinical missions.

Molecular Virology, Immunology, and Medical Genetics Associate or Full Professor The Ohio State University

The Department of Molecular Virology, Immunology, and Medical Genetics has an immediate opening for a research-track position at the Associate or Full Professor level. Candidates should have a Ph.D. and/or M.D. degree, postdoctoral experience, and a strong commitment to cancer genetic research. Experience and background in Microarray Core Facility leadership with full operational responsibilities will be important. The individual will be responsible for all operations within the Microarray Core Facility acting as Core Director in support of ongoing research at the University. Cooperative research and collaboration with internal and external investigators will also be critical to the success of the position. Ongoing leadership will also be required to bring next generation technologies development to the Core Facility to stay at the forefront of gene expression profiling with emphasis in several aspects of human genetics and cancer.

The Department of Molecular Virology, Immunology, and Medical Genetics is under the leadership of **Dr. Carlo M. Croce**, and is affiliated with the Comprehensive Cancer Center and the Arthur G. James Cancer Hospital and Solove Research Institute. The Ohio State University campus includes an NIH-funded Comprehensive Cancer Center, the College of Medicine, the nearby College of Biological Sciences, and other colleges with comprehensive undergraduate and graduate programs.

Applications should include detailed curriculum vitae and description of research experience. Information about the University and the Department of Molecular Virology, Immunology, and Medical Genetics can be obtained by contacting our web sites (**http://medicine.osu.edu/mvimg/**). Application material should be sent to: **Chris Scarcello, MBA, Assistant Director, Administration, The Ohio State University, Comprehensive Cancer Center, 650 Ackerman Road, Room 325B, Columbus, Ohio 43202.**

The Ohio State University is an Equal Opportunity/Affirmative Action Employer. Qualified women, minorities, veterans and individuals with disabilities are encouraged to apply.

MRC Laboratory of Molecular Biology

Postdoctoral Scientist

£25,622 - £27,223 per annum

Postdoctoral Scientists are encouraged to apply for a position in the laboratory of Stephen Williams at the MRC - LMB, Cambridge. The laboratory studies synaptic integration in central neurons and explores the operation of neocortical circuits, using advanced electrophysiological recording techniques and optical recording and stimulation approaches.

We are seeking candidates with skills in electrophysiology, molecular biology or physics that can contribute to this program. You should have a strong interest in cellular and systems neuroscience, be self-motivated with a high degree of creativity and the ability to focus on complex tasks and drive them to completion.

You will be awarded an MRC Career Development Fellowship, which is a three year training and development position for a postdoctoral scientist who has recently completed their doctoral studies or is moving into a new research discipline. For informal enquiries please email srw@mrc-lmb.cam.ac.uk

Your salary is supported by a flexible pay and reward policy, 30 days' annual leave entitlement, an optional MRC final salary pension scheme and excellent on site sports and social facilities.

Applications for this role must be made online at http://jobs.mrc.ac.uk by inputting reference number LMB08/686. Please include a CV and covering letter with your application. If you do not have access to the internet or experience technical difficulties please contact 01793 301280.

Closing date: 2 January 2009.

The Medical Research Council is an Equal Opportunities Employer

THE UNIVERSITY OF HONG KONG

香港大學

Founded in 1911, The University of Hong Kong is committed to the highest international standards of excellence in teaching and research, and has been at the international forefront of academic scholarship for many years. Of a number of recent indicators of the University's performance, one is its ranking at 26 among the top 200 universities in the world by the UK's Times Higher Education Supplement. The University has a comprehensive range of study programmes and research disciplines, with 20,000 undergraduate and postgraduate students from 50 countries, and a complement of 1,200 academic members of staff, many of whom are internationally renowned.

School of Biological Sciences

Applications and nominations are invited for appointments as: (1) Director of the School of Biological Sciences (at Chair Professor level) (Ref.: RF-2008/2009-121); and (2) Chair of Biological Sciences (Ref.: RF-2008/2009-122), on tenured terms, or on a three- to five-year fixed-term basis, tenable from September 1, 2009 or as soon as possible thereafter.

The newly formed School of Biological Sciences aspires to become a top research school in Asia with world-class research and teaching. The School has excellent research facilities and resources, and is supported by a dedicated team of experienced academic and research staff. The areas of expertise include biotechnology, molecular and cell biology, comparative endocrinology, human nutrition, food technology, ecology and biodiversity, marine biology and environmental science.

(1) Director of the School of Biological Sciences

Applicants should have a distinguished international reputation with a substantial research record. They should be able to provide leadership to enhance the School's profile both locally and internationally as a centre of excellence in research and teaching. Experience in management would be an advantage.

(2) Chair Professor

Applicants should have a distinguished research profile and are expected to provide academic leadership in research and teaching.

A highly competitive salary commensurate with qualifications and experience will be offered. The appointment is superannuable (for tenured terms), or attracting a contract-end gratuity and University's contribution to a retirement benefits scheme, totaling up to 15% of basic salary.

At current rates, salaries tax does not exceed 15% of gross income. The appointments carry leave, housing benefits and medical and dental benefits. Research start-up funds will be available.

This is a re-advertisement. Those who had applied before need not apply again. Their candidature will be considered together with that of applicants of this round. The right not to fill the position, or to fill the position by invitation, or to fill the position at Professor level is reserved.

Application setting out in detail why the applicant considers himself/herself suitable for the post, together with a full curriculum vitae and contact information, or nominations should be sent to Mr. T.T. Ho, Korn/Ferry International (HK) Ltd, 2101-2106 Gloucester Tower, The Landmark, Central, Hong Kong; E-mail: hkubiosch@kornferry.com; Fax: (852) 2810-1632. **Closes December 31, 2008**.

The University is an equal opportunity employer and is committed to a No-Smoking Policy

KORN/FERRY INTERNATIONAL

GRANTS

Grant for Postdoctoral Positions in Sweden

This grant enables researchers with doctorates (PhDs or equivalent) to work at Swedish higher education institutions or research establishments. The programme spans up to two years. Research areas: Natural Sciences, Engineering Sciences, Medicine, Humanities, Social Sciences and Educational Sciences.

Call for applications opens early January. Submission deadline is February 26, 2009.

Further information at www.vr.se

Vetenskapsrådet

GRANTS

HOWARD HUGHES MEDICAL INSTITUTE

2009 MED INTO GRAD INITIATIVE

In the second competition for its Med into Grad Initiative, the Howard Hughes Medical Institute will award four-year institutional grants to educational programs that incorporate the knowledge and skills of medicine and pathobiology into graduate education. The awards may be used to enhance existing graduate training programs or initiate new programs to train biomedical scientists who are better prepared to translate the discoveries of basic biological science into the treatment of human diseases.

Applications will be accepted from any institution in the United States that offers a Ph.D. in one or more of the biomedical sciences. The proposed program must be affiliated with a facility that is engaged in medical education. Awards will range from $400,000 to $1 million over the four years of funding. For more information, please visit www.hhmi.org/ref/mig/sci.

Register intent to apply by January 6, 2009
Application deadline: April 27, 2009
Award notification: September 2009

HHMI
HOWARD HUGHES MEDICAL INSTITUTE

Institute of Structural Molecular Biology

Institute of Structural and Molecular Biology (ISMB)
At University College London – Birkbeck College London

Two Lectureships in "Microbial Macromolecular Systems"

The Institute of Structural and Molecular Biology (ISMB) is seeking applications to fill two lectureships in Microbial Macromolecular Systems that the ISMB wishes to fill by September 2009.

We want to recruit outstanding individuals who are capable of developing world-class, interdisciplinary research in the structure and function of complex molecular nanomachines of microbial origins (for example ribosomes, transcriptosomes, secretion systems, etc…). We are especially interested in expertise with systems that are amenable to in vitro reconstitution, and structural and functional analysis using a range of biochemical and biophysical approaches, with potential for antimicrobial drug development. Successful applicants will also be expected to make an appropriate contribution to the affiliated departments' portfolios of graduate and undergraduate teaching.

The ISMB (www.ismb.lon.ac.uk) is a centre of excellence, which jointly consists of the School of Crystallography and the School of Biological and Chemical Sciences at Birkbeck College and the Research Department of Structural & Molecular Biology at University College London (UCL). It was established to foster closer links between the three departments and also to provide a bridge with the Department of Chemistry at UCL. The Institute provides a scientific environment conducive to world-class research in the field of biomolecular science. Work at the Institute seeks to integrate the chemical and physical sciences to provide the molecular basis of protein function. The ISMB also seeks to exploit the knowledge of protein function to further our understanding of human diseases.

The salary range that is offered for these posts will be within the University Lecturer A (£35,239 – £38,250 inc. LW) or Lecturer B (£39,313 – £46,403 inc. LW) range according to experience. Job descriptions can be found at (www.ismb.lon.ac.uk) and at the respective departmental web sites (http://www.smb.ucl.ac.uk/) and (http://www.cryst.bbk.ac.uk/).

Applicants should send their CV and names and addresses of three referees to Ms Caroline Gougerty, Division of Biosciences, University College London, Gower Street, London, WC1E 6BT, UK or email: c.gougerty@ucl.ac.uk. CVs should contain an account of applicant's current research activities together with a plan of future research intentions. The Head of the ISMB, the UCL Research Department of Structural and Molecular Biology and of the Birkbeck School of Crystallography is Professor Gabriel Waksman. He can be contacted informally for general information (email: g.waksman@ucl.ac.uk or g.waksman@bbk.ac.uk).

Deadline for applications is 15th February 2009.

UCL Taking Action For Equality.

Birkbeck UNIVERSITY OF LONDON

UCL

At Monsanto, our talented employees are contributing to our success as a global leader in agriculture. By delivering exceptional results in one of the world's most important industries, we are creating solutions that improve productivity in farming while reducing the impact on our environment.

We are looking for a talented individual for the following position in **St. Louis, MO**:

Marker Discovery Team Lead

PhD in Plant Breeding, Genetics or a related field required.

Our mission is to identify and exploit variation within genes and genomic regions affecting economically important traits, with the ultimate objective of delivering the tools necessary to provide more efficient production of a higher quality product that meets the needs of the marketplace. The successful applicant will have an opportunity to lead, interact, excel, and grow in the company of experts in a number of areas, including molecular Biology, Biotechnology, Biostatistics, and Plant Breeding.

To view a more complete and detailed job description of this exciting position, please visit our website at **www.monsanto.com** and to apply online select **requisition # mons-00009802.** We offer very competitive salaries and an extensive benefits package.

The life of any plant starts with a seed. Within the right environment it grows to become something amazing. At Monsanto, our philosophy is the same – we are committed to helping individuals progress in careers with unlimited potential.

The world, re-imagined

Imagine your world at Monsanto
by visiting us on our website,
www.monsanto.com/careers

Monsanto is an equal opportunity employer who values diversity.

MONSANTO imagine®

SYRACUSE UNIVERSITY

Department of Biology

Tenure-Track Assistant Professor - Biology (024714)

The Department of Biology invites applications for a tenure-track faculty position to be filled by August 2009 in stem/progenitor cell biology, with emphasis on mechanisms of organ and tissue formation, regeneration, and engineering. The successful candidate will have the intellectual freedom to develop an innovative research program in either mammalian or non-mammalian systems using in vivo and/or in vitro approaches to study inter- and intra-cellular signaling and the role of the microenvironment in regulating cell fate. The applicant's interests should augment existing Biology Department strengths in cell signaling and developmental biology (see department website (**http://biology.syr.edu/**). We are hiring at the level of Assistant Professor but, in the case of an exceptionally qualified candidate, appointment at any level may be considered. Candidates are expected to develop an independent, sustainable research program and contribute to departmental teaching at the undergraduate and graduate levels. Competitive salary, start-up funds and new laboratory space will be provided.

The position offers an outstanding opportunity for collaboration with colleagues in Biology, Chemistry and Physics, the new Syracuse Biomaterials Institute (**http://biomaterials.syr.edu/**), as well as in the State University of New York-Upstate Medical University (**http://www.upstate.edu/**), and the State University of New York-Environmental Science & Forestry (**http://www.esf.edu/**). These three institutions (Syracuse University, SUNY-Upstate, and SUNY-ESF) form one nearly contiguous campus. The Syracuse University Biology Department recently moved to the new 110,000 net sq. ft. Life Sciences Complex (LSC), which we share with the Department of Chemistry. The LSC features generous, well-appointed research laboratories designed to promote interaction, and the option to customize a component of research space.

Applicants should visit **www.sujobopps.com** to complete a Dean/Senior Executive/Faculty application form and attach an up-to-date curriculum vita. In addition, we ask each applicant to send electronically as a single PDF file, (1) a cover letter, (2) a description of past research accomplishments, (3) a clearly focused description of future research goals (including, if appropriate, who in Syracuse you might collaborate with) and (4) a statement of teaching interests to: **biosearch@cas.syr.edu**. We also request that applicants arrange to have at least three letters of reference sent directly either to **biosearch@cas.syr.edu** or to the mailing address below. Please include the name, address, phone number and e-mail address of each of your references in the PDF file. Priority will be given to full applications received by December 15, 2008.

The cover letter and reference letters should be addressed to: **John M. Russell, Ph.D., Stem Cell Faculty Search, Department of Biology, 107 College Place, Syracuse University, Syracuse, NY 13244**

Syracuse University is an Affirmative Action/Equal Opportunity Employer.

OAK RIDGE NATIONAL LABORATORY

MANAGED BY UT-BATTELLE FOR THE DEPARTMENT OF ENERGY

Associate Laboratory Director

Support the Laboratory Director in accomplishing the Laboratory's mission by leading the Biological and Environmental Sciences Directorate (BESD), which is an interdisciplinary research and development organization with more than 60 years of achievement in biological and environmental research primarily in the support of the Department of Energy. The vision is to expand scientific knowledge and develop innovative strategies and technologies that will demonstrate national and international leadership in creating world class scientific solutions to biological and environmental dimensions of energy and climate. The Associate Laboratory Director for BESD will be responsible for providing scientific leadership of large complex research programs with a focus on successful implementation and execution of scientific strategy for the Directorate.

KEY ACCOUNTABILITIES:

- Lead biological and environmental research for the Laboratory including developing and implementation of scientific strategy to sustain national and international prominence. Serve as primary liaison to the DOE Office of Biological and Environmental Research (BER) and other sponsors (such as NIH), ensuring the science and technology research programs are meeting client needs.
- Strengthen existing research programs, develop new programs, and drive strategic initiatives for the directorate; current initiatives include: computational biology, climate change, and bio-energy. Work with Laboratory Director and Leadership Team to identify and implement strategic research opportunities, including LDRD (Laboratory-Directed Research and Development) priorities.
- Manage programmatic funds and discretionary investments for research and program development. Act as steward for laboratory operations, facilities, capital, and equipment. Direct line management responsibilities for the Environmental Sciences Division and Biosciences Division and the DOE BioEnergy Science Center.

EDUCATION/EXPERIENCE: Ph.D. in biological or envrionmental sciences or related research field. Prefer research conducted in a large Division or Directorate with 5-10 years of demonstrated executive management experience, including leading large complex and multidisciplinary research programs. Experience with communicating with key stakeholders, clients, program sponsors, internal staff, and regarded as a leading expert and visionary in the field of Biological or Environmental sciences. Demonstrated experience of successfully developing, implementing, and executing scientific strategy with engagement from critical stakeholders. For further consideration and full job description, please visit **http://jobs.ornl.gov/** and reference posting Associate Laboratory Director in the keyword search field.

Oak Ridge National Laboratory is an Equal Opportunity Employer.

POSITIONS OPEN

复旦大学分子与细胞生物学研究室

FACULTY POSITIONS in FUDAN UNIVERSITY

The Molecular and Cell Biology Research Laboratory in Institutes of Biomedical Sciences, Fudan University, invites applications for faculty positions in the areas of biochemistry, molecular and cellular biology, proteomics, metabolism, and cancer. Successful applicants will join an exciting and interactive research group with a well-established facility and are expected to make a quick start. Interested individuals should send a cover letter, curriculum vitae, and two to three letters of recommendation to **Ms. Bing Xu** at **e-mail: mcb@fudan.edu.cn** or **telephone: 86-21-54237450.**

EDNA BIGGS KURTZ ENDOWED CHAIR/ ARBORETUM DIRECTOR POSITION

The University of Denver is seeking applicants for the endowed Edna Biggs Kurtz Chair in Botany in the Department of Biological Sciences. The successful candidate will hold the position of Director of the Chester M. Alter Arboretum with a joint appointment at the **ASSOCIATE or FULL PROFESSOR** level in the Department of Biological Sciences. As Arboretum Director, the successful candidate will provide leadership and long range strategic planning, including fund-raising projects for the Chester M. Alter Arboretum. They will also help develop this resource as a teaching and learning tool for the University community. As a member of the Department of Biological Sciences the successful candidate will be involved in undergraduate and graduate teaching and will maintain an extramurally funded research program that compliments the research interests of faculty in the ecology and biodiversity major offered by the Department. Applications should be submitted to **website: http://du.jobs.org.** Application materials should include: curriculum vitae, a statement outlining one's view on the nature of arboretum on an urban university campus, research statement, and a statement of teaching philosophies. Three letters of recommendation plus two reprints should be sent directly to the: **Chair of the Kurtz Endowed Chair/Arboretum Director Search Committee, University of Denver, Department of Denver, Department of Biological Sciences, Olin Hall Room 102, 2190 E. Iliff Avenue, Denver, CO 80210.** Applications will be accepted until the position is filled.

ASSISTANT/ASSOCIATE PROFESSOR
Biomedical Science (Anticipated Faculty Opening)
St. John's University
Department of Pharmaceutical Sciences
Bringing knowledge to life.
Working for a better world.

St. John's University, one of the nation's largest Catholic universities, currently has a tenure-track faculty position available in our Department of Pharmaceutical Sciences at our Queens campus.

The Department has 34 faculty members with varied research interests in the Biomedical and Pharmaceutical Sciences. Modern instrumentation and Association for Assessment and Accreditation of Laboratory Animal Care-accredited facilities are available.

You will establish an active research program that will attract external funding, mentor students, and teach graduate and undergraduate courses. To qualify, you must have an earned Ph.D. in a biomedical science and postdoctoral experience.

We provide rank and salary commensurate with qualifications, excellent benefits, talented professional colleagues, and a culturally diverse student population. Interested professionals should send letter of application, curriculum vitae, research plan and statement of teaching philosophy, and three letters of reference to: **Dr. Louis D. Trombetta, Professor and Chair, Department of Pharmaceutical Sciences, St. John's University, 8000 Utopia Parkway, Queens, NY 11439. E-mail: trombetl@stjohns.edu.**

St. John's is an Equal Opportunity Employer and encourages applications from women and minorities.

The **European Molecular Biology Organization** (EMBO) recognises excellence, shares information and fosters talented scientists – empowering them to advance the field of molecular biology. EMBO-sponsored funding, training and networking activities impact thousands of scientists every year while leading peer-reviewed publications span a broad spectrum of topics reflecting how science is shaping the world.

Manager | EMBO Publications

A unique opportunity is offered to join the EMBO management group at its administrative headquarters in Heidelberg.

EMBO publishes three high profile journals – *The EMBO Journal, EMBO reports* and *Molecular Systems Biology.* The launch of a fourth journal – *EMBO Molecular Medicine* – is planned for early 2009. The position of Manager of Publications will fall vacant in the course of 2009. The successful applicant will take over the primary responsibility for the successful operation of all four journals. The role of the publications manager encompasses the overall strategic, scientific and financial management of all four EMBO publications and their editorial offices. EMBO publication policy will be developed together with the EMBO Director, the publications staff, the publishers of the journals, the EMBO Publications Committee and EMBO Council. Day-to-day responsibilities include liaison with the senior or executive academic editors of the journals, the Chair of the EMBO Publications Committee, organisation of meetings of this committee and of the Advisory Editorial Boards of the journals including preparation of documentation for and reports of the meetings of these bodies.

The ideal candidate will have a proven research track record, a thorough knowledge of molecular biology and broad interests in diverse areas of the life sciences. He/she should have extensive editorial experience and be familiar with trends in modern scientific publishing. A key requirement for the position is the ability to think critically about the wide range of strategic, scientific, financial and management issues required for the successful operation of high quality scientific journals. Fluent English is essential, as are good communication and organisational skills and the ability to provide leadership to the editorial teams.

An initial contract of 5 years will be offered to the successful candidate. This can be renewed, depending on circumstances at the time of review.

EMBO/EMBL is an inclusive, equal opportunity employer offering attractive conditions and benefits appropriate to an international research organisation.

To apply, please send an English CV (including names and addresses of referees) and covering letter, by e-mail, quoting **ref. no. S/08/096** in the subject line, to: **application@embl.de**

Closing date: 11.01.2009

Web sites:

www.embo.org
www.embojournal.org
www.emboreports.org
www.nature.com/msb/
www.embomolmed.org

EMBO

WAYNE STATE UNIVERSITY

Physiologist

The Department of Biological Sciences at Wayne State University invites applications for a tenure-track position. Rank will be dependent upon qualifications. Preference will be given to candidates who use state-of-the-art approaches to study complex biological problems in any animal model system. While any area of research related to physiology will be considered, we are especially interested in candidates whose work involves cellular / molecular physiology, developmental physiology, neurophysiology, cell regulation and signaling, homeostasis, and membrane biogenesis and transport. Wayne State University is a large, comprehensive, nationally ranked research institution that offers exciting research opportunities and generous start-up packages. Applicants must have a Ph.D. degree, post-doctoral experience and an outstanding record of research achievement. Successful applicants are expected to establish and maintain a vigorous, externally funded research program and participate in graduate and undergraduate education. Candidate must be willing to teach an undergraduate-level course in human physiology on an annual basis.

The position is posted on-line at **jobs.wayne.edu**. Only those application materials that are submitted to this site will be considered. The online application requires a cover letter, curriculum vitae and a two-page statement of research plans. In addition, three letters of reference should be sent to: **Chair, Faculty Search Committee, Department of Biological Sciences, Wayne State University, 5047 Gullen Mall, Detroit, MI 48202**. Review of applications will begin immediately and the search will remain open until the position has been filled. Applications will be considered only when all materials have been received.

Wayne State University is an Affirmative Action/Equal Opportunity Employer. Women and members of minority groups are especially encouraged to apply.

POSITIONS OPEN

CHAIR
Department of Neurobiology and Anatomy
University of Utah School of Medicine

The University of Utah School of Medicine is embarking on a national search for the position of Chair of the Department of Neurobiology and Anatomy. Candidates with a distinguished record of educational and research accomplishments are invited to apply. Past administrative experience is expected. The Department is comprised of 13 full-time faculty members and is part of the broader biological science community at the University. More detailed information is available at the Department **website: http://www.neuro.utah.edu/.**

Interested applicants should submit electronic curriculum vitae, a list of three to five references, and a brief statement describing academic interests and professional goals to:

Jennifer L. Allie
Director, Faculty and Academic Personnel
University of Utah Health Sciences Center
E-mail: jennifer.allie@hsc.utah.edu
Telephone: 801-581-5705
Fax: 801-581-3338

University of Utah is an Equal Employment Opportunity/Affirmative Action Employer and encourages applications from women and minorities.

CHEMISTRY/BIOCHEMISTRY-CANCER CENTER FACULTY POSITION
University of California, San Diego

The Department of Chemistry and Biochemistry of University of California, San Diego **(website: http://www-chem.ucsd.edu)** and the Moores Cancer Center **(website: http://cancer.ucsd.edu/)** invite applications for a tenure-track position in an area of chemistry, chemical biology, or biochemistry contributing to basic knowledge in the field of oncology, translational medicine, or translational pharmacology. Candidates must have a Ph.D., Pharm.D., or M.D. and a demonstrated ability for creative research and teaching at the undergraduate and graduate levels. Salary is commensurate with qualifications and based on the University of California pay scale. Applicants are asked to submit materials online at **website: http://www-chem.ucsd.edu/recruit/index.cfm?addno=5-134.** Materials include cover letter, curriculum vitae, complete list of publications, list of current and past grant support, samples of published research, and statement of your teaching experience. Applicants are welcome to include in their cover letters a personal statement summarizing their contributions to diversity. Please arrange for three reference letters to be sent to: **Chair, Chemistry/Cancer Center Search 5-134, University of California, San Diego, Department of Chemistry and Biochemistry, La Jolla, CA 92093-0332.** The deadline for applications is January 9, 2009, but until position is filled, all applications received will be assured full consideration. *UCSD is an Equal Opportunity/Affirmative Action Employer with a strong institutional commitment to the achievement of diversity.*

Shantou University Medical College, in Shantou, China, is launching internationally competitive research and teaching programs and has many openings for leading and upcoming scientists working at different disciplines. Selected candidates will be sufficiently supported with startup funds, relocation expenses, housing, and competitive salary packages. Please visit the **website: http://www.med.stu.edu.cn/recruit.htm** for more information. Interested candidates should send curriculum vitae to **Mr. Yufang Chen** at **e-mail: chenyf@stu.edu.cn.**

POSITIONS OPEN

FACULTY POSITION
Neural Engineering

The Engineering Science and Mechanics, and Bioengineering Departments at the Pennsylvania State University invite applications for a tenure-track **ASSISTANT PROFESSOR** faculty position in neural engineering at the interface between materials science and neuroscience. Exceptional candidates at the **ASSOCIATE or FULL PROFESSOR** level will be considered. Candidates are sought whose research integrates methods of engineering with neuroprosthetic devices to facilitate treating disabilities and diseases at multiscale systems levels. Expertise may encompass electromagnetics, biomechanics, microfluidics, nanotechnology, and associated engineering fields. Translational research towards the treatment of diseases such as Parkinson's, epilepsy, stroke, depression, hydrocephalus, Alzheimer's, and trauma is desirable. The candidate will be expected to interact with faculty in the College of Engineering, the Materials Research Institute, the Huck Institutes for the Life Sciences, and the College of Medicine. An appointment will also be held in Penn State's Center for Neural Engineering, with new facilities under construction. Candidates will contribute to new undergraduate and graduate curricula, teach in the neural engineering Ph.D. track, and mentor within the M.D./Ph.D. program. Qualifications include a Doctorate in engineering or related area, and a proven record of scholarship. Three years of postdoctoral experience is highly desirable. The Departments are committed to diversity and fostering a welcoming climate for all. Review of applications will begin immediately and applications considered until the position is filled. Send curriculum vitae, statement of professional interests, teaching philosophy, and names and addresses of four references to: **Attn: Neural Engineering Search Committee Chair, Department of Engineering Science and Mechanics, 212 Earth-Engineering Sciences Building, P.O. Box 212, The Pennsylvania State University, University Park, PA 16802-6812.** Electronic applications may be submitted to **e-mail: positions@mail.esm.psu.edu.** *Penn State is committed to Affirmative Action, Equal Opportunity, and the diversity of its work force.*

FACULTY POSITIONS in COMPUTATIONAL BIOLOGY

The University of Colorado at Boulder invites applications for two tenure-track faculty positions in the broad areas of computational biology and bioinformatics, under the auspices of the Colorado Initiative in Molecular Biotechnology (CIMB, **website: http://cimb.colorado.edu).**

Individuals with interests in developing and applying computational or mathematical methods to biological systems are encouraged to apply.

CIMB is a program that integrates faculty from the Departments of Applied Mathematics; Chemical and Biological Engineering; Chemistry and Biochemistry; Computer Science; Ecology and Evolutionary Biology; Integrative Physiology; Mechanical Engineering; Molecular, Cellular, and Developmental Biology; and Physics. A successful candidate may be rostered in any one of these Departments. The positions are at the **ASSISTANT PROFESSOR** level, although outstanding senior candidates at higher ranks may be considered. Candidates must have a Ph.D. degree and a demonstrated commitment to teaching at undergraduate and graduate levels, and will be expected to develop an internationally recognized research program.

Applicants should submit curriculum vitae, statements of research and teaching interests, and arrange to have three letters of reference sent electronically to **website: https://www.jobsatcu.com,** posting #805756. Review of applications will begin on or about December 1, 2008, and will continue until the position is filled. For more information or assistance in submission of materials, contact **Janice McClintock (e-mail: janice.mcclintock@colorado.edu).** See **website: http://www.colorado.edu/artssciences/jobs/** for full job description.

The University of Colorado is sensitive to the needs of dual-career couples, and is committed to diversity and equality in education and employment.

POSITIONS OPEN

RUTGERS
CAMDEN

The Biology Department seeks a broadly trained **EXPERIMENTAL MICROBIOLOGIST** for a tenure-track **ASSISTANT PROFESSOR** position beginning fall 2009. Research interests in systems or computational/integrative biology are desirable. Ph.D. required and postdoctoral experience preferred. This position entails teaching undergraduate and graduate courses in the area of the applicant's expertise and participation in introductory biology courses. Please send curriculum vitae, statement of research interests, and three letters of recommendation to: **Dr. Joseph V. Martin, Biology Department, Rutgers University, Camden, NJ 08102**. Review of applications will begin January 26, 2009, and continue until the position is filled.

SENIOR FELLOWSHIP
Cardiovascular Regenerative Medicine
Regenerative Biology and Tissue Engineering Theme
Institute for Genomic Biology
University of Illinois

A three-year Senior Fellowship (Carle Foundation Hospital-Institute for Genomic Biology) is available immediately to conduct collaborative research in cardiovascular regenerative medicine. Applicants should have a demonstrated interest in cardiovascular medicine and developing stem cell regenerative therapies. Applicants must have either a Ph.D., D.V.M, M.D., or combined degrees. The applicant will be expected to interact with laboratory researchers and clinicians to address critical issues associated with the applications of stem cell biology to treat cardiovascular diseases. A highly competitive salary is provided and the candidate will be housed in the new $75 million Institute for Genomic Biology **(website: http://www.igb.uiuc.edu/)** and actively interact with clinicians at the Carle Foundation Hospital and Clinic Association **(website: http://www.carle.com/)** and the College of Veterinary Medicine Hospital.

Experience with the isolation of adult stem cells, intervention cardiology, or animal models is highly desired. Clinical experience, either in veterinary or human medicine, is preferred. Applicants should also have demonstrated their ability to have published and to create a competitively funded program.

The closing date for the position is January 15, 2009, or until an acceptable candidate is identified. Applicants should submit a letter of intent, curriculum vitae, and the names of three references. Application materials should be forwarded to: **Prof. Lawrence B. Schook, Professor and Gutgsell Chair, Regenerative Biology and Tissue Engineering Theme, Institute for Genomic Biology, University of Illinois, 1206 W. Gregory Drive, Urbana, IL 61801.**

SHULL FELLOWSHIP at the Oak Ridge National Laboratory (ORNL): the Neutron Sciences Directorate of the ORNL invites applications for the Clifford G. Shull Fellowship. The Shull Fellowship provides an exciting opportunity to pursue research applying neutron scattering methods to forefront problems in physics, chemistry, biology, or materials science and engineering. Applications for Shull Fellowships commencing in 2009 are now being accepted. To receive full consideration applications must be submitted by December 12, 2008. For more information, and to apply, go to **website: http://jobs.ornl.gov/index.cfm.** *ORNL is an Equal Opportunity Employer, committed to work force diversity. Applicants need not be U.S. citizens.*

COLUMBIA UNIVERSITY
IN THE CITY OF NEW YORK

THE 2009 LOUISA GROSS HORWITZ PRIZE FOR BIOLOGY OR BIOCHEMISTRY

The Louisa Gross Horwitz Prize was established under the will of the late S. Gross Horwitz through a bequest to Columbia University and is named to honor the donor's mother. Louisa Gross Horwitz was the daughter of Dr. Samuel David Gross (1805-1889), a prominent surgeon of Philadelphia and author of the outstanding Systems of Surgery who served as President of the American Medical Association.

Each year since its inception in 1967, the Louisa Gross Horwitz Prize has been awarded by Columbia University for outstanding basic research in the fields of biology or biochemistry. The purpose of this award is to honor a scientific investigator or group of investigators whose contributions to knowledge in either of these fields are deemed worthy of special recognition.

The Prize consists of an honorarium and a citation which are awarded at a special presentation event. Unless otherwise recommended by the Prize Committee, the Prize is awarded annually. Dr. F. Ulrich Hartl, Max-Planck Institute of Biochemistry, Martinsried, Germany, and Dr. Arthur L. Horwich, Yale University School of Medicine, New Haven, CT., were the 2008 awardees. Dr. Rosalind E. Franklin (1920-1958) was awarded an honorary Horwitz Prize.

QUALIFICATIONS FOR THE AWARD

The Prize Committee recognizes no geographical limitations. The Prize may be awarded to an individual or a group. When the Prize is awarded to a group, the honorarium will be divided among the recipients, but each member will receive a citation. Preference will be given to work done in the recent past.

Nominations must be submitted electronically at: http://www.cumc.columbia.edu/horwitz/

Nominations should include:

1) A summary, preferably less than 500 words, of the research on which this nomination is based.
2) A summary, preferably less than 500 words, of the significance of this research in the fields of biology or biochemistry
3) A brief biographical sketch of the nominee, including positions held and awards received by the nominee
4) A listing of up to ten of the nominee's most significant publications relating to the research noted under item 1.
5) A copy of the nominee's curriculum vitae.

Deadline date: January 31, 2009

SANTA FE INSTITUTE

Summer 2009 at the Santa Fe Institute

Complex Systems Summer Schools

Santa Fe June 7-July 4 • Beijing July 5-August 1
http://www.santafe.edu/csss

An intensive introduction to complex behavior in mathematical, physical, living, and social sciences for graduate students and postdoctoral fellows.

Global Sustainability Summer School, July 12-25
http://www.santafe.edu/global

This program explores global sustainability from many perspectives with particular focus on problems posed by climate change. Targeted for graduate students, postdoctoral fellows, junior and senior faculty and individuals from the private sector.

Research Experiences for Undergraduates
http//www.santafe.edu/reu

Students work with SFI faculty mentors on an individual project focused on some aspect of complex systems. Residence for approximately 10 weeks, within an early-June to mid-August time frame.

See program websites for application requirements and deadlines. Financial support for students available. Women, minorities and students from developing countries are especially encouraged to apply.

BODOSSAKI FOUNDATION

BODOSSAKI ARISTEIO PRIZE 2009

The Aristeio Bodossaki was instituted to give recognition to Greeks who have devoted their lives to science and who, by means of their exceptional, lifelong performance and significant achievements, have made a distinctive contribution towards furthering their field of science. The Aristeio Bodossaki, which is accompanied by the sum of €150.000, is awarded every two years.

The Board of Trustees of the Bodossaki Foundation, at its meeting in September 2008, accepted the proposal of the International Aristeio Committee and decided to award the Bodossaki Aristeio for the year 2009 to a scientist in the field of Bio-Medicine. The award goes to Professor Evangelos Moudrianakis for his pioneering studies on the structure of chromatin, for solving, at atomic resolution, the three-dimensional structure of the histone octamer core of the nucleosome and for computing the first three-dimensional model of the nucleosome. The discoveries of Dr. Moudrianakis' research team have provided us with greater insights into the molecular mechanisms involved in the regulation of the genetic information encoded in the DNA. The recipient is Professor of Biology and Biophysics at Johns Hopkins University, corresponding member of the Academy of Athens and has received numerous international awards. The fundamental contribution of Dr. Moudrianakis' research activities has had enormous impact on the work of other scientists.

POSITIONS OPEN

POSTDOCTORAL POSITIONS
Thomas Jefferson University
Philadelphia, Pennsylvania U.S.A.

Postdoctoral position is available in the laboratory of pulmonary pharmacology for an enthusiastic individual with skills in proteomics, genomics, or gene expression analysis in airway tissues. Ongoing projects explore novel models, mechanisms, and molecular targets for glucocorticoid insensitive (steroid resistant) asthma.

Training in molecular biology, cell culture, and biochemical approaches both in vitro and in vivo is strongly required. Previous experience with siRNA technology, glutathione S-transferase-pull down, chromatin immunoprecipitation, gel shift assays, and site direct mutagenesis, transient and stable transfection are preferred. To apply, please e-mail complete curriculum vitae and contact information of three references to: **Dr. Omar Tliba, e-mail: omar.tliba@jefferson.edu, Assistant Professor, Department of Pharmaceutical Sciences, Thomas Jefferson University-School of Pharmacy, 130 S. 9th Street, Philadelphia, PA 19107.**

ASSISTANT PROFESSOR, TENURE TRACK
Vertebrate Anatomy/Evolutionary Biology

Saint Mary's College of California invites applications for a tenure-track Assistant Professor, beginning fall 2009. The successful applicant will join a team of 10 full-time and adjunct faculty in cell biology, molecular biology, immunology, genetics, botany, marine biology, ecology, evolution, microbiology, vertebrate and invertebrate zoology, physiology, developmental biology, anatomy, and biochemistry. We are seeking a **VERTEBRATE ANATOMIST** who could teach an undergraduate human anatomy course with a cadaver-based laboratory, as well as courses in comparative vertebrate anatomy and evolutionary biology, and undergraduate statistics.

We seek an excellent teacher who is committed both to high quality teaching as well as maintaining an active research program involving undergraduates, in a teacher-scholar fashion. Faculty contractual responsibilities allow a teaching load of six courses per year. Faculty will also serve as academic advisers and on college committees. The successful candidate will be expected to engage in scholarship/research accessible to undergraduates.

Review of applications will begin January 31, 2009. Position is open until filled and subject to availability of funding sources. **Website: http://novushronline.stmarys-ca. edu/jobpostings.aspx.** For complete details and to apply online, please visit our **website: www.http://www.stmarys-ca.edu.** *Equal Opportunity Employer.*

BIOLOGY. Seeking **ACADEMIC ADMINISTRATOR** to manage X-ray crystallographic facility at Mission Bay, University of California, San Francisco. Administrator will facilitate research by the entire macromolecular structure group, and engage in research on high-resolution X-ray crystallographic structural studies of a-lytic protease, an extracellular bacterial serine protease that catalyzes peptide-bond hydrolysis. Studies are conducted at the atomic level, requiring expertise in both chemical behavior of the enzyme and the crystallographic techniques required to study them. Send curriculum vitae and three references to: **Rachel Mozesson, Department of Biochemistry and Biophysics, University of California San Francisco, 600 16th Street, N226, P.O. Box 2140, San Francisco, CA 94158; fax: 415-476-9516.** *UCSF is an Affirmative Action/Equal Opportunity Employer. The University undertakes affirmative action to assure equal employment opportunities for underutilized minorities and women, for persons with disabilities, and for Vietnam-era veterans and special disabled veterans.*

MOUNT SINAI SCHOOL OF MEDICINE

The Department of Oncological Sciences of the Mount Sinai School of Medicine is seeking academic-track **FACULTY** at all levels. Candidates must have Ph.D., M.D., or dual degrees and a strong background in research relevant to cancer biology.

Applicants should submit curriculum vitae, including contact details for at least three references, and a summary of research accomplishments and plans for future research directions no later than December 29, 2008. Applications may be submitted to **e-mail: oncsci.search@mssm.edu,** or by mail to: **Search Committee, Department of Oncological Sciences, Mount Sinai School of Medicine, One Gustave L. Levy Place, P.O. Box 1130, New York, NY 10029.**

AQUATIC SCIENCE GRADUATE FELLOWSHIPS
Great Lakes WATER Institute
University of Wisconsin, Milwaukee

The Great Lakes WATER (Wisconsin Aquatic Technology and Environmental Research) Institute of the University of Wisconsin, Milwaukee (UWM) is seeking outstanding applicants for several multiyear Fellowships, including the James E. Dutton Fellowship and the James D. and Dorothy Shaw Fellowships in Freshwater Science, to support graduate study at the doctoral level. The Great Lakes WATER Institute is located directly on Lake Michigan and is the largest U.S. institution of its kind in the Great Lakes region. Scientists at the Institute conduct research in aquatic ecology and technology, biogeochemistry, aquaculture, fisheries, and environmental health, focusing on the Great Lakes and other freshwater systems. Interested students can look at the Institute website **(website: http://www.glwi.uwm.edu/)** for specific research descriptions and scientist profiles. Under the direction of Institute scientists, graduate degrees can be pursued through programs with existing campus departments in biological sciences, chemistry, geosciences, and engineering. Students are encouraged to contact Institute scientists directly concerning their specific interests in graduate studies. For information concerning how to apply for the fellowships and graduate studies at UWM, contact **Dr. Harvey Bootsma (e-mail: hbootsma@uwm.edu), Great Lakes WATER Institute, 600 E. Greenfield Avenue, Milwaukee, WI 53204.**

POSTDOCTORAL RESEARCH POSITIONS, University of Kansas, Specialized Chemistry Center. The Postdoctoral Researchers will be working with an interdisciplinary team of chemists and biologists to develop new methods to identify targets of small molecules. Ph.D. in organic chemistry, biochemistry, molecular biology, or related fields, and publications in peer-reviewed journals are required. For complete descriptions and application instructions go to **website: https://jobs.ku.edu,** position #00063829 and position #00061793. Review of applications will begin December 19, 2008, and will continue until filled. *Equal Opportunity/Affirmative Action Employer.*

Shantou University Medical School, a dynamic and innovative school located in Guangdong Province, China, jointly funded by Chinese government and the Li Ka-shing Foundation, is seeking M.D.s and/or Ph.D.s to teach undergraduate basic science and clinical courses. Retired or taking sabbatical leave parties are also welcomed. Please send curriculum vitae to **e-mail: karenmai@stu.edu.cn.**